THE UNIVERSITY *of* EDINBURGH

Experimental Investigations of Connections for Robustness of Mass Timber Buildings

by

Alicja Czesława Przystup

Thesis submitted for the degree of Doctor of Philosophy

School of Engineering

The University of Edinburgh

2023

Declaration

I declare that this thesis has been composed solely by myself and that it has not been submitted, in whole or in part, in any previous application for a degree. Except where states otherwise by reference or acknowledgment, the work presented is entirely my own.

Acknowledgements

I want to express my heartfelt gratitude for the unwavering guidance, mentorship and support from my thesis supervisor, Dr Thomas Reynolds, throughout my academic journey. His trust in my research direction and infectious enthusiasm for timber construction have been invaluable and helped me persevere throughout all of the challenges. I would like to extend my gratitude to Professor Yong Lu, who has pushed me towards academic excellence and provided invaluable insights into the world of robustness. I would also like to sincerely thank the technical team of the University of Edinburgh, Jim Hutcheson, and Mark Partington for the work they have put into making my experimental visions come true and making my time in the laboratory so enjoyable.

My sincere gratitude goes out to Professor Thomas Tannert of the University of Northern British Columbia, who through his research collaboration invitation to UNBC has allowed me to expand my experimental campaign beyond what I could have imagined and has since become instrumental in my further academic development. I would like to thank the technical team of the Wood Innovation Research Laboratory Michael Billups, James Andal, and Ryan Stern, who have provided me with the most seamless experimental testing experience a PhD student could ask for.

I'm grateful to my friends and family for their unwavering support, especially my parents for their hard work which helped me get to this point, my sister for being there during the moments of doubt and my brother for lending an ear to my timber tales. And finally, I would like to thank my lovely husband Eddie, whose love and support have been my lifeline throughout this journey.

Lay summary

Recent advancements in the construction of large timber structures have raised concerns about ensuring their safety, particularly in the face of potential collapse triggered by accidental events like explosions, vehicle impacts, or structural damage due to fires. These events can lead to catastrophic failures in these structures. Understanding how large timber connections behave under extreme force combinations is crucial for assessing the safety of tall timber buildings in such design scenarios. However, empirical testing can be expensive and time-consuming, making it challenging to gather sufficient data to enhance our understanding of this topic.

This thesis introduces a novel, more cost-effective, and efficient method for investigating the behaviour of large timber connections. This method aims to address the limitations of testing methods used thus far. The thesis then proceeds to validate these newly proposed methods through extensive large-scale testing and numerical modelling techniques. It goes on to use the proposed method to derive mechanical properties of a variety of connections, discussing factors influencing their performance and providing data on their limitations.

In summary, this research offers a fresh approach to studying how large timber connections respond to combined forces and extreme deformations, providing a more practical and economical way to enhance our knowledge in this critical area. Through using these principles, the thesis provides a wealth of new critical experimental data in the field.

Abstract

Recent growth in mass timber construction has raised concerns about preventing disproportionate and progressive collapse, emphasizing the need for performance-based design due to general lack of understanding the behaviour of mass timber connections under extreme load and deformations. The aim of the research presented was to expand on the current understanding of the mechanical properties of common floor panel-to-panel cross laminated timber (CLT) connections and subsequently floor systems under combined bending and tension, as typically observed under catenary action through experimental analysis. The thesis develops the methods for component-level and full-span substructure tests for CLT floors under extreme deformations that allow for distillation of the necessary parameters. The novelty of the study lays specifically in analysing the changes in these parameters due to increasing tension utilisation of the connections, which is instrumental for robustness performance analysis and has not been previously investigated. The component test developed uses a fraction of resources needed for the standard full-span testing while aiming to provide the same information about the connection behaviour, which can be used in design calculations and modelling alike. Full-span testing was performed to verify the component test results through numerical methods, as well as introducing further parameters such as continuous spanning panels and wall detailing. In total five types of CLT floor-to-floor connections were investigated, including four most commonly used currently in the industry as well as a novel tube connector.

Table of Contents

List of Tables

List of Figures

List of symbols

β – scale parameter in Gumbel distribution

γ – connection efficiency factor (adapted to CLT)

Δ – vertical uplift of the overhang

Δ_h – horizontal opening at the connection at the location of tension resultant

Δ_i – lever arm between the internal resultant couples of the connection

Δ_0 – initial vertical displacement under gravity loading (full-span test)

θ – rotation of the floor

$\theta_{c,Max}$ – maximum rotation of the connection

θ_{max} – maximum rotation of the subassembly/component

$\theta_{M,max}$ – rotation corresponding to maximum moment at the connection M_{max}

μ – location parameter in Gumbel distribution

μ_{Rod} – rod ductility (tube connector)

a – distance from support to the load application (four-point bending)

a_{ax} – distance between two centre axis of top and bottom layers (γ-method)

a_{i} – lever arm to the centroid of layer i (γ-method)

A_i – area of layer i (γ-method)

b – width of the member (γ-method)

C_c – connection's internal compression resultant

d_{cross} – thickness of the traverse layer (γ-method)

E_i – elastic modulus of the layer i

EI_{eff} – panel effective bending stiffness

$F_{max,r}$ – rod peak load (tube connector)

$F_{y,r}$ – rod yield load (tube connector)

G_i – shear modulus of the layer i (γ-method)

G_n – shear modulus of the surface layer (γ-method)

G_r – rolling shear modulus of the traverse layer (γ-method)

$(GA)_{eff}$ – panel effective shear stiffness (γ-method)

h – height of the component section

h_i – thickness of layer i (γ-method)

h_n – thickness of surface layer (γ-method)

i – layer number (γ-method)

I_i – second moment of area of layer i (γ-method)

I_{rob} – robustness index

$k_{c,A}$ – axial stiffness of the connection

$k_{c,R}$ – rotational stiffness of the connection

$k_{s,A}$ – axial stiffness of the support

$k_{s,R}$ – rotational stiffness of the support

k_0 – initial connection stiffness

l – effective span of the member (γ-method)

L – single floor span

M – internal moment in the connection

M_{max} – maximum moment in the connection

M_u – moment caused by uplift of the overhang

P – midspan pushdown force

$P(C)$ – probability of collapse

$P(C|D)$ – probability of collapse given damage

$P(D|E)$ – probability of damage given an abnormal event occurance

$P(E)$ – probability of abnormal event occurance

P_{max} – maximum vertical pushdown force

R – vertical reaction force at the support

r_T – tension utilisation ratio

T – external tension applied on the connection

T_A – active tension imposed on the component

T_c – connection's internal tension resultant

T_i – internal tension forces in the connection

T_{max} – peak tension (strength) of the connection

T_V – vertical component of the tension applied with overhang

u – midspan deflection

U_{max} – maximum vertical deformation at midspan

$U_{T,max}$ – axial deformation at the location of peak tension $\mathrm{T_{max}}$

$U_{T,50}$ – axial deformation at 50% load drop off in axial tension test

w – uniformly distributed load of the floors

x – overhang distance

List of abbreviations

ALP – Alternative Load Paths

ALPA – Alternative Load Path Analysis

ASCE – American Society of Civil Engineers

BS – British Standards

CLT – Cross Laminated Timber

COST - European Cooperation in Science and Technology

CRDC – Collapse Restraint Design Category

DoD – Department of Defence (US)

EWP – Engineered Wood Products

EC – Eurocode

FEA – Finite Element Analysis

FRR – Fire Resistance Ratings

Glulam – Glue Laminated Timber

HIDS – Hazard Independent Damage Scenarios

IBC – International Building Code

ISO – International Organisation for Standardisation

LSL – Laminated Strand Lumber

LVL – Laminated Veneered Lumber

LVDT – Linear Variable Differential Transformer

NBC – National Building Code (Canada)

SEI – Structural Engineering Institute (US)

STS – Self-Tapping Screws

UFC – Unified Facilities Criteria

Chapter 1: Introduction

1.1. Background

Construction industry is a sector with one of the largest overall contributions to the greenhouse gas emissions, with concrete production alone contributing up to 8% of the global CO_2 production (Lehne & Preston, 2018). As the world leaders begin to introduce more ambitious guidance and legislations such as zero net carbon targets, it is both morally and economically necessary to plan for a rapid change in the way modern buildings are being designed. Timber as a construction material is one of the most promising already available and viable alternatives, as it has a potential to become a natural carbon sink (Churkina et al., 2020). Moreover, functioning in timber buildings have been shown to have a positive effect on the wellbeing of the occupants (Green & Taggart, 2020). This along many other factors contributes to the large-scale mass timber construction's rising popularity in the last years with increasing number and scale of the projects year to year. The current tallest timber building is the Mjøstårnet tower (Figure 1. 1a) reaching over 81m in height (Abrahamsen, 2017), with

timber becoming widespread in mid-rise multi-storey buildings. Tall and long-span structures of this scale are required to be designed for robustness and this is a field not yet fully explored for mass timber components (Mpidi Bita & Tannert, 2019c).

Designing for robustness in essence is ensuring that localised accidental damage will not result in disproportionate and progressive collapse and is a vital design step that could save lives (Starossek & Haberland, 2012). Several case studies of progressive collapse activation such as the Ronan Point collapse show (Figure 1. 1b) the direct severe consequences of lack of the robustness consideration and played a significant role in the subsequent introduction of those in the building codes (Pearson & Delatte, 2005).

a)  b) 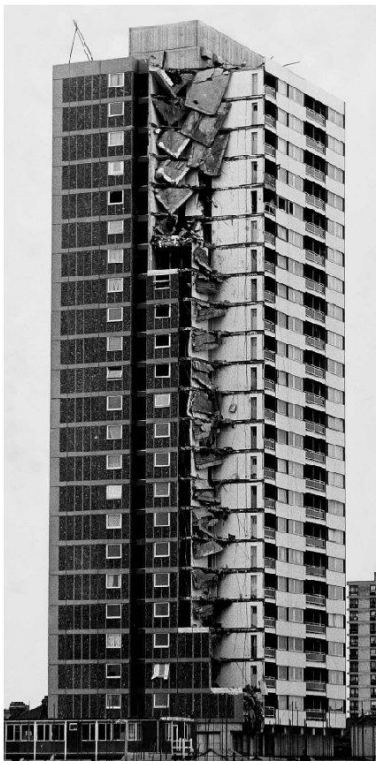

Figure 1. 1 (a) The Mjøstårnet Tower (photo by Ricardo Photo ©) and (b) Ronan Point progressive collapse extracted from Palmisano, (2014)

Eurocode's approach to robustness (European Committee for Standardization, 2006) and many other design guidance and legislation considering the topic is material and event independent, meaning it is the same for all construction materials and assumed to be effective irrespective of the accidental scenario in question. It is also objective based, meaning that there are design checks that aim to introduce some qualities that are thought to increase the robustness of the building, but the actual full performance analysis of the effect of those means is not undertaken.

This becomes a problem for a relatively novel material to be considered in the problems of this scale. The required design objectives have been based on research conducted before mass timber was a commonly used construction material and more empirical research is required to provide design parameters and to ensure that material independent framework can be reliably applied to mass timber. This need for more research and new comprehensive design guidance has been recognised by researchers and industry alike (COST Association AISBL, 2021; Voulpiotis et al., 2021a).

1.2. Alternative Load Path and Timber Assemblies

Alternative Load Paths (ALP) is one of the main strategies for progressive and disproportionate collapse prevention (Starossek, 2007a). It typically entails introducing additional continuity between the elements through either structural ties or designing with increased redundancy. It is not however the only known strategy – the second one being segmentation, which assumes specifically lack of continuity between chosen segments of the structure, to prevent the accidental load from progressing the failure through the elements and stop at strong segment borders. This strategy has

often been overlooked in design guidance, which typically focus on ALP. Segmentation has however often been recommended for large span structures and when the accidental scenario in question is likely to affect multiple elements of the structure (Starossek, 1999). One of the primary ALP mechanisms after the loss of a load-bearing member is catenary action, which allows for redistribution of load in the structure (Kiakojouri, de Biagi, et al., 2020). It is also the main load redistribution mechanism allowed for in Eurocode 1 (European Committee for Standardization, 2006), which provides formulas for horizontal and vertical tie forces required for catenary to form.

Under catenary action, the floors are subjected to combined bending and tension and therefore understanding of the effect of such combined loading on mass timber connections is instrumental for effective modelling and performance-based design. To date some early experimental work (Figure 1. 2) has been performed at a substructure level (C. H. Lyu et al., 2020; Mpidi Bita & Tannert, 2019b) but empirical data is still lacking on the behaviour of variety of connections and types of engineered wood products used in practice especially under varied axial stiffness conditions.

a)

b)

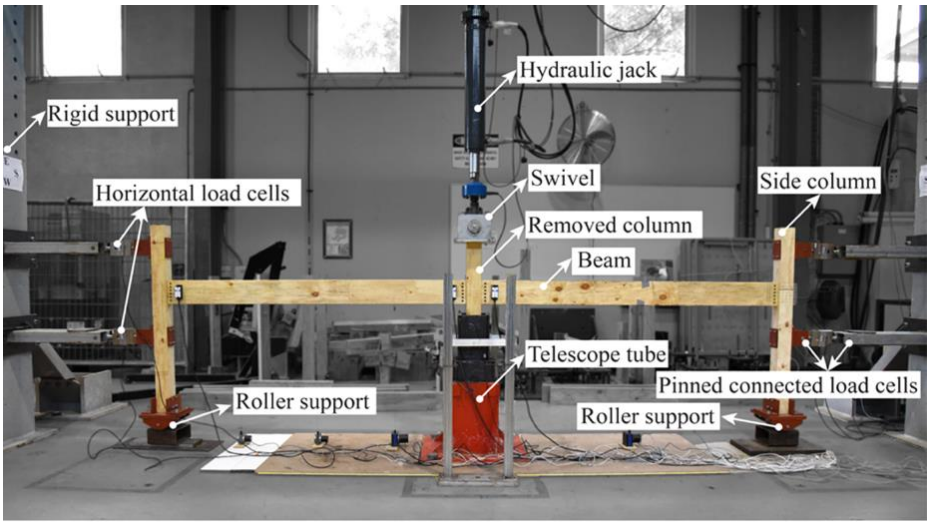

Figure 1. 2 Full span catenary tests performed by a) Mpidi Bita & Tannert, (2019a) and b) Lyu et al. (2020)

1.3. Research gap investigation

Timber as a construction material differs in several crucial ways from steel and reinforced concrete (RC). Most of the progressive collapse cases observed in timber were deemed to have occurred in long span structures (Frühwald et al., 2007) and the most notable examples of progressive collapse such as Siemens Arena and Bad Reichenhall Ice Rink collapse have been deemed to occur due to human error – meaning a systematic error affecting multiple members. Moreover, timber will be differently affected by some accidental scenarios such as fire, which again, is likely to

affect multiple members. All of which means that ALP material and event independent design approach and analysis may not be an appropriate approach and the significance of the consequences when used in the wrong context should be investigated.

The typical approach to investigating the performance of the building and its robustness strategies implemented is exploration of the Alternative Load Paths through notional removal of a vertical element one at a time (Unified Facilities Criteria, 2016). There is no current guidance or strategies available to designers' dictating investigation of other types of accidental scenarios, which as mentioned above, have not yet been confirmed to have a lesser effect on the structure than the typical notional element removal.

1.3.1. Initial accidental load path scenarios modelling

One of the accidental scenarios that is not routinely checked for its unique impact on timber structures in case of structural robustness is fire. When designing for fire the approach for timber is protection of the structural elements and the inclusion of additional sacrificial cross section depth (European Committee for Standardisation, 2004b). However even assuming a perfect protection in case of fire the timber structural elements' mechanical properties are likely to be affected by the heat penetration. Strength as well as elastic moduli of timber decrease with temperatures well before reaching combustion levels which has been codified (European Committee for Standardisation, 2004b) and has been proven to affect engineered wood products (Wiesner et al., 2018, 2019).

The initial stages of establishing the research direction have included producing an FEA model of a 5-storey example CLT building and investigate how a compartment

fire would affect the structure at different temperatures, assuming no combustion of the structural elements occurring. The purpose was to compare how this affected the structure in comparison to nominal element removal (in this case a ground floor wall) Appendix A includes the details of the experimental modelling including calculations of the mechanical properties of the elements, geometry details, and accidental loading modelling approach. The results of this investigation are also available as conference proceedings from World Conference of Timber Engineering 2020 (A. Przystup et al., 2021). In summary the basis of the fire modelling was assumption of the incremental decrease in the modulus of elasticity correlated to increased temperatures ingress. These temperatures also affect the strength of timber, which was reflected through compression strength reduction factors. These values can be seen in Table 1. 1. The reduction factors were applied to four separate ground floor compartments one by one, and a notional wall removal of wall at five locations on the ground floor was performed, altogether forming nine load cases. A comparison was made to maximum compressive strength utilisation ratio seen in the structure which can be seen in Figure 1. 3.

The results have shown that for all of the compartment fire scenarios the compressive utilisation ratio have reached the level equal to column removal in temperatures as low as 50℃

Table 1. 1 Reduced elastic moduli due to increased temperature and the equivalent temperatures and strength reduction factors Eurocode 5

Relative modulus of elasticity	Equivalent temperature in compression (˚C)	Compression strength reduction factor
75%	50	0.7
50%	82	0.25
25%	153	0.18

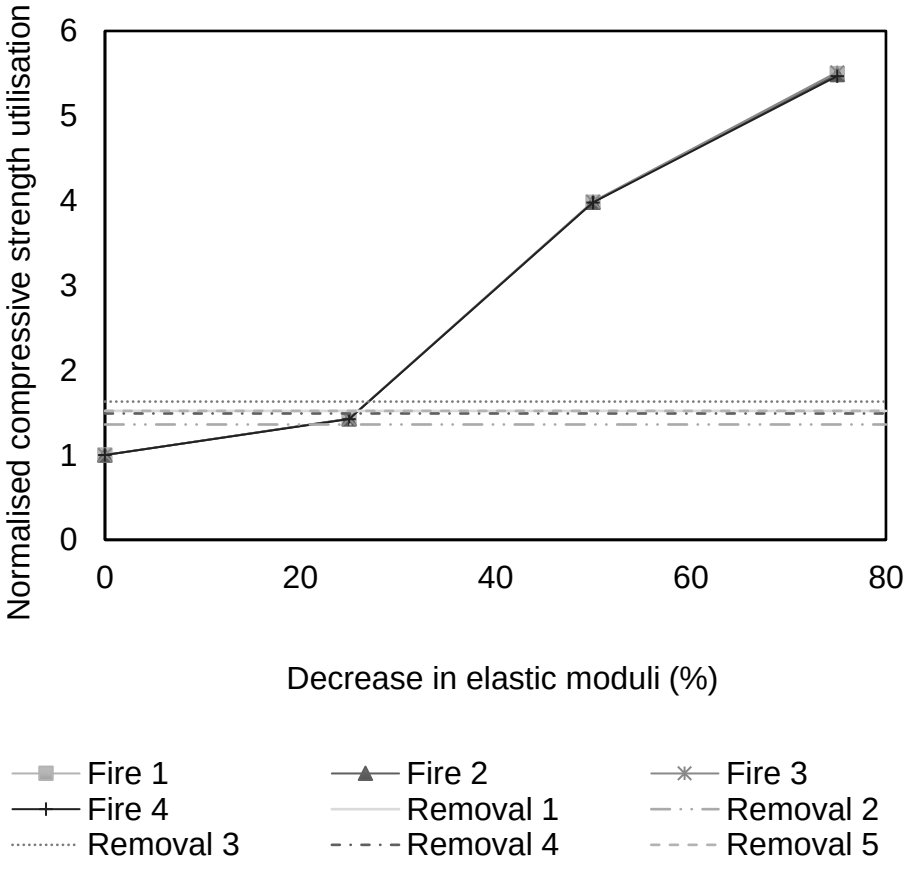

Figure 1. 3 Normalised maximum compressive strength utilisation in wall members vs decrease in elastic moduli due to increased temperatures

The model which yielded the results was simplistic, as it represented only a 2D approach to a 3D problem, was quasi-static and has not accounted for imperfections in structural elements nor temperature gradients. This means that the achieved results could affect the findings presented and the resulting conclusions are to be approached carefully. A bottleneck in modelling was additionally realised, as there was no available method for modelling CLT connections in rotation under combination of loading and extreme deformations, therefore in this case it was simplified to a pin on the basis of rotational stiffness of the connection assumed to be much lesser than the rotational stiffness of the panels. This meant however that the model could not be used to reliably confirm the structural behaviour under robustness scenarios.

Building this model helped in highlighting several important gaps in research. Firstly, it highlighted the importance of investigating the structural performance under various kinds of accidental scenarios, and secondly, that currently there is no reliable method and data one can turn to in order to accurately predict behaviours of connections in any of the progressive collapse scenarios.

1.3.2. Research gap identification

In timber construction the majority of structural design challenges lay in the design of connections, which are often the weakest parts. Since timber connections compared to steel and RC equivalents are particularly brittle in nature, their in-situ behaviour can change dramatically when experiencing large deformations seen after load bearing element loss. Large scale tests can be very informative of the potential problems that the current design approach entails when applied to mass timber and provide information on the subassembly specific behaviour under catenary action type loading. They are not however particularly useful in providing broader view on the mechanical

properties of the connections necessary for a full structure analysis required for the performance-based design approach.

1.4. Summary

The lack of in depth understanding of the robustness behaviours in timber structures means that as of now the use of objective based design principles can be dangerous. This is due to the material specific issues that may arise in various accidental scenarios meaning they will perform differently to their concrete and steel counterparts. Therefore, to increase the safety of the large wooden structures it is imperative that structural performance checks are implemented. However, to model these extreme behaviours one needs to be able to predict the mechanical properties and ultimate limit states of a variety of mass timber connections. The thesis tackles this discussed gap in knowledge through design and implementation of component tests performed alongside “traditional” full-span tests including over 90 specimens in 23 parameter combination varieties including, but not limited to, the connection type and design, support conditions and tension application and utilisation ratio. Fundamental mechanical properties of the connections are distilled based on the component tests and further validated through using them in an FEA, which replicates the large-scale tests in geometry and load application.

In the following chapter a deeper look into the literature is provided to aid in understanding of the current available codified solutions, real life examples of timber structures and their failures, as well as state of the art research in the field of robustness of large timber structure.

Chapter 2: Literature review

2.1. Tall timber structures

In the past decades the mass timber industry has allowed for building taller than ever before through development and mainstream popularisation of Engineered Wood Products (EWP). These include Glued Laminated Timber (Glulam) and Laminated Veneered Lumber (LVL) typically used for large beams and columns and Cross Laminated Timber (CLT), which form floor slabs and walls. Through an array of lamination techniques, these make it possible to create section sizes and element lengths to the designer's liking and therefore allows for higher load carrying capacity, all the while enabling the achievement of dimensional stability not possible in the use of solid timber (Holt & Wardle, 2014)

Since the emergence of first mass timber building over 7 storeys in 2009 and release of the first Canada and US CLT handbooks in 2013, the height and number of such structures has grown substantially (Kuzmanovska et al., 2018). Adaptation of building codes around the world which allow for taller timber construction has been attributed

by some to increased structural and fire testing (Green & Taggart, 2020), however many now conclude that there is still a lot of gaps in the current understanding of performance of large timber structures especially under accidental loading (J. Huber et al., 2019; Mpidi Bita et al., 2022)

2.1.1. Codes and regulations

The International Building Code (IBC) (International Code Council, 2021) has increased the allowable storey height for Mass Timber Structures through the introduction of a new classification of construction types, modified from the previous Heavy Timber construction type (Breneman et al., 2021; Thornburg & Kimball, 2022). This classification now allows for distinction of three categories with varied levels of fire protection, where the category with most conservative Fire Resistance Ratings (FRRs) and required protection with non-combustible materials allows for a building height of up to 18 storeys.

The 2020 amendment to the National Building Codes of Canada (NBC) (Canadian Commission on Building and Fire Codes, 2020) has introduced provisions allowing the construction of encapsulated mass timber buildings for up to 12 storeys. For American designers, most of the jurisdictions in the US follow the IBC provisions, however with variable rates of incorporation of the amendment: as of December 2022, over half of the states had not yet incorporated the new mass timber provisions (Wood Products Council, 2022).

Meanwhile after the Grenfell Tower tragedy, where rapidly spreading fire due to combustible façade system killed 72 people (McKenna et al., 2019), the UK

government amended the Building Regulations, reducing the allowable height of buildings with the combustible materials in the external wall first from 30m to 18m and then further to 11m through amendments to the Approved Document B: Fire Safety (UK Building Regulations, 2022). Due to timber being a combustible material, this although not fully restricting tall timber construction, has made it very difficult in practice.

2.1.2. Case studies

The tallest, “single material” mass timber structure to date (according to classification proposed by Foster et al. (2017)) is the 18-storey Mjøstårnet tower (depicted in Figure 2. 1 and Figure 2. 2a). The total height of 81m is counted including the top floor pergola, while highest occupied floor height stands at 68m (Abrahamsen, 2017). Main load bearing elements consist of glulam beams and columns, as well as large vertical trusses across four sides of the building for increased stability and lateral resistance of the building. Connections used were high capacity slotted-in steel plates and dowels, typically seen in bridges and other large structures. Elevator and stair shafts made from CLT reach 74m total. There is a mixture of timber floors (2-11) and concrete floors (12-18). In the latter, the concrete is added for increased inertia for vibration serviceability. Concrete floors also help to achieve higher acoustic standards. All floors act structurally as diaphragms and have maximum span of 7.5m.

Structural design based on Eurocode 5 (European Committee for Standardisation, 2004a) was implemented in the timber structure. Fire design strategy allows for a sacrificial charring layer, with the remaining cross section calculated according to the Eurocode 5: Part 1-2 (European Committee for Standardisation, 2004b). Robustness

design in the tower accounted for two scenarios: firstly, the loss of horizontal stiffness in one of the timber floors, and secondly for the floors to be capable of withstanding the impact of a falling timber deck.

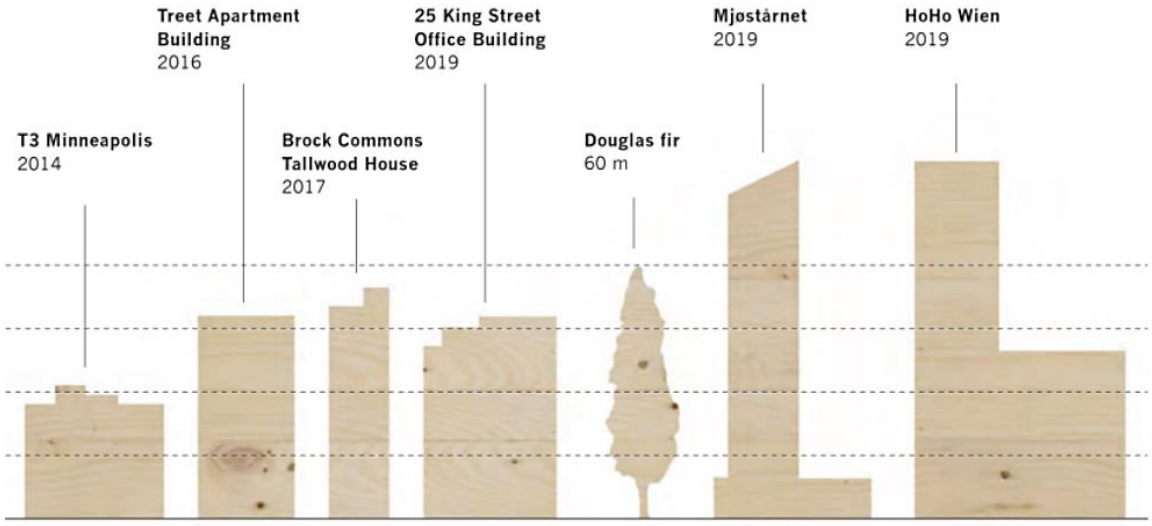

Figure 2. 1 Comparison of the heights of selected modern tall timber buildings to a large Douglas fir tree (Green & Taggart, 2020)

Mjøstårnet uses a vertical truss design as shown in Figure 2. 2a. It was not however the first structure to implement such solution. The 14-storey Treet tower in Norway, constructed in 2016 and shown in Figure 2. 1 and Figure 2. 2b, utilises a similar truss arrangement, with addition of two horizontal trusses under the intermediate concrete floors as its primary load resistance mechanism. Furthermore, it implements modular construction, where the prefabricated modules are connected to the glulam truss (Malo et al., 2016).

The timber structure reaches the height of 49m, and the modules are 8.7m long and vary between 4.0-5.3m in length. The building was designed to the Eurocode standards with the Norwegian National Annexes considered. Malo et al. describe the

truss and modules' design as making it inherently robust (Malo et al., 2016), with debris impact design as well as truss element removal being the main design scenarios considered.

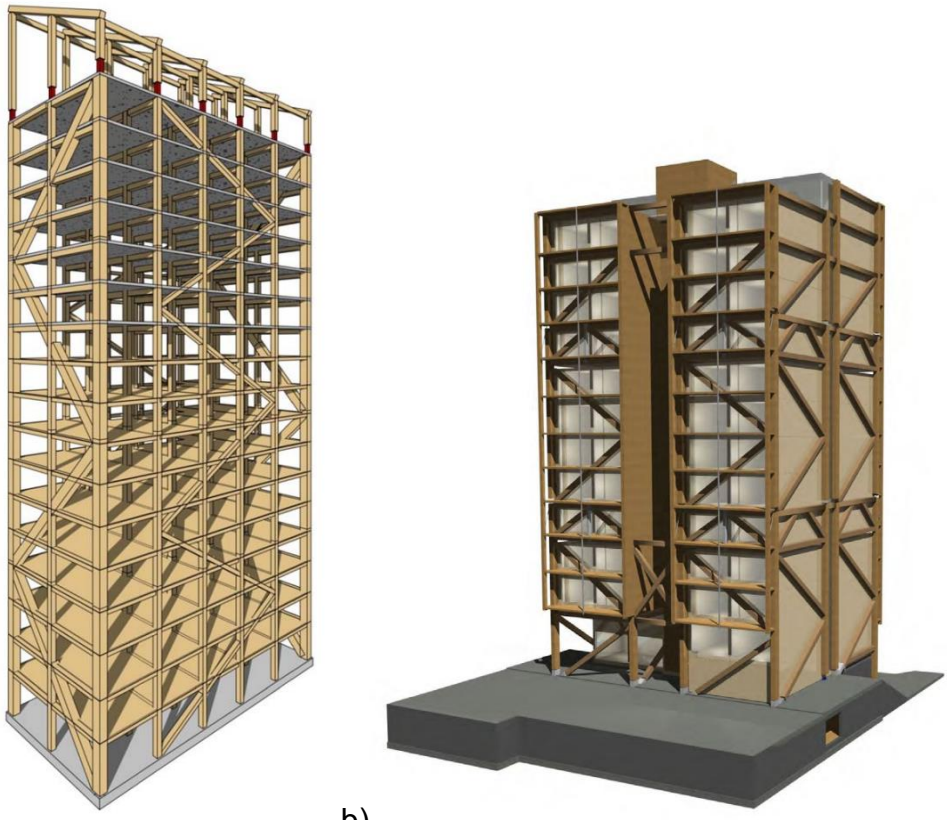

2) b)

Figure 2. 2 (a) Mjøstårnet tower (Abrahamsen, 2017) *(b) – Treet* Tower (Lipasti et al., 2020)

The HoHo building standing at 84m, located in Vienna, although taller than the Mjøstårnet is considered a hybrid structure with over 75% of the system being timber (Entwicklung Baufeld Delta GmbH, 2021). The 24-floor structural system comprises of four prefabricated building elements: supports, joists, ceiling panels and façade elements. These are attached to a concrete core which is the main primary load bearing mechanism (Figure 2. 3) which allows for a simplified wooden structure to be

slotted together without larger timber elements needed. Floors within the structure are composite CLT and concrete.

The robustness design strategy for HoHo relies on the primary concrete core structure to allow for load redistribution in case of damage to the wooden compartments. Design includes vertical and horizontal ties, with each floor tied to the concrete beams through cast-in reinforcement bars, and internal glulam columns vertically tied with glued-in steel rods. The building was designed to allow for removal of one column (J. Huber et al., 2018).

Currently the largest mass timber structure in UK is Dalston Lane, at 10 storeys and 33.8m in height (Figure 2. 4) and at the time of completion was also the tallest CLT platform structure in the world (Harley et al., 2016). The majority of the building comprises residential properties, therefore a “honeycomb” CLT design with many structural internal walls could be implemented with small sized compartments.

This, alongside fully tying the CLT panels to one another, is quoted (Harley et al., 2016)to be the source of robustness in the structure, although it is unknown whether any performance checks were performed. It is worth noting that, as discussed in Section 2.1.1, a timber building of this size with CLT in the external walls would not be permitted in the UK after the recent Approved Document B amendment.

The Brock Commons Tallwood House, built in Vancouver, is an 18-storey, 53m high building considered to be a hybrid structure, due to the inclusion of the concrete core and the steel beams metal decking used for the roof structure, as shown in Figure 2. 5. (Pilon et al., 2017; Poirier et al., 2022). The mass timber components are the Glulam columns and CLT floors. An innovative design of column connections (Figure 2. 6) was implemented in the structure, by ensuring continuation of the vertical load path without

unwanted perpendicular to the grain loading in the CLT floor. This connection allowed for both vertical and horizontal tie design for robustness, incorporating continuous alternative load paths, through which the building was constructed to tolerate the notional removal of a single column (J. Huber et al., 2018; Mpidi Bita & Tannert, 2017).

It ©s important to note that often for large-scale timber buildings, which at the time of construction were pushing boundaries and breaking records, additional testing was done on the project-by-project basis to allow for the proof of concept (Abrahamsen, 2017; Harley et al., 2016; Lipasti et al., 2020). Moreover, these projects are often closely monitored post-construction to assess their in-service performance (Poirier et al., 2022a, 2022b). Such projects are important for development of new technologies – the resources invested in high stakes projects allow to evaluate their collapse resistance response in more detail. However, a vast majority of multi-storey mass timber will be considered in the mid-rise range (Kuzmanovska et al., 2018). Robustness design in those cases is also of importance and therefore understanding of performance of standard connections and assemblies under accidental scenarios, which has not been investigated as closely, is crucial.

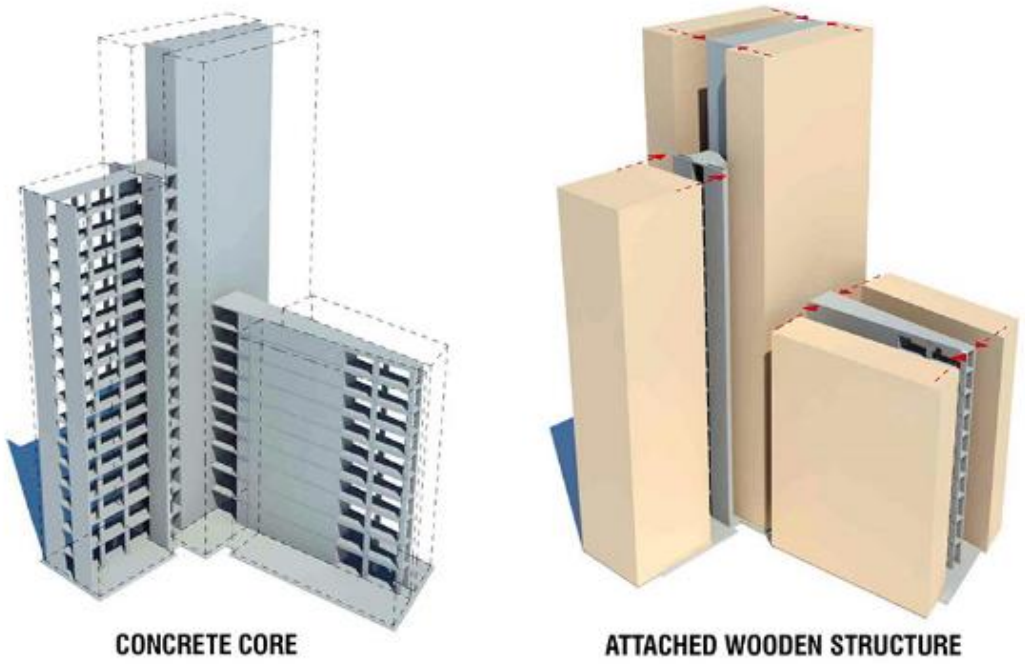

Figure 2. 3 The structural system of the HoHo building, showcasing the concrete core and the wooden structure (Big See, 2022)

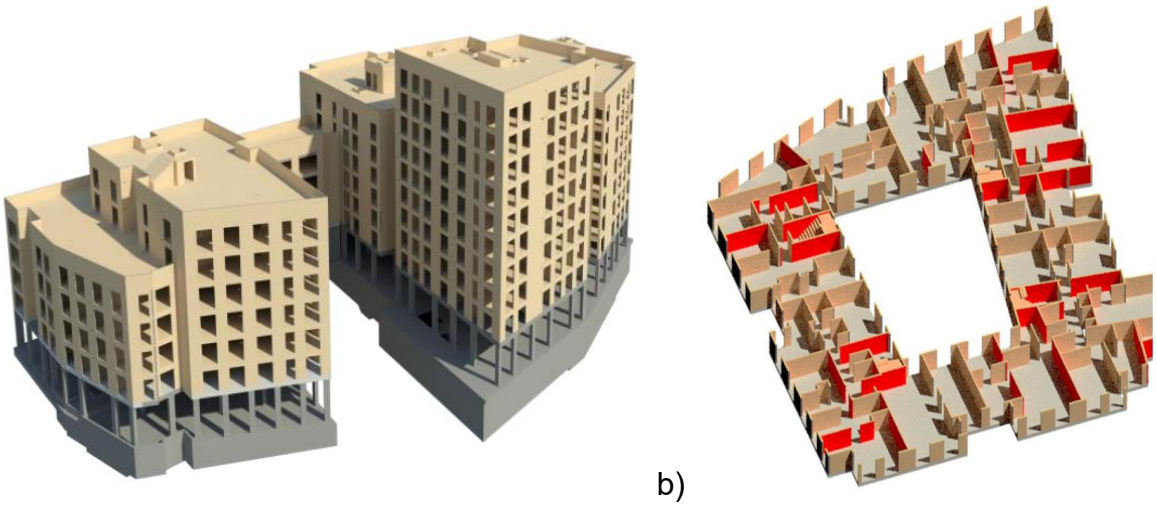

Figure 2. 4 Dalston lane CLT structural system (a) in its entirety and (b) showcase of floorplan arrangement with stability walls highlighted in red (Harley et al., 2016)

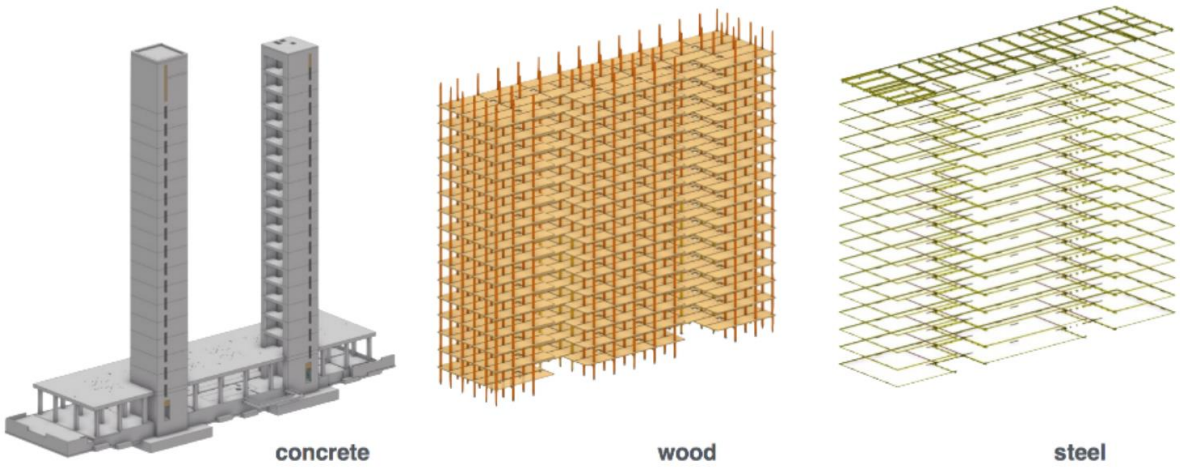

Figure 2. 5 Brock Commons structural system breakdown extracted from Fallahi (2017)*, provided by Action Ostry Architects*

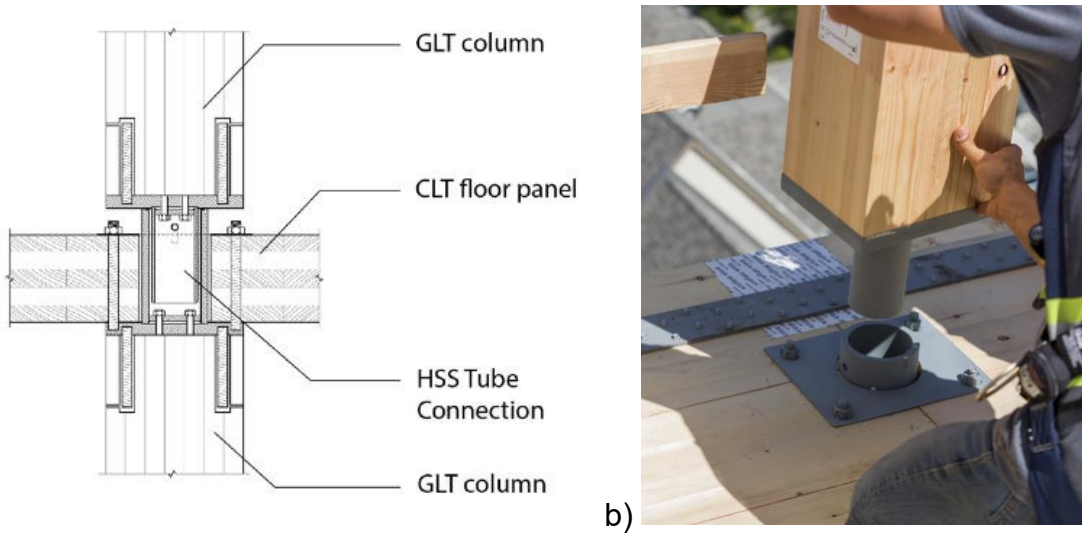

2) b)

Figure 2. 6 Brock Commons' bespoke steel column-to-column in hollow section connection (a) design (Poirier et al., 2022b) *and (b) installation* (Pilon et al., 2017)

2.2. Collapse due to accidental loading

2.2.1. Accidental loading

According to Eurocodes EN 1991-1-7: Eurocode 1: Actions on Structures–- Part 1-7: General Actions–- Accidental Actions (European Committee for Standardisation, 2004b) the accidental actions on buildings and bridges can include, but are not limited to, impact forces (vehicle, rail traffic, ships, and helicopters) and explosions. It further specifies that the code also includes any local failure from an "*unspecified cause*". The most recent draft of the new Eurocode 0 (FrprEN 1990:2022) updates the robustness definition to encompass specific actions originally listed as "*adverse and unforeseen events*" (Palma et al., 2023), leaving more room for interpretation.

North American codes surrounding the issues of accidental action design largely focus on the blast and explosion (Unified Facilities Criteria (UFC), 2005), however the majority of codes dealing with design for accidental loading do not specify the cause of accidental loads and focus on event-independent design (General Services Administration, 2013; Unified Facilities Criteria, 2016).

Although the accidental loading is likely to affect timber in the same manner as other buildings, additional timber-specific accidental scenarios need to be considered. In a study of 127 Scandinavian timber building failures (Frühwald, 2011; Frühwald et al., 2007). 84% of the case studies were large-span structures. The Scandinavian study found that the most common source of failure was human error in design and manufacturing. In designing and manufacturing multiple similar or identical elements and connections, there is a high likelihood that any error affects multiple members of the system, causing the damage or reduction in strength to be systematic and global. A further study investigating the trends present in 230 large-span timber structure

failures found that the majority of cases (58%) were linked to human errors and more specifically related to structural design and construction planning stage, and moreover that in most cases this error had a global effect (Dietsch & Winter, 2018).

The systematic human error was also found to be the main cause of one of the most famous cases of collapse due to accidental loading: the 1986 Ronan Point collapse (Pearson & Delatte, 2005). The collapse, pictured in Figure 2. 7, which initiated due to the small gas explosion, propagated throughout the structure, killing 4 and injuring 16. During the decommissioning poor workmanship was shown on a global level with “not a single joint being correct” (Pearson & Delatte, 2003). This collapse was one of the first triggering factors for research on structural robustness and its consequent incorporation into the building codes.

a)  b) 

Figure 2. 7 Ronan Point collapse (a) during and (b) after the collapse

In addition, timber is the only combustible structural material used in large-scale construction. The conventional knowledge on solid timber (European Committee for Standardisation, 2004b) as well as recent research (Wiesner et al., 2019) on engineered wood products shows significant loss of load bearing properties due to elevated temperatures in the structure. In accidental scenarios involving fire, depending on the size and location of the fire, the strength loss in multiple members could become events statistically dependant on each other.

2.2.2. Robustness and disproportionate, progressive collapse definitions

In structural engineering the three terms: robustness, disproportionate collapse and progressive collapse are terms which often can cause confusion due to the number of similar, but differing definitions out there which often use one of the terms to describe the other and/or interchangeably.

In general terms system robustness has been described as “the ability of system to maintain function even with changes in internal structure or external environment” (Callaway et al., 2000). The term can be used to describe this system quality in many fields of study, this thesis however will focus on the structural engineering definitions of robustness. The direct meaning of structural robustness has long been discussed and to date there are multiple descriptive definitions in standards, guidelines, and research articles (Starossek & Haberland, 2010). ISO 22111:2019 (International Organization for Standardization, 2019) as well as Eurocodes (European Committee for Standardization, 2006) define robustness as the ability of a structure to withstand accidental events or consequences of a human error, without enduring damage disproportionate to its original cause. The most recent draft of Eurocode 0 (FrprEN

1990:2022) updates the robustness definition to more general "*adverse and unforeseen events*" instead of defining the accidental loads one by one. Swiss Standard (SIA, 2004) additionally states that it is the ability of structure as well as its members to keep the degree of failure and deterioration within reasonable limits in relation to the cause – implying that robustness can also be considered on the member level, and that ensuring the prevention of member deterioration is a part of the designing for robustness. The standards in general aim to explain and present robustness as a structural quality that designers should aim to achieve.

Progressive and disproportionate collapse are often used interchangeably or a part of the same definition. Ellingwood et al., (2007) proposes a definition based on the American ASCE code 7-05 (ASCE, 2006), where progressive collapse is defined as "*the spread of local damage, from an initiating event, from element to element resulting, eventually, in the collapse of an entire structure or a disproportionately large part of it; also known as disproportionate collapse".* This definition is additionally included in the UFC 4-023-03 Design of Buildings to Resist Progressive Collapse (Unified Facilities Criteria, 2016)

Some researchers and practitioners have been more specific, arguing that progressive collapse and disproportionate collapse are two different, although often occurring concurrently, types of phenomena (ARUP, 2011; J. Huber et al., 2019; Starossek & Haberland, 2010). Progressive collapse signifies the *nature* of the collapse, where one initial damage spreads from element to element in a progressive manner. Whereas disproportionate collapse directly talks about the outcome quantification, where relatively small initiating event should not lead to extensive damage. This outcome-based description of disproportionate collapse is referred to in the Eurocode 1-7:

General Actions (European Committee for Standardization, 2006) in the already mentioned definition for structural robustness, described as "*the ability of the structure to withstand events (…) without being damaged to an extent disproportionate to the original cause*.". The extent of damage is furthermore quantified as the smaller of the two values: 15% of area of one storey or 70m^2.

European and American standardisation organisations are, at the time of writing, working on new generation of codes, where the aspect of the disproportionate and progressive collapse design is developed further, particularly with development of specific performance definitions (Dusenberry, 2022; Palma et al., 2023). The new draft of the SEI/ASCE for the Disproportionate Collapse Mitigation Standard has been quoted to define disproportionate collapse as *"a collapse that is characterised by a pronounced disparity between the original cause and the ensuing collapse of a major part or the whole of the structure*" (Dusenberry, 2022).

The extent of the allowable perfo"manc' there is quoted (Dusenberry, 2022) to be based on the Hazard Independent Damage Scenarios (HIDS) and the Collapse Restraint Design Category (CRDC), with the former specifying the design values for the initial damage scenario and the latter specifying acceptable outcomes, as shown in Figure 2. 8. CRDC categories are based on the ASCE/SEI 7-16 (ASCE, 2017) building risk categories and associated risk. For the CRDC A not pictured on the chart, as long as the structure complies with material code specific minimum structural integrity it does not require any additional analyses.

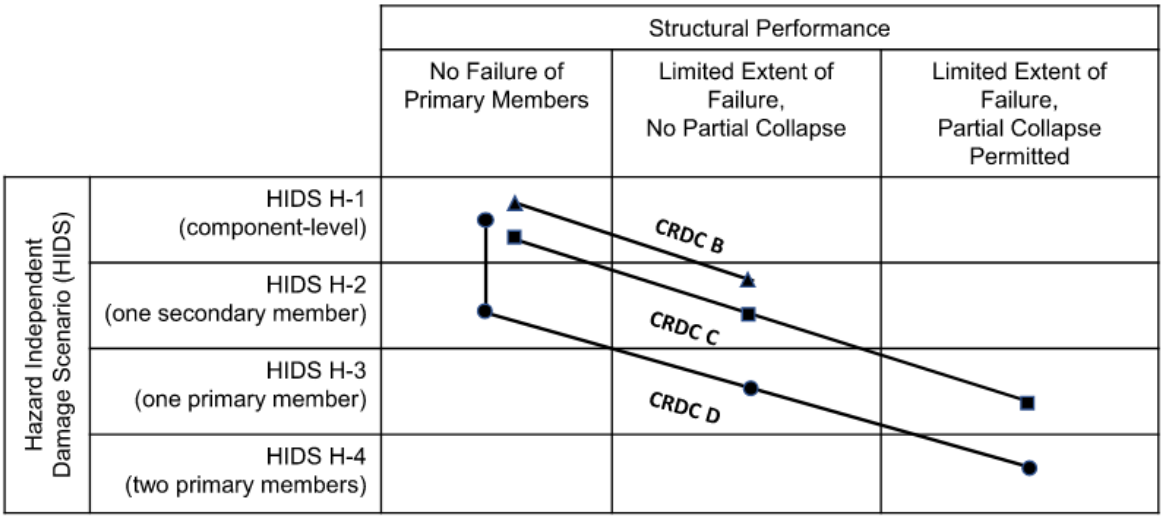

Figure 2. 8 New SEI/ASCE acceptable collapse outcomes based on HIDS and CRDC (Dusenberry, 2022)

Meanwhile the newest publicised information of the robustness-related updates to the Eurocodes (Palma et al., 2023) specify that no general rules regarding hazardous scenario specification or performance objectives are to be expected from the new generation of the code. These are said to be too complex and include too many variabilities and therefore will be expected to be assessed on a project-by-project basis, involving stakeholders beyond the building owner and the structural team, including local building authorities and insurance companies. It is unclear whether more specific guidelines for such assessment and specification will be available at the time of publication.

2.2.3. Collapse typology

One of the most commonly cited classifications of the progressive collapse is the typology proposed by Starossek, (2007b) who outlines five main types: pancake-type, zipper-type, domino-type, section-type and instability-type.

Pancake-type collapse is characterised by a loss in the bearing capacity of multiple vertical load-bearing components, resulting in a downward movement of either a portion or the entirety of the structure. This type of collapse entails the conversion of gravitational potential energy into kinetic energy, consequently generating substantial impact loads in the vertical direction. This is a type of system-level failure and can described as a series system. An example of this type of collapse is the World Trade Centre towers collapse, shown in Figure 2. 9 (Clifton, 2001), which is to date one of the most devastating examples of modern building collapse.

When loss of a single member (such as cable in a bridge) consequently leads to an overloading and failure of adjacent members, this is classified as a zipper-type collapse. In this case – sudden, dynamic redistribution of forces to remaining members may prove detrimental to the stability of the structure when the alternative load paths become overloaded. The system here is a parallel, rather than series system. The example of such collapse given by Starossek (2007b) is the Tacoma Narrows Bridge. The domino type collapse happens due to chain reaction movement cause by the overturning of the initial element and falling onto a neighbouring structural component causing large lateral impact leading to its overturning and causing the same impact on next neighbouring element.

Section type collapse is the loss of part of the cross section induces force redistribution into remaining cross section – causing progression of failure into the remaining

sections of an element, somewhat akin to the system level progressive collapse. Voulpiotis et al. (2021) also introduces the concept of the member-level collapse progression, which could be classified as section type, even expanding on that idea downwards in size to robustness of fasteners. Member-level robustness provisions in Swedish Standards (SIA, 2004) also address this issue.

Finally, Instability-type collapse can occur due to the localised failure of a bracing element which leads to the entire system becoming unstable. Example of this behaviour can also be seen in determinate trusses such as the FIU pedestrian bridge (Hu et al., 2021), which collapsed onto a highway in 2018.

In reality, more than one of the processes described above can occur at the same time. An example of a recent progressive collapse case is the 2021 Surfside condominium collapse (Lu et al., 2021), where pancake-type as well as zipper-type behaviour can be observed initially, and simulations performed by Lu et al. (2021) suggest that these further led to shear wall failures which triggered the building instability. In this case this could be classified as a mixed-type collapse.

Figure 2. 9 World Trade Centre pancake type progressive collapse (Clifton, 2001).

2.2.4. Timber structures collapse examples

Most of the collapse case scenarios investigated to date for timber structures are long-span structures (Dietsch & Winter, 2018; Frühwald, 2011; Frühwald et al., 2007), and so are the two most notable examples of serious structural collapse in timber. Both have been shown to have suffered to global and systematic errors in both the design and construction stages (J.D. Sørensen et al., 2010).

In 2003, the Ballerup Siemens Arena, a Danish velodrome, experienced a collapse of 2 out its 12 trusses (pictured in Figure 2. 10) only one year after construction (Hansson & Larsen, 2005; Munch-Andersen & Dietsch, 2011),. The trusses were fish-shaped with a spacing of 10.1m between trusses, and a span of 72m. The failure initiated in only one truss, but spread further into a neighbouring one, effectively doubling the area of collapse.

Investigations revealed that the design tensile strength used was about 50% higher than the one provided by the design code, effectively making the strength of the failed joint only between 25%-30% of the actual required strength (Munch-Andersen & Dietsch, 2011). Moreover, the truss members were joined by very stiff elements, inducing large moments in the connections, while design assumed hinged connections (Hansson & Larsen, 2005). Lastly, reduction in timber cross sections due to steel plates, bolts, and dowels, as well as reduced height near ends of the arches were not considered.

It was deemed that because the purlins were not tied directly to one another as part of the robustness strategy, it potentially saved the rest of the structure. Overall, although the fall of the second truss was shown to be progressive, it was deemed that the collapse was not disproportionate to its cause, given that the number and scale of

the design errors was so high and yet still the collapse has not spread beyond 2 trusses (Munch-Andersen & Dietsch, 2011).

In contrast, the second example discussed, the 2006 Bad Reichenhall ice rink collapse, was shown to have no evidence of robustness design considerations (Munch-Andersen & Dietsch, 2011), during design stage nor the lifetime of the building. The collapse of the 75m long and 48m wide building, using specialised timber box girders, is described in detail by Winter & Kreuzinger, (2008). There, similarly to the Siemens Arena, the collapse was found to be due to multiple causes. This included use of moisture-sensitive glue combined with the high moisture changes characteristic of an ice rink, and deviation from the technical approval for the box girders. Another serious issue flagged was the lack or regular inspection and maintenance which would have revealed the evolving issues. The ice rink, in contrast to Siemens arena which collapsed less than a year into its service life, was built over 35 years prior to its collapse, meaning that the arising moisture issues could have been flagged before they became a serious concern. The collapse of the structure was deemed to be progressive in nature (Winter & Kreuzinger, 2008), with the stiff cross girder structure causing the spread of the initial failure of an individual support to the remainder of the structure, pictured in Figure 2. 10.

Although the current focus of investigations into robustness of large timber structures mostly revolve around tall timber, it is still important to learn the lessons from the large-span collapses as in many cases the mistakes made apply to other large structures. Additionally, the lack of tall timber collapse examples does not indicate their inherent robustness but is likely due to the relatively recent development of the tall mass timber, with the tall timber buildings as we know today only starting to substantially increase

in numbers past 2013 (Kuzmanovska et al., 2018). The Siemens arena collapse has highlighted the need for an independent third-party performing quality assessment of the design (Munch-Andersen & Dietsch, 2011).

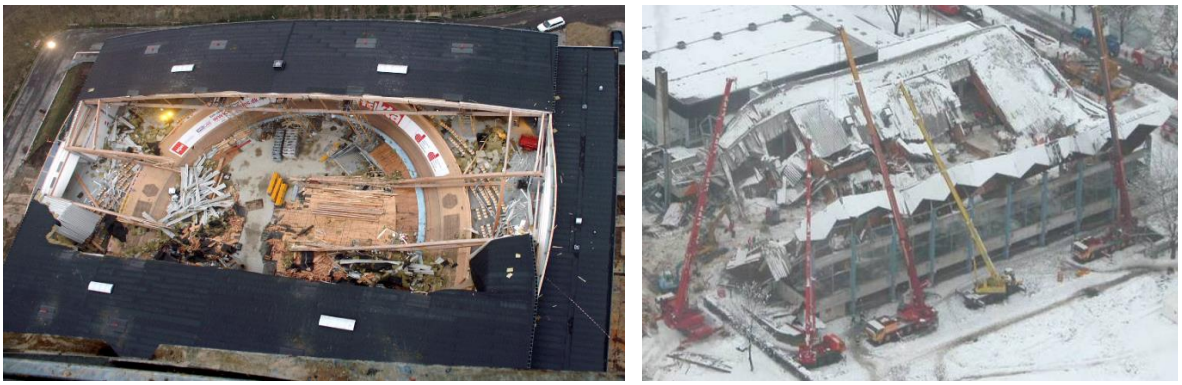

Figure 2. 10 Left–- Ballerup Siemens Arena (Hansson & Larsen, 2005), right – Bad Reichenhall Ice Rink (J.D. Sørensen et al., 2010)

2.2.5. Robustness design framework

Robustness as a concept has now had decades of research to allow for emergence of various design strategies, the adequacy of which can be assessed and quantified by a variety of sophisticated as well as more simplistic methods. Figure 2. 11 is a summary of the analysis methods, quantification methods and design strategies for robustness collated from a range of review publications across years (Agarwal et al., 2003; ARUP, 2011; Brett & Lu, 2013; Ellingwood et al., 2007; J. Huber et al., 2019; Nam & Luu, 2015; Sørensen, 2011; Starossek & Haberland, 2008, 2011). The diagram highlights the quantification and design strategies available currently in the Eurocode 1-7 (European Committee for Standardization, 2006).

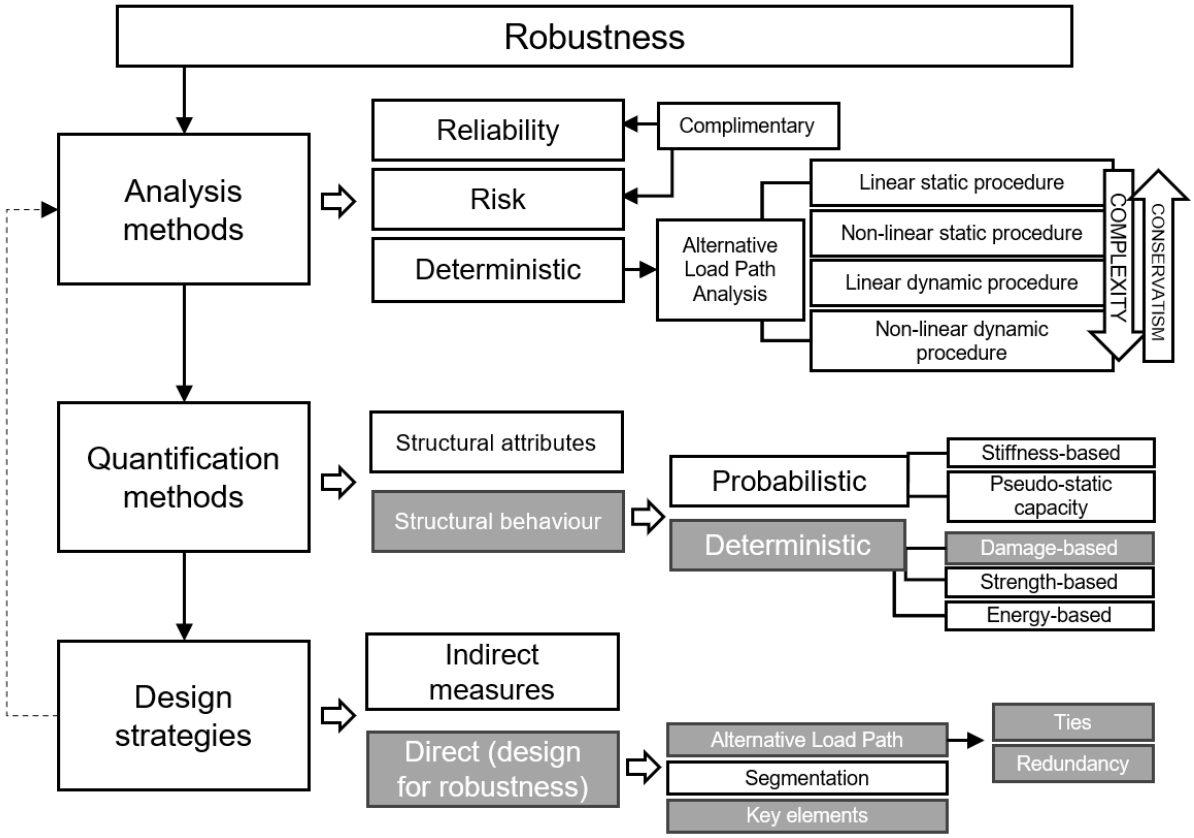

Figure 2. 11 The summary of the robustness analysis, quantification, and design methods, with the highlighted fields for the methods currently included in the Eurocodes

2.2.5.1. Quantification and analysis methods

Previously mentioned descriptive definitions of robustness from design standards and codes fail to assign a quantifiable measure of robustness which would make it possible to compare design methods. For this purpose, researchers often turn to risk and reliability analysis. Robustness as a structural property can be described as a general insensitivity of the structure to local failure (Starossek, 2007b; Starossek & Haberland, 2010). In statistical reliability terms where the probability of the accidental event occurring is $P(E)$, $P(D|E)$ is probability of localised damage given the event occurring and finally $P(C|D)$ is the probability of collapse given the occurrence of damage, the

probability of collapse is $P(C)$ is calculated as shown in Figure 2. 12. In these terms the probability of collapse given initial damage $P(C|D)$ is what we would call the structural robustness.

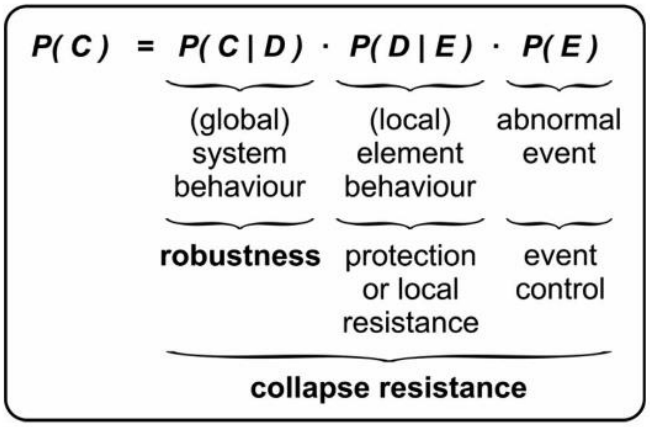

Figure 2. 12 Reliability definition collapse resistance and of robustness (Starossek, 2007b; Starossek & Haberland, 2010)

An alternative way of quantifying robustness within the risk and reliability framework was proposed: the structural vulnerability method (Agarwal et al., 2003). This allows for identifying non-robust structures by analysing the connectivity of the structural components in the system and their degrees of freedom. Advanced statistical models, although capable of revealing important quantifiable features of various structures, require a base understanding of the nature of the components investigated. The analysis framework by Voulpiotis et al. (2021, 2022) proposes a version of the robustness index I_{rob} originally introduced by Baker et al. (2008). The amendment to the formula proposes the use of damage-based criterion of damaged area A_{fail} to quantify the consequences C in the original formula in a more concrete way. Therefore, through ALPA of a variety of potential collapse scenarios of a structure it would be possible to compare different design scenarios to one another empirically.

This way of implementing quantification into the design (Figure 2. 13b) proposed by Voulpiotis et al. (2021, 2022) attempted to bridge the higher level of complexity types of statistical analysis and the current design practices. Figure 2. 11 highlights that although the Eurocodes include (limited) design guidelines, and basic damage-based performance criteria, they do not provide the analytical tools and procedures to connect the two.

a)

$$I_{Rob} = \frac{C_{Dir}}{C_{Dir} + P(C|D) \times C_{Ind}} \longrightarrow I_{Rob} = \frac{A_{Fail,Dir}}{A_{Fail,Dir} + \sum_{i=0}^{n} (P(C_i|D) \times A_{Fail,Ind,i})}$$

b)

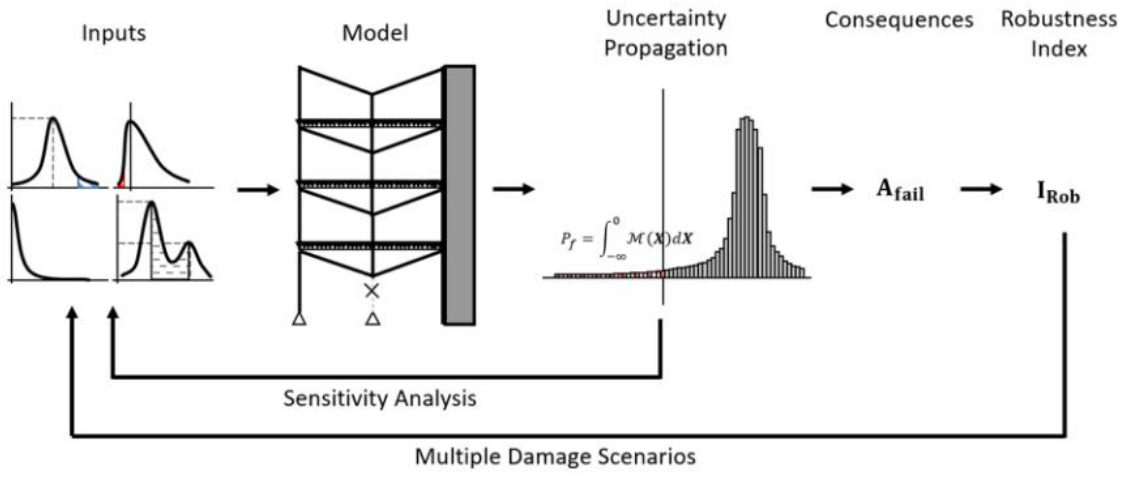

Figure 2. 13 The proposed (a) updated robustness index adapted from Baker et al. (2008) *and (b) proposed implementation of the index into design process by* Voulpiotis et al. (2021, 2022)

2.2.5.2. Design strategies

Choosing which strategy to use is dependent on the safety requirements outlined for the structure, evaluated either through its class or on a case-by-case basis. Starossek & Haberland (2012) provide a detailed classification of design methods presented in Figure 2. 14. There, a differentiation between robustness and event prevention is

made, collapse resistance being the sum of the robustness strategies and control of behaviour on the component level. The design strategies are also classified by Starossek & Haberland (2012) as structural and non-structural and lastly for robustness two main design categories are outlined: the indirect measures such as connection detailing or direct design measures – confining the spread of initial damage. Direct design indicates that a structural analysis on the specific structure is being carried out under a notional event scenario and made sure to meet the outlined specifications, whereas indirect design means incorporating design features which implicitly enhance system robustness based on previous experience. Direct design is preferable in large, novel, competitive structures, whereas smaller, relatively common types of construction can benefit from the indirect measures (Starossek & Haberland, 2012).

The design strategies for disproportionate collapse prevention in the Eurocode 1-7 (European Committee for Standardization, 2006) and their classification can be seen in Figure 2. 15. Although similar to the direct and indirect design methods classified in literature (Starossek & Haberland, 2012), the Eurocode's categories bear some important differences. The design strategies are divided into ones based on identified accidental action and ones focusing on limiting the extent of the local failure. Although the Eurocode's identified accidental action category (Figure 2. 15) could be seen as analogous to indirect design methods (Figure 2. 15), as prevention of incidents and protection of structures are included, designing for robustness is part of this category as well.

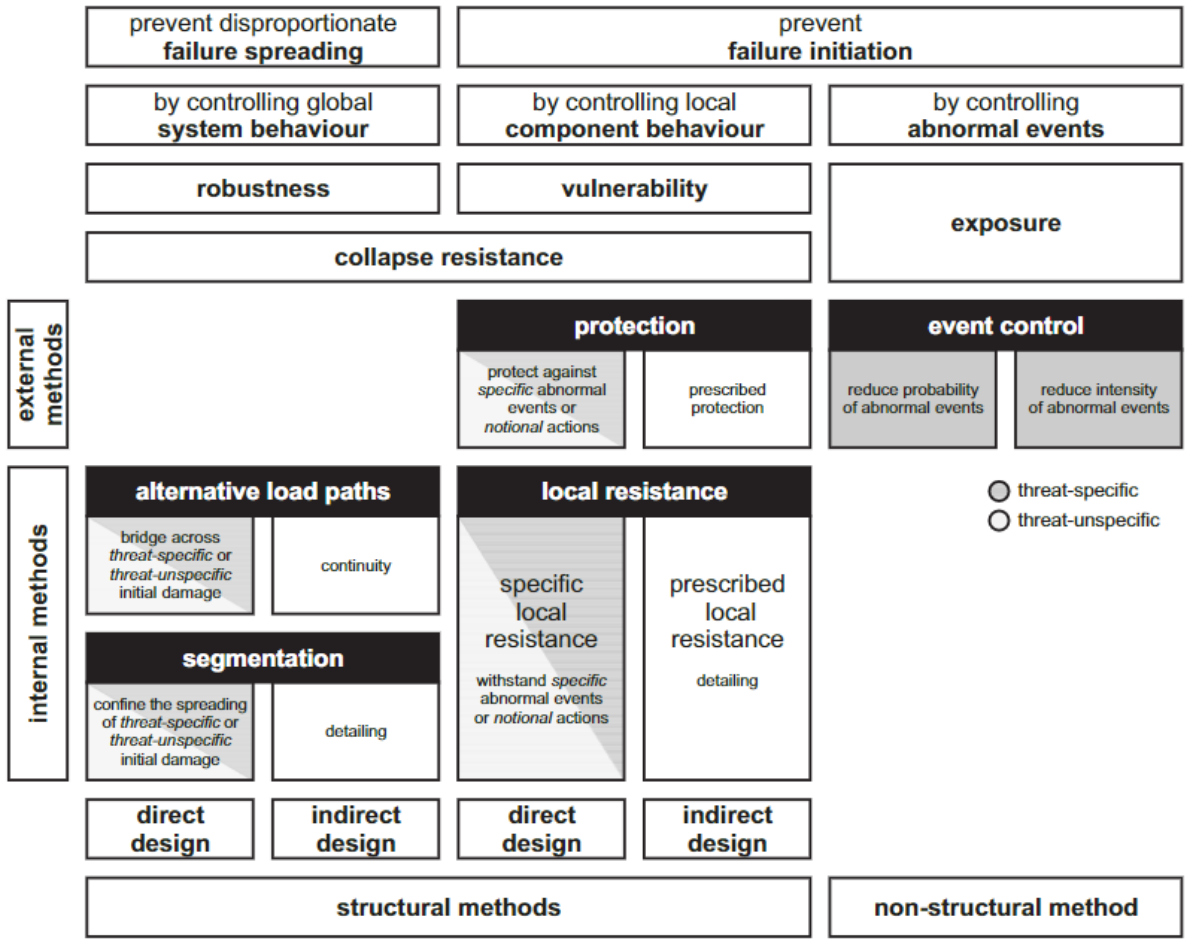

Figure 2. 14 Disproportionate collapse prevention methods in Starossek & Haberland (2012)

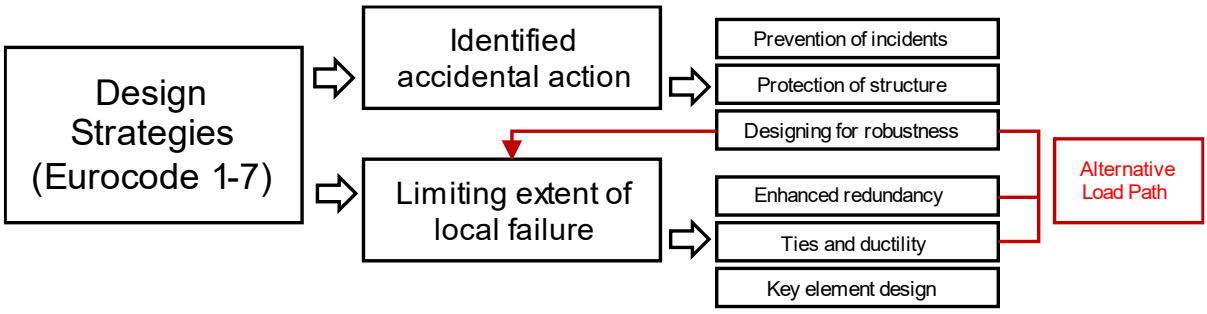

Figure 2. 15 Current Eurocode 1-7 robustness design strategies (annotated in red by author)

However, the known robustness design strategies, connected to Alternative Load Path Design specifically are listed under the limiting of local failure categories (Figure 2. 15 in red shows this connection). Overall, more clarity in the definitions as well as the implementation is needed in the new generation of codes. A survey of timber engineering practitioners (Mpidi Bita et al., 2019) has shown that for the most common reason for the participants not considering disproportionate collapse design was lack of specific code requirements.

There are two main approaches to Alternative Load Path development in the robustness framework in Figure 2. 11: as a method of analysis, and as a method of design. In alternative load path analysis, a study is conducted on a structure or part of it, which through introduction of some damage, typically notional element removal, allows to assess the ability for load redistribution (ARUP, 2011; Ellingwood et al., 2007; Unified Facilities Criteria, 2016). The design method, on the other hand, means introducing features into the structure that will allow for those alternative load paths to form (European Committee for Standardization, 2006). These typically will revolve around introducing redundancy to the structure and ensuring tying of the elements.

Alternative load paths in timber structures can form in various ways (ARUP, 2011), such as cantilever of continuous elements (bridging) (Palma et al., 2023), deep beam action of the CLT walls (J. Huber et al., 2018, 2019). The most referred to way of load redistribution, to which the tie force requirement is inherently connected, is the catenary action. Catenary action allows for tensile forces to develop within a subassembly after deforming downwards over a lost element (Figure 2. 16). Studies investigating the practical implementation of reinforced concrete (Y. Li et al., 2011) and

steel (Johnson & Mahamid, 2010) tie force design are available in literature, confirming the suitability of the method.

Moreover, catenary performance criteria for connections can be found both in the current, as well as the new draft SEI/ASCE Disproportionate Collapse Mitigation Standard for the steel and concrete structures (Dusenberry, 2022; Unified Facilities Criteria, 2016). These requirements dictate minimum allowable rotation of the central connection to be 0.112 rad for life protection and 0.15 rad for disproportionate collapse prevention. These values are based on material-specific research and experience, and although they can be used as an initial point of reference for mass timber, we currently do not have the same level of understanding of the mass timber connections as for steel and reinforced concrete, and therefore more research is needed to establish these values for timber.

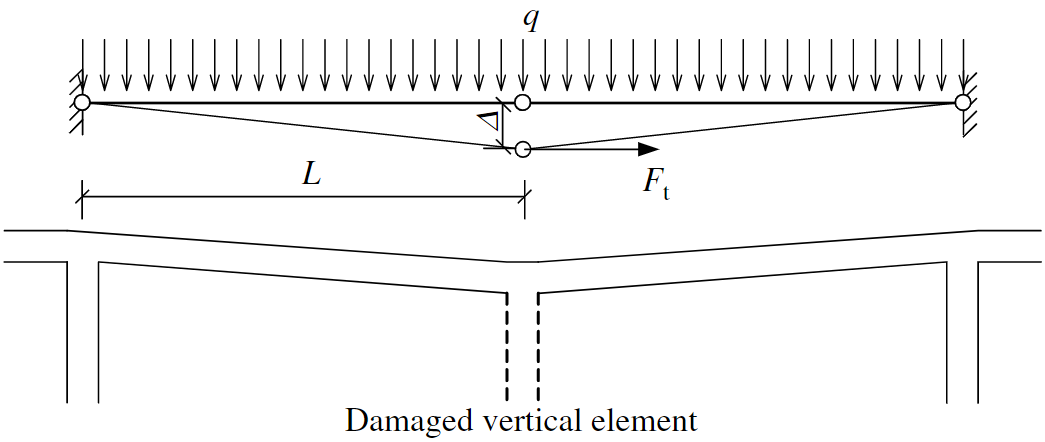

Figure 2. 16 Catenary action mechanism for tie force calculation (Y. Li et al., 2011)

Segmentation, in some literature referred to as compartmentalisation (Ellingwood et al., 2007; J. Huber et al., 2018) is a design strategy that ensures that an element failure will not cause a chain reaction, progressively overloading the neighbouring structural

elements by introducing deliberate breaks in load paths, allowing a segment of a structure to collapse while leaving the rest intact (ARUP, 2011). Segmentation is described as one of the two main design methods of preventing the disproportionate collapse in structures by Starossek & Haberland (2012).

One example of segmentation in the literature is the case study of the Confederation Bridge, investigated by Uwe Starossek, (1999). The paper shows the differences between the preliminary design before progressive collapse study and the final design after the analysis. The designers have incorporated an additional plastic hinge to prevent a potential local failure pulling the remaining structural elements down. It is deliberate consideration of segmentation in design which made the difference between the collapse of Siemens arena – which was limited to 2 out of 12 trusses – and the Bad Reichenhall arena, where the whole roof collapsed (Munch-Andersen & Dietsch, 2011).

The “Design for Robustness of Timber Structures” report (J.D. Sørensen et al., 2010) in their recommendations show possible deign of connection detailing in a timber structure that would allow for transfer of both horizontal as well as vertical load under regular loading conditions, but with a possibility of the complete detachment in case of an element failure. In current Eurocode 1-7: Accidental actions, segmentation design has not been considered (European Committee for Standardization, 2006), however the recent presentation of the new draft of the code does mention that not only it will be now included, but also timber specific guidelines for segmentation are to be expected (Palma et al., 2023). It is a vital inclusion as the majority of collapse cases seen so far have been long span structures (Dietsch & Winter, 2018; Frühwald, 2011) and in these cases, tying between members and increased redundancy could be

expected to be detrimental to robustness, the additional loading causing adjacent substructures to fail progressively (Sørensen et al., 2010).

The last strategy available in Eurocodes is the so-called key element design. A key element of a structure is one upon which the stability of the remainder of the structure relies (European Committee for Standardization, 2006). Such an element is to be designed to withstand a notional accidental load onto it. In terms of timber buildings, it is asserted that key element design should be used as last resort (ARUP, 2011), since the notional loading is generally arbitrary.

2.2.6. Experimental testing

2.2.6.1. Progressive collapse testing

There are two general groups of testing regimes for progressive collapse: dynamic and quasi-static (Alshaikh et al., 2020). Dynamic testing typically involves simulating the gravitational load of the building through placing weighted blocks throughout the structure and quick release of one of the supports, while quasi-static tests use an actuator to provide steady pushdown. The concrete and steel progressive collapse tests performed on the structures can also be classified in the three groups according to size: connection tests, sub-assembly or assembly, and full-scale tests (Kiakojouri, De Biagi, et al., 2020).

Some full-scale tests have been performed through removal of elements in real life buildings prior to the demolition (Sasani, 2008; Song et al., 2013). The advantage of these tests is the ability to account for all of the real-life elements such as infill walls and other dead loading. However, no live loads are present or accounted for typically

in those cases. Moreover, investigating structures that are scheduled for decommissioning generally means that the methods of construction used will be outdated and therefore they are less likely to provide useful information for modern construction. They can be however, of great value when it comes to assessing the safety of some older existing structures.

To date one of the largest tests performed on laboratory-build experimental frames include the dynamic testing of a half-scale three-storey reinforced-concrete frame retrofitted with carbon-fibre reinforced strip cables seen in (Liu et al., 2017), seen in Figure 2. 17. True full-scale testing is extremely time consuming and therefore many researchers opt for scaling down their reinforced concrete and steel frames to help in minimising these limitations (G. Q. Li et al., 2018).

Figure 2. 17 Half-scale reinforced concrete frame retrofitted with carbon-reinforced strip cables progressive collapse column removal test (Liu et al., 2017)

Connection and small sub-assembly level testing designed to investigate the behaviour of the central connection under large deformations seen after loss of element typically involve a central vertical actuator simulating pushdown action and a variety of boundary conditions simulating various level of restraints (Dinu et al., 2017; Forquin & Chen, 2017; Yang & Tan, 2013), an example of which can be seen in Figure 2. 18.

Reinforced concrete and steel frames, when designed and maintained properly, offer ductility, and retained tensile load transfer under large deformations which was shown numerous times under a large variety of parameters to be appropriate for proprietary alternative load path formation (Alshaikh et al., 2020; Kiakojouri, De Biagi, et al., 2020). The wealth of experimental investigations performed on reinforced concrete and steel and consequently presented in literature is vast at various test sizes and the material independent design approach used today largely draws from this knowledge. There is no guarantee however, that these conclusions can be extrapolated to mass timber structures.

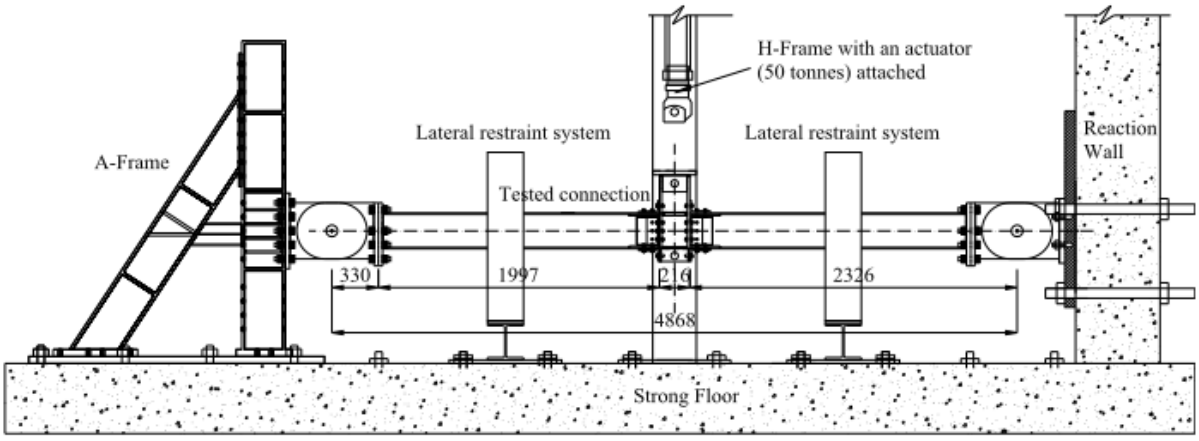

Figure 2. 18 Component experimental setup for the beam-column connection progressive collapse performance test (Yang & Tan, 2013)

2.2.6.2. Combined load testing

The forces within the beam or floor elements during the progressive collapse pushdown scenarios are going through a range of combined loads – firstly in the compressive arching stage it is combined bending and compression, and later in the catenary action it is tension and bending (Alshaikh et al., 2020). Similarly, combined loading can be found in a number of other structural elements. There has been a number of experimental studies that have focused on load interactions in more detail, through designing experimental setups to reflect such combinations.

Examples include steel composite columns tested under axial-force and moment interactions (Lai et al., 2019) composite beams tested under combined flexure and torsion (Tan & Uy, 2009) or shear wall under tension, bending and shear cyclic loading (Nie et al., 2020). Some methods use load and restraint placements to induce the combined loading directions (e.g., off-centre load application placement introducing eccentricity such as in Figure 2. 19 b). Other ways of achieving the similar effects is using two separate actuators (Figure 2. 19 a). Another example of using two-axis actuators on the shear walls can be seen in the reinforced concrete shear wall study (Nie et al., 2020), showcased in Figure 2.20.

The advantage of testing smaller components in general is the ability to increase the sample sizes and isolation of the specific combined load behaviours. It is thought that this approach could be beneficial in the timber progressive collapse testing due to the current focus on performance of connections and the present need for more empirical data in the field. Moreover, introduction of the actuator along both axes instead of restrained horizontal condition, which has been done previously for other purposes,

can be of great benefit in timber to allow for a better understanding of the influence of tensile force on the timber components.

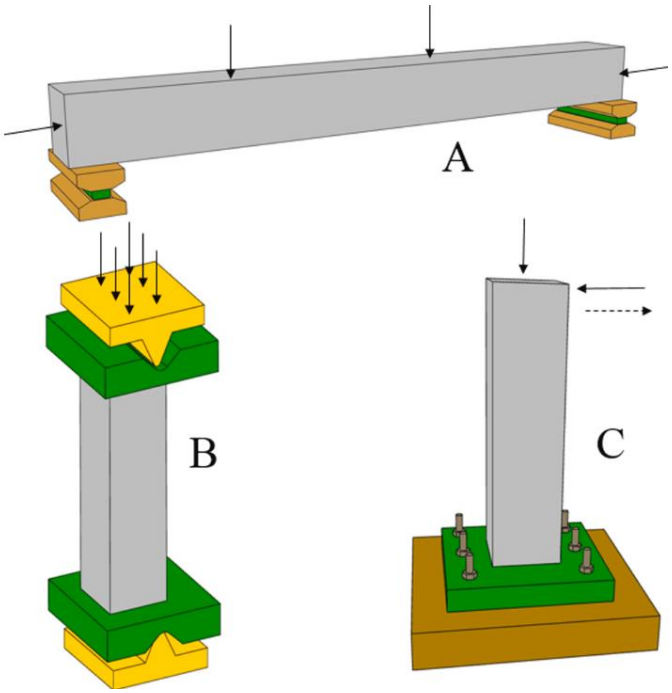

Figure 2. 19 Experimental setups for evaluation of the axial force-moment interactions in columns a) combined compression and traverse loading b) eccentric compression c) cyclic loading (Lai et al., 2019)

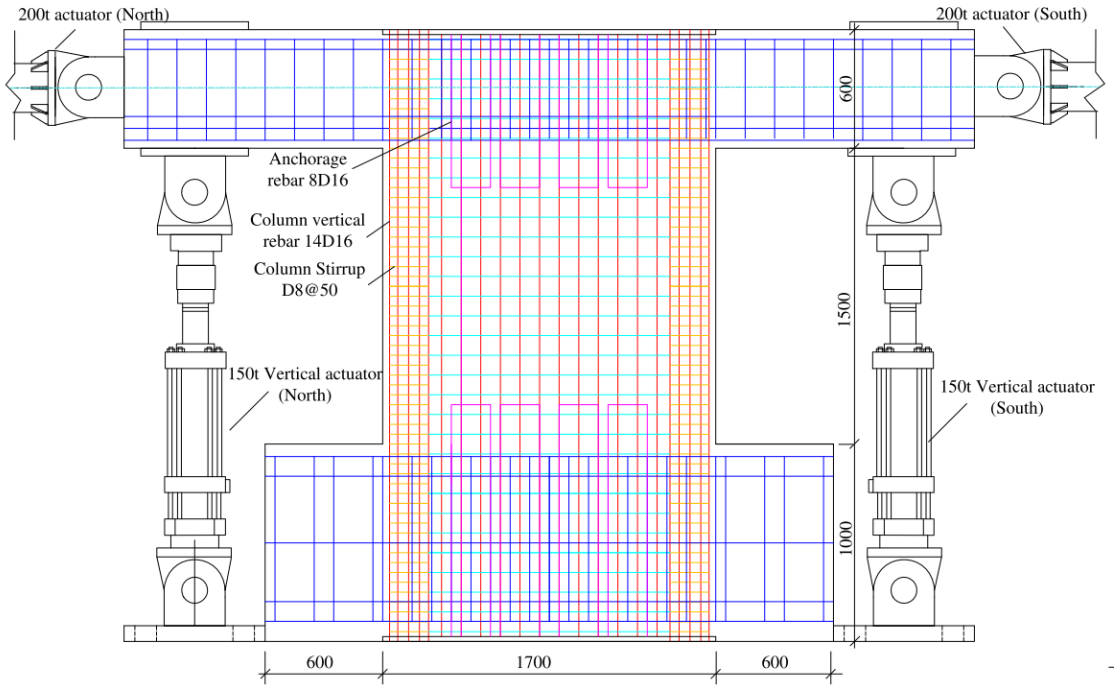

Figure 2. 20 Experimental setup for combined cyclic tension-bending-shear loading on reinforced concrete shear walls (Nie et al., 2020)

2.3. Robustness in timber

A comprehensive review of robustness design measures in general in view of their use in timber construction, including light timber frame as well as mass timber considerations is carried out by J. Huber et al. (2018, 2019). They conclude that although the low weight-to-strength ratio may be advantageous in the collapse scenario, the brittle nature of the material is of concern. They highlight that there is no well-established deterministic approach currently available in for timber robustness design. Another review study (Mpidi Bita et al., 2022), which considers resources, for design, quantification, and analysis as well as ongoing research activities regarding the robustness of large timber buildings, advises against using any prescriptive design rules developed for steel and concrete buildings when designing multistorey mass timber. Despite certain similarities between the mass timber structure and other

methods of construction, which in the past was used as justification for objective design methods, their performance is simply unknown. Voulpiotis et al., (2021) identifies some of the major timber-specific challenges that need to be addressed and considered when pushing the limits of timber construction to be: the orthotropic nature of material, low stiffness, and high brittleness of the material. All of these will drastically affect the way the system behaves under extreme loads.

Robustness as an arising issue in the design of taller timber structures has been recognised by extensive inclusion of the topic in the COST (European Cooperation in Science and Technology) Action CA20139 HELEN – Holistic Design of Taller Timber buildings (Fink et al., 2023). Working Group 1 deals directly with the issue of robustness, while Working Group 2 looks into the Accidental Load Situations which aside from seismic design includes fire and blast which are both important factors to consider in disproportionate collapse prevention. Another COST action, E55 Modelling of Performance of Timber Structures, has also considered robustness as an important issue to consider (COST Domain Committee, 2010), however due to the action taking place before tall mass timber structure become more prevalent, the Design for Robustness of Timber Structures guideline (J.D. Sørensen et al., 2010) deals only with long span structures.

2.3.1. Effect of accidental loads on timber elements

One of the focuses of the COST action HELEN (Fink et al., 2023, personal meeting minutes) is the investigation of the effect of accidental actions on tall timber structures. Two of the accidental actions relevant to robustness outlined in the Working Group 3, alongside seismic design, are blast and fire. Moreover, the group work focuses on

identifying the interaction between the potential hazards through, as it has been recognised that often these often occur together. A good example of which can be the World Trade Centre collapse, where mechanical impact followed by fire has occurred (Clifton, 2001).

There is a substantial body of literature on the performance of timber buildings in fire, therefore for the scope of this thesis the focus will remain on the research yielding potential implications to ways in which the timber robustness should be considered. Recent research (Wiesner, 2019; Wiesner et al., 2018, 2019) found that the post-extinction delay phase of the fire, where the heat begins to propagate through the structure in the hours following the fire, the temperatures to which the timber elements are likely to be elevated to can be detrimental to the compressive strength and stiffness of the elements. Due to the general lack of information on the behaviour of the mass timber components under dynamic loading, several research studies have delved into the experimental investigations regarding the topic.

Behaviour of CLT and Glulam components after simulated blasts was investigated by Viau & Doudak (2019, 2020), who start developing the dynamic increase factors library for the mass timber components. The studies also concluded that while the components lack the ability for energy dissipation, the performance improvement is seen in cases where the end connections are designed to allow for ductile deformations. In a similar vein mechanical impact has been studied by Cao & Frangi (2023) to allow for better understanding of the dynamic effects for accurate modelling of collapse scenarios, however the findings of those studies are still preliminary and so far and have not investigated effect of variable support conditions.

2.3.2. Load redistribution capabilities of timber structures

Multiple recent research studies approach the performance-based design question through various approached to connection modelling and Alternative Load Parth Analysis. One of the methods is utilising Finite Element Analysis software.

J. A. J. Huber et al. (2020) performed a nonlinear quasi-static pushdown analysis on isolated comparment models representing a bottom, middle and top comparment of an 8 story platform type CLT building. The ALPs in this study were shown to be formed in transverse shearing of the floor panels, deep beam action of the walls, catenary action on the short span of the floor panels as well as hanging action from the roof. All of the above, aside from the shearing of floor panels, are direcrly dependent on the behaviour of respective connections. A linear-elastic ALP analysis of a 6-storey post and beam building, performed by Mpidi Bita & Tannert (2019a), has also pointed to limited axial and shear capacities as well as limited deformation capacity, all necessary for the formation of ALPs. In this case the most effective load trasfer was observed throught the continuous sections.

Another recent FEA parametric study of an experimentally validated post-and-beam model has investigated the influence of inclusion of CLT floor and their various arrangements on the strength of the system(C. Lyu, 2022; C. Lyu et al., 2023). It was concluded that the staggering of the floor panels can improve the strength of the subassembly by 60.2%. They also argued that the post-and-beam load paths were crucial for the load redistribution behaviour and that CLT floors alone have shown not to provide sufficient ALP formation.

Voulpiotis et al. (2022) implemented the previously proposed (Voulpiotis et al., 2021a) method of using the modified robustness index I_{rob} as a tool for quantifiable

comparison of robustness of designs. The method in practice allowed for sensitivity analysis of various design parameters. The case study designed by the researchers was a 15-storey, CLT core post and beam timber structure, and the ALPA was performed in ABAQUS FEA software. The study found that improvements to the system level design such as introduction of strong floors yielded a more significant improvement of robustness performance than improving strength and ductility of connections. The study however points out the need for further experimental validation of the floor and connections behaviours.

Although FEA is currently the most commonly used tool for the ALPA in research, running complex large-scale models including discontinuous is very computationally intensive (Cao & Frangi, 2023a). A mixed element method is hence proposed that allows for non-linear dynamic model for ALPA, which could be used to perform multiple parametric studies. Preliminary results highlight, that changes to one property of the connection, could directly influence other properties (Cao et al., 2023), and therefore emphasizing both the need for deeper understanding of the connection mechanical behaviour as well as computationally efficient, yet accurate method of analysis for subsequent performance checks.

2.3.3. Load redistribution capabilities of timber subassemblies

The presented studies investigating whole system behaviour all have one thing in common – they either use experimental methods to validate the accuracy of the models and behaviour of system components or highlight the need for further validation of them through experimental methods. It can therefore be asserted that to

investigate the more complex system level response under accidental load scenarios, the empirical behaviour of the initial building blocks needs to be established.

The simplified beam model proposed by Izzuddin et al. (2008) treat the large deformations due to the removal of a column due to an accidental scenario as a series of structural components connected by rotational and axial springs. This method was further developed and implemented in case studies (Izzuddin, 2022; Stylianidis et al., 2016a, 2016b; Stylianidis & Nethercot, 2021) and was an important basis for the following experimental work, as it allows for distillation of smaller subassemblies as small as individual beam systems seen in Figure 2. 21.

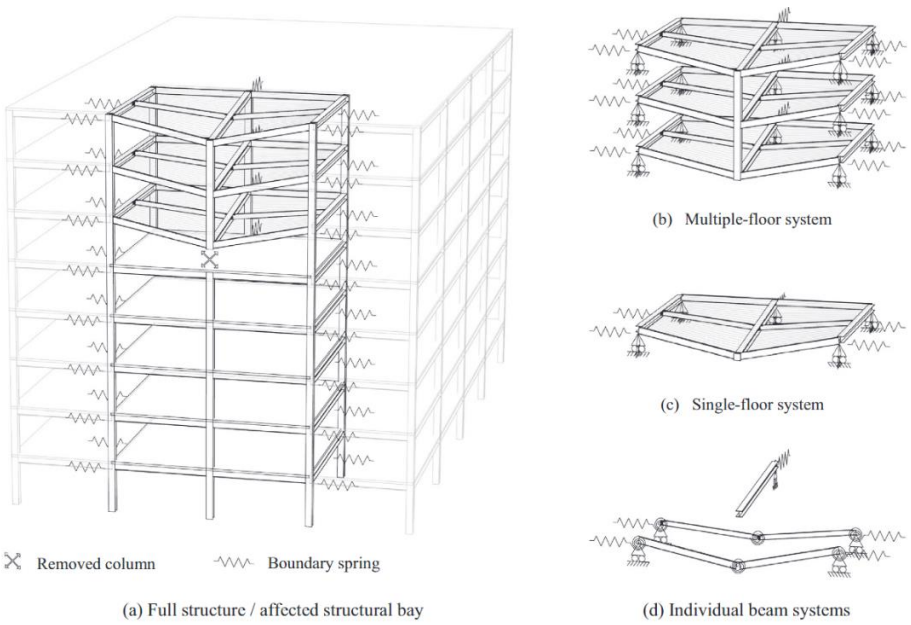

Figure 2. 21 Simplified beam models for load redistribution post column loss (Stylianidis et al., 2016a)

To date, several testing campaigns have been performed to attempt to quantify the ability of timber substructures to deform and redistribute the loads. Mpidi Bita et al. (2020) performed quasi-static floor-to-floor tests on cross-laminated timber (CLT),

laminated veneered lumber (LVL) and laminated strand lumber (LSL). Their experimental test setup can be seen in Figure 2. 22a). The specimens tested were 2000mm in the single span and 580mm in width, and two central connection types were tested – a standard half-lap connection utilising self-tapping screws, and the novel tube connector. The vertical support implemented for both sides of the specimen was a bracketed floor-to-wall connection typical to platform-type construction, and the end of the panels were additionally held own over the supports, providing a level of rotational stiffness. The study found limited ability of the conventional connection for load redistribution, with most of the load resistance being attributed to compressive arching, however the novel tube connection was shown to significantly increase the vertical load bearing capacity through catenary action activation. The performance of the tube connector was further investigated by J. Huber et al. (2023), who implemented testing setup shown in Figure 2. 22b) featuring quasi static 4-point bending tests, with the floor spans of 2600mm and the lever arm to the spreader beam of 2000mm and a hinge support allowing for free rotation of the floor elements. The tube connectors have shown desirable behaviour of ductile deformation modes and provide consistent result of high subassembly deformability.

C. H. Lyu et al., (2020) performed quasi-static experimental tests on a 25% scale LVL post-and-beam subassembly, seen in Figure 2. 22c). The specimen investigated the central beam-column-beam connection, with the scaled-down spans of 2000mm each beam. The support conditions included beam-to-column connections with the columns held in place by two steel sections with load cells attached at different heights of the column allowing for estimating the moment present at the ends of the subassembly.

It found that the subassembly was capable of achieving a deflection sufficient for catenary action deformation in the standard Megant ® type connector and additionally proposes improvement through introduction of a novel double plate connector. The authors disclaim however, that the results of the study are only applicable to the exact connections used. (Cheng et al., 2021) used the same, slightly modified experimental setup to investigate the influence of the dynamic loads on the tested subassemblies. The study concluded that although the static tests yield similar results, their initial stiffness and moments in the connections are overall lower and putting forward Dynamic Increase Factors (DIF) for the tested subassemblies.

The largest pushdown mass timber tests to date have been the 25% scale 2x2 bays of 2000mm in length of LVL post-and-beam with CLT floors performed by C. H. Lyu et al., (2021) investigating the performance of such subassemblies to loss of a corner column. The experimental setup can be seen in Figure 2. 23. The loading sequence was a combination of gravitational load through application of steel blocks on the 3 undamaged bays and the active pushdown with an actuator on the bay with the failed column. Two quasi-static tests were performed and the results from the tests were additionally used for FEA model validation, which was then used to perform the parametric tests discussed in Section 2.3.2 (C. Lyu, 2022; C. Lyu et al., 2023). It was found that 64% of the load applied was transferred directly to the column adjacent to the lost element in the primary CLT direction, signifying the importance the floor arrangement has to the load redistribution.

a)

b)

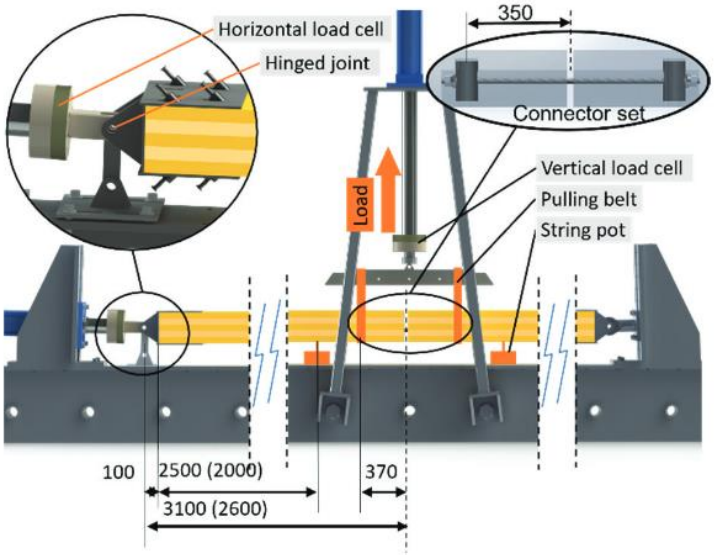

c)

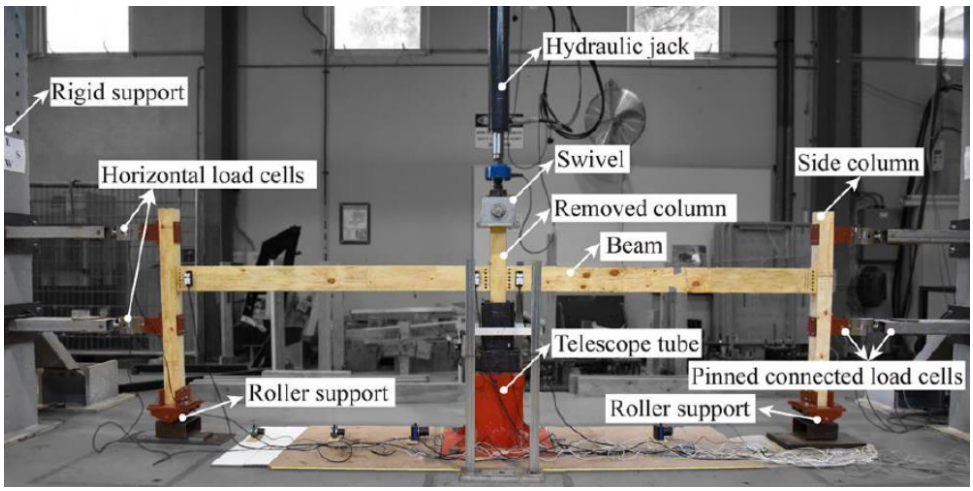

Figure 2. 22 Mass timber catenary action pushdown experimental setups (a) (Mpidi Bita et al., 2020) *(b)* (J. Huber et al., 2023) *and (c)* (Cheng et al., 2021; C. H. Lyu et al., 2021)

a)

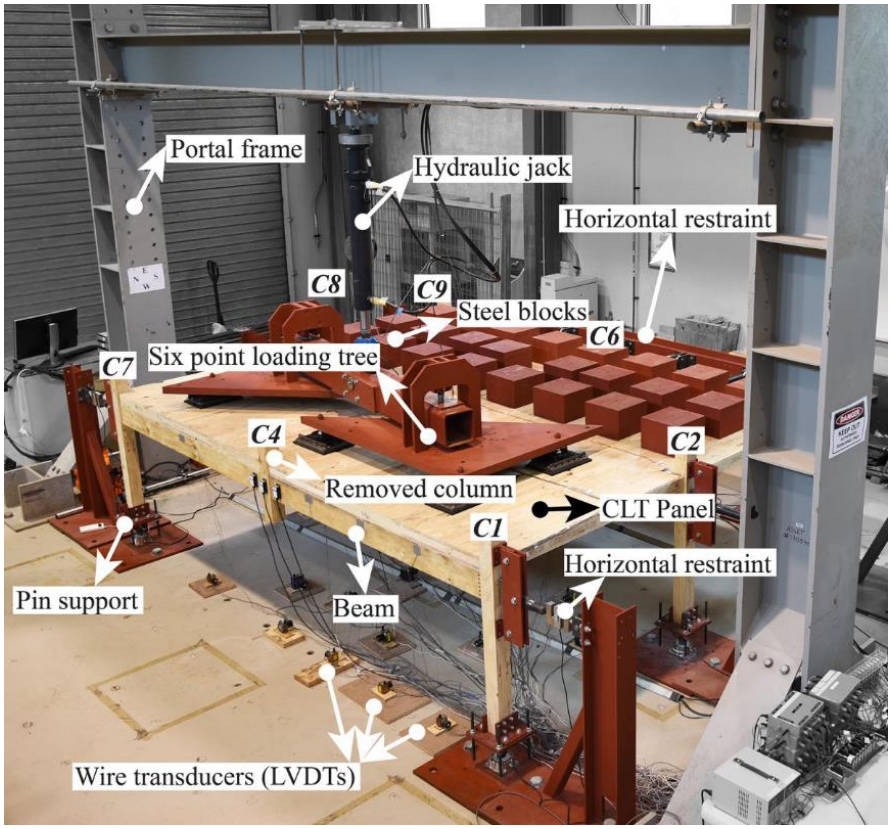

b)

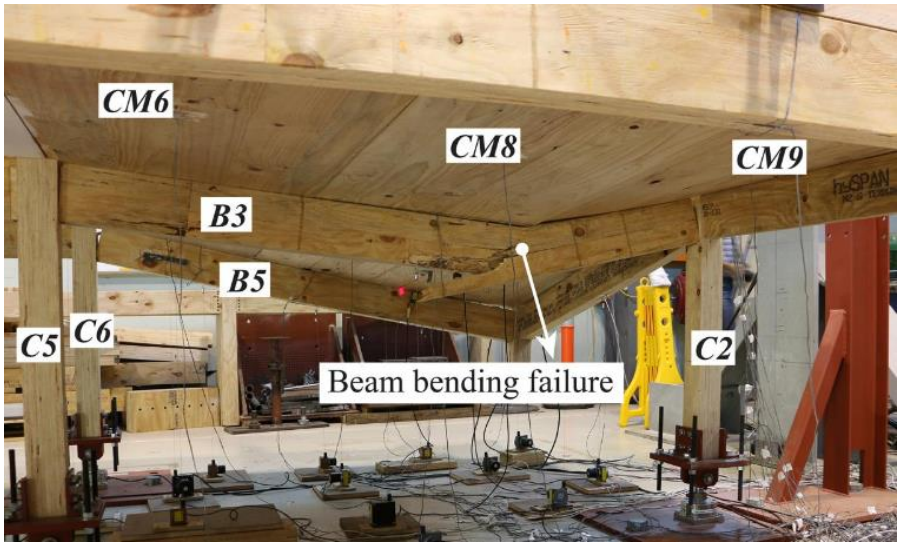

Figure 2. 23 3D post and beam 2x2 bay with CLT flooring experimental test setup (C. Lyu, 2022; C. H. Lyu et al., 2021)

2.4. Summary

The use of timber structural systems in mid- to high-rise buildings has become more commonplace in the past decade, and taller than before buildings are already in the planning stages. This means that the consequences of potential progressive collapse due to accidental loading are also increasing for those types of structures. The investigated timber progressive collapse case studies have shown that the human error in connection design as well as moisture ingress have been the main causes of collapse. In cases where the triggering event is likely to systematically affect multiple structural members, objective based alternative load path robustness design strategies are not advised. These however are the only codified methods available to designers today.

These types of errors are likely to affect timber structures disproportionately to steel and concrete counterparts and therefore it is thought that structural performance checks for material specific accidental scenarios are vital. Moreover, subassembly studies have shown that even under regular notional removal scenarios CLT floor-to-floor as well as LVL beam-to-beam connections often do not perform in favourable manner for catenary action activation, which is the basis of the design objectives in the codes.

To dates some studies have been performed modelling the full structure behaviours of the tall mass timber buildings under notional column removal, however the connection behaviour of these models has not been verified empirically. Due to the large number of types of timber connections, varying in grain directions, lamination techniques and types of fasteners, each of those types needs to be considered and investigated separately with regards to its mechanical properties under large deformations.

The current progressive collapse resistance testing methods previously employed in concrete and steel structures are vary in size. Large subassemblies, although desirable for investigating the full structure behaviours, require a lot of time and resources and limit the test matrix significantly. Moreover, even those tests often require to be half-scale or smaller, due to the large cost and complicated and time-consuming assembly. Mass timber is currently still experiencing a lot of innovation, meaning that a lot more data needs to be collected, and therefore smaller scale tests could be favourable for best contribution to the state of knowledge today.

Chapter 3: Methodology

3.1. Aim of the study

As previously discussed, the objective-based approach is currently the only one provided in Eurocode 5 and is based on research conducted before mass timber was a commonly used construction material. Therefore, an in-depth investigation is required to establish how mass timber structures practically function after accidental element loss. This means establishing how existing popular mass timber connections, technically designed to standards, behave under extreme deformations and combined loading typically seen after loss of an element. In these scenarios predictable ductility is a desirable quality of the structural components, and timber is a brittle and orthotropic material known for challenging connection design. Rotational and axial stiffness, maximum deformations and consequently ultimate limit states of individual connectors are all parameters that will define the structural response in Alternative Load Path (ALP) formation, one of the primary robustness design strategies.

There is a great need for more empirical data on these behaviours both to verify whether assumptions made in the existing design frameworks are valid and ALP

formation is possible and to provide reliable inputs for the numerical modelling often used to predict progressive collapse scenarios. Simultaneously, full-scale testing of subassemblies is costly, time-consuming, and often only gives information about how the specific geometry considered will behave. One of the aims of the following study is investigating feasibility of alternatives to full-scale testing.

3.2. Objectives

The following objectives are targeted in the study:

1. Investigate the possible limitations of current objective-based design practices when implemented in mass timber structures.
2. Distil the vital parameters of CLT connections allowing for load redistribution in alternative load path design. Design a component test method for the said parameters and implement it on a variety of connection types.
3. Design and perform full-span CLT floor pushdown tests in combined axial tension and bending with a range of connection types and under a variety of boundary conditions for empirical investigation of the catenary action formation in different subassemblies.
4. Validate the component test results through direct comparison of the test results with the full span tests as well as through implementing a numerical model.

3.3. Research outline

Overall, the study challenges the many assumptions made in the process of creation of the current material and event independent robustness design guidelines. The main research question aims to develop a kind of testing regime that will allow for testing combined loading on mass timber connections to estimate their potential for load redistribution. Reduction in test specimen was prioritised as it allows for reduction of testing cost and time and therefore high repeatability allowing for increased test volume and parametric study approach to experimental work.

- Limitations of the past experimental work with relation to their usefulness in design were investigated and combined loading theoretical framework was created for the alternative load path of catenary action formation (Chapter 4)
- Boundary conditions and loads applied were numerically related to the connection stiffness and resultant internal forces (Chapter 4)
- Combined loading test set-ups that allow for axial load application were developed allowing to mimic different boundary conditions without full-span subassembly test (Chapter 5)
- Component test method was developed to test the changes in moment capacity and rotational and horizontal stiffness of connection under different axial tension utilisation (Chapter 5)
- Four CLT connections – half-lap in 3-ply CLT, half-lap in 5-ply CLT, single surface spline in 5-ply CLT and butt-joint in 5-ply CLT were tested using the above method, resulting in moment-rotation curves under a range of tension utilisations (Chapter 5)

- A full span combined loading CLT floor test was designed and a butt-joint, double incline butt joint, single surface spline and a novel tube connection were tested under various boundary conditions and tension utilisation levels (Chapter 6)
- The full-span and component test results of the butt-joint and spline connection were compared using the axial load – moment capacity failure envelope (Chapter 7)
- A numerical model of the full-span test subassemblies was built based on the component-test inputs and compared to the empirical full-span test results (Chapter 7)

Chapter 4: Theoretical Framework for Load Redistribution Mechanism

4.1. Alternative load path formation after element loss

After presumed element loss, there is a variety of ways in which a structure can redistribute loads. Figure 4.1 depicts such scenario in an example three-storey building, which could be representative of a CLT platform construction or other mass timber post and beam assemblies. Element loss represents an internal column failure, albeit this can potentially occur at various locations. Therefore, a comprehensive analysis necessitates the identification and examination of multiple worst-case scenarios independently.

In the following presented case, the primary mechanisms after the loss of a load-bearing member is catenary action, which allows for redistribution of load in the

structure after an element loss as visualised in Figure 4.1. Under catenary action, the floors which typically act in bending and shear only are subjected to combined bending, shear and tension and therefore understanding the effect of that combination of load on mass timber connections is instrumental for effective modelling and performance-based design.

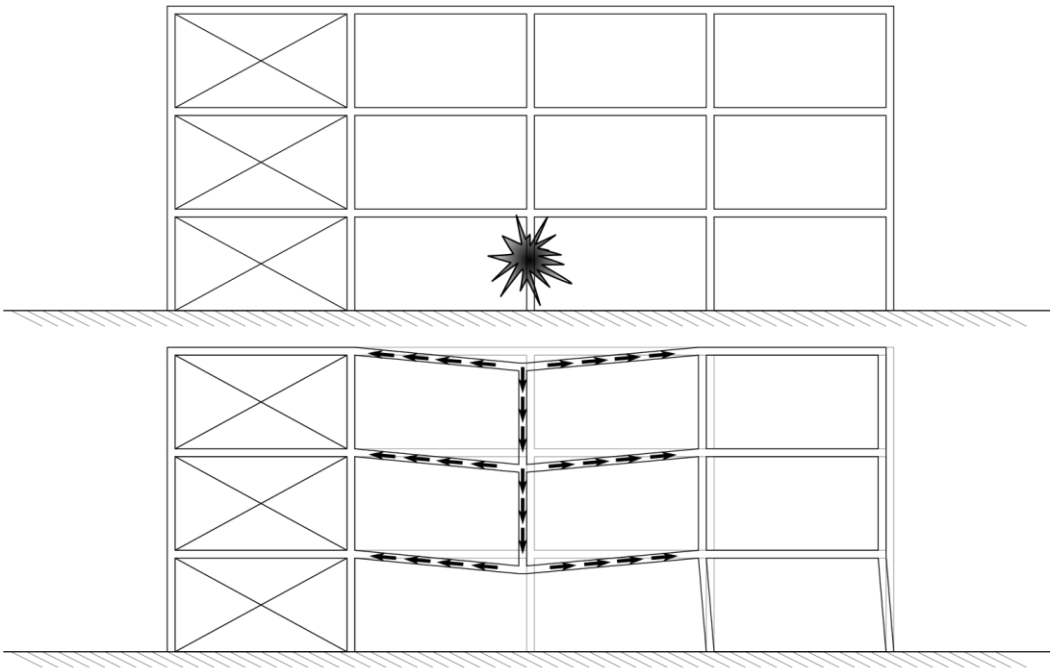

Figure 4.1 Catenary action activation after element loss at ground floor

It should be noted that apart from catenary action, there are several valid alternative load redistribution mechanisms in large timber buildings. These include, but are not limited to, deep beam action of the walls, cantilever action of continuous spans and redistributing the loads to a secondary large truss system as seen in Treet Tower and Mjøstårnet are all valid alternative ways of achieving ALPs in large timber buildings.

However, for the purposes of this thesis, the investigation primarily focuses on the catenary action and the accompanying mechanisms in the subassemblies, as not only it is one of the only concrete strategies presented in the Eurocode through introduction of tie force calculations. Furthermore, it is an area that has received limited empirical research and one with potentially most complicated parameter interactions due to the anticipated extreme deformations necessary for its achievement. In contrast, the alternative load redistribution strategies mentioned above will largely rely on the new load bearing elements remaining static and redistributing the load throughout mostly within their elastic limits. In the case of catenary action, it is a mechanism that we rely on working and achieving system equilibrium through the connections accommodating significant plastic deformations. This presents a significant challenge, considering the inherently brittle nature of timber connections. Consequently, addressing this issue is of paramount importance within the realm of robustness design for mass timber structures.

After the element removal the structure initially will go through the compressive arching stage, however this is only relevant in relatively high depth to span ratios. Since compressive arching works through achieving an arch like effect between the compressive faces of the lateral restraints and the upper part of the connection (as pictured in Figure 4. 2), the floor assemblies with the high depth to span ratio will allow for a greater angle of the compressive arching load path and therefore can provide a significant vertical load resistance. However, when trying to achieve larger building spans that will allow for greater flexibility of use, this ratio will be lower.

Compressive arching also relies heavily on the ability to provide a near rigid lateral restraint at the supports, which cannot always be guaranteed. Furthermore, large

accidental loads acting on the structure can potentially influence the lateral rigidity of the supports. Lastly, compressive arching load redistributions works in a way that the increase in the midspan deformation will have a negative effect on the ability of this mechanism to withstand the vertical loading, as the vertical component of the compressive load path will continue to decrease.

To sum up the above-mentioned points, it is important to note that while compressive arching may have a potential role in preventing disproportionate collapse, its effectiveness is significantly limited. Therefore, it is generally not considered adequate when employed as the sole measure in this regard, especially when considering assemblies of a lower depth to span ratio.

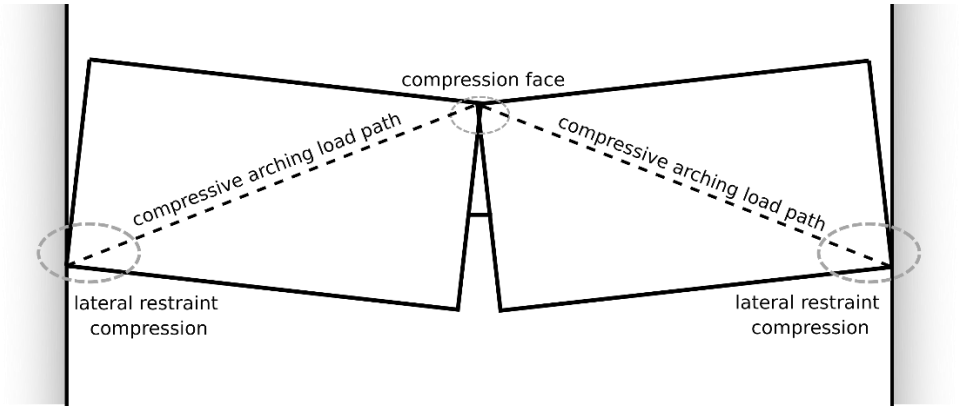

Figure 4. 2 Compressive arching diagram

4.1.1. Central connection and boundary conditions under catenary action

The following analysis will focus on this primary assumed scenario of internal column or wall removal, focusing on a quasi-static approach of assumed equilibrium reached after force redistribution. It is important to note, that the dynamic effects are likely play

a significant role in this scenario, initially increasing the load demand and potentially influencing the load resistance depending on imposed strain rates. However, the expansion of the current understanding of those subsystems needs to begin with a thorough investigation of the static cases.

When considering catenary action in isolation from other load resisting mechanisms and simplifying it to 2D elements, the loads in the system develop as shown in Figure 4. 3. Assuming the loss of the central wall or a column, the point load equivalent of what that element would have carried is considered to act as a pushdown force at the centre. If that force imposes moment on the central connection that is greater than the bending capacity of the central connection, the floor begins to deflect downwards. With the assumption that the floor elements have a much greater effective stiffness than the central element, these will be considered to follow a rigid body movement motion.

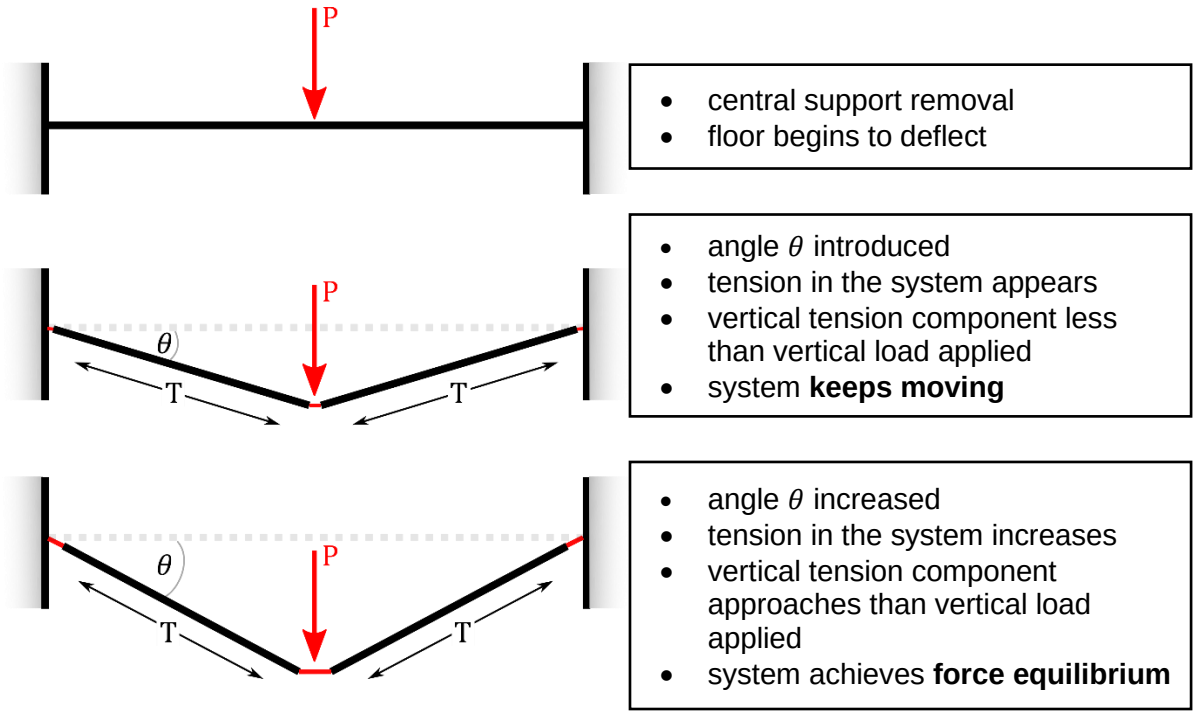

Figure 4. 3 The progression of catenary action in a single floor-to-floor assembly

Once the floor starts to deflect, axial deformation needs to occur at supports, central connection, or both. The stiffness of the supports will dictate the magnitude of the tension developed at each of position. While the angle θ remains relatively low, so will the vertical tension component of the tension which will be what is expected to accommodate the vertical load applied. The floor will keep moving downwards increasing the floor angle of rotation, and while doing so two factors will help achieving the equilibrium and consequent final position of the system:

- more axial displacement will be required, causing higher tension in the system (assuming the ultimate tensile capacity is not reached)
- deeper angle will increase the vertical component of the tension allowing for a greater vertical load resistance

This simplified model was presented for the purpose of distilling the most rudimentary steps and elements playing role in formation of the catenary action. In reality, this

mechanism works in tandem with the compressive arching, as well as the rotational stiffnesses of both the connection and the support conditions of within the floor assembly. For the purpose of the remainder of the chapter, a spring model is used as shown in Figure 4. 4. Herein the catenary action in a singular subassembly of two adjacent floor panels with a central connection is considered, while representing the rest of the structure through a series or rotational and axial non-dimensional springs (Figure 4. 4b). Here there are two structural components that will affect the behaviour during midspan downwards deformation due to the additional loading previously carried by the lost member at the ground floor.

The first component, and the main focus of the thesis, is the properties of the central connection. In case, where we presume that three identical connections are present at each end of the panel, the central one will be subjected to an angle twice as large as the one of the edge connections and therefore its limits will likely dictate the failure of this subassembly. The second factor is the boundary conditions on either side of the panel, namely rotational and axial stiffness of the supports. Quantifying the behaviour of this structure component however requires assuming a variety of parameters and boundary conditions. Figure 4. 4a) for instance shows how introduction of bracing causes increased lateral stiffness of a part of the structure. This would result in an increase in the rigidity of the equivalent axial spring in the spring model.

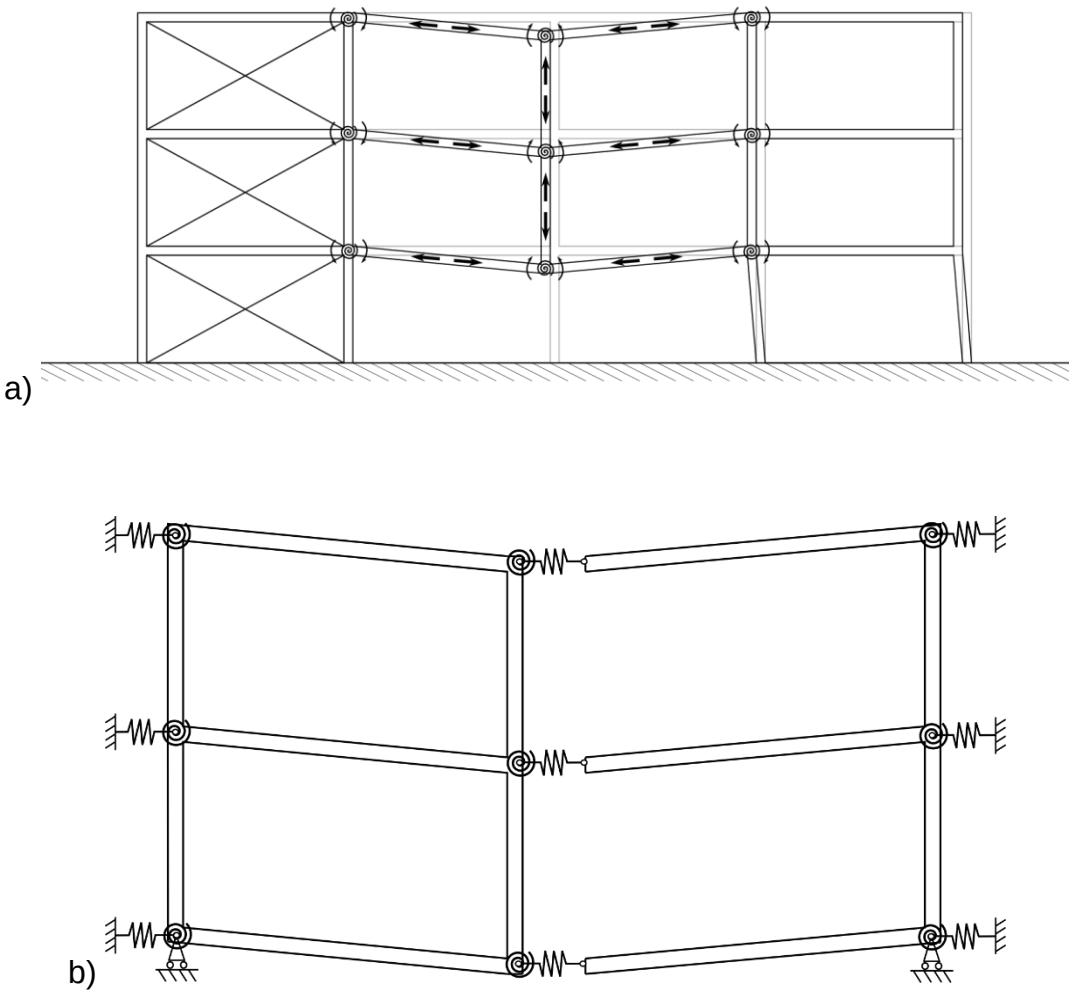

Figure 4. 4 Catenary action load resistance mechanisms (a) and isolated subassembly spring model (b).

Under this scenario when analysing the second-order state there will be two types of forces that counteract the gravity loads – the first being tensile catenary forces, for creation of which sufficient horizontal ties need to be implemented between the floor/beam elements. The axial stiffness will dictate the development of the tension withing the system. The second will be the moments present in the connections and continuous span floor elements.

4.2. Experimental recreation of catenary action

With all of the aforementioned arguments of the significance of the catenary action and the accompanying mechanisms as a means of load redistribution as well as the complicated nature of the parameter interactions within the catenary action formation, it is clear that the necessary next step to further the understanding of disproportionate collapse prevention through this strategy is a more in-depth experimental investigation into the topic. To investigate the loads forming within the context of catenary action through experimental means, a number of decisions must be made

- **Level of abstraction** - the experiment should strike a balance between recreating a real-life scenario and simultaneously acquiring information useful for broader applications
- **Design for result usability** - recreating an exact scenario might give information on that subassembly alone, but a good experimental series should aim to push beyond that
- **Method of load application** - the appropriate investigation of characteristics of the support condition and subsequent imposed horizontal and vertical loads should inform decision making during the experiment design stage of the study
- **Size of the experiment** – recreating multiple storeys or even spans might not be necessary, if the key parameters are able to be measured; typically limited by the equipment availability, practicality, and repeatability of the experimental setup as well as time and cost, therefore smart experiment design is vital

The experiments shall be designed in a manner that will allow to distil the crucial parameters which need to be identified. The challenge here arises due to those

parameters not existing on their own, but in many cases influencing one another in more way than one.

4.2.1. Identification of relevant mechanical properties

Based on the spring model of a two-span subassembly of the building as shown in Figure 4. 4 Catenary action load resistance mechanisms (a) and isolated subassembly spring model (b)., the following parameters can be identified of a singular floor-to-floor subassembly as shown in Figure 4. 5.

- **Rotational stiffness of the connection** - $k_{c,R}$
- **Axial stiffness of the connection** - $k_{c,A}$
- **Maximum rotation of the connection** - $\theta_{c,Max}$
- **Maximum axial displacement of the connection** - Δ_h
- **Rotational stiffness of the support** - $k_{s,R}$
- **Axial stiffness of the support** - $k_{s,A}$
- **Panel effective bending stiffness** - EI_{eff}

The three examples shown in Figure 4. 5 represent the possible support conditions which can represent various connections to and stiffness of the remainder of the substructures. Model (a) allows for representation of any type of conditions, especially faithful to the true conditions if non-linear spring stiffnesses are introduced. This general case can be simplified when certain conditions are met. For instance, when the support rotational stiffness is much lesser than the central rotational stiffness of the connection $k_{s,R} << k_{c,R}$ the rotation point may be assumed as a pin

connection (Figure 4. 5b). The reverse can also be true. In cases where the support rotational stiffness is much larger than the central is much lesser than the rotational stiffness of the connection $\boldsymbol{k_{s,R} >> k_{c,R}}$ and the same is true for the axial stiffnesses $\boldsymbol{k_{s,A} >> k_{c,A}}$ then this subassembly may be abstracted as one with fixed support conditions (Figure 4. 5c). This by no means are the only possible cases, however they are vital to illustrate the importance of proportionality of the various stiffnesses that can play a role.

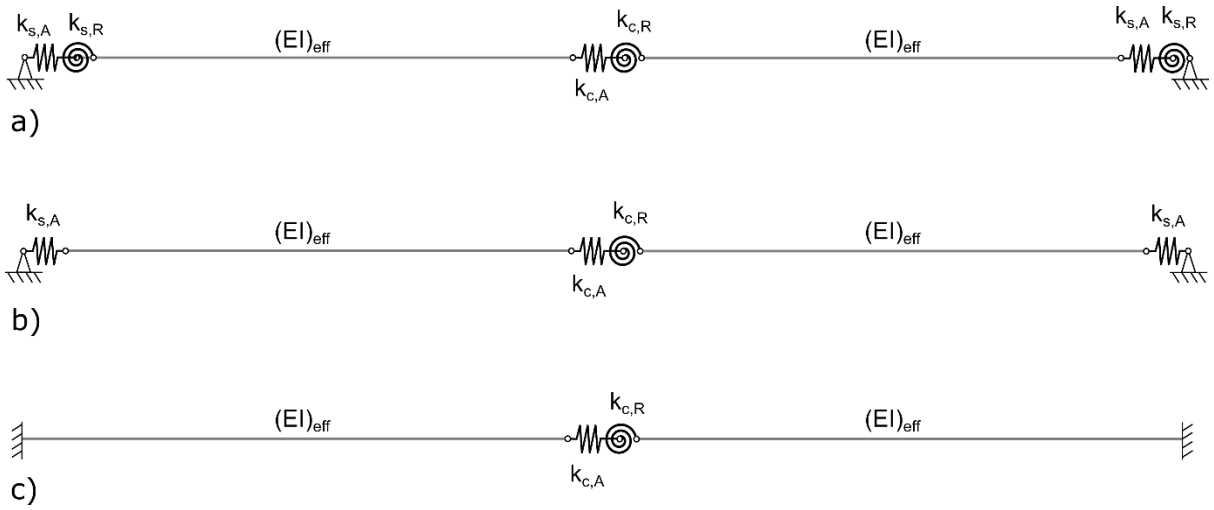

Figure 4. 5 Two-span floor-to-floor subassebly structural diagram with examples of various support conditions

Similarly, the effective bending stiffness $\boldsymbol{EI_{eff}}$ of the floor panels should be considered in some cases, namely when either or both of the rotational stiffnesses $\boldsymbol{k_{s,R}}$ and $\boldsymbol{k_{c,R}}$ are high enough to impose sufficient moment on the panel end for their elastic deformation to occur. This will most notably be of interest in the case (c) which in reality will most often represent continuous span over the support. The effective bending stiffness $\boldsymbol{EI_{eff}}$ of the CLT panels can be calculated through the use of modified $\boldsymbol{\gamma}$ −method was first introduced out of attempts to design composite timber beams (Möhler, 1956). Mohler derived equations for mechanically jointed beams

composed of two or three elements, starting from the basic principles. This method is widely used in EC5 appendix B (European Committee for Standardisation, 2004a) as the go-to technique for designing mechanically jointed beams. The modified γ −method assumes the longitudinal layers to the beam elements with the cross-layers acting as semi-rigid connectors (Swedish Wood, 2019).

In remainder of the cases, when considering CLT construction, the moment transfer capability of the connections has been shown to be limited and rigid body movement of the panels was detected. In those cases, the capacities of the joints will be dictating the behaviour of the entirety of the subassembly.

4.2.2. Mechanical parameter interactions

Calculating and or estimating the parameters identified above is necessary in order to perform any second-order analysis necessary for Alternative Load Path Analysis (ALPA). In the first-order analysis this could in theory be achieved numerically through calculating the rotational stiffnesses based on the properties of the material and connectors used, either from provided by the manufacturers or through performing material testing. However, as the connection component moves through its elastic region, which is what it is designed for and into extreme deformations it is unclear whether these numerical predictions are reliable, as there is empirical basis for calculating these parameters at large deformations and post-peak strength behaviour does not currently exist.

Numerically, the change in rotational stiffness is rooted in the nonlinear nature of the stiffness at large deformations, but equally through the change in respective contact

points present with those deformations. An example is illustrated in Figure 4. 6 of the interactions for any screwed CLT floor-to-floor connection, such as a butt-joint or half lap connection, assumed for the central connection.

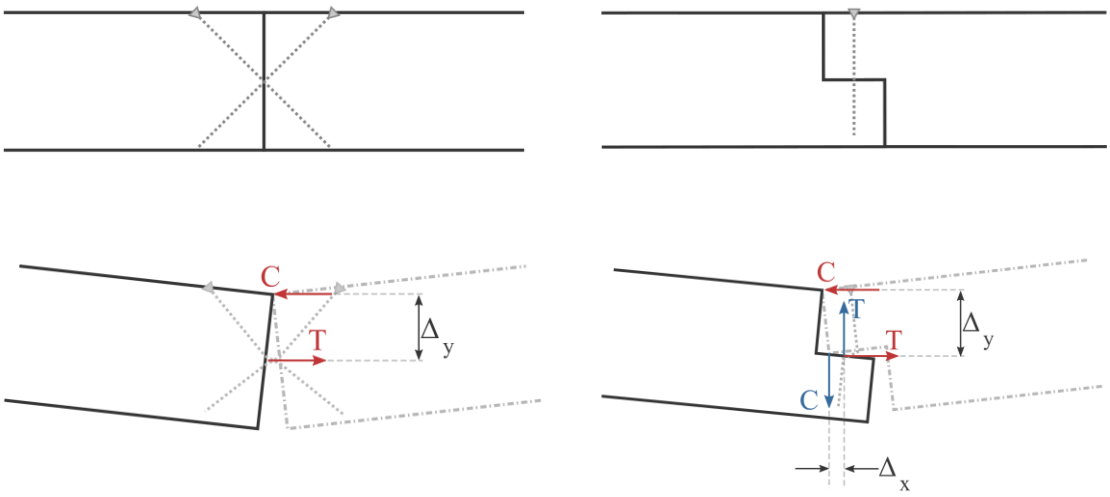

Figure 4. 6 Deformation of the screws illustrating the changes in moment lever arms of butt joints (left) and half lap (right) connections

As vertical deformation at midspan increases and the metal screws experience plastic deformation combined with partial withdrawal and embedment crushing, allowing for significant rotation and change in the geometry without immediate failure. The change in the angles of resultant forces causes the decrease in the lever arms to the moment couples forming within the connection. This will have an effect on the rotational stiffness which will be variable as the connection moves through the deformation stages. As previously mentioned, the embedment crushing can affect the withdrawal stiffness of the screws and combined with changes in the screw geometry which will change the load on the screw e.g., from acting in pure shear to acting in shear, bending and withdrawal. Both of those can affect the horizontal

stiffness of the connection, both positively and negatively depending on the type and initial geometry of the connection used.

Notably, similar interactions will be simultaneously happening at the support connections if considering single spanning floor systems. Although the central connection will see approximately double the deformation as the peripheral counterparts, there are some timber connections not symmetrical round the central horizontal axis and therefore will act differently when hogging and sagging. A good example of such connection is a single surface spline connection (as depicted in Figure 4. 12b)

The significance of the respective change in parameters with one another really becomes apparent when related back to the catenary action formation parameter relationships first explained in section 4.1.1. Altogether those interactions can be summarised as presented in Figure 4 .7. There the vertical load level dictates angle of rotation and tension demand all the while the angle of rotation affects the tension demand due to the increased proportion of vertical component of the tension – higher the angle, lower the absolute tension demand. In turn, the angle of rotation affects the rotational stiffness, if considered rotations past its elastic limit – and this is necessary when considering such large deformations. How this affects different types of connection is discussed in more detail in Section 4.3.1. Moreover, the axial stiffness of the connection as well as the support stiffness will affect the tension development, the stiffer they are, the higher the tension will develop. We need tension development in order to achieve catenary, however if the stiffness is too high, the tension will reach the maximum connection tension capacity and fail before managing to reach the needed equilibrium. Furthermore, the angle of rotation in tandem with axial stiffness affects the maximum tension developing in the system, as it will

geometrically translate into the total horizontal elongation needed to achieve the needed deformation.

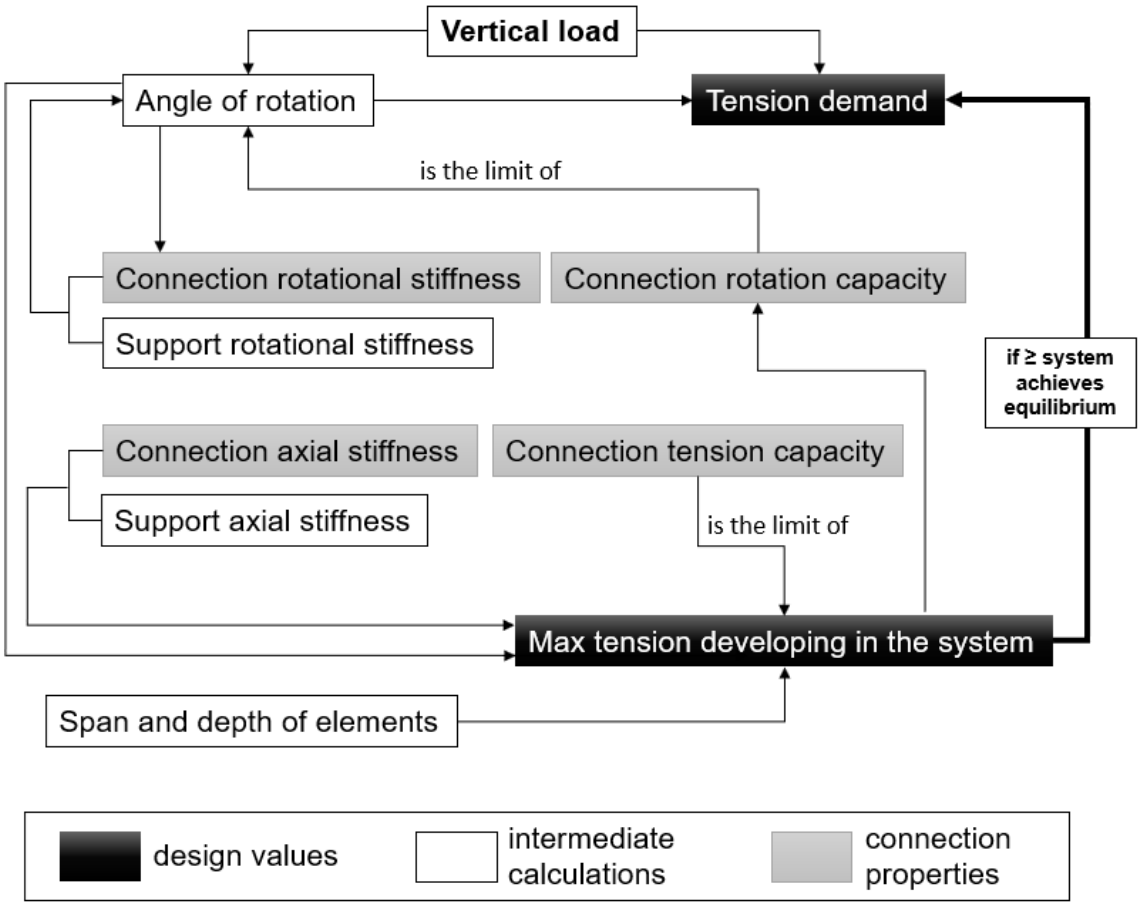

Figure 4. 7 Interaction between the properties under catenary action

Finally, the connection tension capacity, which directly limits the tension level that the system is capable of developing; and additional interaction there exists, with the rotational stiffness. Note that the diagram here does not focus on interaction between the connection properties for clarity of presentation. Given the outlined complexities of the numerical predictions, stiffness of timber connections under extreme deformations should be backed up by empirical data. With that being said, recreating the combined tension and bending conditions in a laboratory setting can be

challenging and many decisions need to be made with respect to the experimental setup based on its influence on the accuracy of representation of a real-life scenario as well as the feasibility and repeatability. The following sections explore the most relevant factors and provide the theoretical basis on which those decisions were made in the remainder of the thesis.

4.2.3. Horizontal load application

Considering the instrumental role that the tension level plays in the entirety of the catenary action behaviour, a careful consideration is to be made when deciding on how to induce the axial loads in the system, both in the technical sense as well as deciding on the appropriate and realistic load levels.

4.2.3.1. Passive and active load application methods

The first factor when discussing the experimental setup is the difference between the passive versus active tension development. A standard way of inducing the horizontal load in such arrangements is through some form of lateral restraint at the supports on both sides of the deforming floor elements, which depending on the axial stiffness of said restraints combined with the axial stiffness of the central connection will impact how much tension can evolve in the system. This type of load application is what has been presented through the axial springs in Figure 4 .5 and is here considered a passive load application method. The passive load application use in an experimental setup introduces some challenges that arising from trying to recreate the horizontal support conditions assuming support conditions in the structure. The support stiffness depends on a variety of factors such as the bracing of the adjacent structure or the

level of potential damage to the supports resulting from the accidental action imposed, and not only will be largely variable across different structures but also across different locations within the same structure (e.g. bay near a concrete core versus an edge bay). Therefore, to achieve a set of usable data that could be used in a variety of cases it is potentially counterproductive to assume one arbitrary support condition. as it introduces more noise for interpretation of the connection properties alone.

The second way of imposing tension is the active load application method, namely introducing a secondary horizontal actuator. This method allows for full control of the tension application, choosing the magnitude throughout the test as a result opens a whole new area of exploration in terms of the combined loading combination investigations. However, it does still mean that the magnitude and application slope of tension need to be assumed for the tests, and so a test matrix design can become more complicated. Significance of the road to achieving the maximum tension (load hold/ramp/nonlinear) is potentially one of the important research questions to be answered, as knowing that can be helpful in simplifying the future testing requirements.

4.2.3.2. Tension utilisation

Variety of connection types use different load resistance mechanisms, and their ultimate strength value can be adjusted through size and number of the connectors used. Therefore, comparing their performance to one another through absolute load resistance values may not always be productive. This holds especially true for the performance in load redistribution after member loss.

Moreover, the following experimental series aims to be able to be replicated easily by other researchers and the results presented in a manner that those test results could be compared to the previous ones with ease. To accommodate that the tension utilisation concept is therefore introduced here to aid in understanding of the influence of tension across the full range of load and deformation in each of the connections. The ability to distinguish the changes in mechanical properties in various connections and compare them to one another as a function of this vital parameter is absolutely necessary for development of a foolproof horizontal tie design.

The r_T in Equation (4.1) is the tension utilisation ratio value of the connection, T represents the tension applied to the connection and T_{max} is the ultimate tension strength that the connection can take when loaded axially and not under combined loading scenario.

$$r_T = \frac{T}{T_{max}} \tag{4.1}$$

It is crucial to highlight that this value is referring to the tension that the connection sees from end of the component to the end of the component and does not represent the utilisation of the fastener alone. It is possible then to predict fastener tension in some of the connections, where a large lever arm introduces big moment stiffness (such as internal tension calculations for butt joint and half lap shown in Section 4.3.2). In those cases, it is expected that under combined loading the fasteners will reach the 100% utilisation r_T well before the connection. There are other joints however where this relationship is not as straightforward and therefore having an objective measure such as tension utilisation r_T is extremely useful to allow for adequate comparison across the board.

4.2.4. Vertical load application

When designing an experimental setup to test bending capacity, a common approach is to use 4 point bending experimental approach. This allows for elimination of shear force in the central stretch between the two points of load application. However, in the case where the effective bending stiffness of the panel is much higher than the one of the connections, the shear failure is an unlikely mechanism, as pivot at the connections will occur way before achieving the panel shear capacity. Moreover, quite often in a building system the point load will be present due to the presence of the wall/column as the primary load path.

Simultaneously, four-point bending allows for distillation of the behaviour of the connection without additional interaction with the wall/column element above and consequently reduce potential sources of error resulting in clearer data. In the experimental series described in more detail in Chapters 5 and 6, both four- and three-point bending was performed on various floor to floor assemblies, and therefore the force equations must be derived for both. Figure 4. 8 Free body diagram of the three-point bending showcases the free body diagram of the floor-to-floor assembly under three-point bending combined with the axial tension applied to 2D beam elements. In many instances, these experiments are typically analysed under the assumption of marginal deflections. However, when intentionally introducing extreme deformations, it becomes necessary to consider second-order effects. The following derivation allows for the calculation of the moment in the connection given the central pushdown load $\boldsymbol{P}$, uniformly distributed load $\boldsymbol{w}$, tensile horizontal load at the end $\boldsymbol{T}$ as well as the span $\boldsymbol{L}$ of the assembly and its vertical midspan deformation $\boldsymbol{u}$. The vertical reaction force at the supports is depicted here as $\boldsymbol{R}$.

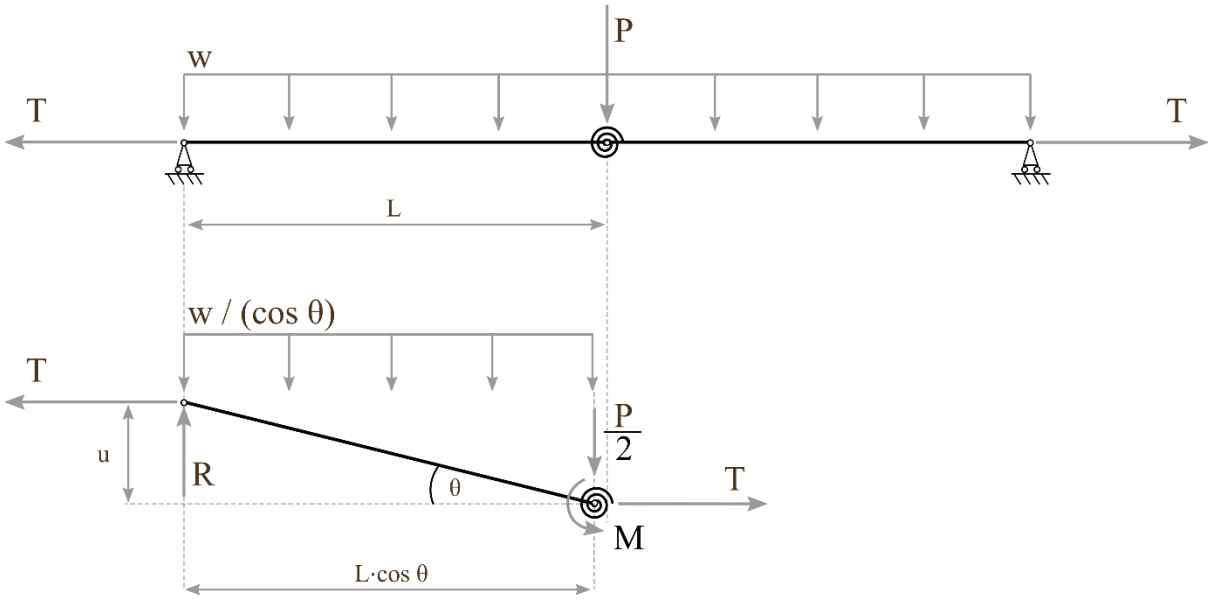

Figure 4. 8 Free body diagram of the three-point bending and its second order state

The vertical and moment equilibrium equations for the free body diagram are derived:

$$\sum V = 0$$

$$R - \frac{P}{2} - w \cdot L = 0 \qquad (4.2)$$

$$\sum M_{support} = 0$$

$$Tu + M - \frac{wL^2 \cos\theta}{2} - \frac{PL\cos\theta}{2} = 0 \qquad (4.3)$$

The angle of rotation $\boldsymbol{\theta}$ can be calculated from the vertical displacement at midspan $\boldsymbol{u}$ and the span of the assembly $\boldsymbol{L}$:

$$\theta = sin^{-1}\frac{L}{u} \qquad (4.4)$$

After calculating rotation and rearranging equation (4.3) we receive the moment resistance of the connection:

$$M = \frac{(P+wL)\,L\cos\theta}{2} - Tu \qquad (4.5)$$

Solving for load given known moment $\boldsymbol{M}$ and rotation $\boldsymbol{\theta}$ will yield:

$$P = \frac{2(Tu+M)}{L\cos\theta} - wL \qquad (4.6)$$

Solving for tension in the connection $\boldsymbol{T}$:

$$T = \frac{L\cos\theta}{2u}(P + wL) - \frac{M}{u} \qquad (4.7)$$

Similarly, the four point bending assebly is presented below in Figure 4. 9. The distance from support to the point of load application is here depicted as $\boldsymbol{a}$.

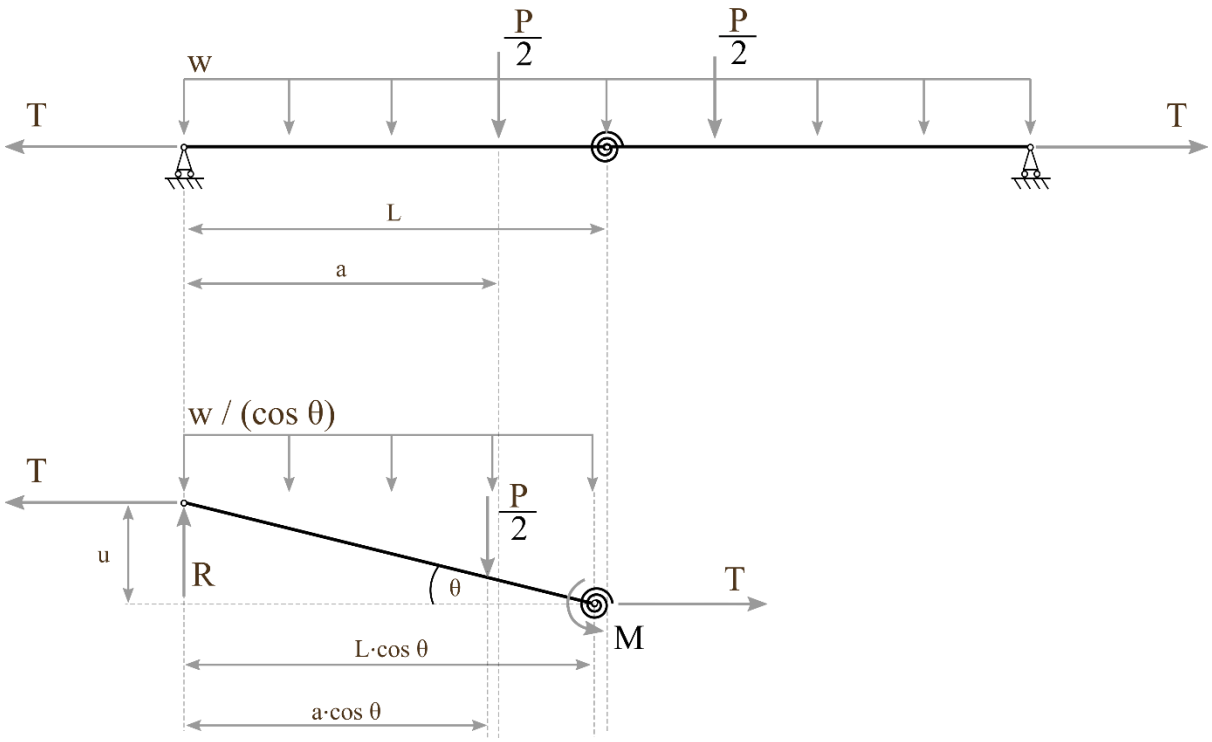

Figure 4. 9 Free body diagram of the four-point bending and its second order state

The vertical and moment equilibrium equations for the free body diagram:

$$\sum V = 0$$

$$R - \frac{P}{2} - w \cdot L = 0 \qquad (4.8)$$

$$\sum M_{support} = 0$$

$$Tu + M - \frac{wL^2 \cos\theta}{2} - \frac{Pa\cos\theta}{2} = 0 \qquad (4.9)$$

The angle of rotation can be calculated from the vertical displacement at midspan $\boldsymbol{u}$:

$$\theta = sin^{-1}\frac{L}{u} \qquad (4.10)$$

After calculating rotation and rearranging equation (4.3) we receive the moment resistance of the connection:

$$M = \frac{(Pa+wL^2)\cos\theta}{2} - Tu \qquad (4.11)$$

Solving for load given known moment $\boldsymbol{M}$ and rotation $\boldsymbol{\theta}$ will yield:

$$P = \frac{2(Tu+M)}{a\cos\theta} - \frac{wL^2}{a} \qquad (4.12)$$

Solving for tension in the connection $\boldsymbol{T}$:

$$T = \frac{\cos\theta}{2u}(Pa + wL^2) - \frac{M}{u} \qquad (4.13)$$

4.2.5. Support conditions

Designing a test which includes a roller support, where great vertical deformations are expected, can be challenging due to considerations that need to be made in terms of the resulting travel distance of the support. There are several ways of achieving the roller effect, three of which are presented below in Figure 4. 10.

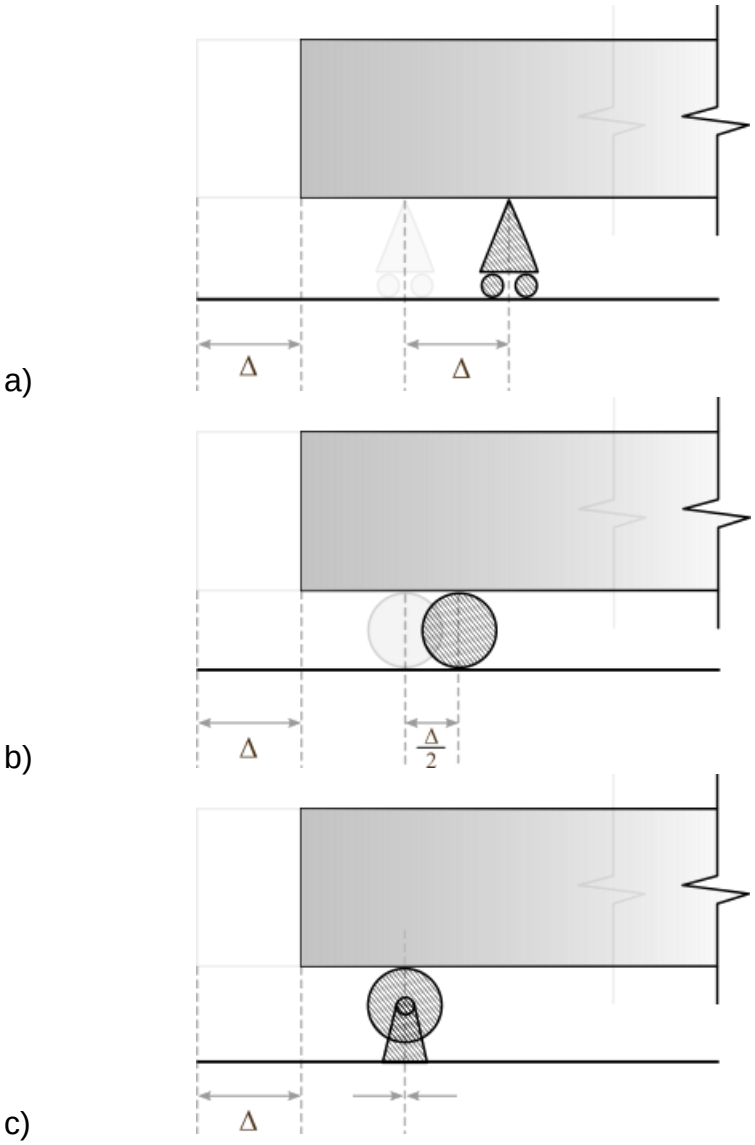

Figure 4. 10 The different ways of achieving a roller support condition a) pin roller b) cylindrical steel section c) stationary bearing

The first way (a) is one that reflects the typical structural diagram presentation of the roller support. The advantage of such support is that it the location of the support with relation to the element remains constant, which means a greater ease of calculation and elimination of calculation errors related to the changes in span. The lack of relative movement also means that overhang, significance of which is explained in Section 4.2.6, is not necessary in this case. It is however not an easy support to practically achieve in the experimental setup.

The second way (b) is the simplest version of the roller, which is a solid rigid circular section, typically steel, on which the element rests. The challenge in this particular experimental series here involved the relative travel between the element and the support. As seen in the Figure 4. 10b) for every unit of travel the element moves horizontally, the position of the roller moves half of that distance in the opposite direction with relation to the element. Meaning that there is a minimum overhang distance required for this support to adequately provide support throughout the entire test duration. Moreover, once the element begins to develop a significant angle, that position being maintained will rely largely on the friction between the element and the roller as well as between the roller and the ground. To accommodate for that potential slip, overhang is thought to need an additional margin to prevent loss of support. It is also a potential safety concern.

The final way of achieving a support mimicking the roller condition is a stationary bearing (c). Such approach allows for a safe and stable solution that, given use of appropriately chosen bearings, can take large loads in as close to a frictionless manner as possible. One of the main disadvantages of this approach is that it is more complicated and therefore harder to achieve in some laboratory conditions, involving

making bespoke steel parts. It also, once again, introduces the need for the overhang.

4.2.6. Overhang calculations

Due to the need for the overhang as discussed through the lens of second order horizontal displacements in Section 4.2.5, there will be an additional rotational moment present in the two-span assembly. This moment will be resisting the pushdown force alongside the catenary action and the moment resistance of the connection and given sufficient lever arm and vertical deformation might be significant. The following derivation is presented as a tool to investigate the overhang significance and correct for it in calculations if needed. A free-body diagram of a single span of the assembly deformed by an angle $\boldsymbol{\theta}$ is presented at Figure 4. 11.

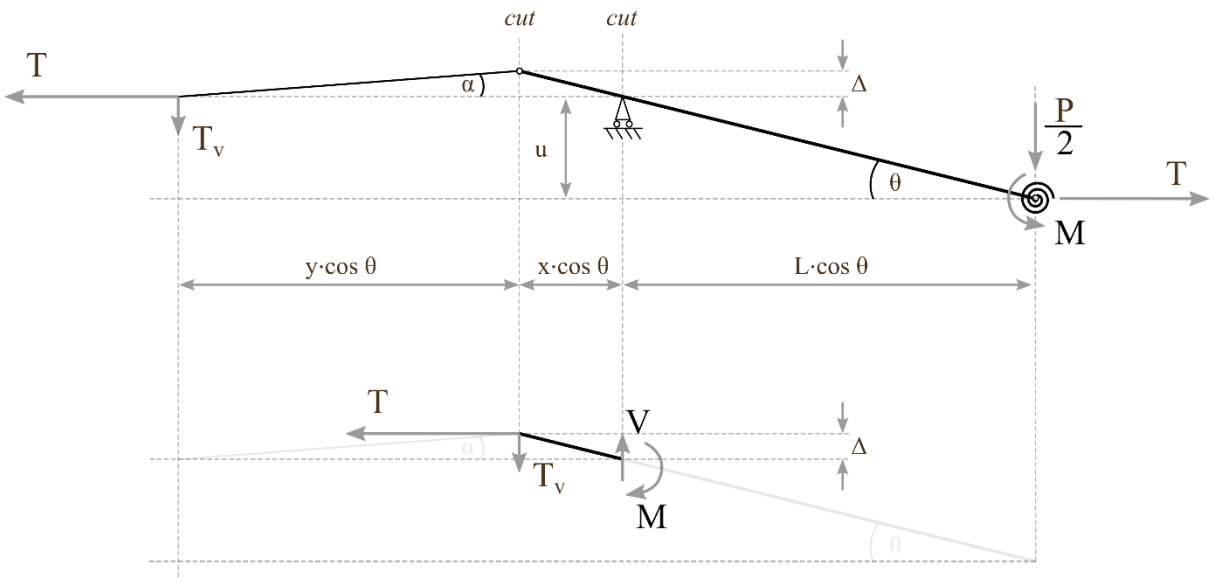

Figure 4. 11 Forces acting on the overhang section

If vertical uplift of the overhang of the length $\boldsymbol{x}$ is considered as $\boldsymbol{\Delta}$, the initial distance between the sample and of the point of tension application is $\mathbf{y}$ and the point of tension application remains stationary, an angle $\boldsymbol{\alpha}$ will develop along the path of load

application (this specific arrangement is used in the experimental series described in more detail in Chapters 5 and 6).

Vertical uplift **Δ** can be calculated regarding the proportions of other known values:

$$\Delta = \frac{ux}{L} \tag{4.14}$$

And knowing this value will allow for calculation of the angle of tension application $\boldsymbol{\alpha}$*:*

$$\alpha = \ sin^{-1}\left(\frac{\Delta}{y}\right) \ = \ sin^{-1}\left(\frac{ux}{yL}\right) \tag{4.15}$$

The moment of the uplift $\mathbf{M_u}$ at the support will be therefore calculated through introduction of a section cut at the support as presented in Figure 4. 11 resulting in Equation (4.17). There will be two forces with lever arms contributing to the moment, the vertical ($\mathbf{T_V}$) and horizontal ($\mathbf{T}$) components of the tensile load. The value of the vertical component $\mathbf{T_V}$ is a function of the $\mathbf{T}$ and the previously calculated angle of tension application $\boldsymbol{\alpha}$ (equation 4.16).

$$M_u = T \cdot \Delta + T_V \cdot x \cos\theta \tag{4.16}$$

$$T_V = T \tan\alpha \tag{4.17}$$

Substituting Eq. (4.16) into (4.15) will yield the equation for the total moment enacted at the support.

$$M_u = T \cdot \Delta + T \cdot x \tan\alpha \cos\theta$$

And further incorporating Eq. (4.13) we arrive at the moment due to overhang $\boldsymbol{M_u}$ as a function of the tension $\boldsymbol{T}$**,** overhang length $\boldsymbol{L}$, midspan deflection $\boldsymbol{u}$.

$$M_u = T \cdot x \left(\frac{u}{L} + tan\,\alpha\, cos\,\theta \right) \quad (4.18)$$

Therefore, in order to minimise the uplift effect from the tension load application the length of the overhang $\boldsymbol{x}$ as well as the angle $\boldsymbol{\alpha}$ are ought to be minimised and for each experimental setup this predicted uplift force is to be calculated.

Finally, incorporating the above derivation into the total moment in the connection as derived in Section 4.2.4 for three-point bending results in:

$$M = \frac{(P+wL)\, L\, cos\theta}{2} - Tu - M_u \quad (4.19)$$

And for four-point bending results in:

$$M = \frac{\left(Pa+wL^2\right)\, cos\,\theta}{2} - Tu - M_u \quad (4.20)$$

4.3. Analysis of connection internal forces

The above calculations can be representative of any material, timber or otherwise, and within the mass timber category these can be applied to both CLT floors as well as LVL and Glulam beams. However, once the decision is made on which materials and consequently connections will be tested, further analysis can and should be undertaken to investigate the actual internal forces and possible fastener capacities. This thesis will focus on CLT floor-to-floor connections, and the following divulges the some of the details of the relationships between the external forces and the rotational behaviour of the components investigated.

4.3.1. Internal forces under bending

As already discussed, all of the moment capacity in a CLT connection can be reduced to one or more significant resultant forces forming a moment couple. When referring to the moment couples in the vertical direction the lever arm between the forces will be referred to as Δ_y horizontal direction lever arm as Δ_x. The compressive forces will always occur at the contact points between the timber elements and the tensile forces can either form from bending the spline (Figure 4 .7.b) or the withdrawal and shear resistance of the metal connectors like seen in butt joint (Figure 4 .7.a), half-lap (Figure 4 .7.c) and tube connector (Figure 4 .7.d).

The total moment in the connection $\boldsymbol{M}$ can be assumed to be a sum of all of the discrete moments due to present resultant forces and their lever arms. Assuming compression $\boldsymbol{C}$ and tension $\boldsymbol{T}$ will always be equal this will result in:

$$M = \sum (T_i \cdot \Delta_i) \qquad (4.21)$$

The connection using both butt joint for regular moment and shear restoration of the panel-to-panel connection as well as the tube connector specifically for the second-order catenary action performance maximisation (Figure 4. 12d) will exhibit two separate couples in tube connector, these however can be simplified to one resultant as presented in the diagram. This is possible due to compression point remaining the same at the top face regardless of the location of the tension resultant, and the tension resultant locations being equal to one another

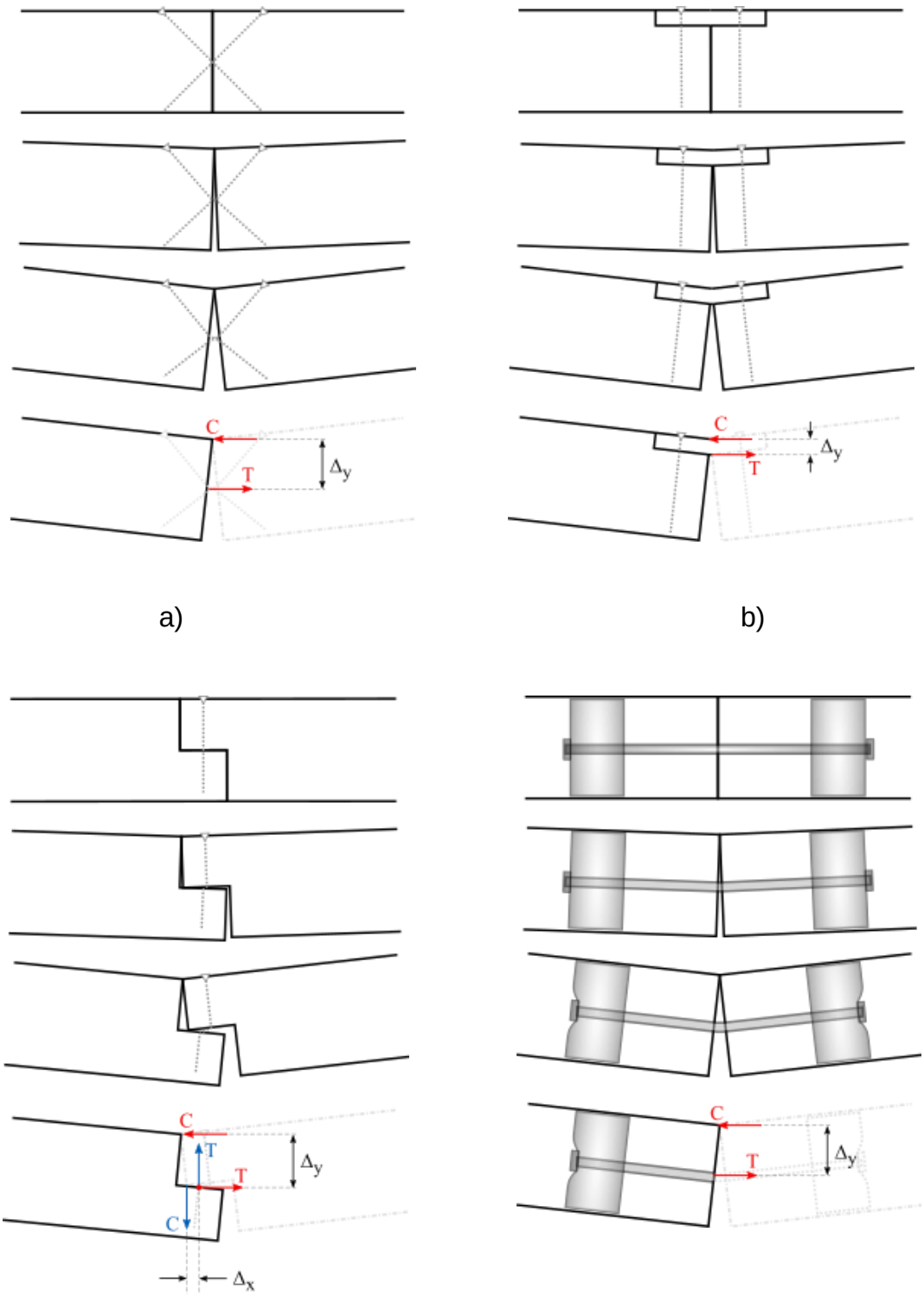

Figure 4. 12 The moment couples forming in the timber connections a) butt joint, b) single surface spline joint, c) half-lap joint b) tube connector.

Once and internal moment in the connection $\mathbf{M}$ is also calculated through the incorporation of the catenary influence on the system as shown in Equations (4 .5) and (4.11), and in some cases the influence of the overhang in the subassembly when necessary (Equations 4.19 and 4.20) the internal forces can be calculated.

In some of the presented cases this will be more easily achieved than the others. As already mentioned, the surface spline connection will pose a more complicated case as the location of the resultants in the rotating spline itself will not be straightforward to numerically deduce and the moment and the failure modes present will be a combination of a variety of factors. When considering the cut at the middle of the spline as shown in the diagram, the horizontal couple is present due to the pure plywood bending at the centre and the internal forces resultants arising from that. The way in which this bending is induced and how it translates from the connection will however be dependent on several factors. The compressive connection point at top left of the spline on the diagram and the point where the spline is screwed in through the fastener will induce some moment on the plywood.

The second mechanism in which the spline is being bent is it through the compressive contact on the bottom face and the tensile resultant in withdrawal at the point of connectors. Neither of these are prefect connections and they will vary greatly depending on embedment crushing, withdrawal, loosing compressive contact points due to external tension etc. Spline therefore proves to be one of the more complicated cases to consider.

Similarly, half lap also presents two separate couples, horizontal and vertical, as presented on the diagram. The horizontal couple is simple to analyse as it can be compared to the butt joint, with compressive point at the top face and tension point

at the connector. However, the vertical couple, although initially significant to the stiffness, has a variable lever arm, which is directly lessened alongside the opening in the connection. This is not true for any other lever arms, which mostly only change due to the angle or rotation. Once the opening at the connection reaches the length of half the half lap with (location of the screw) the influence of this couple becomes negligible. Since it is the behaviour at large deformations that is of interest, it is asserted here that the half lap can be effectively analysed using only horizontal couple making it a very similar case to the butt joint.

4.3.2. Combined bending and tension

When a singular significant couple is present in some cases discussed above, another simple way to analyse the internal forces is to consider the geometry of the connection as 3-D as opposed to the 2-D beam elements so far presented. As an example, the butt joint (Figure 4. 13) as well at the half lap joint (Figure 4. 14) are presented below showcasing the forces analysed under three-point bending of the load P, imposed active tension T_A, angle of rotation θ, component span L, internal compression C_c and tension T_c in the connection, the depth of the connection h, vertical midspan displacement u and opening of the connection at the location of tension resultant Δ_h. The resultant tension force T_c is of interest here as this force imposed on the connectors governs the failure of the entirety of the component. Based on the presented diagrams through simplifying a series of equilibrium equations and solving to the tension T_c it can be calculated as per Equation (4.22).

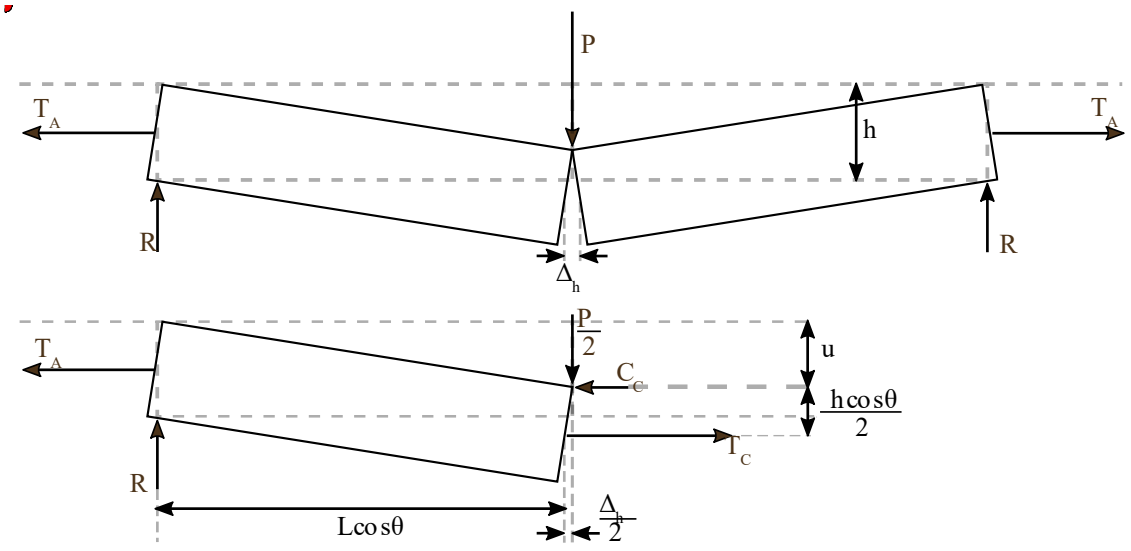

Figure 4. 13 Butt joint combined load internal connection force formation

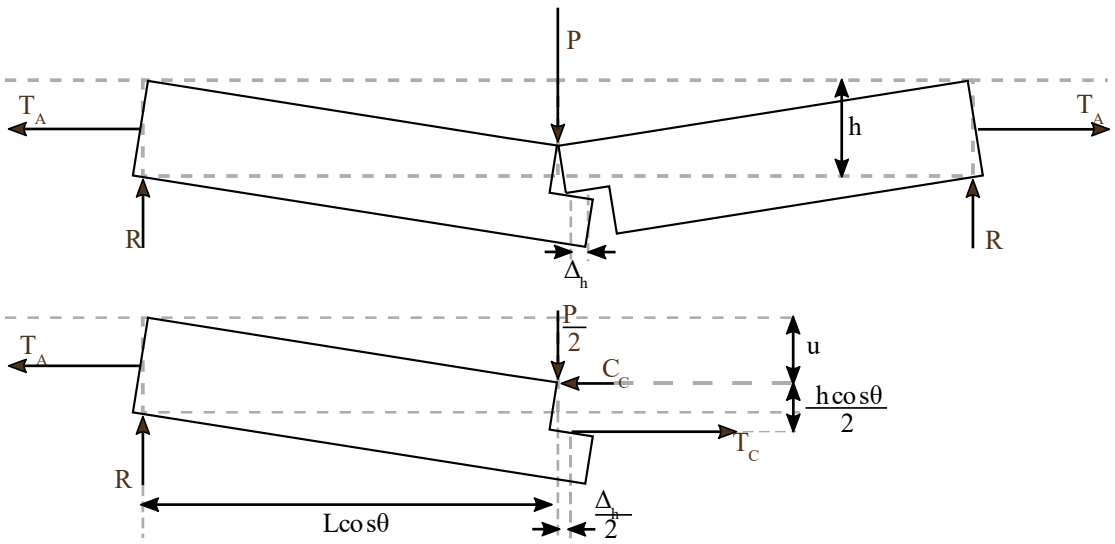

Figure 4. 14 Half lap joint combined load internal connection force formation

$$T_c = P \cdot \frac{L}{h} + T_A \cdot \left(1 - \frac{2u}{h}\right) \qquad (4.22)$$

Calculating resultant connection tension can reveal a lot about the mechanisms of the combined loading in the components and more importantly the predict the failure, and therefore is an imperative parameter to account and calculate for. Calculating

this internal parameter in its deformed state also presents an opportunity to compare its performance to uniaxial tension. One of the secondary research questions is to investigate whether these two behaviours are comparable and if so, would simple axial test be able to predict the final behaviour of larger components and eventually subassemblies without the need for full-scale testing.

4.4. Summary

The chapter investigates in detail the theoretical basis for the experimental portion of the thesis. The relationship between the external forces implemented on a floor-to-floor subassembly and the internal forces in the central connection is necessary to understand before adequate design of the tests. This is approached by first isolating a theoretical subassembly from a structural frame and investigating the mechanical properties and ultimate limit states relevant to the alternative load path formation under large deformations after notional element removal at the ground floor. Consequently, this subassembly is reimagined in the context of an experimental setup and potential factors such as boundary conditions and load application methods are investigated. Furthermore, equations for calculation of the relevant unknowns such as internal forces and relative displacements are derived which are used for data analysis in the following experimental chapters.

Chapter 5: Component tests

5.1. Experimental objectives

The goal of this experimental series is the realisation of Objective 2 as described in Chapter 3: “Distil the vital parameters of CLT connections allowing for load redistribution in alternative load path design. Design a component test method for the said parameters and implement it on a variety of connection types.”.

This chapter will primarily focus on assessing the behaviour of individual connections in detail under the combined loading typically seen in catenary action which will involve assessing the change in various mechanical properties across the spectrum of tension utilisation and observing the effect of those changes on the overall performance of the component. With the tension utilisation used as a primary parameter, the study will allow for the obtained data to be used as modelling input for predicting catenary action behaviour in larger subassemblies as well as full structure models. The use of the obtained data will be explored in more detail in Chapter 8, however it is necessary to take this into consideration at the experiment setup and

test matrix design stage. The crucial mechanical parameters of the floor panel-to-panel connection to be extracted from the experiments are:

- Rotational and axial stiffnesses
- Ultimate strength
- Maximum angle of rotation

A test method adequate for this purpose is one that can be replicated for multiple connection types, therefore aiming for localised testing of the components including the connection in question is thought to be the most cost and time effective solution. The full-scale floor tests presented in Chapter 7 however can be used further to confirm the accuracy of the component test results.

5.2. Materials and methods

5.2.1. Experimental setup

The testing method developed for span reduction in combined axial and bending load on connections has several novel features, which allowed for a greater control and increase in number of tests per testing day, while still mimicking the combined loading conditions under catenary action faithfully.

The reduction in span is possible thanks to implementing the secondary horizontal active method of load application. The previous full-span catenary action experimental set-ups (Cheng et al., 2021; C. H. Lyu et al., 2020; Mpidi Bita et al., 2020) typically have a connection on each side providing various levels of horizontal and rotational restraint. By doing so the tension developed in the connection is a direct result of the stiffness of the connections, geometry of the assembly (element

depth/thickness, span, connection detailing) meaning that those tests only represent one specific combination of loads at the moment of failure. By controlling the force withing the system manually, a whole array of tension conditions can be investigated and therefore provide fuller understanding of connection behaviour. A secondary issue for developing component experiments is compressive arching, as its impact becomes significantly higher along with span reduction. Using the active load application method and a true roller support, while not restraining the movement of the supports outwards, the compressive arching effect will be minimised down to the system friction and assumed to be negligible. Consequently, the investigation can focus on extreme rotations and deformations and their effect on the second-order analysis.

The component tests were performed in two different institutions with different available equipment and resources, which allowed for investigating different set setup parameters, such as load application method, support conditions, component size and data acquisition methods. One of the goals of the study is to provide a jump off point for development of future test standards and therefore investigating different ways of achieving the same goal is beneficial. Table 5.1 summarises the main characteristics of Setup A and Setup B.

Table 5. 1:Summary of characteristics of Setup A and Setup B

Parameter	**Setup A**	**Setup B**
Vertical load application	4-point bending	3-point bending
Horizontal load application	Symmetrical, manual	Single-sided, automated
Component size	1000mm total	1600mm total
Roller type	Bearings	Steel roller
Support rotation	Hinge	Continuous over support with overhang
Data acquisition	Wire pull potentiometers (string pots) + DIC + load cells	Wire pull potentiometers (string pots) + load cells
Connectors	1 per specimen	4-6 per specimen

5.2.1.1. Setup A

The first experimental setup (Figure 5.1) was developed to provide the most optimum support conditions for the idealised version of the combined loading model. This included developing a custom-made steel C-clamp to be attached to each end of the connections with steel screws rigidly connecting them all the way through. The clamp would then be connected through a pin to a steel section elongating the component from the pin out, which was placed between two bearings, one at the bottom and one at the top. This allowed for elimination of the potential rotation and moment resulting from the lever arm introduced with the steel component. That moment elimination was necessary to be able to safely connect these ends to the load cell and eventually hydraulic Enerpac cylinders on both sides.

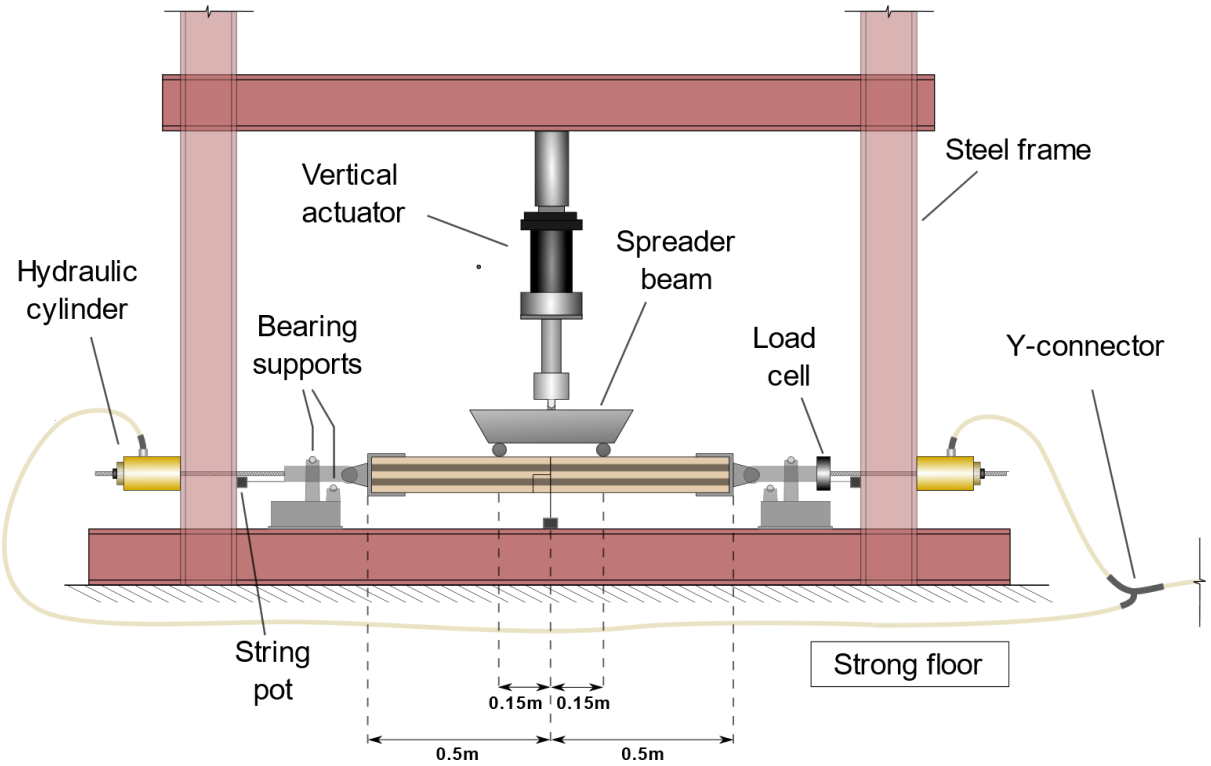

Figure 5. 1 Diagram of the experimental setup A

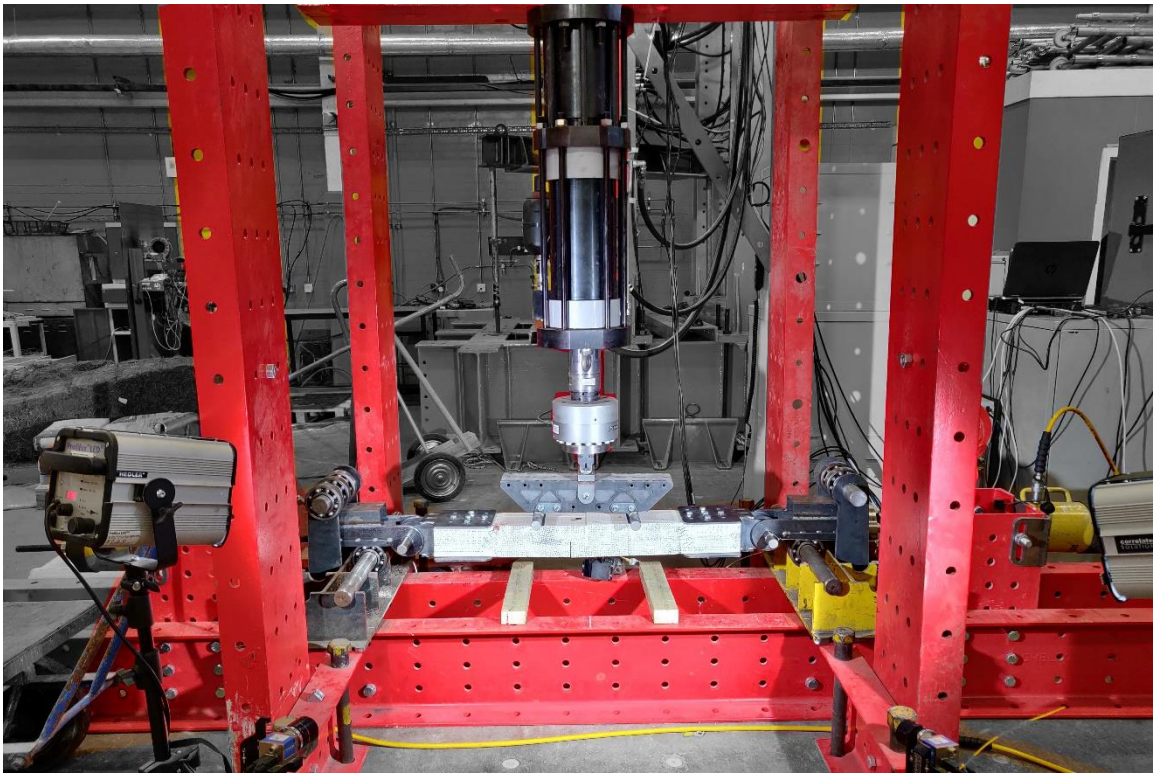

Figure 5. 2 Photograph of the experimental setup A

The cylinders were connected through a Y-connector together and then to a manually controlled Hydraulic UTM Losenhausenwerk 400kN. This allowed for the pressure to be evenly distributed through both cylinders and in principle enable to impose axial tension on the specimen perfectly symmetrically. The vertical load was implemented through a spreader beam, which was attached on a swivel to the Instron 8800 250kN actuator.

Data acquisition for the forces was performed by a recording the integrated load cell output from Instron for vertical force and a load cell installed horizontally. The displacements were recorded in three ways:

1. String pots, one vertical at the midspan and two horizontals at either side of the frame.
2. Actuator displacement output
3. Digital Image Correlation system

The DIC system was assumed to be the primary data set to be used in analysis, with the other two mainly there to allow to cross-check the results and correct alignment of data sets in post processing.

5.2.1.2. Setup B

The experimental setup B was used for both component level testing (shown in Figure 5. 3 and Figure 5. 4.) as well as corresponding full-span test, where the wall supports were moved outwards (see Chapter 6, section 6.2.1). The setup used a number of different solutions to the challenges encountered in experimental setup A. The bespoke steel C-clamp and bearings were here replaced by regular steel rollers

placed on top of thick wall supports and the horizontal movement was provided by the overhang on the other side of the support. This made it possible to drastically reduce the experiment preparation time and use off-the-shelf elements but meant that the influence of the overhang on the overall vertical load capacity had to be accounted for in the calculations at the analysis stage of the investigations. The tension anchors were installed using 180mm long fully threaded self-tapping screws installed at 90° to the end face of the specimen. Adjustable chains where then used to attach one end of the specimen to a 250 kN actuator (Figure 5. 6) and the other to a steel frame. This meant that, unlike Setup A, once displacements begin to increase, the specimen was predicted to drift slightly to the right-hand side.

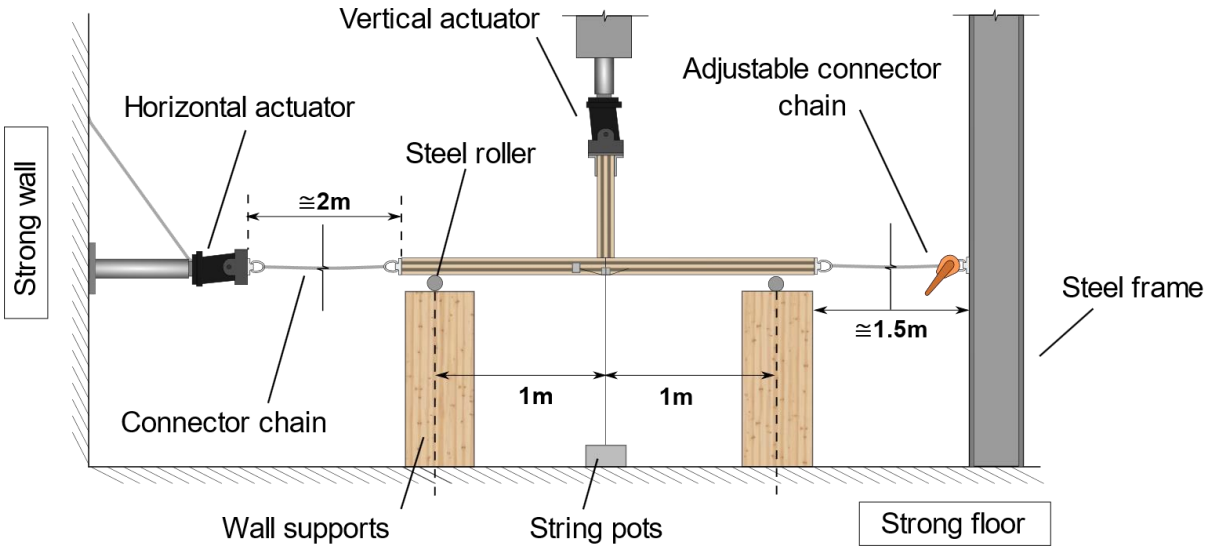

Figure 5. 3 Diagram of the component test expertimental setup B

Figure 5. 4 Photograph of component test experimental setup B

Vertical load application was performed using 3-point bending through a CLT wall element attached to another 250kN actuator (Figure 5. 6). The movement of the components was assumed to be mostly rigid, based on the previous work (A. C. Przystup et al., 2020) as well as the string pot checks in full-span tests (Chapter 6, section 6.3, Figure 6. 10). The use of a wall stub was decided for all the tests to mimic a platform construction type of point loading.

The data acquisition of both the horizontal and vertical load was possible due to the integrated load cells in both actuators. The displacements were measured using a series of string pots. Two of each measurement were taken, one on each side of the specimen. The vertical string pots were placed on the floor and encapsulated in wooden casing to be protected from the potential impact of the failed specimen. Their reach was elongated with a non-flexible string to allow for minimising the error

introduced by the sideways drift. The axial deformation was measured at the very bottom of the connection with string running across two metal elements on both sides reaching the bottom as shown in Figure 5. 5. For both axial and vertical string pots, strong magnets were used as attachments to allow for decoupling of the elements after sudden failure in order to preserve the equipment.

a) 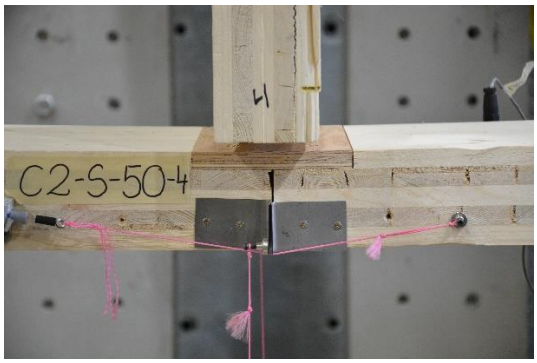

b) 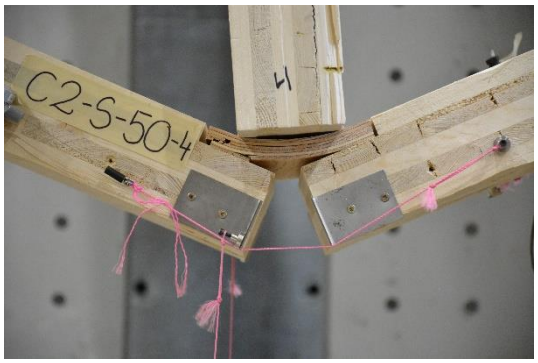

Figure 5. 5 Axial opening string pot installation (a) before test and (b) in its deformed state

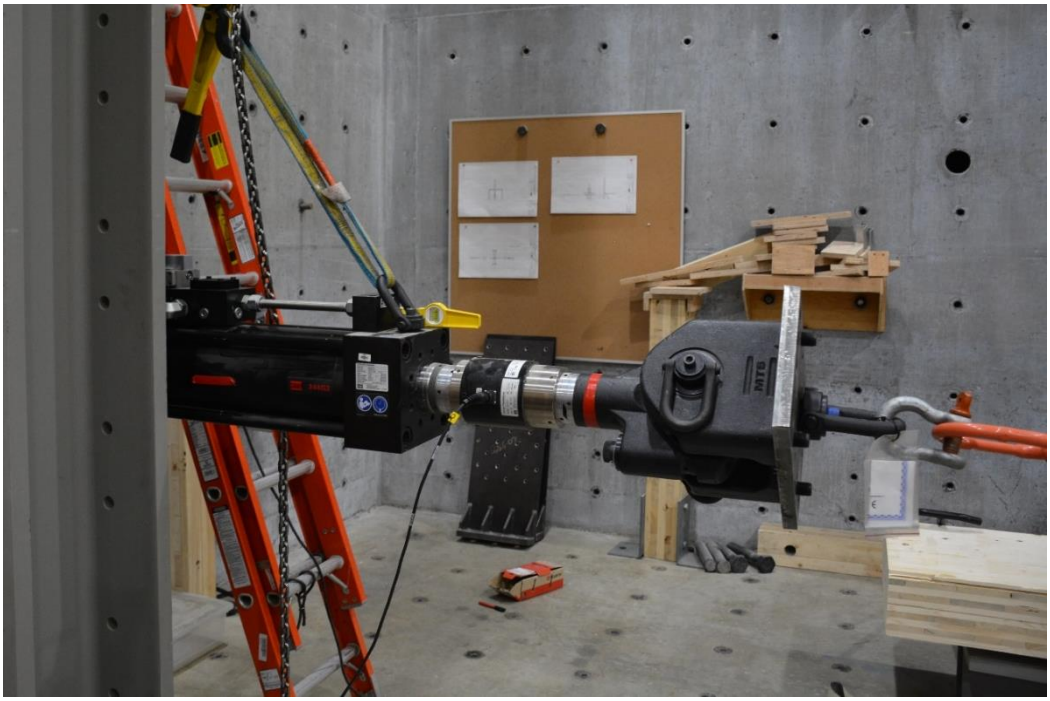

Figure 5. 6 Experimental Setup B horizontal actuator installation

A different approach was used for the components tested under axial tension only. The horizontal force and stiffness of the connection is instrumental in dictating the force-displacement behaviour and it was deemed necessary to measure the mechanical behaviour of the connection under pure axial loading. Setup B however assumed a larger size of the components both in width as well as length, neglecting the weight of the specimen in this scenario was deemed to be inappropriate. Therefore, to eliminate any bending effects of gravity loading, an upright configuration was chosen (Figure 5.7).

The samples were attached with 6 tight fit 15 mm diameter steel dowels on each side to minimise the slack in the system. Displacement was measured by two potentiometers installed on either side of the connection. The connections design was the same as in the component tests and therefore tension test results were also used as the equivalent of the combined test loads under maximum utilisation of tension (100% r_T).

Figure 6. 7 Tension experimental setup

5.2.2. Specimen characteristics

CLT panels used in Setup A were produced by the Construction Scotland Innovation Centre to order and had two different panel layups. The 5-ply setup consisted of the 20-20-20-20-20mm panels, and the 3-ply setup consisted of 33-34-33mm panels, both with the total thickness of 100mm. The CLT panels used for tests in Setup B were 5-ply 100 mm thick Binderholz BBS 125 of 20-20-20-20-20 mm layer thickness and 10% moisture content.

5.2.2.1. Half-lap connection

The half laps connection for both of the specimen used a single self-tapping screw installed at a 90-degree angle to the top panel to connect the two notched parts of the component together. The screws were installed without predrilling. The main difference between the specimen and the reason for testing two layup setups is to investigate the influence of different variances of the grain orientation on the overall performance and failure behaviour of the components.

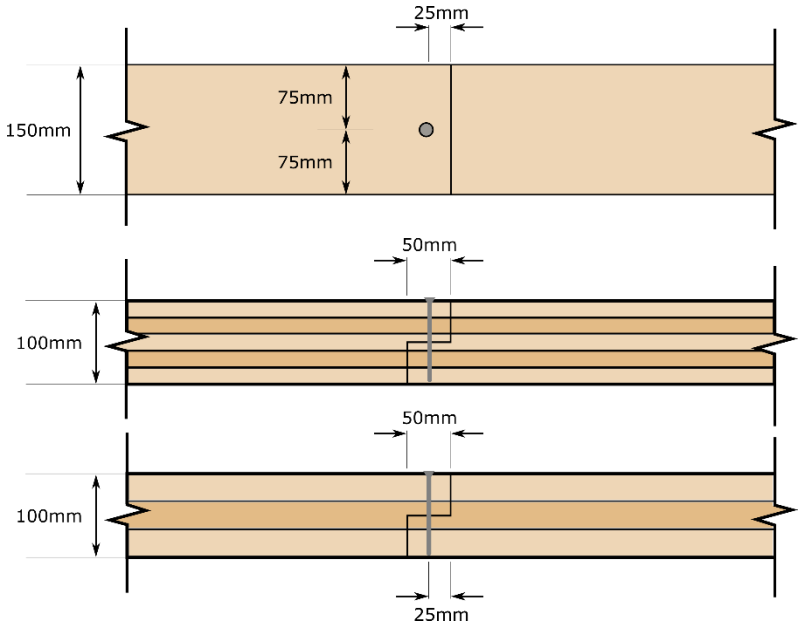

Figure 5.8 Half lap design with 5-ply (a) and 3-ply (b) CLT

5.2.2.2. Butt joint

SWG fully threaded self-tapping screws (STS) of 8mm diameter and 140 mm in length installed at 45° angle were used to make a butt joint connection, as shown in Figure 5. 9. Minimum edge spacing was 110mm and screw-to-screw spacing between the screws on the same side was 160mm. The cross-screws were installed

as close to one another as was practical in order to minimise potential problems connected with asymmetrical design such as variable rotation of the specimen at failure across the width of the panel.

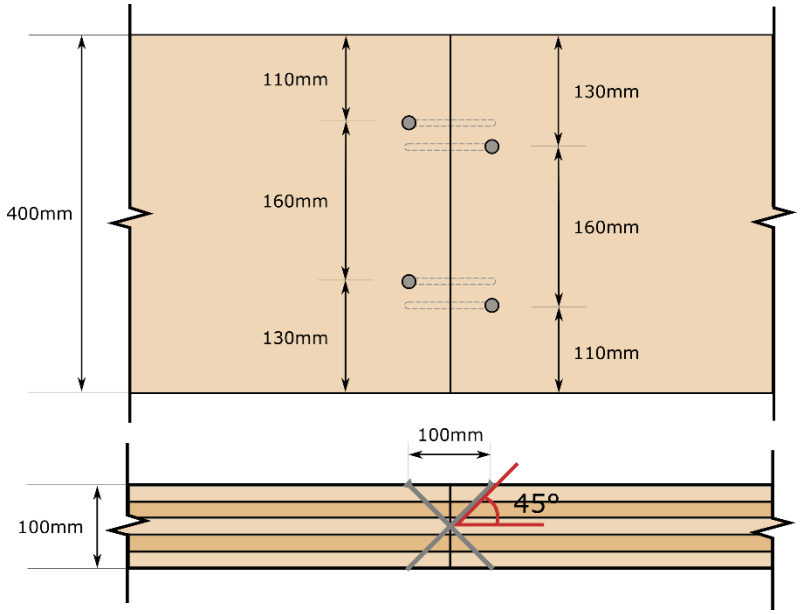

Figure 5.9 Butt-joint component design

5.2.2.3. Spline connection

For the spline connection the tension as well as component specimens used 8x100 mm SWG fully threaded self-tapping screws STS installed through the ¾ inch plywood perpendicular to the surface into the previously cut out notch in the CLT matching the depth of the plywood. Each of the notches reached 80mm from the end of each of the floor elements and therefore the plywood spanning both was 160mm in total. The notch has penetrated almost the entire top longitudinal layer as visualised in Figure 5. 10. 60mm spacing from the edge and 90mm from one another was implemented along the width of the specimen for the connectors and were placed symmetrically along the cut-out with 40mm spacing on either side of the notch.

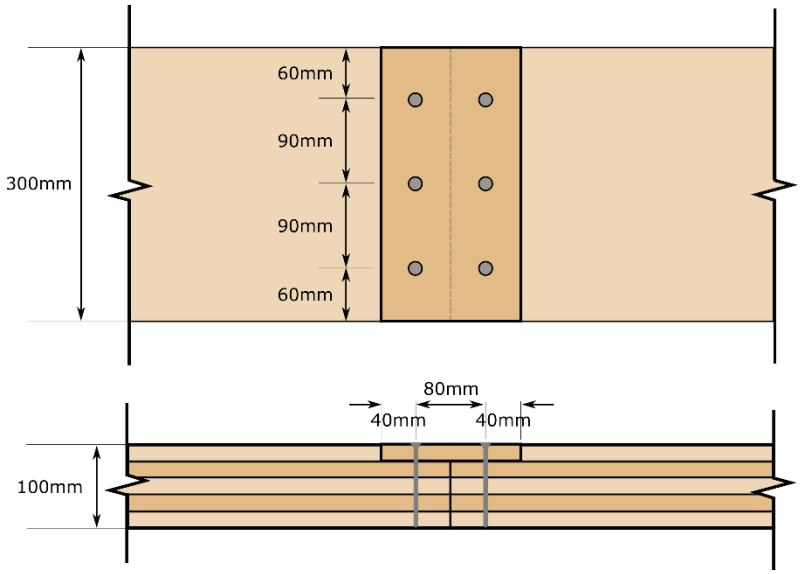

Figure 5.10 Single surface spline connection design

5.2.3. Testing plan

The aim of the component tests was to gather information on the influence of tension level on the moment rotation behaviour and ultimate limit state values; therefore, the test series were designed in even increments of tension utilisation from 0%-75% r_T (Table 5. 2). These utilisation ratios were based on the average ultimate strength obtained from the axial tension tests. Together with the axial tension tests this allows for investigating of the changes in mechanical bending properties depending on the tensile utilisation ratio.

Table 5. 2: Setup A

Series	Tension utilisation r_T	Tension (kN)	STS connectors
T1-B	100%	To failure	4x120mm
C1-B-0	0%	0.00	4x120mm
C1-B-25	25%	7.96	4x120mm
C1-B-50	50%	15.91	4x120mm
C1-B-75	75%	23.87	4x120mm
T2-S	100%	To failure	6x100mm
C2-S-0	0%	0.00	6x100mm
C2-S-25	25%	4.48	6x100mm
C2-S-50	50%	8.95	6x100mm
C2-S-75	75%	13.43	6x100mm

Table 5. 3 Setup B

Series	Tension utilisation r_T	Tension (kN)	STS connectors
T3-H3	100%	To failure	1x100mm
C3-H3-0	0%	0.00	1x100mm
C3-H3-25	25%	0.81	1x100mm
C3-H3-50	50%	1.62	1x100mm
C3-H3-75	75%	2.43	1x100mm
T4-H5	100%	To failure	1x100mm
C4-H5-0	0%	0.00	1x100mm
C4-H5-25	25%	0.98	1x100mm
C4-H5-50	50%	1.96	1x100mm
C4-H5-75	75%	2.95	1x100mm

5.3. Results

5.3.1. Axial tension tests

The butt joint axial tension test results are shown in Figure 5.11. An initial high-stiffness elastic region is followed by a peak and a softening branch. The mean value of the maximum force is 31.8 kN from the four tests. After around 6 mm displacement, the load reached a plateau, in most cases, at approximately 15 kN, until failure. The initial stiffness $\boldsymbol{k_0}$, maximum tension force $\boldsymbol{T_{max}}$, and its corresponding deformation $\boldsymbol{U_{T,max}}$ as well as the deformation at 50% load drop-off $\boldsymbol{U_{T,50}}$ are summarised in Table 5. 4 The latter is presented to investigate the extreme deformation behaviour which was relatively plastic.

The stiffest behaviour was exhibited by the butt joint connection (Figure 5. 11a) with k_0 of 8.99kN/mm, in contrast to the remainder of the connections ranging from 1.22-2.10kN/mm. The butt joint force-displacement curves does however exhibit the long plateau of plastic behaviour after the initial drop-off past peak value which could potentially allow for sufficient deformation to decrease tensile demand during catenary action. However, the rapid loss of stiffness could lead to accelerations in the system and further release of kinetic energy. This would likely negate the initial benefits from this type of deformation and still result in connection failure. As discussed in more detail in Chapter 7, this post peak plateau is not therefore considered in modelling the failure, as it is considered unreliable.

Spline connection has shown the most brittle failure of all, with no force retention present past maximum load at all, however the stiffness of the connection around 10mm while maintaining the load increase, allowed for achieving deformations of

50mm or higher at peak load, which in combined loading scenario would allow for development of substantial rotation, a property desired in catenary action. The 3-ply half lap did show potential of desirable plastic plateau behaviour in two out of three samples, however the third sample has only exhibited half the strength and no-load retention. The 5-ply half lap allowed for higher deformation and less brittle failure mode than its 3-ply counterpart.

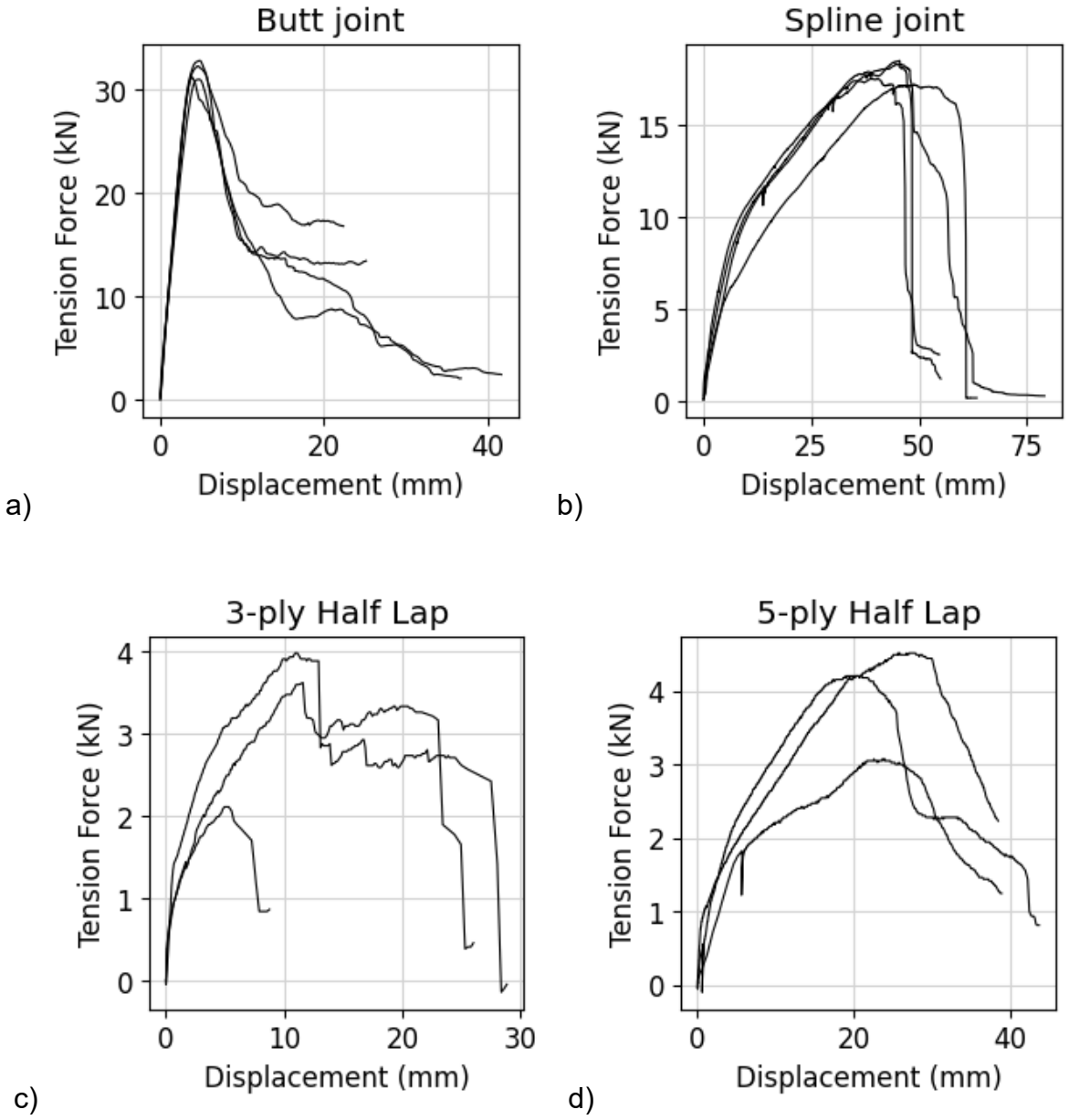

Figure 5. 11 3-ply half lap joint axial force displacement curves

Table 5. 4 Axial force test results summary

Specimen	k_0 (kN/mm)	T_{max} (kN)	U_{Tmax} (mm)	U_{T50} (mm)
T1-B-1	8.36	31.00	4.67	10.80
T1-B-2	9.29	32.80	4.78	9.27
T1-B-3	9.19	32.28	4.55	18.33
T1-B-4	9.13	31.22	3.85	9.98
mean	8.99	31.83	4.46	12.09
CoV	4%	2%	9%	34%
T2-S-1	2.27	18.52	35.64	37.44
T2-S-2	2.75	18.32	32.95	38.11
T2-S-3	1.71	17.21	34.98	42.53
T2-S-4	1.65	17.55	32.48	46.23
mean	2.10	17.90	34.01	41.08
CoV	25%	3%	5%	10%
T3-H3-1	2.33	3.63	11.58	27.85
T3-H3-2	1.78	3.99	10.92	24.50
T3-H3-3	1.60	2.11	4.94	7.66
mean	1.90	3.24	9.15	20.00
CoV	20%	31%	40%	54%
T4-H5-1	2.29	4.51	25.70	38.50
T4-H5-2	1.03	4.20	18.94	36.21
T4-H5-3	0.34	3.07	22.60	37.39
mean	1.22	3.93	22.41	37.37
CoV	81%	19%	15%	3%

5.3.2. Component tests

The numerical results of the maximum force P_{max}, displacement U_{max}, moment M_{max}, and rotation θ_{max} of the component-level tests are summarized in the following Table 5. 5 – Table 5. 8. Additionally, a value for the corresponding to the peak moment $\theta_{M,max}$ is also outlined as the peak moment and peak vertical force were often achieved at different displacements. The significance of maximum rotation θ_{max} shows the total displacement possible to achieve before full load drop off. The ability to compare $\theta_{M,max}$ with the θ_{max} allows to investigate how far past the elastic limit the connection is capable of deforming before total loss of contact between the two parts of the component.

5.3.2.1. Butt joint

Table 5. 5 below shows the results for the butt joint, which was achieved through the 3-point bending in Set-up B 25% r_T is shown not to have failed after reaching the maximum stroke of the vertical actuator, reaching 1.1rad rotation. This, however, is a high upper outlier. In each of the test series there is at least on outlier which achieves a significantly higher performance. The location of maximum moment did not vary greatly across the test series, largely staying around the value of 0.03 rad with a very slight increase across the series, with the exception of the 75% r_T test series, which produced a large variation of results, but ultimately averaging around the same value also.

Table 5. 5: Butt joint component test results numerical summary

Series	P_{max} (kN)	U_{max} (mm)	θ_{max} (rad)	M_{max} (kNmm)	$\theta_{M,max}$ (rad)
C1-B-0	4.10	55.2	0.111	1668	0.028
	4.10	62.3	0.125	1668	0.025
	4.03	95.2	0.192	1640	0.028
	3.58	249.6	0.520	1461	0.025
C1-B-25	10.90	476.0	1.102	1779	0.031
	5.91	241.4	0.502	1336	0.035
	3.71	133.7	0.271	1349	0.036
	6.29	253.1	0.528	1278	0.035
C1-B-50	4.39	84.9	0.171	910	0.048
	4.24	91.1	0.183	894	0.036
	7.57	155.3	0.316	1068	0.037
	3.77	73.3	0.147	898	0.035
C1-B-75	5.78	65.8	0.132	1101	0.053
	0.11	16.0	0.032	71	0.003
	3.96	76.2	0.153	692	0.033
	5.41	270.7	0.568	960	0.054

The graphic representation of the results can be seen in Figure 5. 12. Looking at the non-combined bending only set of specimens, the 0% r_T graphs (Figure 5. 12) shows a shape curve exhibiting clear elastic region ending in a peak and subsequent drop off of force with displacement and total failure. The force displacement graphs for the combined loading cases of 25% and 50% tension utilisation r_T (Figure 5. 12) show two distinct phases of the curve – the first one being the initial elastic range ending in a yield-like bump, similar to the initial uni-axial 0% r_T case, corresponding to the location and magnitude of the maximum load. While showing a drop off in load (25% r_T case) or just a slight decrease in curve slope (50% r_T case) in that location, the second part of those graphs shows a strain hardening like behaviour of the system.

This is directly related to the activation of the catenary action, and it can be asserted that the influence of the moment resistance of the connection here drops off, while the majority of the load is resisted directly by the catenary action.

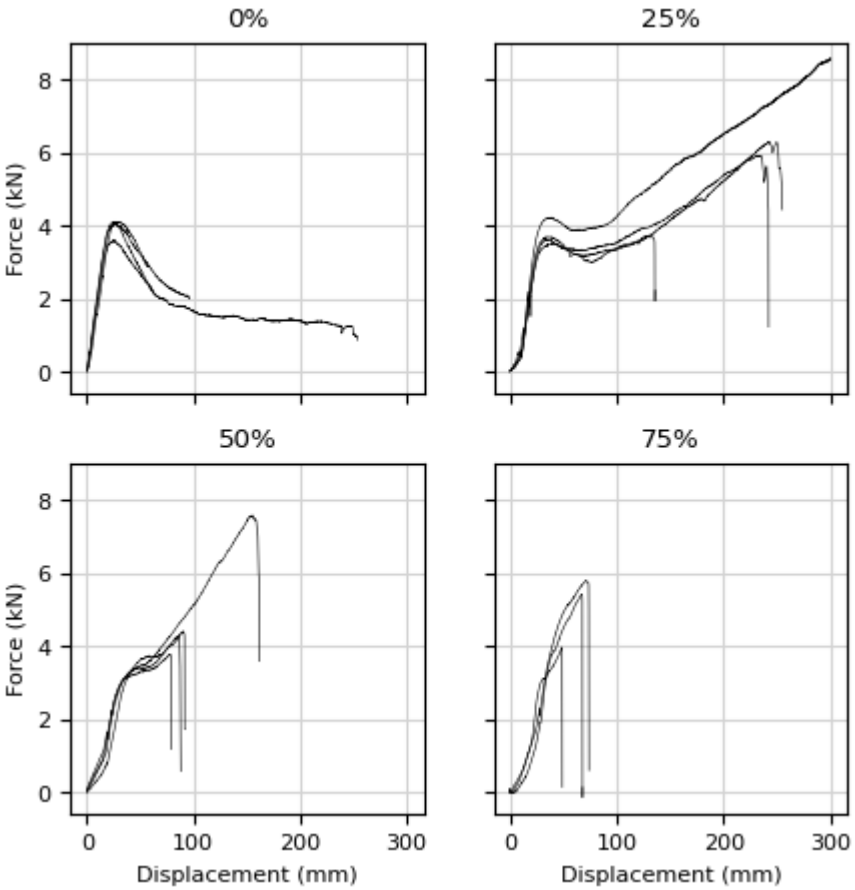

Figure 5. 12 Butt joint force displacement graphs

The maximum moment capacity of the connection, which can be observed as the peak values in Figure 5. 13, reduces with increase of the level of tension applied to the connection. It can also be observed that the specimens loaded to the middle range of force between 25-50% r_T performed best, both in maximum deformation and maximum force. However, all the tests reached their maximum moment at a similar rotation of approximately 0.04 rad. Any further increase in vertical force resistance for the C1-B-25 and C1-B-50 samples occur directly from catenary action activation, which is only possible through the post-failure plastic plateau. The

phenomenon of the post failure plastic plateau is necessary given the really high initial stiffness of the undamaged connection in its elastic range.

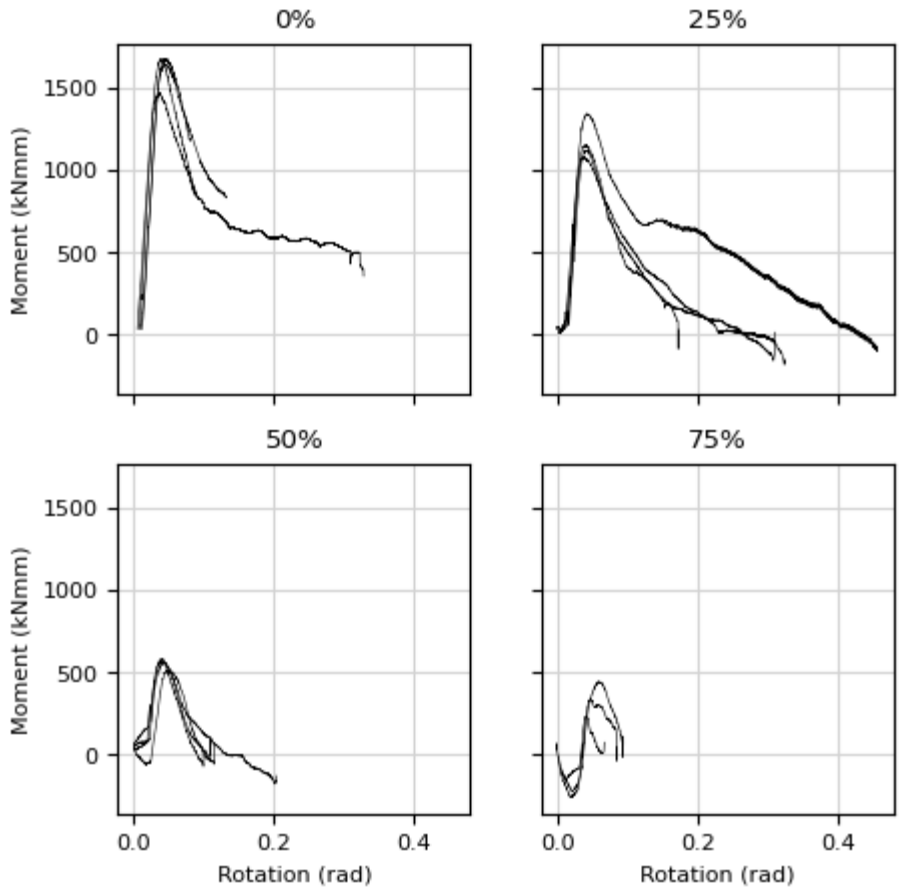

Figure 5. 13 Butt joint moment rotation graphs

Failure of the screws in the component tests was observed in two different modes. Screws failed in withdrawal, with some having punched through the material from the headed side of the screw (Figure 5. 14b). In either scenario material in the traverse layers of the panels was pulled due to the tension perpendicular to the grain. Some of that failure was shown to split all the way to the edge of the sample, indicating that a higher edge spacing and therefore more material to distribute the localised stresses could have a positive impact on the overall strength of that connection.

a)

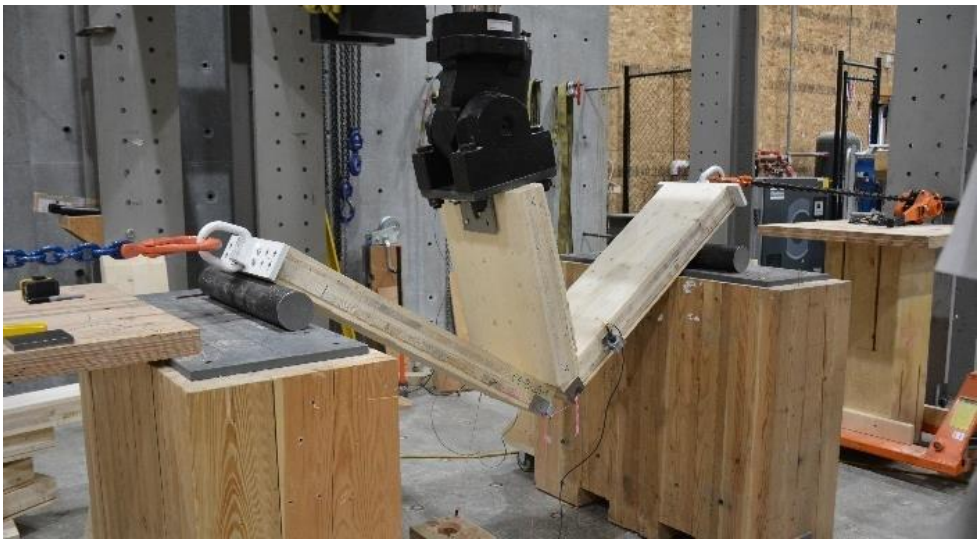

b)

Figure 5. 14 Butt joint component tested to maximum stroke (a) and to failure (b)

5.3.2.2. Single surface spline joint

The numerical representation of the spline joint results can be seen in Table 5. 6. Tests were performed using the 3-point bending tests in Setup B. This shows that the joint reaches optimal performance when tensioned with around 50% of its maximum tensile strength (50% r_T). The variability of the results does not show outliers as major as the ones present in the butt joint in either of the parameters. The location of the maximum moment remains in within the region around 0.1-0.2, with slight increase from the 0% r_T samples to the 25-50% and a consequent decrease in the values to the 75% r_T series. Overall, the initial stiffness is much lower than the butt joint, despite using more connectors, which is understandable given the connection has not been designed to resist a sagging moment. This results in a longer elastic region allowing for greater pre-moment-failure deformation allowing for a stronger catenary formation, visible in the tenfold jump in the vertical force resistance from 0% to 25% r_T and further, although not as dramatic, increase within the 50% r_T series.

The graphical representation of the results in Figure 5. 15 and Figure 5. 16 allows for the comparison of the curve shapes. Both force displacement as well as the moment rotation behaviours are qualitatively different to the butt joint curves shown in Figure 5. 12 and Figure 5. 13. The force-displacement behaviour is very smooth and seems to become increasingly close to linear the higher the tension utilisation. The force resistance of the bending-only samples is minimal, which explains the linear-approaching behaviour of the curves as the whole system relies solely on the catenary activation without the “noise” caused by the connection stiffness.

Table 5. 6 Single surface spline joint component test results numerical summary

Series	P_{max} (kN)	U_{max} (mm)	θ_{max} (rad)	M_{max} (kNmm)	$\theta_{M,max}$ (rad)
C2-S-0	0.55	125.31	0.253	248.89	0.086
	0.53	80.98	0.163	240.51	0.122
	0.54	59.71	0.120	244.36	0.089
	0.49	56.88	0.114	224.723	0.085
C2-S -25	5.60	469.81	1.084	329.21	0.186
	5.20	401.24	0.891	288.03	0.175
	5.25	407.66	0.909	311.72	0.175
	5.65	439.70	0.997	380.26	0.181
C2-S -50	8.28	303.91	0.646	386.38	0.157
	10.79	459.59	1.054	379.02	0.214
	7.77	279.01	0.587	331.35	0.161
	8.81	337.75	0.728	427.56	0.234
C2-S -75	3.47	210.43	0.433	36.36	0.119
	5.27	120.52	0.243	372.37	0.111
	11.02	285.10	0.602	284.15	0.125
	6.52	184.10	0.377	306.84	0.142

The moment-displacement curves shown in Figure 5. 16 show an initial uptick in the moment at the very beginning of the test which is due to the initial pre-tensioning before introducing the vertical displacement. This is not thought to have affected the connection as this calculated moment lasting a very short increment of time has never been truly resisted by the connection, as the component would immediately start deflecting before reaching an equilibrium at higher deformations. Visual inspection of the connections after pre-tensioning and before the application of the vertical load further corroborated lack of visible damage to the connection. This effect however increased with the value of pre-tensioning resulting in the only series where this is

thought to possibly have had an influence was the 75% r_T series, as the initial moment was twofold the magnitude of the peak moment achieved and the samples have shown a decrease in the total moment resistance.

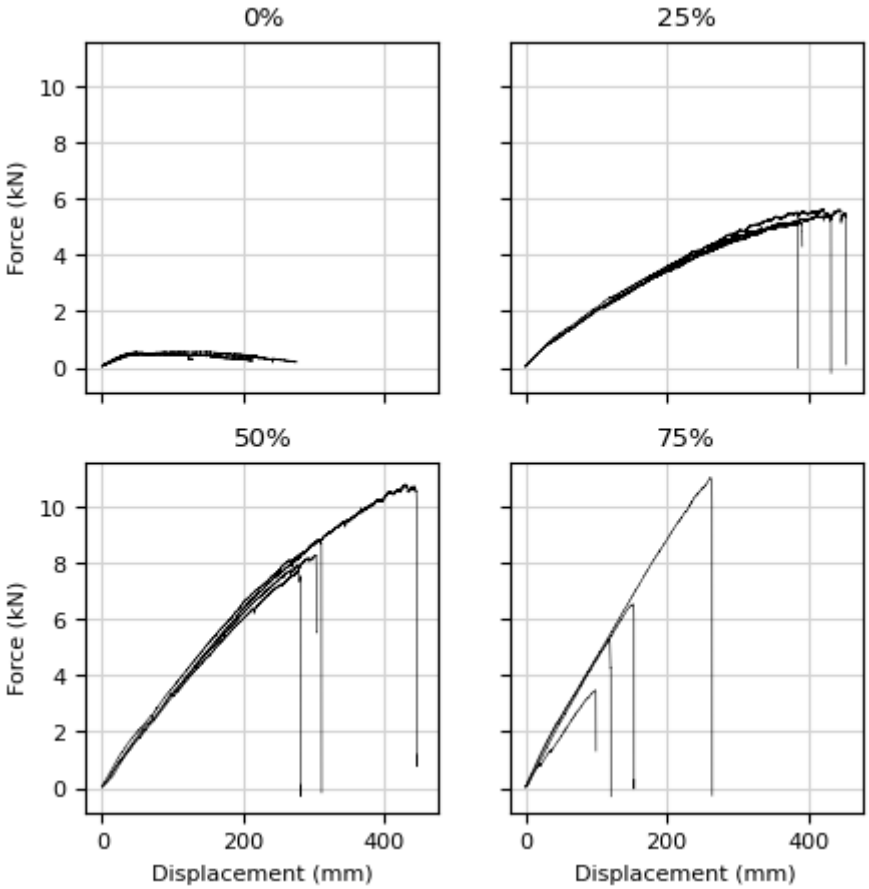

Figure 5. 15 Force displacement curves of the surface spline connection

That decrease cannot however be fully attributed to this effect since this behaviour of lowered performance is present across all of the connections and is thought to be mainly a result of the variability of the material closer to its ultimate limit state. The total maximum rotation here seems to be a good failure predictor across 0%-50% r_T samples. Despite the lack of significant vertical force resistance in the pure bending series, the ability of the deformation to persist an increase while maintaining the load way past its maximum moment and force has been reached is what play the instrumental role in the very successful activation of the catenary action.

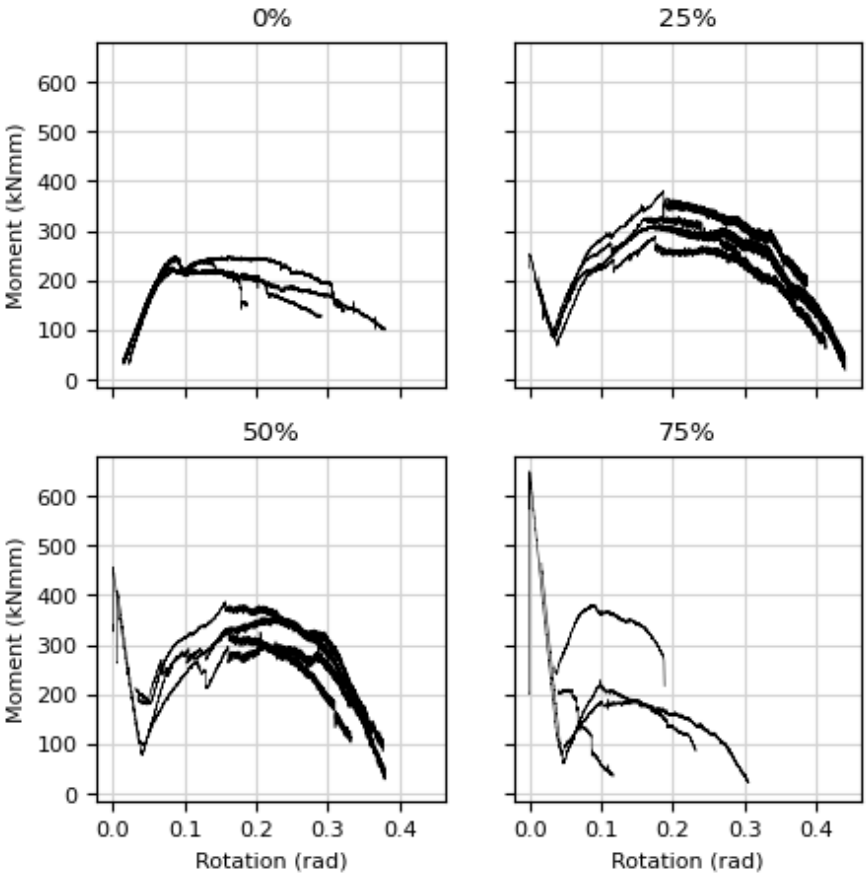

Figure 5. 16 Moment rotation curves of the single surface spline connection

5.3.2.3. Half lap

5.3.2.3.1. 3-ply

The numerical representation of the 3-ply CLT half lap tests are shown in Table 5. 7. The results regarding all of the parameters remain replicable for the 0% and the 25% r_T test series, with small variabilities across all of the variables. At 50% and 75% r_T test series this increases and there is a reasonably large spread. This is thought to be due to use of a single fastener as opposed to a series, which was necessary due to the constraints of material availability and the testing setup. It is, however, still possible to investigate the trends present in the changes to the overall behaviour

using three replicated of each of the tests. Looking at the $\theta_{M,max}$ in comparison to the θ_{max} it is possible to see that the maximum location of the peak moment and peak force capacity are here significantly closer in this connection when compared to the butt joint and the spline connection. What that means in this case is that once the connection leaves the elastic limit, it is not capable of sustaining significant catenary action.

Table 5. 7 3-ply half lap connection component test results summary

Series	P_{max} (kN)	U_{max} (mm)	θ_{max} (rad)	M_{max} (kNmm)	$\theta_{M,max}$ (rad)
C3-H3-0	1.15	70.55	0.142	213.94	0.126
	1.23	106.18	0.214	226.66	0.173
	0.93	88.84	0.179	175.34	0.159
C3-H3-25	1.30	72.66	0.146	182.65	0.122
	1.41	77.92	0.156	200.26	0.126
	1.42	82.35	0.165	195.12	0.141
C3-H3-50	3.16	212.44	0.438	202.83	0.390
	1.42	90.77	0.183	143.71	0.046
	1.93	129.30	0.261	166.50	0.107
C3-H3-75	2.45	119.95	0.242	148.80	0.214
	0.46	12.09	0.024	67.61	0.022
	1.75	64.96	0.130	169.55	0.098

This is further visualised in the force-displacement and the moment-rotation graphs presented in Figure 5. 17 and Figure 5. 18. There is no significant imrovement in the joint performance from 0% to 25% tension utilisation r_T and with some, but not very reliable improvements in the 50% r_T and the 75% r_T sections. This repeatability especially in the 50% r_T series is thought to be able to be improved alongside the introduction of multiple fasteners.

Overall the best deformation capacity was exhibited by the uni-axial samples when no external tension was applied. One significant reason this is thought to be the case is the performance of the cross-wise layer, which in the 3-ply the location of the half lap horizontal cut. There were two significant failure modes in this test, the direct shearing of the screw and the splitting of the cross-layer. This is shown in Figure 5. 19 below.

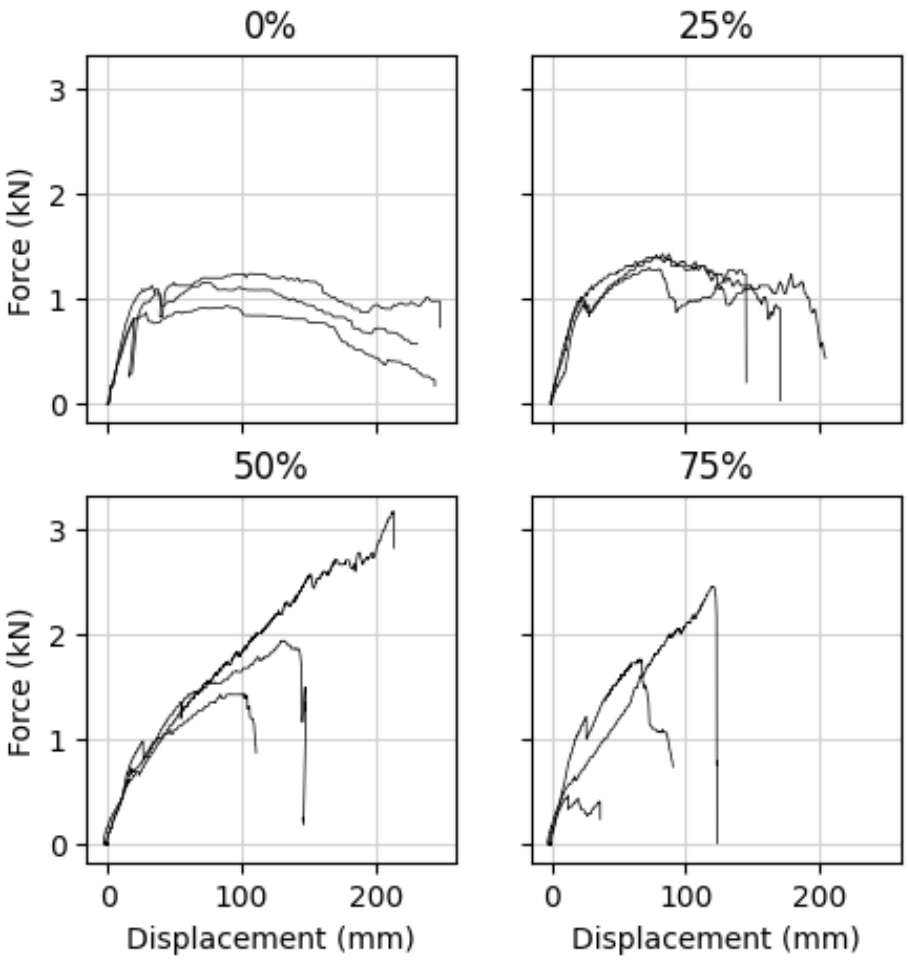

Figure 5. 17 Force displacement graphs for the 3-ply half lap component tests

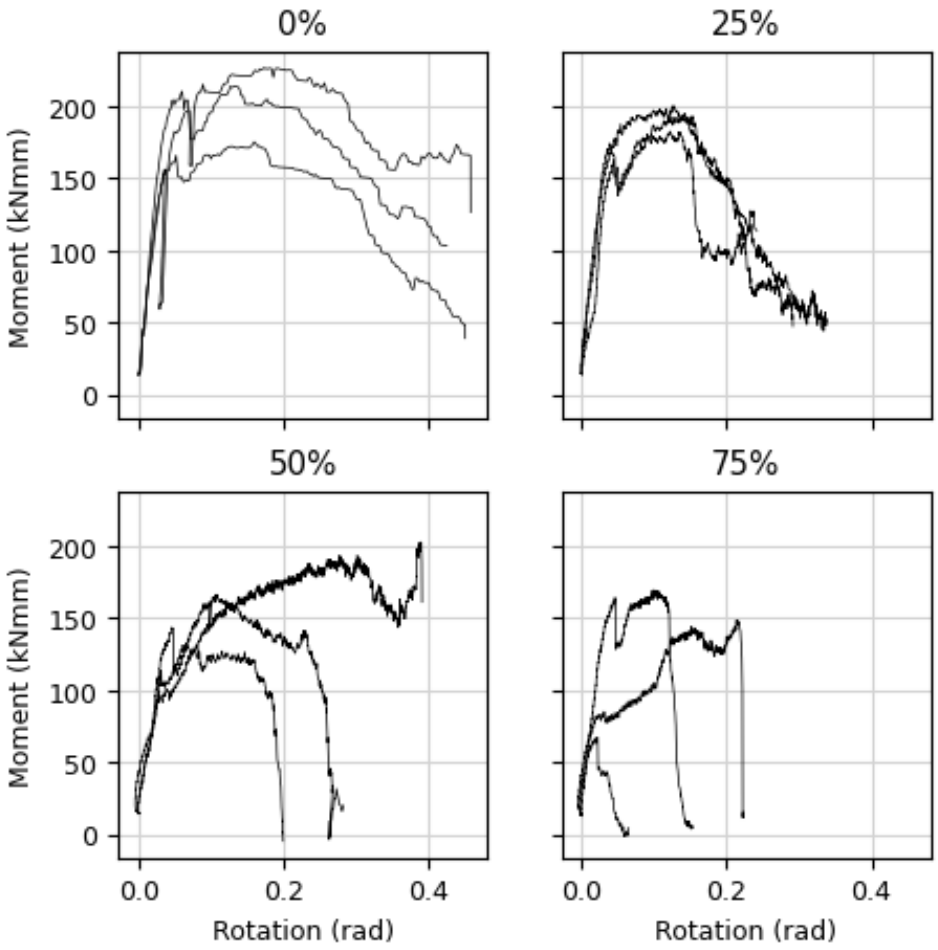

Figure 5. 18 Moment rotation graphs for the 3-ply half lap component tests

a)  b)  c) 

Figure 5. 19 Failure modes of 3-ply half lap: a) cross-layer split, b) & c) screw shearing

5.3.2.3.2. 5-ply

The numerical results of the half-lap connection in the three-ply CLT are presented in Table 5. 8. The location of the maximum achieved force and moment in the 0% r_T samples coincide very closely when looking at the comparison of values $\theta_{M,max}$ and θ_{max}, however the maximum force in the majority of the remainder series where tension was present shows a further increase in force resistance past reaching the point of maximum moment, indicating a successful catenary action activation. The greatest variability in the presented values has been observed in the 75% r_T series, this is however considered to be normal due to the external tension perceived approaching the ultimate tension load. Similar to the 3-ply test set however it is thought that the variability could be reduced with the introduction of multiple screws in the connection.

Table 5. 8 5-ply half lap connection component test results summary

Series	P_{max} (kN)	U_{max} (mm)	θ_{max} (rad)	M_{max} (kNmm)	$\theta_{M,max}$ (rad)
C4-H5-0	1.38	84.49	0.170	252.97	0.151
	1.18	32.50	0.065	221.40	0.058
	1.31	66.76	0.134	241.92	0.120
C4-H5-25	2.07	201.87	0.415	187.12	0.182
	1.55	178.98	0.366	162.28	0.079
	2.41	171.68	0.350	253.55	0.290
C4-H5-50	1.23	72.01	0.145	136.77	0.063
	2.19	125.43	0.254	173.86	0.142
	1.78	94.18	0.189	150.60	0.124
C4-H5-75	0.63	28.43	0.057	78.39	0.019
	2.57	123.11	0.249	144.06	0.123
	2.34	112.48	0.227	141.41	0.097

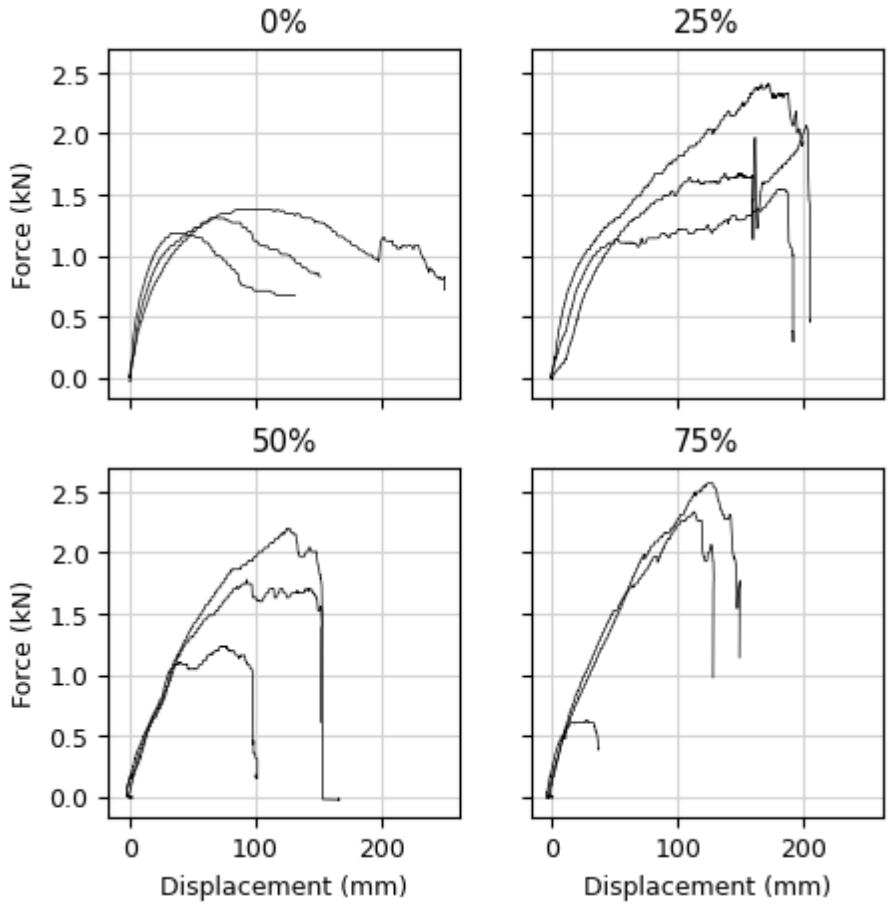

Figure 5. 20 Force displacement graphs for the 5-ply half lap component tests

Looking at the shape of the force displacement graphs in Figure 5. 20, significant improvement in the force performance can be seen from series 0% to 25% r_T, in contrast to the 3-ply series. The behaviour becomes increasingly linear with the further increase of the tension, however with no significant improvement to the total force taken and a small but steady decrease in the maximum deformation.

Shape of moment-rotation graphs are presented in Figure 5. 21. The 25% r_T series graph when compared with the equivalent force-rotation reveals that the maximum force is achieved after the maximum moment has done so. Moreover, the average deformation achieved was improved upon from the 0% r_T series here. Both of these indicating a good catenary action activation in the 25% r_T series. In contrast, for

samples in the 50% r_T series the location of the maximum moment coincides largely with the location of the maximum force, where the force in the system reaching a plateau as soon as the peak moment is achieved and consequently dropping off for most samples. No significant improvement in performance is therefore seen past the 25% tension utilisation r_T, while variability of the results and the deformation capacity decreases.

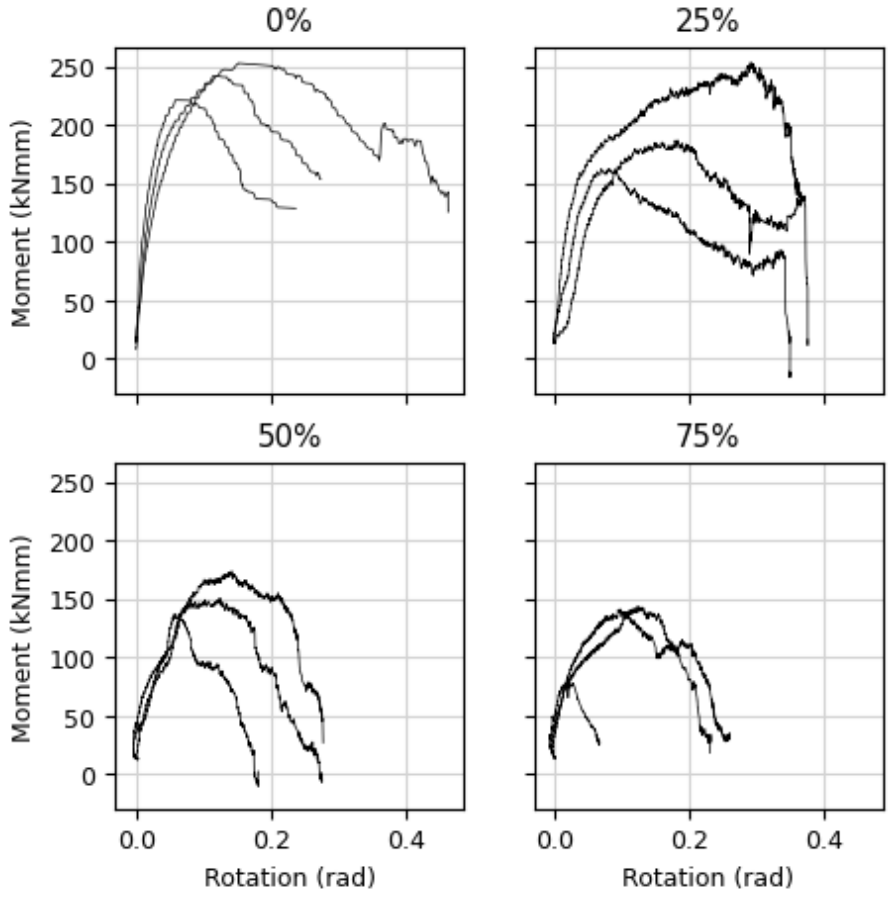

Figure 5. 21 Moment rotation graphs for the 5-ply half lap component tests

5.4. Discussion

5.4.1. Connection performance

To approach the comparison of the four presented test sets of three connections, one of the connections being introduced into 5-ply and the 3-ply CLT, the summary graphs in figures from Figure 5. 22 to Figure 5. 25 are presented. These graphs combine the results for each of the connections across all of the tension utilisation level series from 0% to 75% r_T, differentiated by colour. It allows for both quick visual recognition of the way in which the increased tension impacts the characteristics of both force-displacement and moment-rotation graphs as well as across the different types of connections. For clarity of the presentation, a single test has been chosen from each of the series that was thought to be most representative of the series, however for the broader understanding of the behaviour of the array of the behaviours present in each of the series it is advised to refer back to the Section 5.3.2.

Looking at the summary graphs of the butt joint results in Figure 5. 22Figure 6.22 a clear trend in change of both force-displacement as well as moment-rotation can be observed. The force-displacement curves end up turning upwards and becoming shorter, with the initial displacement capacity decrease being minimal and decreasing faster after 25% r_T. A similar trend can be seen in spline connection curves in Figure 5. 23. The main difference is that the starting condition of the uniaxial load is much less favourable, with the vertical force resistance as well as displacement capacity being minimal. The performance decrease in the combined loading cases there also only starts to deteriorate only after 50% utilisation r_T. The reason why the two connections behave in such different manner can be seen in the moment diagrams, where it is shown that the moment rotation behaviour does not change as

dramatically in the spline connection as it does in the butt connection, with the initial moment capacity being actually better in 25% and 50% r_T series than in the 0% r_T, and only deteriorating back down when reaching 75% r_T. Another interesting observation can be that the location of maximum moment reached in butt joint seems to remain largely the same, while in spline joint there is a shift forward in the cases of 25% and 50% r_T series, which were the better performing ones. The exact location of these moments could be influenced by increase in the influence of overhang error at higher rotations, discussed in more detail in Section 5.4.3.

The comparison between the half lap 3-ply and 5-ply components based on the visual investigation of the summary graphs in Figure 5. 24 and Figure 5. 25. The major difference between the location of the peak performance and the influence of the tension utilisation on the shape of the curves. The 3-ply connection exhibits almost negligible change to the behaviour from the 0% to the 25% r_T series and a major improvement in the total vertical load carried at 50% r_T, all the while maintaining almost unchanged moment capacity. 75% r_T series still performs better than 0% r_T and 25% r_T, however moment and deformation capacity deterioration isvisible. This trend of drastic initial improvement is replicated in the 5-ply but at an earlier point of 25% T_u , however it is not sustained through to the 50% r_T and 75% r_T series. Overall although the 3-ply samples had initially lower force capacity in the uniaxial scenario, they lean seem to be more successful in catenary, offering higher load resistance at higher tension utilisations than the 5-ply samples. All of the above results gathered during both Setup A and Setup B series are further simplified into normalised graphs and charts in the Chapter 7, where the numerical results achieved in the process of component testing are transformed to be of more practical use for the purposes of modelling larger subassemblies.

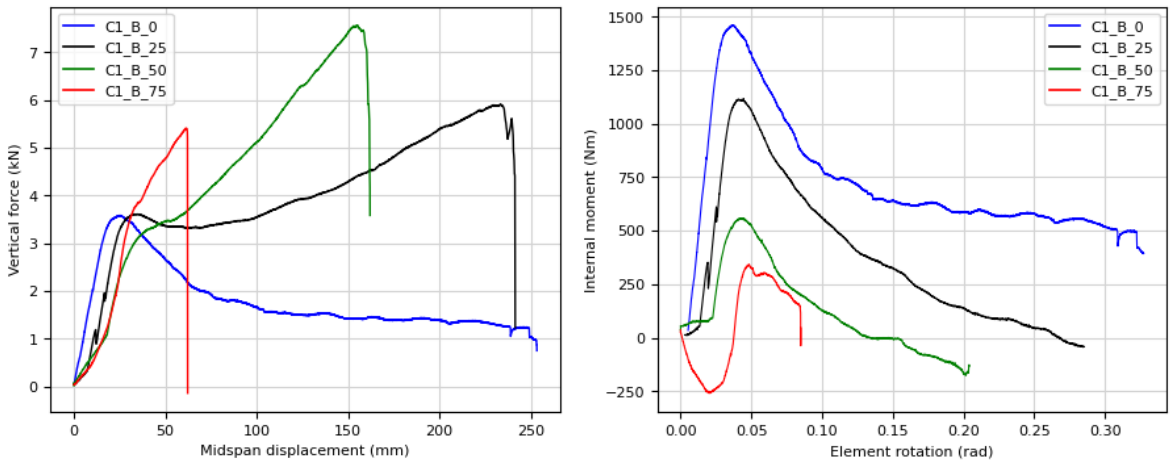

Figure 6.22 Summary graphs of the butt-joint conneciton component tests (left: force displacement, right: moment rotation)

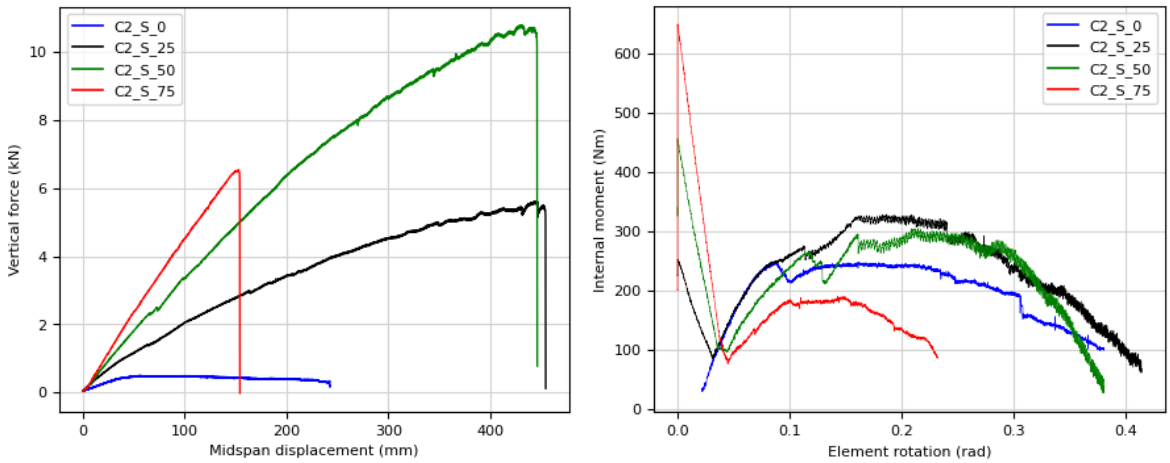

Figure 6. 23 Summary graphs of the single surface spline connection component tests (left: force displacement, right: moment rotation)

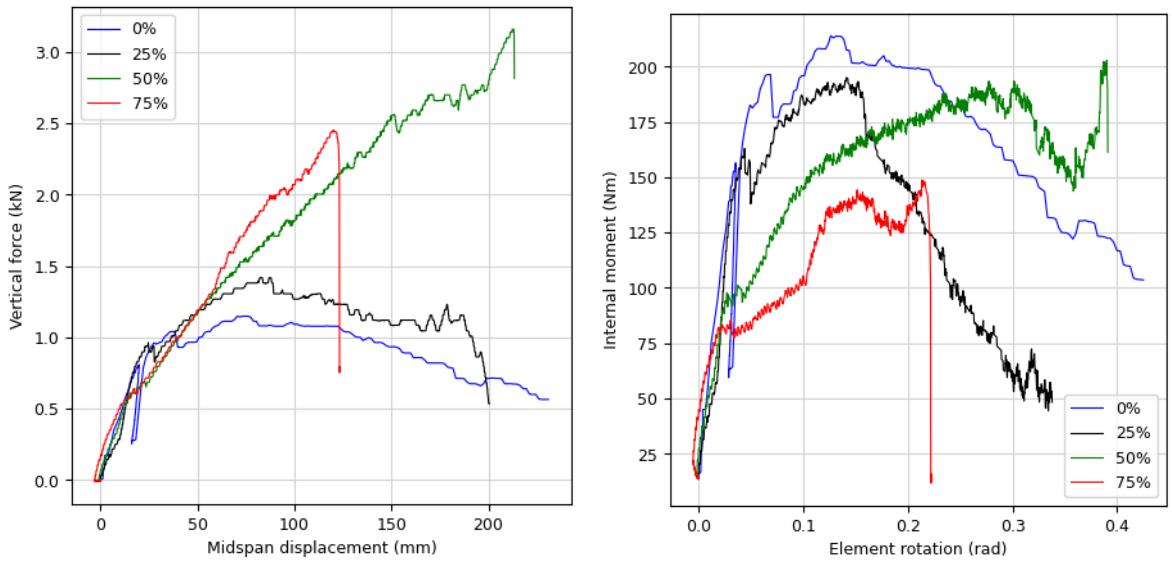

Figure 6. 24 Summary graphs of the half lap 3-ply connection component tests (left: force displacement, right: moment rotation)

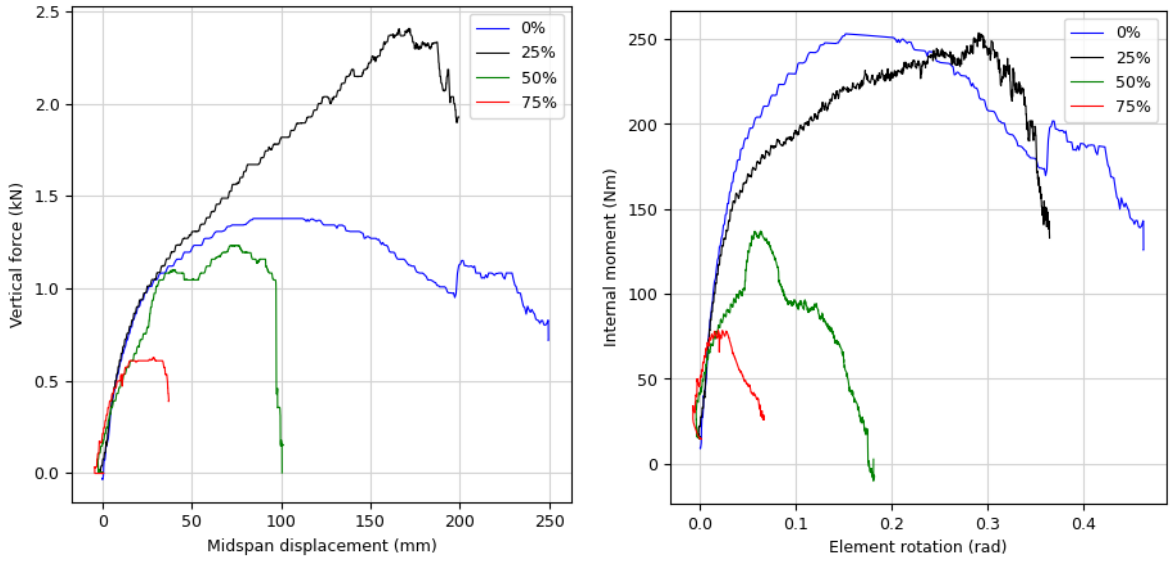

Figure 6. 25 Summary graphs of the half lap 5-ply connection component tests (left: force displacement, right: moment rotation)

5.4.2. Stiffness and catenary action

There are several design decisions that have shown to be of importance. The initial stiffness of the connection as well as the ability of the connection to sustain some loading past its ultimate values have been the two that have shown to be of utmost importance to consider here.

Connections of low initial rotational stiffness in the tested direction, such as the spline connection, perform better under catenary as there are lower internal stresses present to achieve deformation levels necessary for the catenary activation. This difference in stiffness is due to the geometry and screw placement. In the spline connection there is minimal deformation of the screws themselves necessary to achieve the opening at the bottom of the connection, with local plywood crushing and plywood bending being an important mechanism of deformation. In contrast, the butt joint will require withdrawal and bending of the screws as the connectors span both floor component. It is for this reason that the spline connection does not follow the similar trend of reduction in moment capacity to the other, stiffer, connections, as there is not a direct correlation between the increased tension on the component and the reduction in the peak moment. In fact, the moment capacity initially increases. One of the potential mechanisms behind this is that the introduction of the wall section above the connector combined with sufficient downwards deformation allowed for the corners of the wall to maintain contact with the plywood and through friction help transfer some of that compressive load. This is visualised in Figure 5. 26.

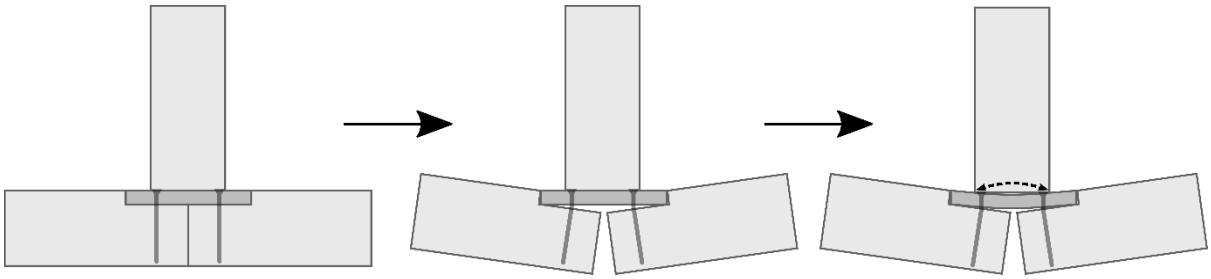

Figure 6. 26 The visualisation of the possible new compressive bridging route in spline connection

The comparison of both of the half-laps is also a great example to support these findings. The 3-ply connection's behaviour leans itself better to the catenary action activation, due to the major splitting of the cross layer which allows for greater joint opening and smaller stiffness. This causes the moment capacity to not diminish drastically as the internal stresses in the connector do not increase as much with the midspan deformations increasing. Comparing that to the 5-ply, where a stiff longitudinal layer is present at the centre, the maximum load capacity improvement here is lesser and peaks early at 25% r_T, while the moment capacity is drastically diminished more drastically to its 3-ply counterpart.

5.4.3. Experimental setup practicalities

The comparison of Setup A and Setup B has brought up several findings that could inform future testing based on the priorities in the type of results gathered and the payoff of labour versus the perceived benefit to the achieved results.

Setup A, which was built first chronologically, has implemented several features that were thought to be more labour-intensive in the setup stage. The creation of the specifically designed bearing and hinge systems as a support condition required additional setup time. Moreover, the preparation and mounting of the samples also cost additional time. The perceived benefit of implementing such solution was the

exclusion of the overhang error, which at small loads and variable overhang throughout the movement of the regular roller could reduce the applicability of the results to investigation of the catenary action. Additionally, the tension application setup here was fixed to one axis with rods and therefore there needed to be no upwards movement of the ends of the samples.

In contrast, Setup B has solved this issue by introducing chains for tension transfer, and the overhang error was accounted for in the numerical processing of the results. The end connections implemented here were off-the-shelf anchors, and their application was fast and convenient. However, the error calculations are thought to be only approximate, as the values of overhang were taken as constants, while their influence in reality was variable due to the moving across the rollers and the rollers additionally travelling on the supports as a result. For that reason, the accuracy of the moment calculations would reduce alongside the increase in the vertical midspan deformation.

Another significant difference between the two setups was the attempt at symmetrical application of the load. With active load application, the simple approach would be to fix one side completely and apply tension from the other side. However, since the experiments specifically delt with extreme deformations, the vertical pushdown in this case equated to the horizontal travel of the active support, translating across to the centre of the sample and therefore the connection.

To solve this problem Setup A, where the tension application was done manually through hydraulic jacks, identical hydraulic cylinders were installed on both ends of the sample and connected through the pipes of the same length to a Y-connector. In principle this applied the same tension from both sides, which, along with stabilising

friction from the vertical point load application, would result in symmetrical horizontal deformation on each of the supports. This did not in fact work in practice, with the samples still exhibiting sway up to 40mm towards the right-hand ride support, which is thought to be due to the differential frictions in the cylinders. Therefore, Setup B has used the simpler one-side-fixed approach. Although the sway was still consistently higher in this case, reaching approx.120mm to towards the restricted side at full extension, it was at least consistent and predictable and therefore a more favourable solution. Setup B also improved on the consistency of the tension applied, using a horizontal servo-controlled actuator.

The Digital Image Correlation introduced for displacement data collection in Setup A, alongside the string potentiometers and was prioritised in the final data analysis, as the location and accuracy of the string sensors were shown to be lesser. However, the process of data collection and post-processing needed just to achieve linear displacement values was inefficient. DIC in this case could not be used to show the significant stresses present in the samples as these were either concealed or located too close to the edge in the compressive one for the software to be able to pick it up. Setup B in used multiple string potentiometers.

The last major difference between the two setups was the three-point bending implemented in Setup B, versus four-point bending in Setup A. The four-point bending is thought to be a better solution where the behaviour of the connection alone is of more interest, while the three-point bending could capture the load transfer through the wall above, and any interaction between wall and joint.

5.5. Summary

The chapter has introduced two experimental set-ups from two different institutions designed to extract the same information about the connections – the rotational performance under various levels of tension. Four test series were performed – on Set-up A: half-lap joint in 3-ply CLT, half-lap joint in 5-ply CLT, and on Setup B: spline and butt joint connections (both 5-ply CLT). The tension levels applied were implemented with reference to their experimentally measured tensile strength, represented by the tension utilisation ratio r_T: 0% (bending only), 25%, 50% and 75%. The tension was applied in load control and remained equal throughout the entire experiment, which has allowed for a controlled way to investigate the difference in connection performance across tension spectrum. Force displacement and moment rotation graphs were presented for each of the tests, which allowed for discussing the most favourable tension levels for each connection, and through comparison between one another discuss the sources of performance differences between the connections.

These tests were relatively easy to perform once an appropriate experimental setup design has been reached. They have revealed crucial mechanical properties which can be used in modelling and is variable with tension, which has not previously been achieved with other experimental setups. Chapter 6 focuses on scaling the tests up to full subassemblies and experimental data from both scales is brought together in Chapter 7 to further explore the correlation between the two and potential implications of the results achieved to the alternative load path formation in CLT floors.

Chapter 6: Full scale tests

6.1. Experimental objectives

The goal of this experimental series was to directly address Objective 3 outlined in Chapter 3 “Design and perform full-span CLT floor pushdown tests in combined axial tension and bending with a range of connection types and under a variety of boundary conditions for empirical investigation of the catenary action formation in different subassemblies.”. The full-scale floor tests can be used further to both confirm the accuracy of the component test results as well as investigate the behaviour of more complex subassemblies, which is the basis of Objective 4: “Validate the component test results through direct comparison of test and a numerical model. Use the validated component parameters and numerical model developed to investigate other subassembly and boundary condition scenarios”, which is fully explored in Chapter 7.

One of the main advantages of testing full-span tests was that is allows to investigate the behaviour under passive tension loading (i.e. tension developing due to restrained horizontal support and increased vertical midspan deformation), which is

not possible to achieve in the component test scenario, as this will depend largely on the interaction of the subassembly geometry with the rotational and axial stiffness of the connection. An important question that the following attempts to address - are the failure loads of the connection, in terms of combined tension and bending, affected by the time-history of tension and bending development through the experiment?

Here two main scenarios are to be considered. The first is the passive tension development in the system, meaning that the tension starts at zero for a vertical midspan deformation of zero and develops due to the introduction of that deformation, increasing with through the motion of the pushdown force. The second scenario assumes active tension load implementation, meaning that the secondary actuator was used to impose specific load level throughout the test.

6.2. Materials and methods

6.2.1. Experimental setup

The full-span pushdown tests were performed in 3-point bending on two CLT floor panels connected at the centre with an effective length (midspan to support) of 3000 mm, see Figure 6. 1a). Due to the limited stroke of the actuator, especially for the vertical direction, the 3m span tests only allowed for maximum of 17% midspan deflection to single span ratio. To allow for a further investigation into the more extreme deformations a supplementary test series of 2000mm span was introduced as shown in Figure 6. 1b). Vertical string pots on either side were placed at 1 m increments and two additional string pots at the underside of the connection to monitor the joint opening. The first full-span floor specimens were tested in a simply supported arrangement. This was used to verify whether moment rotation behaviour

of the connection remained the same in such larger subassemblies as the component tests. Later specimens were tested using a variety of wall details and support conditions outlined in Section 6.2.3

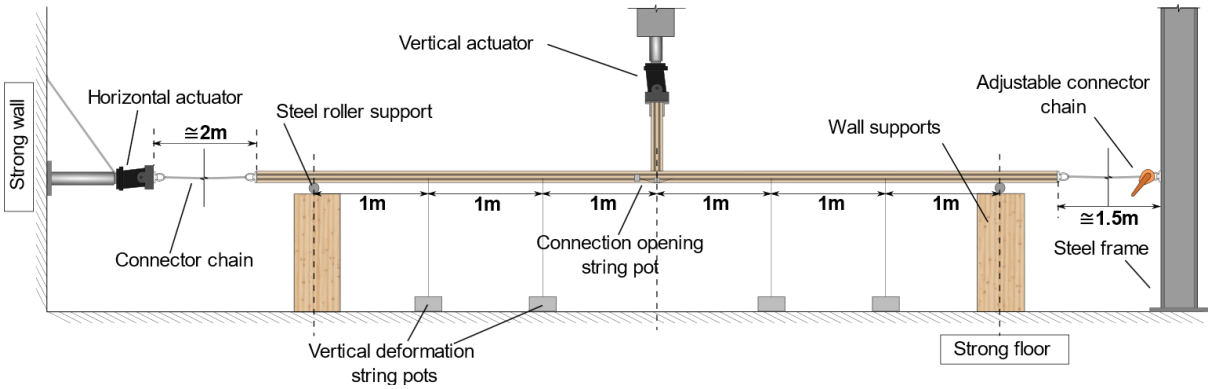

a)

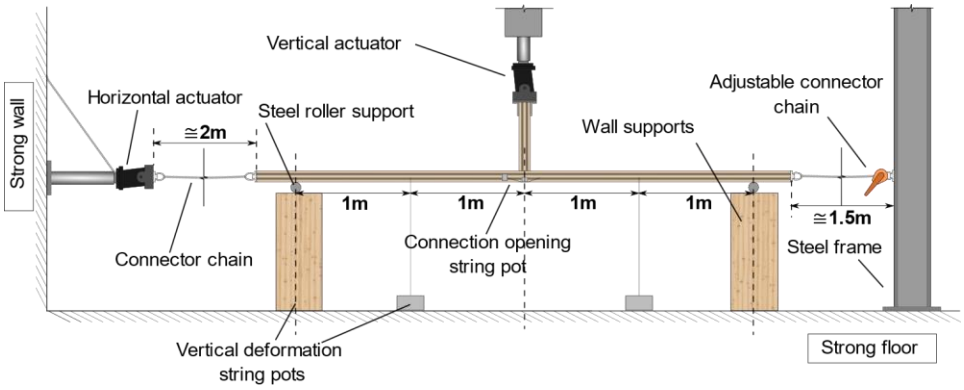

b)

Figure 6. 1 Experimental setup diagrams for 3m (top) and 2m (bottom)

The problem with comparing tests of different spans while section size and connection design remain unchanged is the increase in relevance of the compressive arching alongside the increase in the section depth to span ratio. To mitigate that issue, the tension was applied utilising chains rather than fixing the support to another member or directly to the strong wall, while the sample rested above steel rollers.

a)

b)

Figure 6. 2 Experimental setup 3m span (a) and 2m span (b)

That way, there was no horizontal compressive reaction possible aside from friction from the rollers which can be assumed to be negligible. Therefore, in this setup compressive arching was eliminated. The load was applied by two actuators both of 500mm maximum stroke, one vertically at midspan for pushdown and one installed horizontally on one end of the assembly for axial load application.

The full-scale experimental setup was similar to the Setup B in component tests (Section 5.2.1), tested during the same experimental campaign but under different parameters and with increased span and width of the specimen. No full-scale equivalent was made for component Setup A as limited material availability in the institution at the time meant that component tests were the most economical way forward and therefore Setup A was not designed to accommodate larger specimen.

The tube connector (described in detail in sections 0), which has been tested alongside traditional floor-to-floor connections, has been specifically designed for the ability to deform plastically exhibiting high ductility, and since it was expected to outperform the other joints by an order of magnitude, some adaptations had to be made to the test setup. The end connections for tension application were changed from perpendicular screws to a stronger dowel connection, allowing for testing the tubes fuller capacity. Moreover, the pushdown test was performed in two stages, after initial deformation the vertical load was removed and a wall stub with additional 200mm height was introduced to be able to test the tube to its full capability.

6.2.2. Specimen characteristics

CLT panels used were edge bonded Binderholz BBS 125 100mm 5-ply of even layers 20mm in thickness, produced with C24 strength class Norway spruce (*Picea abies*). The moisture content was 10%, recorded near the time of experiment. Cutting and milling of the panels and other timber components was done on site at the University of Northern British Columbia structures laboratory. Four types of connections were tested in total: butt joint, double incline butt joint, single surface spline connector and the novel tube connection. The detailing of each of the connections can be seen in the figures 6.3 – 6.6. fully threaded self-tapping screws (STS) manufactured by SWG (Schraubenwerk Gaisbach GmbH) were used for all of the connections.

For the regular butt joint 8 mm diameter 140 mm long screws were installed at 45° angle to the vertical. Double incline used the 8 mm diameter 140 mm long STS which were installed at 45° angles both in plan as well as the side view. Both butt joint variants tested a 6-screw variant and a 4-screw variant, the 4-screw variant maintaining the position of the two edge pairs from the 6-screw and removing the central pair, as depicted in Figure 6. 3 and Figure 6. 4 Spline connection used the 8 mm diameter, 100 mm long screws which were installed through the plywood perpendicular to the surface of the panels. Two arrangements of screws were tested, 8-screw variant and 6-screw variant, differentiated by numbers (1) and (2) respectively in the Figure 6. 5, both maintaining even spacing between the screws and the same edge spacing between the two variants.

For the tube connector specimen depicted in Figure 6. 6, the 4-screw butt joint variant was included, as the tube connector would not be used alone in regular design scenario - since the tube connection does not the have the ability for accommodating

moment and shear strength as well as rotational stiffness therefore the “traditional” connection would need to be used alongside it. However, as the capacity of the tube connector in catenary is thought to be much higher, it is thought to have minimal impact which can be confirmed thorough comparison with the regular 4-screw butt joint test results. The steel used for the tube was A/SA 106 Grade B (minimum yield strength 240 MPa). The tube was 3 inches (76.2 mm) external diameter, 100 mm in length, and 3 mm in thickness. The steel rods used were fully threaded ASTM A193 grade B7 with a diameter of 19.1 mm. Their mean yield and ultimate load-carrying capacities were determined on six samples. The yield and peak loads $F_{y,r}$ and $F_{max,r}$ were on average 170 kN and 190 kN, respectively, with the coefficients of variation (CoV) of 1.1%. Ductility, μ_{Rod}, calculated in accordance with ASTM E2126 as the ratio of ultimate to yield displacement was roughly 7, therefore these rods can be classified as highly ductile (T. Tannert, personal communication, 6 April 2023).

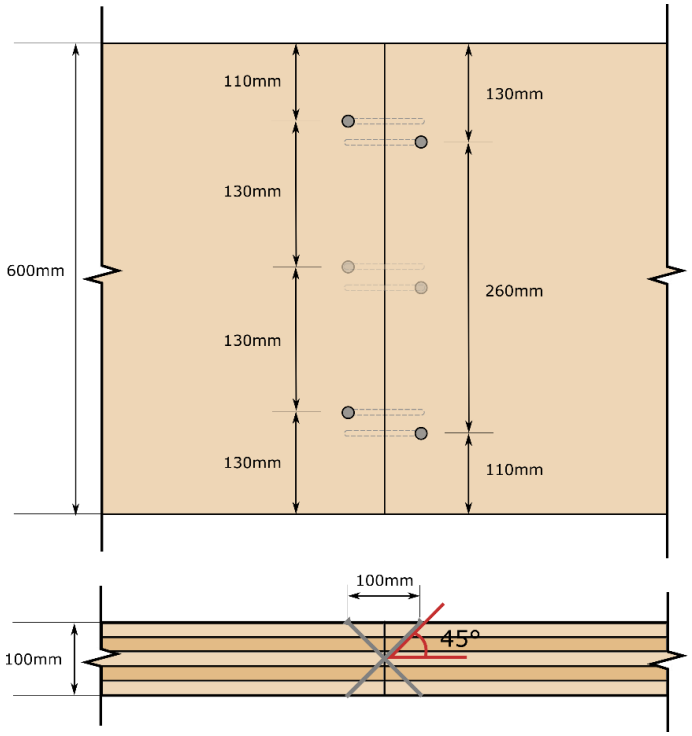

Figure 6. 3 Butt joint connection design

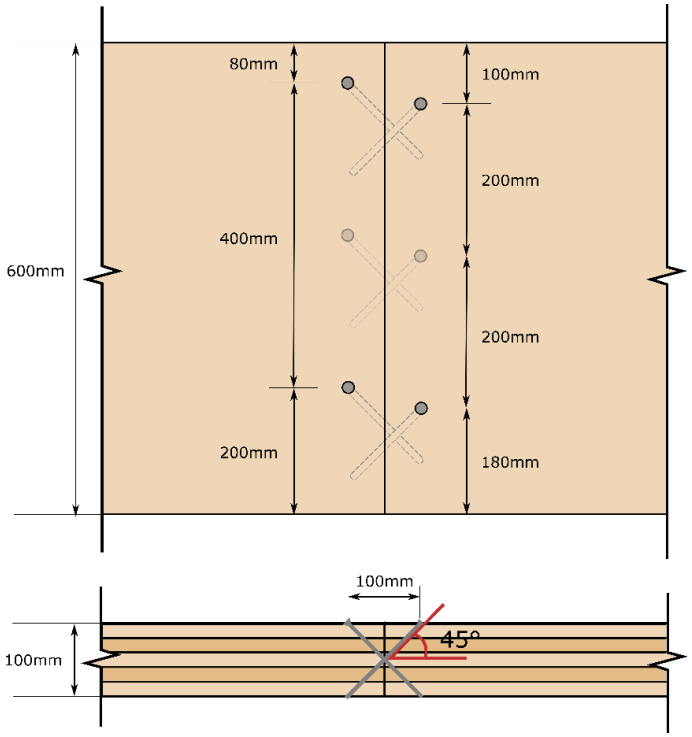

Figure 6. 4 Double incline (DI) butt joint connection design

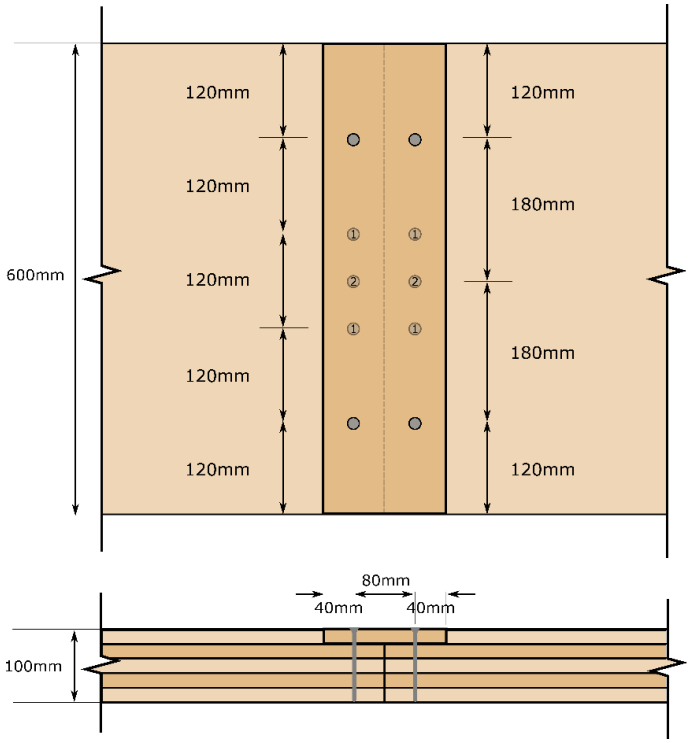

Figure 6. 5 Single surface spline connection design

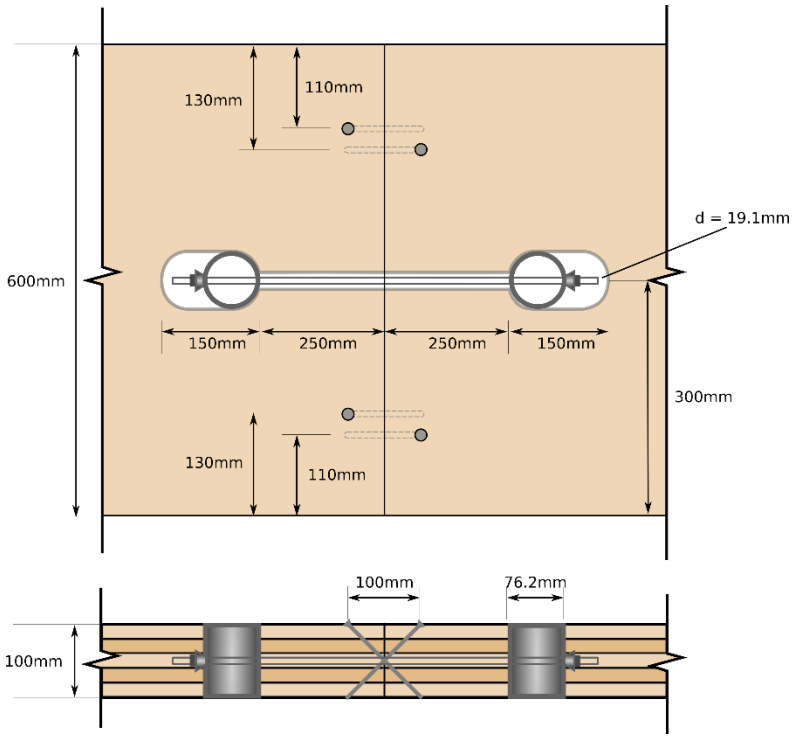

Figure 6. 6 Tube connection design (installed alongside regular butt joint)

6.2.3. Testing plan and variables

Large scale testing requires high volume of time, labour, and materials, therefore a testing plan needed to be designed in a way that allows for the best use of those resources. The two paths of investigation were chosen. Firstly, a detailed investigation, changing a variety of load combinations and support conditions, primarily looking into the influence of those conditions on the capability of the connection to achieve catenary action. Secondly, several test series were performed on three additional types of joints, with the main intention of comparing the performance between the types of connectors.

For the joint investigated in detail, the butt joint was chosen, commonly used in the industry due to its simplicity of implementation. Five parameters were changed across the butt joint test series, summarised in Table 6. 1. The first is the point of load application through the wall stump, which was either done by placing the wall loosely on top (L -*loose)* or attaching the wall stub with one pair of Simpson ABR105 CLT angle bracket angle brackets (Figure 6. 7) installed on both sides close to the centre (A - *anchored).* The second parameter was the support condition which was either simple *pin* (P) or simulated double continuous span behaviour through restraining the overhang (*restrained).* The tests had either 6, 4 or no screws (*#screws*). The series with no screws (N) relied solely on the angle brackets (S5-N-P-A-15) and was performed as a control of the remainder of the tests using that connection alongside the butt joint.

The last variable was the manner of horizontal load application. The experimental setup allowed to perform load holds of constant horizontal tension (15 and 30kN), allowing to investigate load combinations irrespective of the geometry and stiffness

of the system and therefore compare the joints to one another under the same load combinations. However, a test series was also designed to investigate the maximum tension developed in the system passively, akin to a real-life scenario of catenary action activation. In that case, the horizontal actuator was set to displacement control at minimal tension needed for taking out the slack out of the system and then locked at that position before the vertical actuator began to apply pushdown at midspan. This case is indicated in the test summaries as fixed (F).

The purpose of comparing these two scenarios was to investigate whether achieving the same load combinations through constant active tension and natural tension gradient will yield comparable results. This in timber is not obvious, since at such extreme deformations the embedment crushing, cracks and other post-elastic region damage will occur.

The supplementary reduced span tests were performed under the simply supported condition for each of the regular connections (Table 6. 2). The last variable investigated was the introduction of a short span spreader beam 4-point bending (S8-4PB-15) as an additional check on the potential effect of the wall stub on the load redistribution within the joint. A decision was made to perform these alongside the 2m tests to allow to record a fuller moment-rotation curves, since the connection in 3m tests was shown to often reach their maximum moment capacity under the gravity loading alone.

The two remaining tests involved three different types of joints – the double incline butt joint, typically used for lateral shear resistance and membrane action (Table 6. 3), single surface spline (Table 6. 4), and a tube connector (Table 6. 5), offering a novel approach to load redistribution.

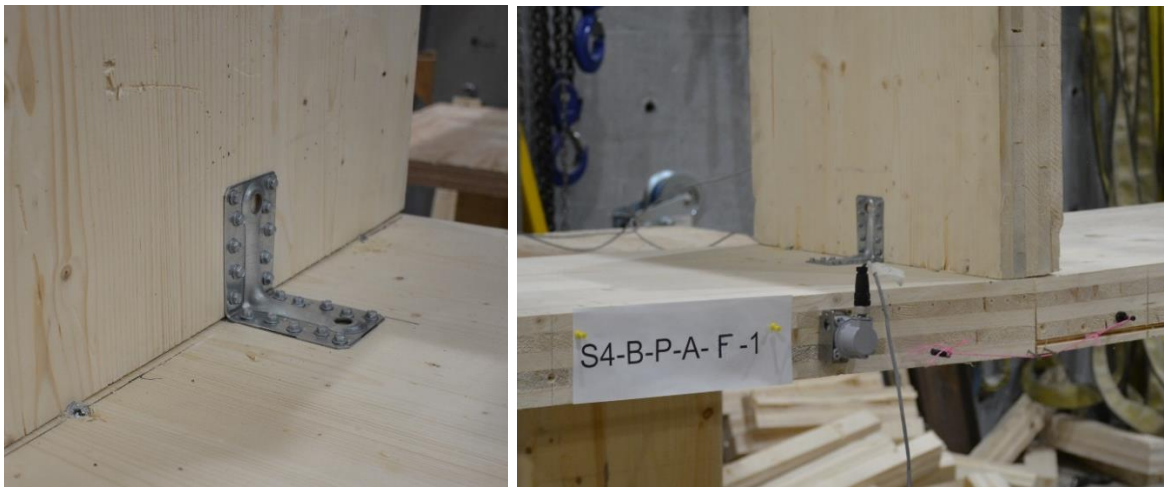

Figure 6. 7 Angle bracket

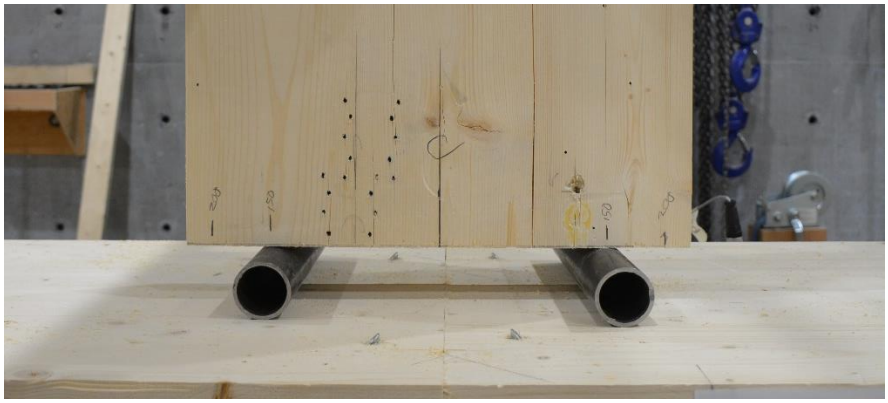

Figure 6. 8 Four-point bending spreader arrangement

The double incline butt joint as well as spline connectors were tested under two tension levels and three tension utilisation levels. The third tension utilisation level was achieved by changing the number of screws used in these samples. The tube connectors were tested under the 30kN load level as well as the *fixed* axial displacement condition with gradual tension development to allow for direct comparison with the overall test series outlined here as well as the literature results, where the passive tension condition is used.

Table 6. 1: Test series overview for butt joint full-span tests

Series	Load	Support	T (kN)	#screws
S1-B-P-L-15	Loose	Pin	15	6
SS1-B2-P-L-15	Loose	Pin	15	4
S2-B-P-L-30	Loose	Pin	30	6
S2-B2-P-L-30	Loose	Pin	30	4
S3-B-P-A-15	Anchored	Pin	15	4
S4-B-P-A-F	Anchored	Pin	Fixed	4
S5-N-P-A-15	Anchored	Pin	15	0
S6-B-P-L-F	Loose	Pin	Fixed	4
S7-B-R-L-30	Loose	Restrained	15	4

Table 6. 2 Test series overview in reduced span tests

Series	Joint	Load	Support	T (kN)	#screws
S8-B-P-L-15	Butt	Loose	Pin	15kN	4
S8-4PB-15	Butt	4-point	Pin	15kN	4
S9-D-P-L-15	DI butt	Loose	Pin	15kN	4
S10-S-P-L-15	Spline	Loose	Pin	15kN	8

Table 6. 3 Test series overview for double incline butt joint full-span tests

Series	Load	Support	T (kN)	#screws
S11-D-P-L-15	Loose	Pin	15kN	6
S11-D2-P-L-15	Loose	Pin	15kN	4
S12-D2-P-L-30	Loose	Pin	15kN	4

Table 6. 4 Test series overview for single surface spline connection full-span tests

Series	Load	Support	T (kN)	#screws
S13-S-P-L-15	Loose	Pin	15kN	12
S13-S2-P-L-15	Loose	Pin	15kN	8
S14-S-P-L-30	Loose	Pin	30kN	12

Table 6. 5 Test series overview for tube connector full-span tests

Series	Load	Support	T (kN)	#screws
S15-T-P-L-30	Loose	Pin	30kN	4
S16-T-P-L-F	Loose	Pin	Fixed	4

6.3. Results and discussion

The summary of all of the standard full-span connection tests is shown in Figure 6. 9. The legend for the test types captioning can be found in Table 6. 6. The results are presented in form of the map between two values which are indicative of the ability of the connection to form catenary action. The y-axis depicts ratio of midspan deflection at the point of failure to the single span of the floor, which is used to describe the minimum necessary deflection for achieving the catenary action formation, and therefore is one of important predictors of good load redistribution capabilities. The x-axis shows the tension values read from the horizontal actuator load cell at the point of failure, normalised to the maximum axial tension test results from Chapter 5.

Presenting the relationship between these two values allows for visual investigation of the test results where, broadly speaking, further along both of the axis to the top right the better potential for good catenary action activation. It is vital to understand however that this is only indicative of the approximate performance differences between the tests of different parameters and is not to be taken as a definitive measure of the appropriateness of the connection for use in robustness design. The dashed line at 15% deflection ratio on the y-axis signifies the minimum deflection required for collapse prevention according to the ASCE/SEI 41-13 (ASCE, 2014) and the 11.3% dashed line corresponds to the requirement for life safety, both values discussed in more detail in Chapter 2.

Table 6. 6 Test captioning legend

	Connection	Support	Wall detail	Tension
B-P-L	Butt joint	Pin	Loose	Active
B-P-A	Butt joint	Pin	Anchored	Active
B-P-A-F	Butt joint	Pin	Anchored	Passive
B-P-L-F	Butt joint	Pin	Loose	Passive
B-R-L	Butt joint	Restrained	Loose	Active
D-P-L	DI Butt joint	Pin	Loose	Active
S-P-L	Spline	Pin	Loose	Active

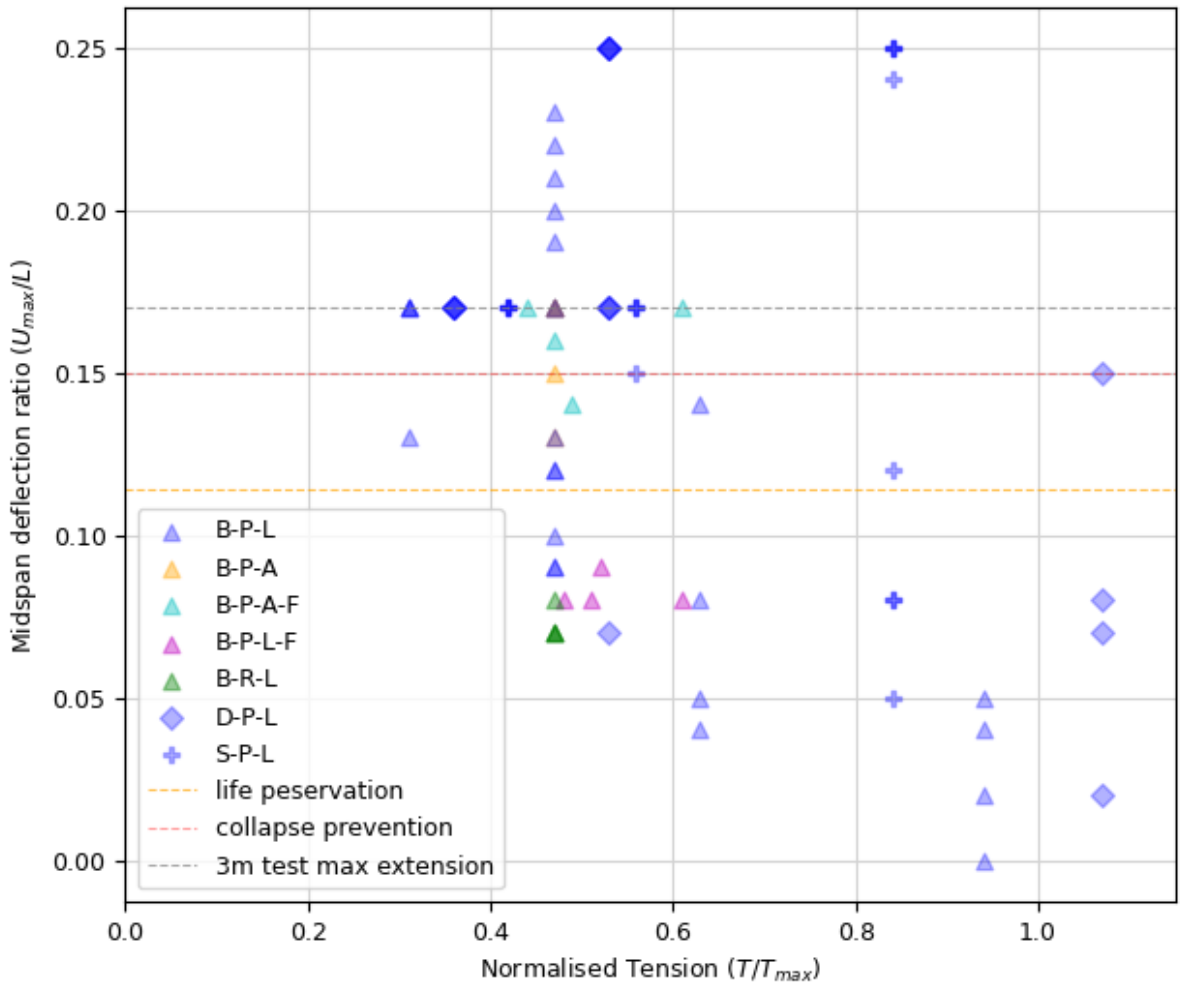

Figure 6. 9 Test results depicting the tension utilisation and midpsan deflection ratio values.

This graphic representation of results allows for the observation of the biggest difference in performance between the spline connection and the butt joint. The spline continues to perform well past the 0.8 tension utilisation mark, however with increasingly variable results. Similar behaviour may be observed in the double incline butt joint, with the butt joint seemingly increasing the tensile capacity past 1.0 normalised tension (uniaxial testing resulted in mean of 28.1kN, for this series while load hold imposed was 30kN) It appeared that the redistribution of internal forces due to the large rotations allowed for the deflected connections to outperform the ones loaded only axially. This trend cannot be observed in the regular butt joint despite other similarity between the series. Mapping of the results relating to the parameters within the butt joint allowed for first impressions of the general influence of the other variables on the catenary behaviour of the subassembly.

For instance, the specimen with the wall stub anchored with steel brackets under constant horizontal load hold (B-P-A) have shown a behaviour consistent with the load hold specimen without the brackets (B-P-L), with the anchored specimen result placing around the median value of the loose wall specimen. However, when comparing the non-anchored and anchored specimens under the fixed horizontal restraint (passive tension) instead of active load (B-P-L-F versus B-P-A-F) the discrepancy of the rotational capacity becomes visible, with the anchored specimen able to achieve a better deformation overall. The loose wall passive tension specimens (B-P-L-F) also generally stayed within the range of the active load hold tension specimen results (B-P-L) at similar tension levels, however noticeably grouping on the lower end of the rather broad spectrum of displacements. This is investigated in more detail in Section 6.3.1.1.

Maximum force, displacement, moment, and rotation values recorded for each test are summarized from Table 6. 7 through to Table 6. 12. One of the challenges of full-span testing was the relatively low vertical stroke to span ratio, which led to some of the samples not failing throughout the duration of the test (greyed out fields), meaning that their maximum values will likely be larger than the tabulated data shown. This was particularly true for lower utilisation levels. This was one of the reason the reduced 2 metre span tests have been introduced to allow for a deeper span to vertical displacement ratio, exceeding 17% span L.

For all of the tests using the pin connection support condition the panel bending checks were performed through projecting the midspan deformation value from sets of string pots at increments of 1m on both sides. The example below (Figure 6. 10) shows that values projected from string pots are a perfect match and therefore minimal bending is occurring in the panels under those conditions.

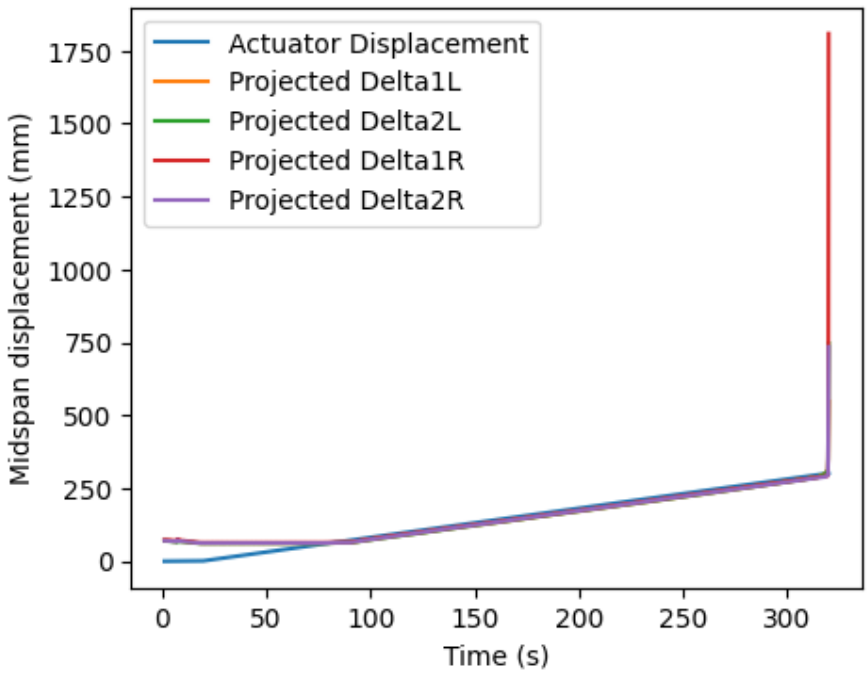

Figure 6. 10 Projected midspan deformations from string pots versus the actuator displacement values

6.3.1. Butt joint

The numerical representation of results of the butt joint is shown in Table 6. 7. The butt joint was the specimen that was investigated in most variants and details, and therefore the following section includes discussion of the performance of the butt joint as well as attempts to answer some more general question about the influence of the parameters on the catenary of the subassemblies. Although the findings can be seen as connection specific, they can be representative of the type of influence those parameters would have on connections which redistribute loads in a similar manner (these connections would include the Double Incline butt joint as well as half-lap connections presented in Chapter 5, and considered in detail in Chapter 7, where their similarities are discussed in detail).

In the butt joint series there were numerous specimens, mostly within the 15kN load hold specimen, that were not able to be tested to failure after reaching the maximum stroke. The 6-screw variant at 15kN load hold specimen resulted in such censored data in 3 out of 4 specimens.

Table 6. 7: Full span butt joint test results summary

Series	P_{max} (kN)	Δ_0 (mm)	U_{max} (mm)	θ_{max} (rad)	U_{max}/L (%)	M_{max} (kNmm)	Fail (y/n)
S1-B-P-L-15	5.53	42.83	456.91	0.167	17%	1403.95	n
	5.81	42.76	457.21	0.167	17%	1631.45	n
	5.57	8.79	394.48	0.135	13%	2068.12	y
	5.68	22.44	480.63	0.168	17%	1878.55	n
S1-B2-P-L-15	5.30	58.59	444.65	0.169	17%	1728.92	n
	2.29	44.65	208.58	0.219	22%	959.38	y
	2.44	72.52	222.73	0.099	10%	992.89	y
	2.07	75.84	193.54	0.090	9%	784.43	y
	3.36	80.05	266.25	0.116	12%	1277.14	y
	5.17	82.24	416.36	0.167	17%	1573.26	n
S2-B-P-L-30	3.05	41.11	116.10	0.052	5%	1385.98	y
	2.46	43.67	89.45	0.044	4%	1236.88	y
	8.31	54.76	357.85	0.138	14%	1463.58	y
	4.26	52.60	188.06	0.080	8%	1324.72	y
S2-B2-P-L-30	1.90	60.72	68.84	0.043	4%	417.75	y
	0.02	0.00	0.00	0.000	0%	1.11	y
	2.06	55.94	81.48	0.046	5%	885.86	y
	0.43	57.35	13.05	0.023	2%	4.95	y
S3-B-P-A-15	5.12	22.00	431.24	0.152	15%	2298.80	y
	4.25	19.95	368.08	0.130	13%	2344.34	y
	5.20	19.04	483.72	0.168	17%	2086.11	n
	5.34	21.84	481.04	0.168	17%	2214.84	n
S4-B-P-A-F	3.39	94.34	408.50	0.168	17%	1286.43	n
	3.72	107.10	392.96	0.167	17%	1288.48	n
	3.68	65.76	400.24	0.156	16%	1421.13	y
	2.99	72.15	335.28	0.136	14%	1428.93	y
S5-N-P-A-15	0.54	9.81	0.00	0.003	0%	2212.47	y
	0.55	73.85	39.94	0.038	4%	1595.43	y
	0.24	50.50	0.00	0.017	2%	1648.39	y
S6-B-P-L-F	2.86	90.98	153.20	0.081	8%	1362.03	y
	2.26	109.84	159.18	0.090	9%	1270.89	y
	1.96	74.69	155.99	0.077	8%	1414.78	y
	1.73	121.02	109.97	0.077	8%	1135.04	y
S7-B-R-L-15	16.49	23.88	198.22	0.074	7%	1168.31	y
	15.25	21.62	195.44	0.072	7%	1471.04	y
	14.09	20.07	180.00	0.067	7%	1582.55	y
	18.31	22.74	222.03	0.082	8%	1236.23	y

The maximum tension values at supports for these test series are shown in Table 6. 8. The presence of angle brackets connecting the wall stub to the floor panels did not have a great influence on the maximum tension capacity; however, it did allow for a greater deformation, which positively affects the overall force capacity presented in Figure 6. 11.

Table 6. 8 Maximum tension in the fixed horizontal displacement tests

	T_{max} (kN)	U_{Tmax} (mm)
S4-B-P-A-F	14.0	243.5
	19.4	227.8
	15.0	167.6
	15.7	185.6
mean	16.0	206.1
CoV	15%	17%
S6-B-P-L-F	19.5	152.9
	16.5	120.6
	16.3	155.9
	15.2	113.8
mean	16.9	135.8
CoV	11%	16%

Force displacement curves of the standard simply supported series S1 and S2 (with active tension application and loose wall detailing) can be seen in Figure 6. 11. The detailed results of the remainder of the series are discussed in more detail in further sections. The stiffness of the system is largely governed here by the tension and therefore the test series S2_B and S2_B2 (Figure 6. 11b and d), which are under 30 kN horizontal load hold, are visibly stiffer in comparison to the S1_B, S1_B2 (Figure 6. 11a and c), which were loaded with 15kN. Notably, the number of screws (S1_B and S2_B with 6 screws total and S1_B2 and S2_B2 with 4 screws total) did not visibly affect the stiffness. Although the best performing singular specimen was observed in the S2_B series (Figure 6. 11b), the variability of the results in this series

brings the median down significantly. The samples that have been tested to full failure were observed to have failed in screw withdrawal, an example of which can be seen in Figure 6. 12. The screw withdrawals were generally characterised by withdrawal of the threaded end from the timber, however some did show a head pull-through. This did not seem to follow a specific pattern. In both cases of withdrawal, a pullout and splitting of the crosswise layer has occurred. In most cases the layer split travelled close to the edge of the sample (Figure 6. 12 right), on average up to around 20mm from the edge, however in some cases the layer fault did travel to the edge fully (Figure 6. 12 left).

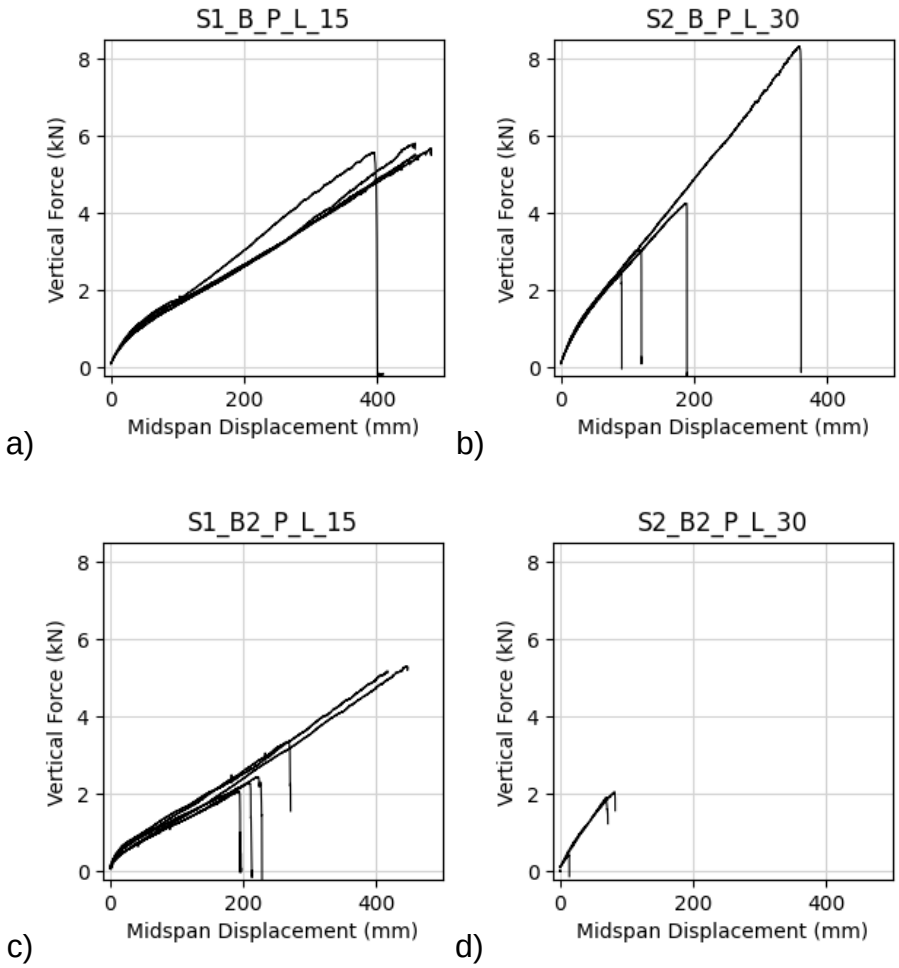

Figure 6. 11 Force displacement curves of the four variants of simply supported butt joint full-span test

Figure 6. 12 Screw failures in S2-B-P-L-2 sample

6.3.1.1. Influence of wall bracket anchoring

The addition of wall brackets, like the inclusion of an additional pair of screws, did have a positive effect on the ultimate load and moment capacity and maximum deformation/rotation as seen in Table 6. 7 and Figure 6. 13. The biggest positive difference can be seen in the Figure 6. 13b), depicting the passive tension formation. The addition of brackets was seen to increase the deformation capacity by over 2 times, allowing for a corresponding increase in the vertical force capacity. The effect of the additional brackets in samples S3-B-P-A in the load hold is less apparent, showing almost exactly the same behaviour as their S1 counterparts under the same 15 kN loading, however it can still be seen. It is thought that if the samples were able to be tested to failure, this effect could be replicated.

Figure 6. 14 depicts the tensile loads which developed in both of the passive tension tests. The samples with no angle brackets were not able to maintain the tension past the peak, resulting in absolute failure of the samples. The brackets in allowed for a very favourable ductile behaviour of the samples, which can be attributed to the deflections in the brackets as presented in Figure 6. 15. It is thought that potentially

if brackets with longer upper parts were used, this effect could be further increased to the advantage of robustness design.

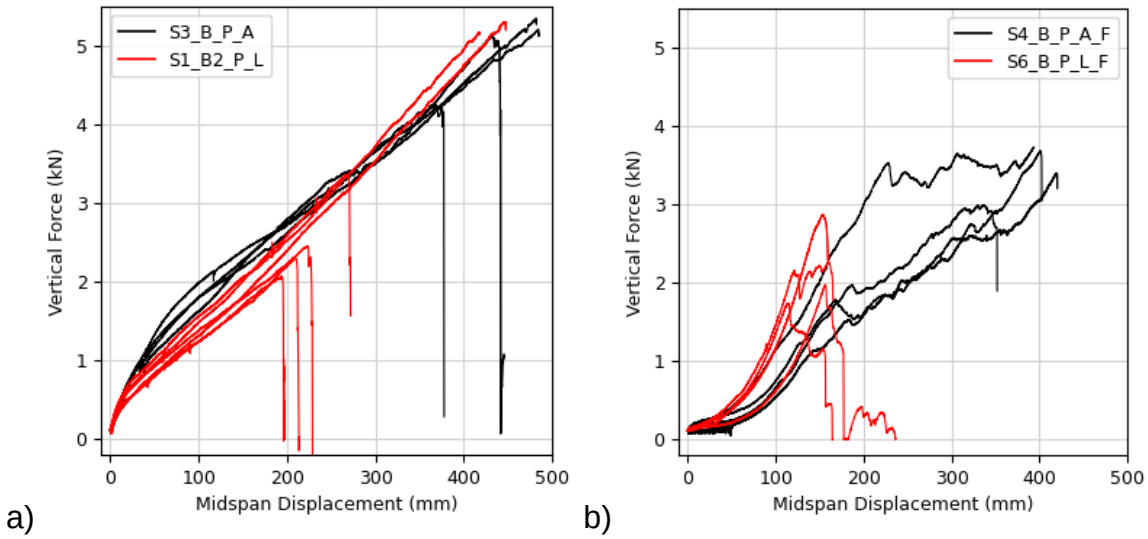

a) b)

Figure 6. 13 Comparison of the influence of the wall bracket anchor influence (a) under constant tensile load and (b) under fixed horizontal displacement at the supports

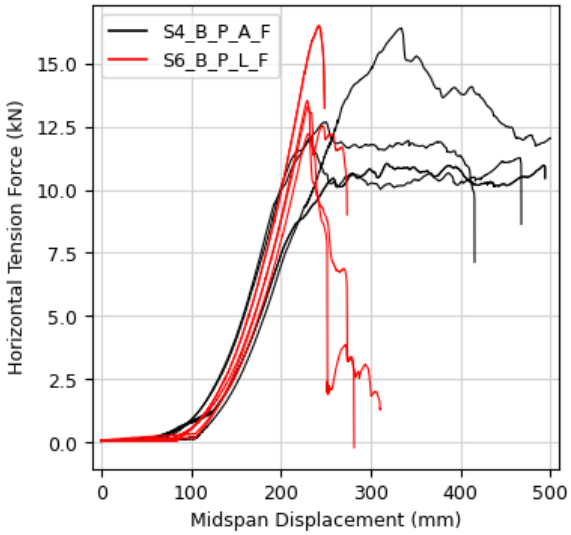

Figure 6. 14 Tension developed at the connection in the fixed horizontal displacement at support specimen with and without wall bracket anchor

Figure 6. 15 Angle bracket deformation examples

a) 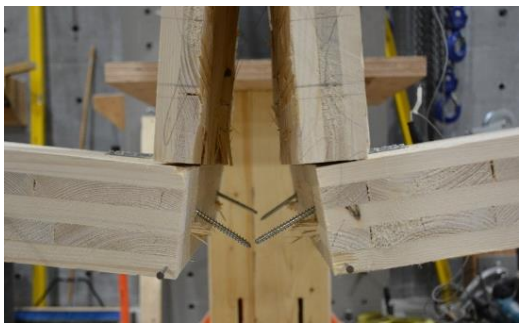 b) 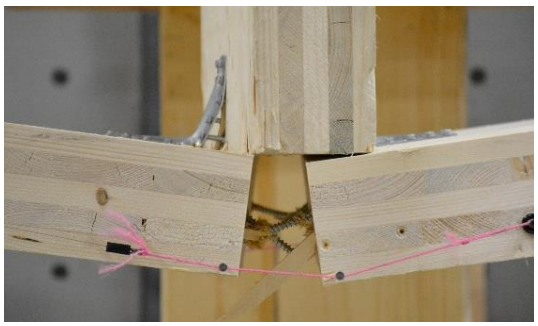

Figure 6. 16 Failure with wall splitting (a, S3-B-P-A-15), failure without wall splitting (b, S4-B-P-A-F)

However, it must be noted that an unexpected behaviour was observed when the wall stub completely split apart due to the tensile forces imposed upon it from the brackets as seen in Figure 6. 16a. This was more likely to occur in the load hold samples and was not observed in all specimens in either of the series; sometimes the total failure occurred as expected purely in the connection (Figure 6. 16b). This failure mode should be kept in mind if attempting to use the angle brackets as a tie force reinforcement in the robustness design.

6.3.1.2. Active versus passive load application

To answer whether it matters how we achieve a certain combination of loading – progressively increasing the tension versus sustaining the same level of load throughout – a comparison was made between the load profiles of the load hold samples and passive tenseion samples. These are shown below in Figure 6. 17, Figure 6. 18 and Figure 6. 19. The shape of the load displacement curve is strongly influenced by the way in which the axial tension is applied, which confirms that the catenary action is the primary load resistance mechanism. For instance, in the test series with passive tension formation (S4 and S6), the stiffness of the system increased throughout the test (Figure 6. 17, Figure 6. 19), while the load hold examples after the first 10-20mm of vertical deformation have maintained linear force displacement curve relationship for the remainder of the test until failure Figure 6. 18.

The comparisons of the effect of wall brackets in section 6.3.1.1 has already pointed to the different level of influence this connection makes between the active and passive tension application techniques. Figure 6. 9, Figure 6. 13 and Table 6. 7 show that both the maximum force capacity as well as the maximum rotation achieved allows for the anchored specimen to position themselves in the range of higher outliers of the load hold specimen. The load hold tests seem to allow for greater deformations and therefore yield a higher vertical force resistance. This could be due to the fact that, in the load hold tests, if the connection has some remaining strength after that initial peak, but reduced stiffness, this will allow for greater deformation and therefore decreased tension demand, allowing to potentially achieve load equilibrium once again. However, the majority of these connections being relatively brittle do not have a large enough residual strength to be able to accommodate the resulting kinetic

effect. Moreover, with the large variability of timber, especially in the region close to failure, it would not be safe to rely on this behaviour past the peak strength as a robustness design feature. Another possible explanation for the differences in behaviour is that the moment at the connection in the early stages of the deformation in the passive tension samples will be higher due to the low catenary effect. This could mean that the samples are being brought closer to their ultimate moment capacity and then unloaded in moment as the tension takes over, causing some initial damage which does not allow for the final results to achieve the same deformation.

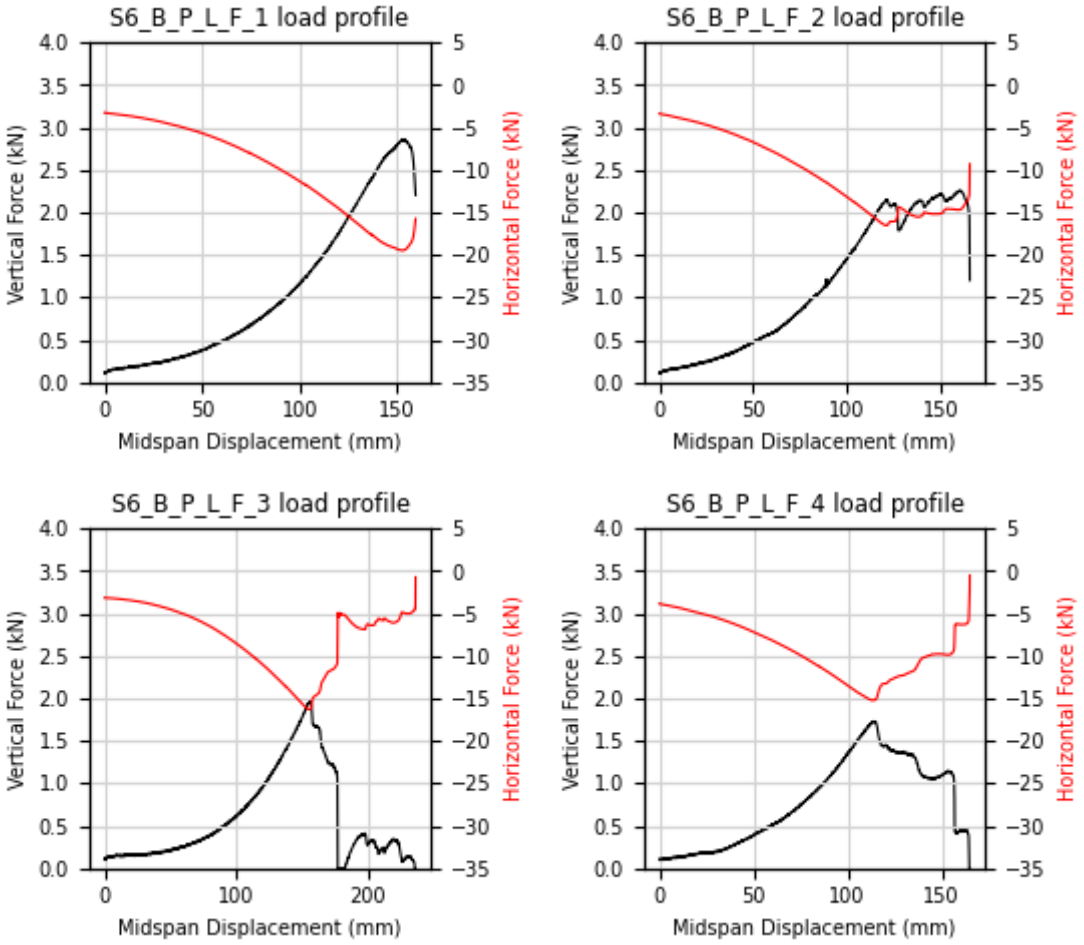

Figure 6. 17 Catenary action activation load profile for samples with no angle brackets

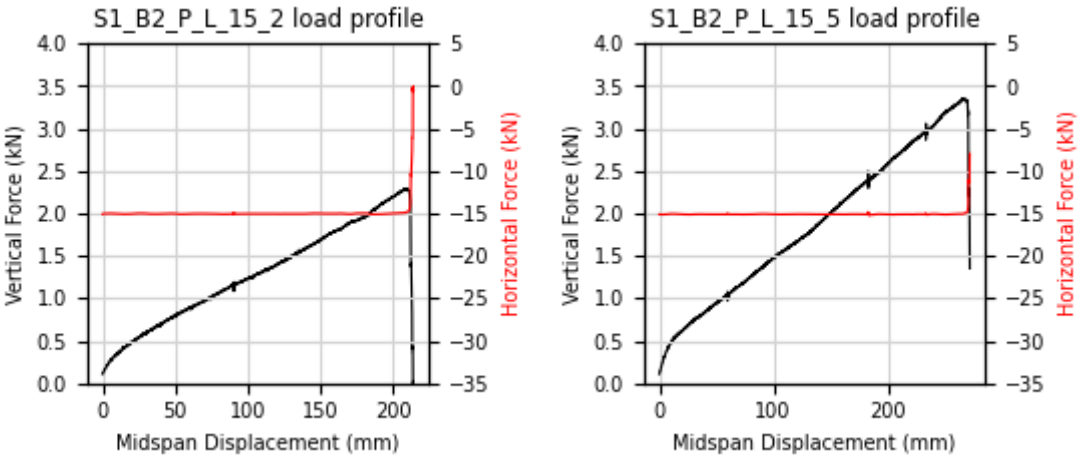

Figure 6. 18 Examples of load profiles from the equivalent load hold samples

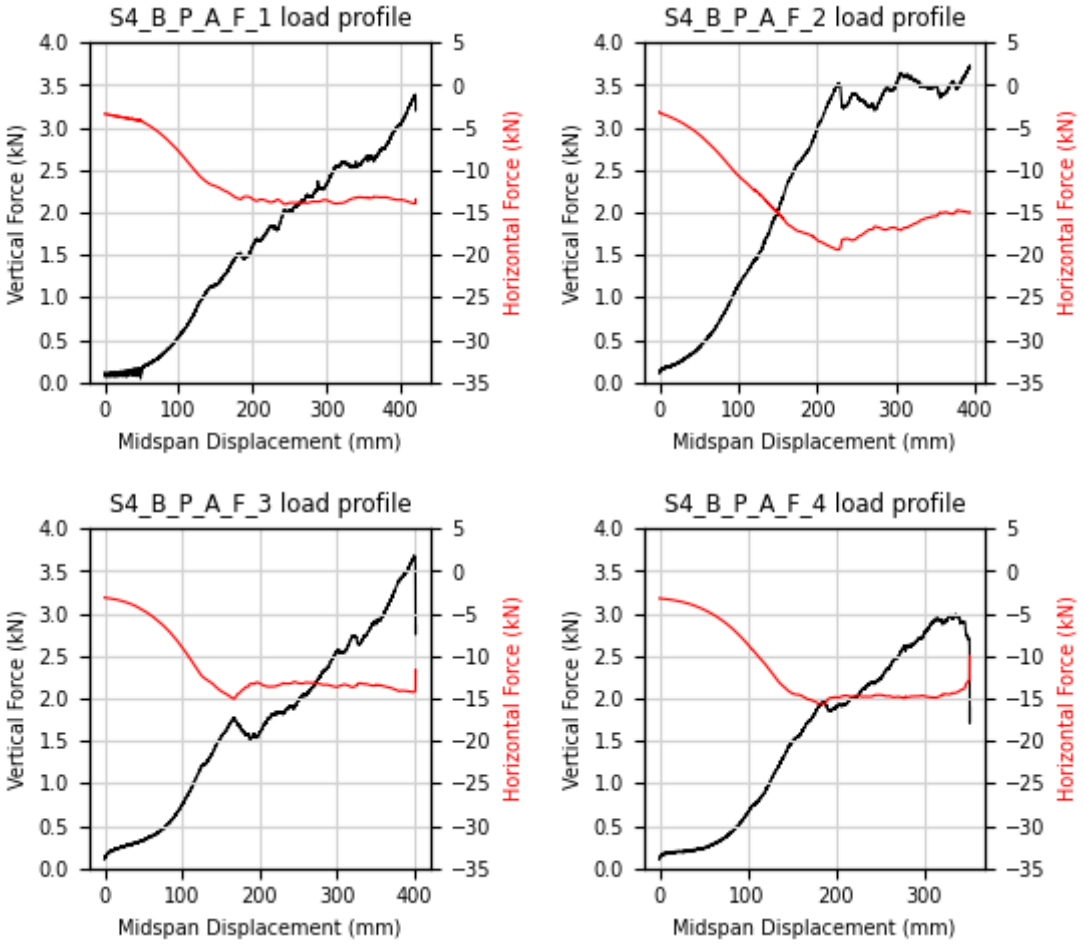

Figure 6. 19 Catenary action activation load profile for samples with angle brackets

It is important to note that changes in strength can be attributed to the high variability in of the material that is wood. The load hold specimen on their own exhibit a very wide range of strengths and rotation capacities, with the load hold specimen fitting within the ranges. The wall bracket presence does influence the repeatable results of where those results fit within the range, increasing their force and deformation capacities. The above results show that the influence of the internal load redistribution in catenary action testing especially in the case of large rotations could potentially be significant and should be considered when designing an experiment.

6.3.1.3. Continuous span

Samples with the continuous span have produced the highest vertical force resistance of 14-18 kN, with more than 3x higher resistance than the catenary action. The failure mode of these samples was initially rolling shear in the traverse layers and eventually tensile splitting of the uppermost layer (Figure 6. 21). In all of the samples coinciding rolling shear failure was observed at the locations of the tensile failure (Figure 6. 22) The test was stopped after this first load drop off due to the panel failure and before the ultimate failure of the connection due to safety concerns. The maximum moment exhibited by the connection was on average lower than but approaching the values in series S1-B2 of the equivalent connection properties and magnitude of tension applied. This explains lack of connection failure but also implies that it was imminent, and the overall force capacity of the system was unlikely to rise back up above the initial peak. In this case the catenary action plays a secondary load redistribution role, with the cantilever being the primary alternative load path in this scenario due to the relatively high stiffness of the panels. This although a viable

load route, does mean there would be a significant uplift force on the other side of the support, and this would need to be considered in design.

Another danger of such arrangement is that due to the axial stiffness of the supports, the only possible way of horizontal deformation is at the connection itself. If a wall is supported on top of such system, a possibility arises where the wall can slip through downwards, causing a large amount of energy to be released which could have significant consequences (which was the reasoning behind the premature stopping of the test despite not reaching full test stroke).

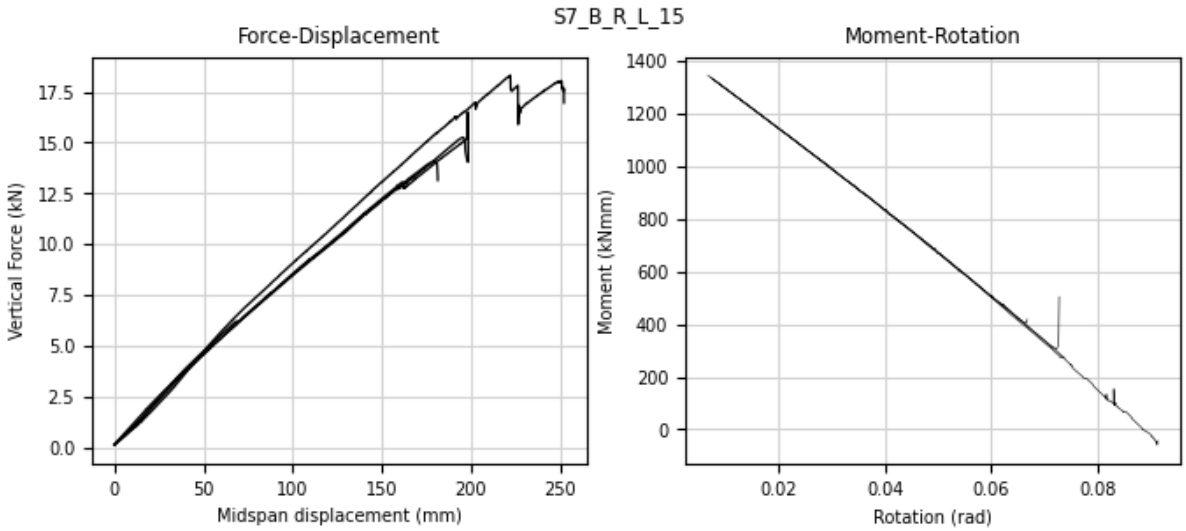

Figure 6. 20: Selected axial load hold tests force displacement curves

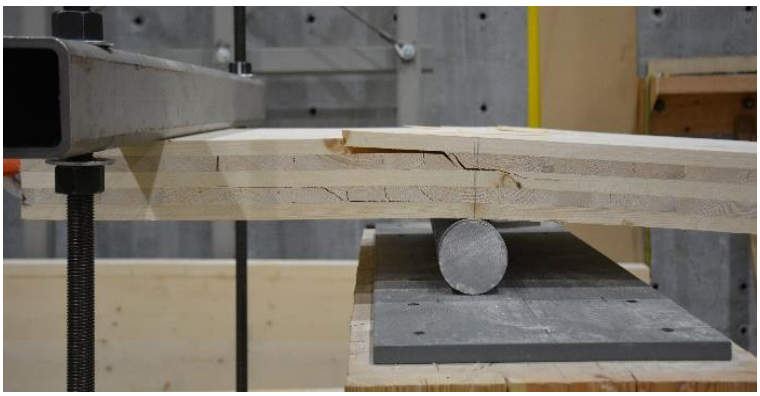

Figure 6. 21 Failure of the panel over the support in test series

Figure 6. 22 Rolling shear failure with tensile failure at the top over the knots

6.3.2. Double incline butt joint

The numerical summary of the full-span test results of the double incline butt joint are shown in the Table 6. 9. Overall, the joint has shown a higher strength than the regular butt joint, despite performing almost identically during the axial tension tests. The major difference there was the small increase in the post-peak behaviour ability with the residual tension which seems to have induced a major improvement in the ability for development of the catenary action. One of the major differences observed between the 6-screw (S11-D) and 4-screw (S11-D2) variants was the displacement under gravity loading Δ_0, which was within the 3.88-27.17mm range for the 6-screw and 66.23-96.15mm for 4-screw. The maximum moment observed in the 4-screw was also significantly smaller, however the overall load capacity for the non-failed samples here was shown to be comparable with the moment of the 6-screw samples.

Table 6. 9 Full span double incline butt joint test results summary

Series	P_{max} (kN)	Δ_0 (mm)	U_{max} (mm)	θ_{max} (rad)	U_{max}/L (%)	M_{max} (kNmm)	Fail (y/n)
S11-D-P-L-15	5.64	20.81	481.72	0.168	17%	1783.96	n
	5.26	13.58	489.30	0.168	17%	1764.20	n
	5.40	27.17	475.74	0.168	17%	1576.95	n
	5.78	3.88	498.68	0.168	17%	1724.51	n
S11-D2-P-L-15	4.66	71.45	425.53	0.166	17%	844.42	n
	4.85	66.66	433.20	0.167	17%	982.34	n
	6.13	96.15	405.41	0.168	17%	1581.96	n
	1.64	66.29	132.08	0.066	7%	1080.39	y
S12-D2-P-L-30	4.24	47.91	194.69	0.081	8%	835.40	y
	1.52	8.27	60.19	0.023	2%	1777.75	y
	8.46	49.37	408.30	0.153	15%	728.03	y
	4.22	44.21	163.16	0.069	7%	1454.19	y

There is one sample in the S11_D2 (Figure 6. 23b) series which shows a significant increase in stiffness, as well as total moment and force capacity, comparable with the S11_D ((Figure 6. 23a) series. It is unclear why this occurred, as the specimen reached maximum extension of the vertical actuator before failure of specimen therefore difference in the screw behaviour could not be properly investigated. It is speculated this could be due to fortunate embedment within a higher stiffness knot. The 4-screw 30kN load hold samples seen in Figure 6. 23c again outperforms their single incline butt joint equivalents (Figure 6. 11c), although the high variability would generally deem this behaviour not reliable.

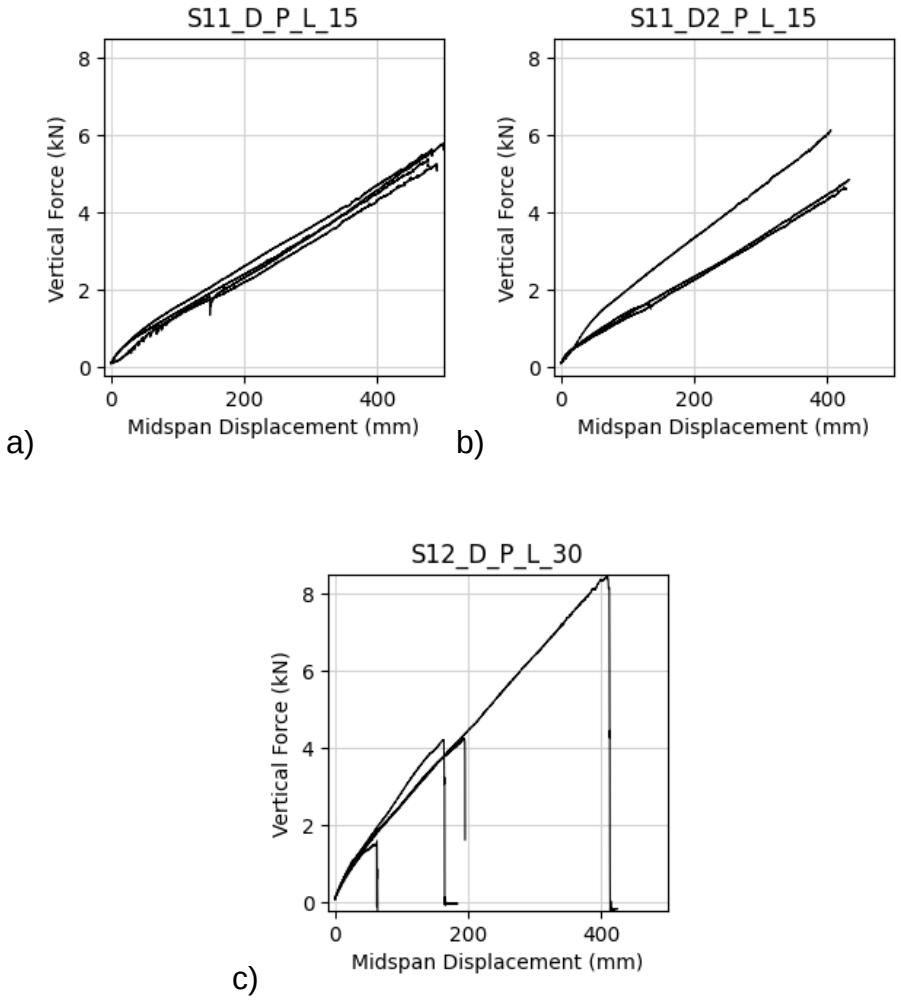

Figure 6. 23 Force-displacement graphs of the double incline butt joint specimen

The failure mode of the DI butt joint has predictably been total screw withdrawal, as pictured in Figure 6. 24. The prevalence of the cross-layer pull-out behaviour has generally been larger in comparison to the single incline equivalent, often with entire sections pulled out across the whole of the sample. This is due to the secondary angle inducing direct pull-out load pressing back against those layers while the single incline only does so through withdrawal effect alone. Overall, the greater performance can be attributed to the longer pull-out distance due to use of longer screws.

Figure 6. 24 Double incline butt joint screw withdrawal failure

6.3.3. Spline joint

The numerical summaries of the spline joint can be seen in Table 6. 10. Majority of the 15kN load hold tests have not failed after reaching the full stroke of the test. Figure 6. 25a) and b) showcase the behaviour of the 8-screw variant and the 6-screw variant of the joint respectively. As seen in these graphs they exhibit the exact same stiffness behaviour, independently of the number of connectors used, which is to be expected considering the plywood spline being the main element of rotation. The lack of stiffness change is here further corroborated by very close values of the initial midspan deformation Δ_0. The change however does occur in the S14 series, these cannot be compared however due to the values being recorded post tensioning and therefore only comparisons can and should be made across samples of the same tension load. Total vertical load in spline samples although slightly lower than the butt joint equivalents, despite achieving a much higher tension utilisation ratio.

The failure modes in every single scenario followed the same pattern of ripping out inner layers of the plywood spline. Some bending was clearly present in the screws, with which the spline was shifting axially out of the indent. No major damage was seen in the CLT at the location of the screws, other than small embedment crushing which facilitated the bending of the screws.

Table 6. 10 Full span single surface spline joint test results summary

Series	P_{max} (kN)	Δ_0 (mm)	U_{max} (mm)	θ_{max} (rad)	U_{max}/L (%)	M_{max} (kNmm)	Fail (y/n)
S13-S-P-L-15	4.32	145.88	357.55	0.169	17%	2627.98	n
	4.81	130.15	372.94	0.168	17%	2639.26	n
	4.68	123.35	379.91	0.169	17%	2480.44	n
	4.54	99.49	403.51	0.168	17%	2224.43	n
S13-S2-P-L-15	4.61	126.84	375.43	0.168	17%	2617.97	n
	4.48	125.09	378.22	0.169	17%	2489.31	n
	3.78	130.72	310.58	0.148	15%	2576.27	y
	4.43	130.18	369.74	0.167	17%	2461.26	n
S14-S-P-L-30	1.50	97.55	61.75	0.053	5%	2904.82	y
	3.75	95.47	153.60	0.083	8%	2897.41	y
	3.60	98.54	151.70	0.084	8%	2869.52	y
	6.43	96.08	275.62	0.124	12%	2898.69	y

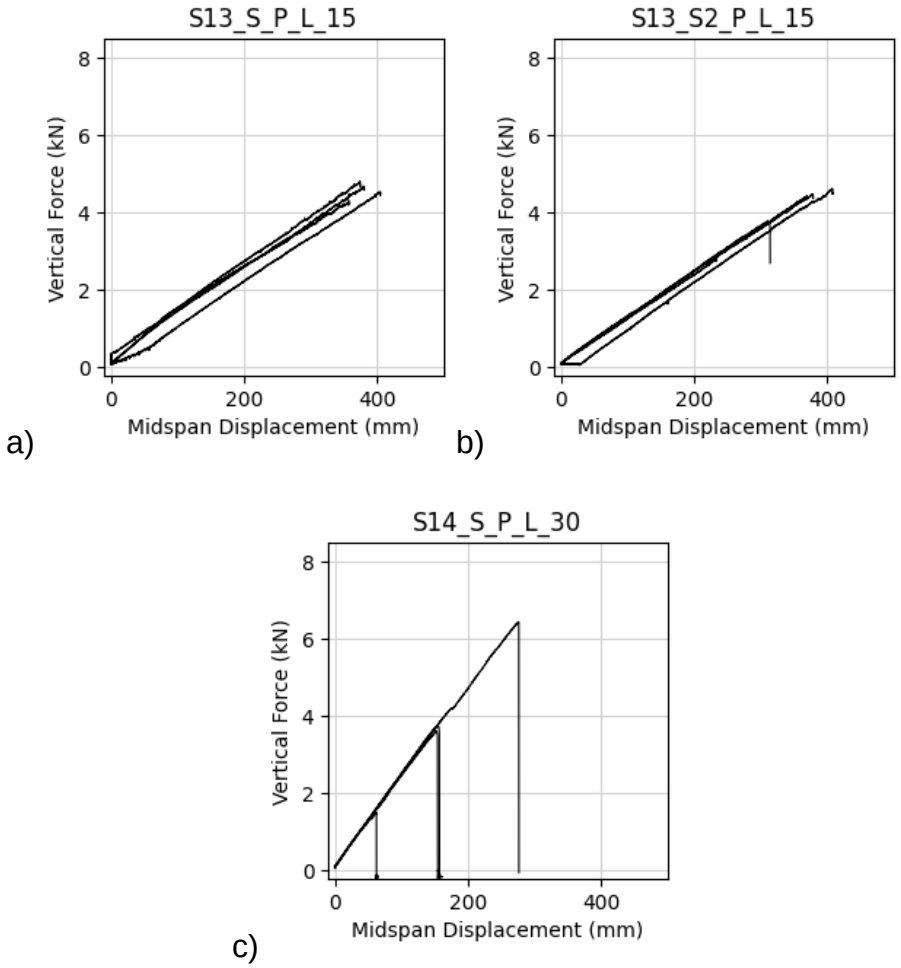

Figure 6. 25 Force-displacement curves of the spline connection specimen

Figure 6. 26 Examples of the spline failure

6.3.4. Reduced span tests

The numerical summary of the 2m test results can be seen in Table 6. 10. The reduced span tests served an important supplementation role to the full-span counterparts, as they allowed for achieving a higher displacement to span ratios in the same setup, when pin-connections were used. Moreover, the self-weight of the sample comprising a smaller fraction of the total load imposed, a more complete moment rotation curves were possible to extract, seen Figure 6. 27, Figure 6. 28 and Figure 6. 29.

Table 6. 11 Reduced 2m span test results summary

Series	P_{max} (kN)	Δ_0 (mm)	U_{max} (mm)	θ_{max} (rad)	U_{max}/L (%)	M_{max} (kNmm)	Fail (y/n)
S8-B-P-L-15	6.80	29.86	371.35	0.202	20%	1345.27	y
	3.67	29.92	214.07	0.122	12%	846.41	y
	3.82	31.67	219.04	0.126	13%	941.38	y
	5.00	33.57	307.19	0.171	17%	845.51	y
S8-4PB-15	6.45	49.67	329.01	0.190	19%	956.91	y
	8.03	48.34	406.45	0.229	23%	1132.76	y
	7.50	41.72	377.32	0.211	21%	1141.20	y
	2.73	41.02	142.45	0.092	9%	921.10	y
S9-D-P-L-15	8.36	45.04	454.71	0.252	25%	962.25	n
	8.44	36.42	463.58	0.253	25%	972.83	n
	7.47	38.20	461.59	0.252	25%	806.76	n
	8.21	51.32	448.34	0.252	25%	835.46	n
S10-S-P-L-15	7.96	85.15	415.27	0.253	25%	2556.34	n
	8.12	82.74	415.97	0.252	25%	2586.55	n
	8.06	84.94	414.87	0.253	25%	2558.26	n
	7.41	87.01	384.89	0.238	24%	2801.32	y

For the majority of the 3m tests these graphs lacked a large portion of the moment-rotation curves at the front, as due to the experimental constraint the gravity loading had to be slowly released manually prior to starting the test. Moreover, less of those tests, especially in the butt joints, were able to achieve full failure. For the samples that did not fail still, the ability to push the rotation further allowed for fuller understanding of post peak moment behaviour, essential for catenary action activation.

The four-point bending test variant comparison can be seen in Figure 6. 30. The tests have shown that although there is a slight indication of an increase in strength and maximum moment achieved before first fracture under the four-point bending. The biggest difference here seems to be the ability to achieve larger deformation signified by the longer and flatter plateau past the peak moment on moment rotation curve in the four-point bending test series. Overall, however the behaviour was comparable.

Observing the resulting graphs, it can be noted that the two best performing connections as the spline joint and double incline butt joint connections, achieving vertical load resistance around the values of 8kN at full extension. None of the double incline joints have failed and only one spline did. Notably the main difference in the double incline versus single incline butt joints was not in the maximum moment but the post peak-moment behaviour, with the moment resistance plateauing with the DI butt joint, while SI kept falling. Spline connection have behaved completely differently in comparison, with the moment increasing alongside the vertical load increase, and failure occurring seemingly at or close after the peak moment was reached. This is due to the failure mode being purely withing the spline alone and once its moment capacity is reached, post-peak behaviour is not possible. The moments achieved

however are very high compared to the butt joint equivalent and it is thought that it cannot be attributed to the spline alone but is connected to its interaction with the wall above. This is discussed in more detail in Chapters 5 and 7.

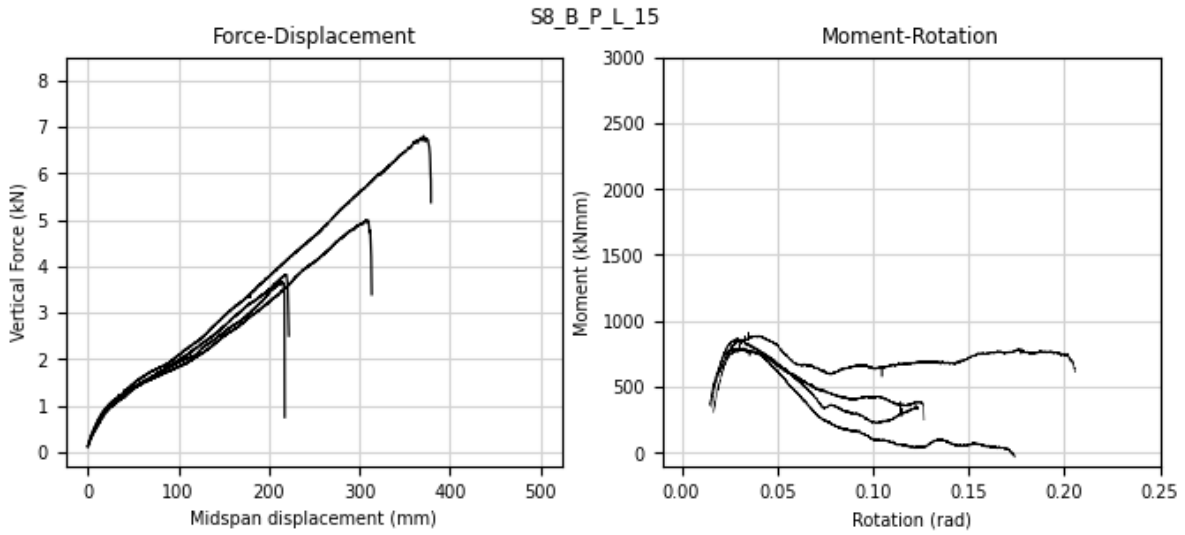

Figure 6. 27 Force-displacement and moment-rotation graphs of 2m butt-joint tests

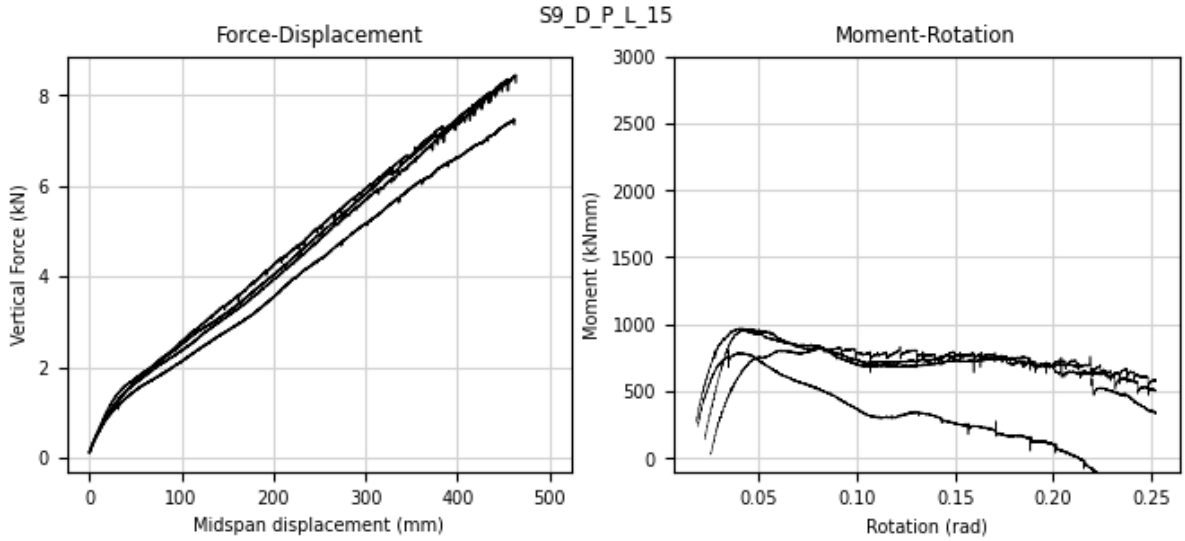

Figure 6. 28 Force-displacement and moment-rotation graphs of 2m double incline butt-joint tests

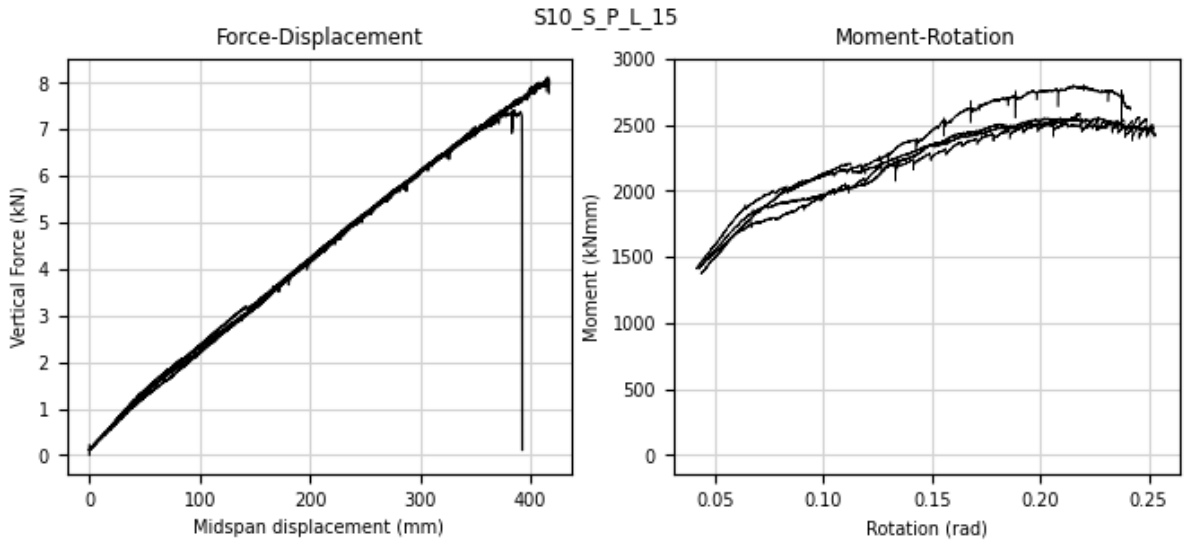

Figure 6. 29 Force-displacement and moment-rotation graphs of 2m single surface spline tests

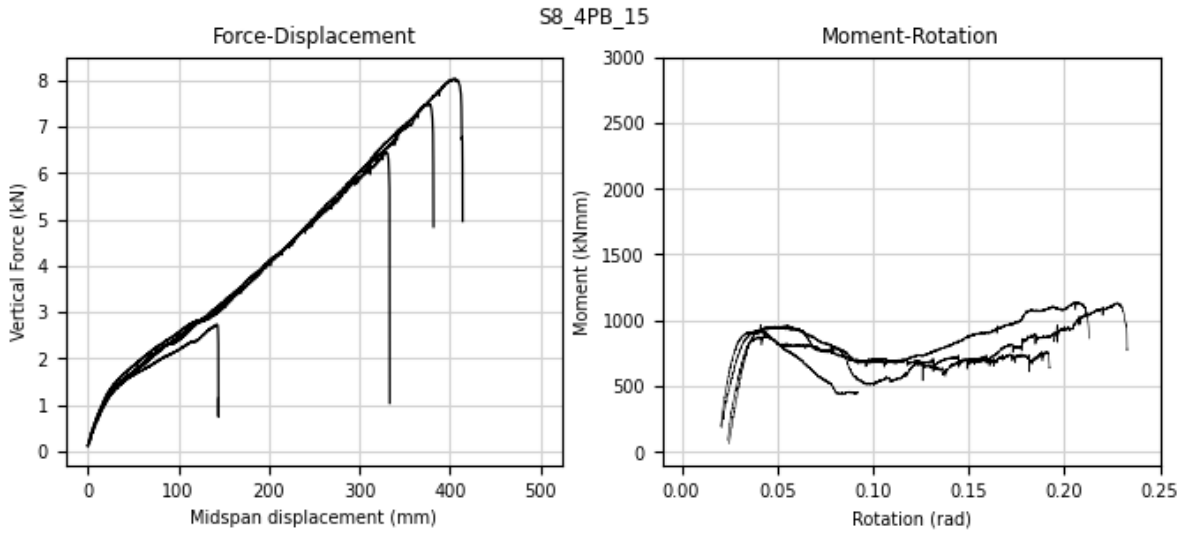

Figure 6. 30 Four-point bending 2m test results

6.3.5. Tube connector

The tube connector was the only one that was specifically designed to withstand the catenary loads, through designing elements that are capable of reliable plastic deformations. This was achieved by avoiding localised timber failure around the connector through increasing the surface area of contact between the connector and the embedment by using the tubes which were designed to buckle and collapse inwards, allowing for the horizontal extension of the central connection by approximately double inside diameter of the tubes. There were two test series employed, first one using the 30kN tension load hold shown in Figure 6. 31 (active tension) and second one fixing the horizontal displacements of the supports (passive tension) shown in Figure 6. 32. The numerical summary of the tests can be seen in Table 6. 12.

Table 6. 12 Full span tube connector test results summary

Series	P_{max} (kN)	Δ_0 (mm)	U_{max} (mm)	θ_{max} (rad)	U_{max}/L (%)	M_{max} (kNmm)	Fail (y/n)
S15-T-P-L-30	12.13	53.77	446.25	0.253	0.17	4373.40	n
	12.00	53.76	444.56	0.252	0.17	4155.50	n
S16-T-P-L-F	53.51	270.30	681.65	0.494	0.48	15329.44	n
	53.17	274.96	676.97	0.494	0.48	16232.97	n
	48.84	273.73	666.03	0.487	0.47	16889.78	n
	50.73	265.04	666.22	0.483	0.47	17641.49	n

The active tension test results presented in Figure 6. 31 although unable to provide ultimate values for the tube connectors themselves, are a great experimental representation of almost idealised catenary action activation under constant loading.

The two tests' results in identical load-displacement curves and close to identical moment-rotation behaviour. The rotational stiffness begins to decrease towards with the increase of the angle, however, which is reflected in the slight bend in the force-displacement behaviour. As the moment resistance decreases all the way to the bending of the rod alone, this bend would become fully linear.

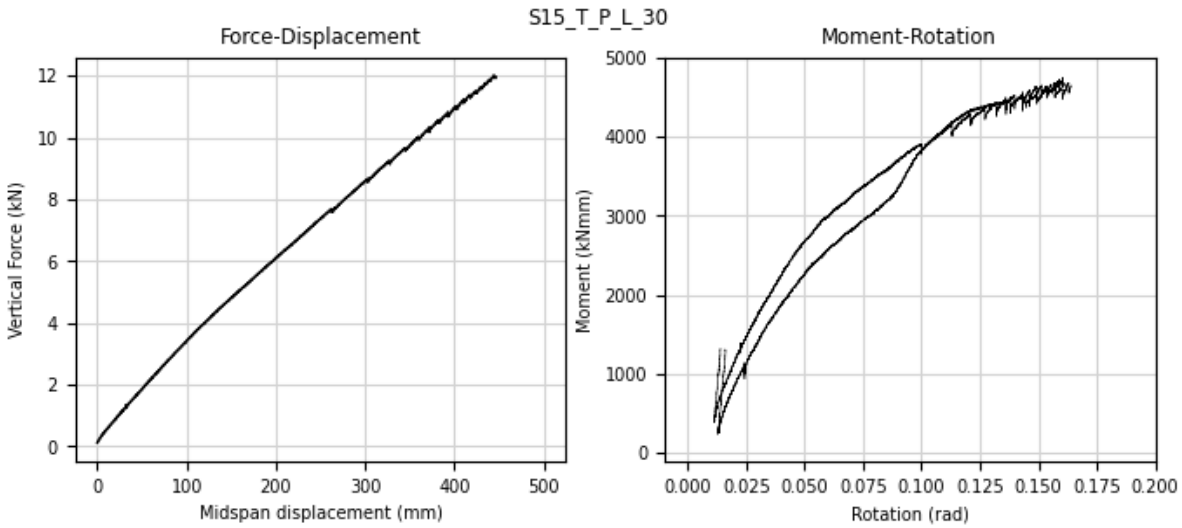

Figure 6. 31 Force-displacement graph of the 30kN load hold tube connector test

For the passive tension samples, force-displacement of which can be seen in Figure 6. 32, none of the specimen failed. Only two tests were performed in the load hold series, as the specimen were nowhere near failure at the end of the extension of the vertical actuator, and therefore it was concluded that performing more of the passive tension tests would be more beneficial to understanding of the tube behaviours. Moreover, during the passive tests, the vertical midspan deformation was increased by introducing two stage testing, where after initially reaching close to full stroke of the actuator, the test was stopped, the specimen unloaded, and the central wall stub which was used for applying the load was replaced by one 200mm larger. This was possible thanks to the plastic deformation introduced by the initial loading,

and since there was no brittle timber failure present, the test was able to continue. This unloading and reloading can be seen in Figure 6. 32 between 200-300mm marks.

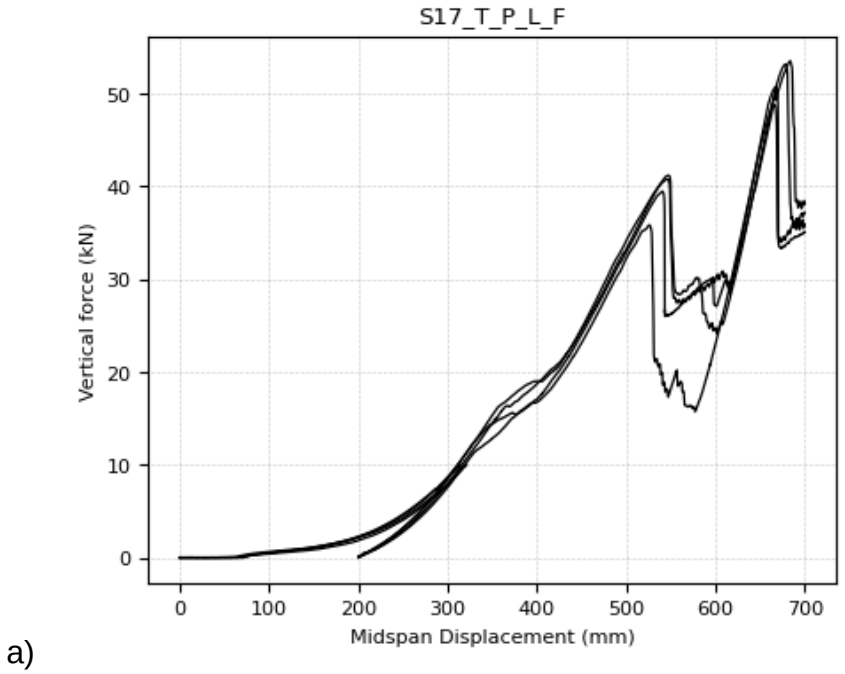

a)

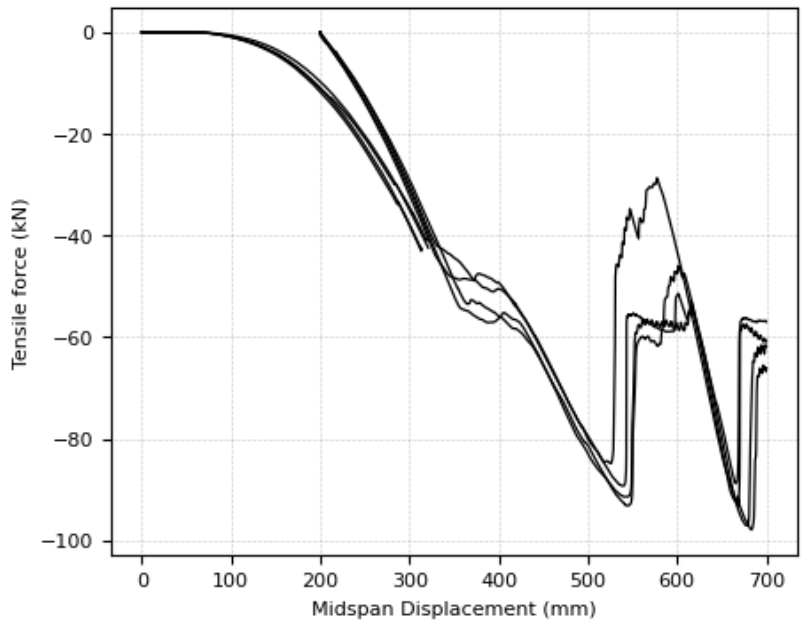

b)

Figure 6. 32 Force-displacement graphs for the vertical pushdown force (a) and developed tensile force (b) in the tube connector test

a)

b)

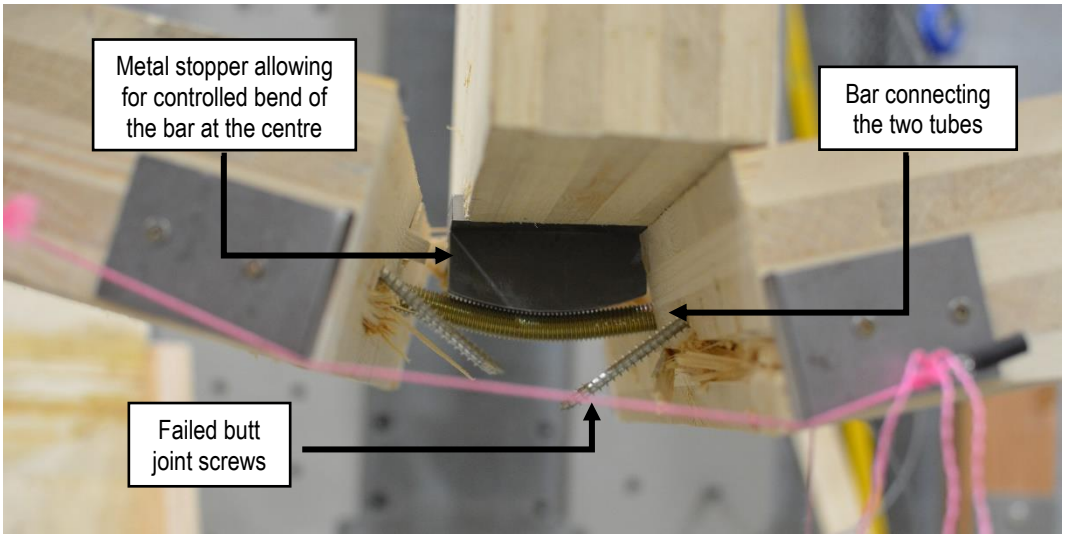

c)

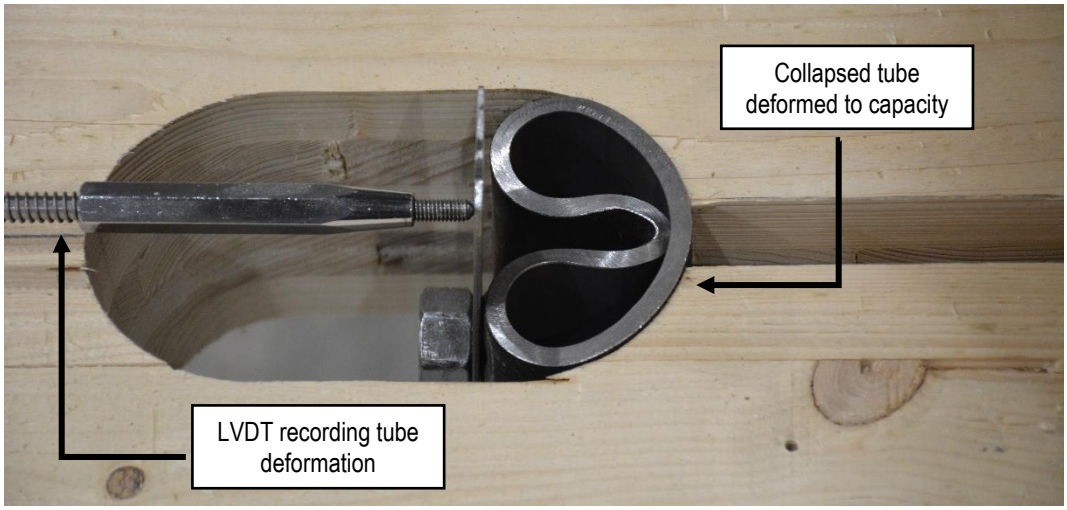

Figure 6. 33 Tube connector tests (a) fully deformed specimen (b) showcasing of the wall attachment (c) shape of the fully deformed tube

6.4. Testing challenges and sources of errors

One of the challenges of representing the catenary action with sufficient accuracy and yet managing to perform a larger number of tests was introducing the overhang approach. Although accounted for in the calculations, the real behaviour of such system differs significantly due to the asymmetry of the testing in the laboratory and the subsequent variable overhang on both sides increasing with the increase of the midspan vertical deformation. Therefore, the moment calculation is increasingly prone to errors along with the deformation increasing.

However, at small rotations, where for most of the connections the maximum moment is achieved, this error was deemed acceptably small to conclusively compare those values to one another. Moreover, the parameters changing along with the increasing asymmetry should have a very similar effect on the results of specimen of similar geometry. This study was focused on investigating the differences in performance due to a number of parameters outlined in Section 6.2.1 and so the conclusions drawn about those differences are to be considered the main findings, not the definitive answer about the performance of a singular subsystem or connection.

The stroke of the main actuator although achieving a deformation allowing to surpass the minimal requirement of 15% u/L ratio for catenary action activation, did not allow to fully investigate the catenary capabilities in the stronger assemblies, which is why the reduced span 2m series was introduced. Another issue with quasi-static investigations in the full-span test was that the maximum moment has often been achieved through application of the gravity loads alone and therefore it was not possible to fully capture the slope of the elastic region of force displacement curves with the setup used.

The variability of screw spacing is likely to have played a role in the total capacity of the connections, despite it being designed well within the acceptable limits, the samples where screws were spaced closer (6 screw butt joints and 12 screw spline connectors) at the same total width of the sample have exhibited the splitting of the wood across the secondary layers travel all the way between the screws. Since the pullout and embedment failure have been shown to be significant failure mechanisms, increasing the spacing would potentially have impact on the total capacity.

6.5. Summary

The full-scale subassembly tests were performed on four types of connections – butt joint, double incline butt joint, single surface spline and tube connector. The first three are popular design choices for CLT-to-CLT panel connections and the tube connector proposed previously by other researchers has been specifically designed for purpose of alternative load path formation. Additional parameters were used in the butt joint series to investigate the influence of wall brackets and tension application method.

The size of the experimental setup combined with limited actuator travel distance has limited the experiments to 17% u/L ratio, meaning a lot of tests had to stop before sample failure. Although useful to know that the subsystem meats this level of deflection, the resulting data is considered censored and does not provide the full picture, limiting its usefulness. The following chapter attempts to answer the research question, whether the results of the full-scale testing could be predicted by the component method, in which acquisition of the full deformation range data is possible.

Chapter 7: Connection properties characterisation for Alternative Load Path Analysis

7.1. Analysis approach

When considering the second order effects of load redistribution under general loss of column or wall in an Alternative Load Path Analysis, the displacements and forces present in the final presumed static equilibrium will depend directly on the rotational and axial behaviour of the connections and geometrical arrangement of the structure. The geometrical structure arrangement in question includes the location of the connection (centrally over the support or offset), span length, section properties, and any continuity of span over the supports present.

These variables can be accounted for using a variety of structural analysis methods, where internal force and moment relationship to applied loading can be derived as a function of these spatial measurements and boundary conditions as well as material properties, and finally, mechanical behaviour of the connection. The experiments were designed to specifically target the connection mechanical behaviour as in timber

structural design this is the part of the entire analysis that both will dictate the strength of structure as a whole but is also the most challenging to predict through calculations alone.

As discussed in Chapter 4.2, these vital parameters are the following:

- Maximum moment capacity of the connection M_{max}
- Maximum rotation of the connection θ_{max}
- Rotational stiffness of the connection $k_{c,R}$
- Axial stiffness of the connection $k_{c,A}$

7.2. Mechanical properties

One of the most important questions that the study aims to answer is the level of influence of the tension utilisation on the moment and rotation capacity of the connections. Figure 7. 1 shows the interaction diagram of moment and tension for all tested connections, and Figure 7. 3 shows the maximum rotation and tension utilisation interaction diagrams. For each test series, 95% confidence intervals (CI) were calculated based on the Extreme Value Distribution Type I (Gumbel, 1948), to account for asymptotic behaviour of the upper outliers of the datasets.

7.2.1. Moment-tension interaction curves

The half-lap and the butt joints showed an inversely proportional relationship of the moment capacity and tension utilisation due to the direct increase of the resultant tension through increased bending. The 5-ply half-lap joint (Figure 7. 1a) and butt joint (Figure 7. 1c) showed an almost perfectly linear relationship, while half-laps in 3-ply test (Figure 7. 1b) showed a decrease of about 25% in its moment capacity until

60% utilisation r_T, with sharp drop off after that point, attributed to splitting failure occurring in the transverse layer of the 3-ply panels. In contrast, the spline connection (Figure 7. 1d) exhibited an increase in moment capacity up until about 50% r_T, with steep drop off after that point.

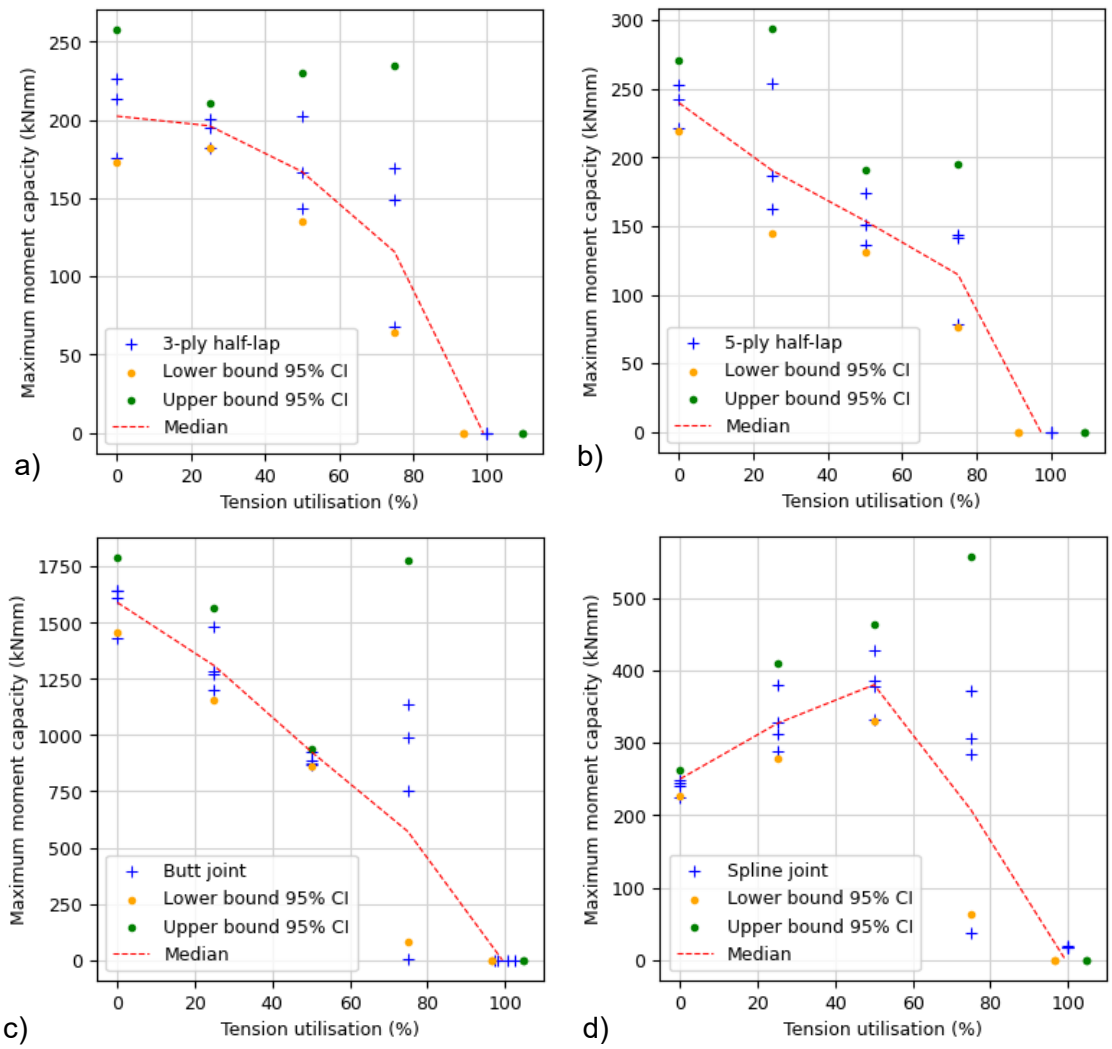

Figure 7. 1 Force interaction curves from Setup A: 3-ply (a), 5-ply (b) half lap joint and Setup B: butt joint (c) and spline joint (d)

The interaction in this connection cannot be simplified down to two resultant point loads but is directly caused by the bending and splitting of the plywood. The capacity increase may be attributed to the direct interaction between the wall-stub point load and the spline, discussed previously in Chapter 5, Section 5.4.2. Catenary action enables greater overall force and rotation, facilitating sufficient friction between the wall stub and the connection to transfer compressive loads. Moreover, that type of perfect contact between both sides of the wall as seen in Figure 7. 2, was only possible due to the deformation in the plywood and was not observed in the butt joint equivalent.

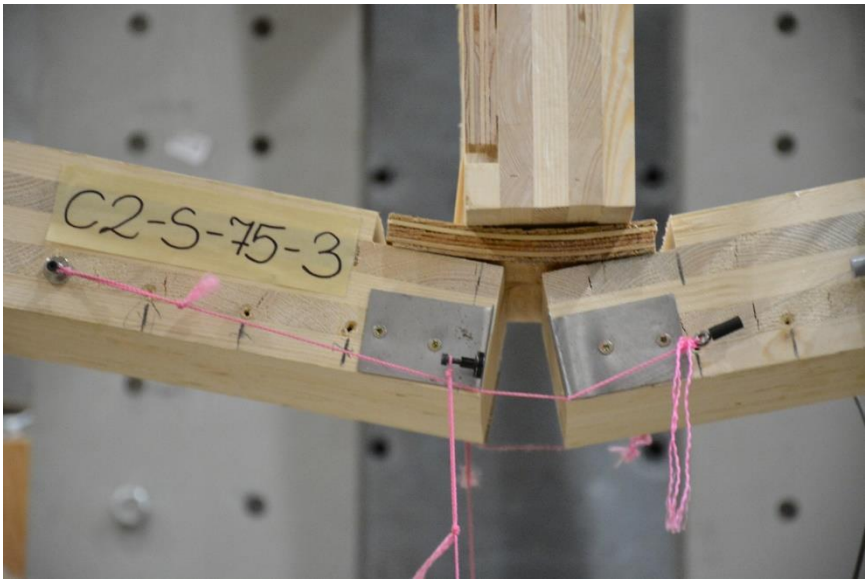

Figure 7. 2 The deformed spline component test, showing the corners of the wall pressed tightly against the top plywood layer

7.2.2. Rotation-tension interaction curves

Sufficient rotation of the elements is vital for the tension to be able to develop appropriate vertical force resultant effective in withstanding the vertical load applied. Therefore, a second possible criterion to be used as a limit state is the rotational deformation of the connection. Moreover, knowing the stiffness of the connection a corresponding force can be approximated, however this could be tricky to establish and is discussed in more detail in Section 7.3.1. Looking at the rotation capacity interaction curves, 5-ply half lap (Figure 7. 3b), butt joint (Figure 7. 3c) and spline joint (Figure 7. 3d) show significant increase until 25% $r_T$and subsequent drop off, with spline having by far the largest increase. The 3-ply (a) is an outlier here and it is also thought to be due to the failure modes being distinctly different than the 5-ply half lap and butt joint equivalents. The splitting of the cross layer, that only occurs past the 25% r_T in this series, allows for greater deformation initially without overstressing the connectors, however the splitting will also reduce the effective embedment depth and therefore result in consequent fast decrease in the rotation capacity when further stressed in tension.

5-ply half lap and butt joint share the same characteristics not only of the median trend, but also of the general variability of the strengths, with 25% r_T yielding the widest range of results. This larger variability at 25% r_T is important to note, as this means that with the upper outliers skewing the results, the increase in performance shown on the graph for the majority of the results may not be sufficiently reliable for design. Therefore, on this basis it is suggested that for both of the half-laps as well as the butt joint designer should not hope for improvement of performance, but to account for reduction in performance past that point.

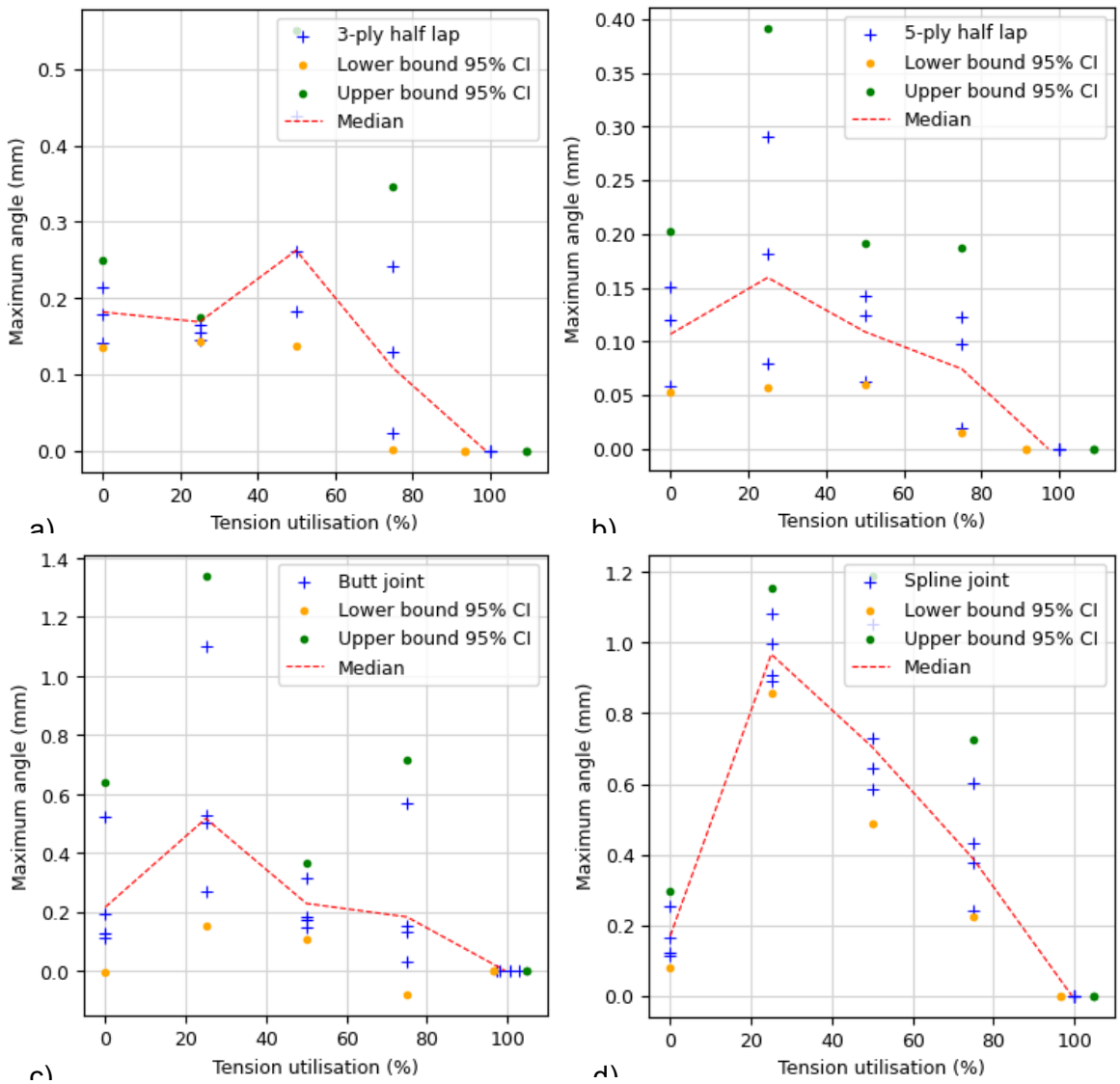

Figure 7. 3: Rotation failure envelope curves from Setup A: 3-ply (a), 5-ply (b) half lap joint and Setup B: butt joint (c) and spline joint (d)

7.2.3. Full span and component test

Results of the pin-support tests under variable vertical load and constant axial tension have been summarised as a failure envelope for combined tension and bending in Figure 7. 4. Each datapoint represents the maximum moment experienced by the sample and the corresponding tension utilisation value based on the axial load tests.

An extreme value distribution fitting was performed on the results from 4 specimen in each of the component test series. The 95% CI were developed by fitting a straight line utilising the method of least squares on the CI values for each separate test type calculated through the EV1 distribution, as shown previously in Figure 7. 1a. The moment capacity of both component and full span tests drops proportionally to the increased tensile utilisation. Horizontal withdrawal of the screw is the governing failure mode and both increased system tension as well as bending of the connection increase the tension resultant at the screw, therefore this relationship is physically justified. The tension resultant calculations are discussed in more detail in section 7.2.4.

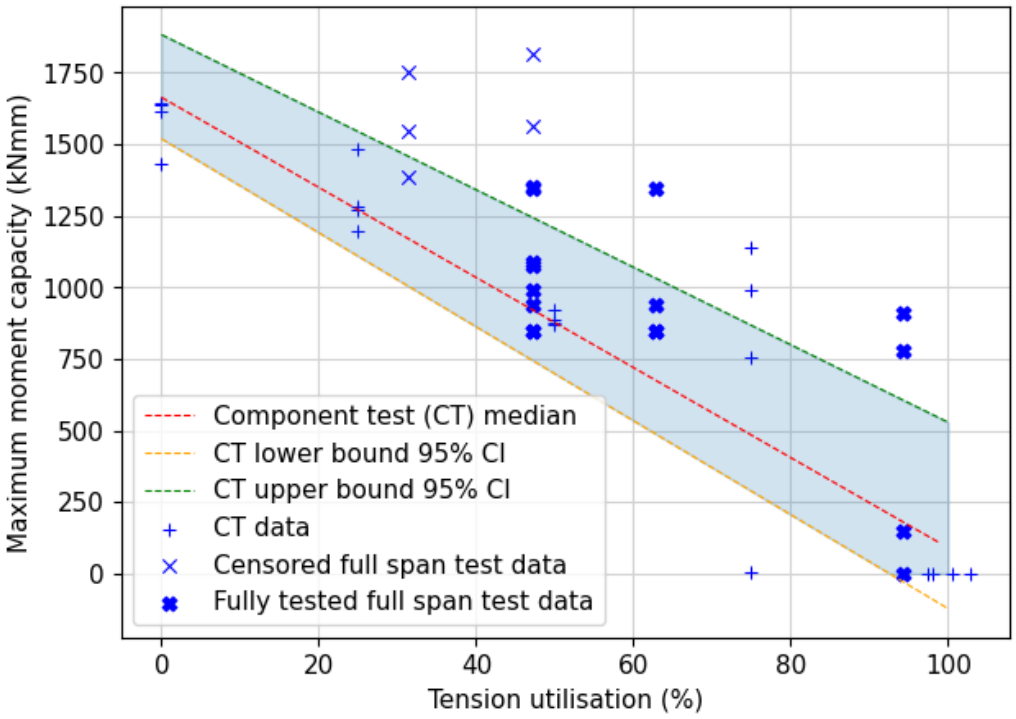

Figure 7. 4 Correlation between the component and full-span test

The values of the full-span tests when compared to the component test data fit does fall on the higher side of the data distribution. This could be due to a multitude of factors such as data errors and the active changes in the effective span due to the horizontal travel distance of steel rollers, small changes in screw spacing and proportionally large variability of timber properties. Although some of the full-span tests show a higher moment resistance, the lower confidence interval does a good job of capturing the bottom boundary of large-scale test values, which is the more crucial for design. Therefore, they can be deemed to follow the same trend and are a deemed a good predictor of the large-scale behaviours.

There are several possible reasons for the small discrepancies between the two levels of testing, many of which will be due to the small discrepancies in the experimental setup necessary for reduction in the span, that could not feasibly all be accounted for numerically. These include the differences in the length of the chain resulting in different angles for the overhang calculations, the need for propping up the chain length to account for sagging and an increase in string-pot accuracy after refining the setup halfway through the full-test series (necessary for protecting the equipment).

Another plausible factor had to do with the spacing of the connectors. There were two types of full-span test screw arrangement, one with four and another with six connectors, both of which however had the minimum edge spacing of 110mm. The component tests however allowed only for 90mm of edge spacing, which being still over ten times the screw diameter, remains sufficient to mitigate edge splitting according to Eurocode 5: 1-1 (European Committee for Standardisation, 2004a). However, in many of the component tests, the withdrawal failure of the screw was

combined with the splitting and pulling out of the crosswise layer, which propagated to the edge. This phenomenon was not observed in the full-span specimen at all. The side-by-side comparison of the full span and component test failed specimen can be seen in Figure 7. 5. It could be therefore asserted, that although in-keeping with Eurocode (citation) design principles, there is a possibility that in cases of extreme deformations such as the ones seen in the catenary action deformation, additional edge spacing could provide some additional resistance. This is specifically important in the CLT, as the splitting brittle failure of the crosswise layers is an unfavourable failure mode for developing post-peak force plateau for the individual connectors, discussed in detail in Section 7.2.4

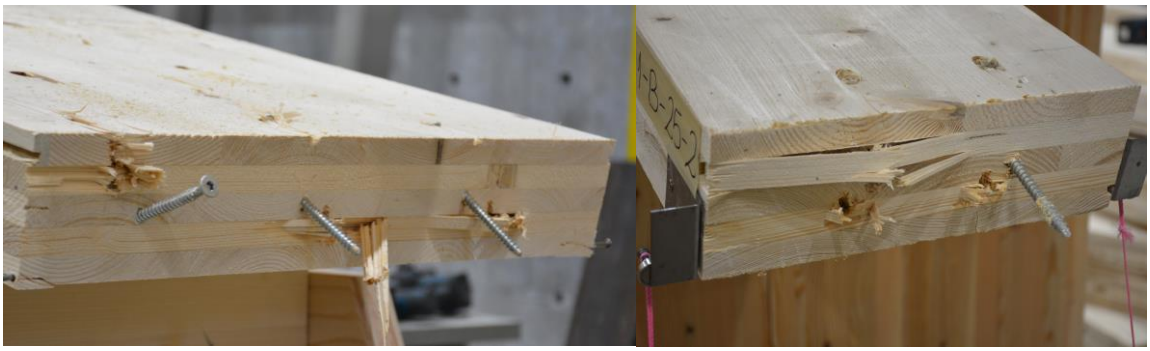

Figure 7. 5 Side by side compassion of the full span (left) and component (right) tests

7.2.4. Axial properties and internal forces

The following internal resultant tension forces in the connector were calculated according to Equation 4. 22 from section 4.3.2 for all of the butt joint component tests. In essence the tension present in the connection is a combination of the moment couple present from the opening of the joint and the tension resultant from catenary forces. The horizontal deflection at the bottom of the connection was measured using string potentiometers installed on both sides of the specimen and the deflection at

the connector and therefore the location of the tension resultant was assumed to be half of that opening given the connection geometry.

Several differences can be observed between tension displacement behaviour when comparing the bi-axial samples to the uniaxially loaded specimen, shown visually in Figure 7. 6. This was due to the slight changes in the failure modes, as the bent screws redistributed internal loads differently based on the angle of deformation. However, for most of the tension utilisation levels the maximum tension force as well as the relating deflection corresponds to the uniaxial tension tests. Despite different bi-axial load combinations this can therefore be used as a reliable parameter for failure checks. The overall shape of the curves also remains unchanged when compared to uniaxial tension tests. One of the most notable observations is that a positive correlation between the ability to progress through the post peak plateau within the connection, as seen in the 25% $r_T$series and to limited extent in the 50% r_T, which resulted in much higher overall force and deformation capacity.

The main purpose of the analysis is to investigate whether the screw withdrawal behaviour changes significantly based on the combination of forces. An observation can be made that the 25% and 50% r_T tensile utilisation series, despite reaching the maximum force at around the same magnitude and corresponding displacement, both manage to achieve greater displacements after this initial withdrawal before total failure. This occurs because, as the rotational stiffness decreases and midspan deflection increases, a greater load is transferred to the supports through catenary action. As a result, both the moment demand and moment capacity decrease. In practical application of the joints in buildings, the tension applied will generally not remain constant as in the artificially designed experiment, and sudden drop in

rotational stiffness will correspond to a spike in tension in the system causing rapid collapse. Therefore, for purposes of analysis of real catenary formation, the maximum tension force at the connector is to be used as the limit state for this type of load redistribution.

Visibly the main outlier in the comparison of all of the results is the 75% r_T series, where the tension in the connector manages to climb to levels above 40kN in three out of four samples, however one sample fails before the full tensile load was even applied and no vertical load aside from gravity load was present. This could be explained by the fact that unlike the other series, due to the high-tension application level, the top contact point has been initially lost which was revealed by the visual investigation (Figure 7. 7). Moreover, at those edge cases the result variability is expected to be higher regardless. This hypothesis is supported by a larger spread of the total maximum values than the series' counterparts both in the resultant tension as well as maximum rotation and moment calculated as seen in Figure 7. 1 and Figure 7. 3. Even so, the specimen which failed during the pre-tensioning does bring the average down from the high-strength specimens and therefore overall, the approximation of the uniaxial tension test is still thought to be of relevance here.

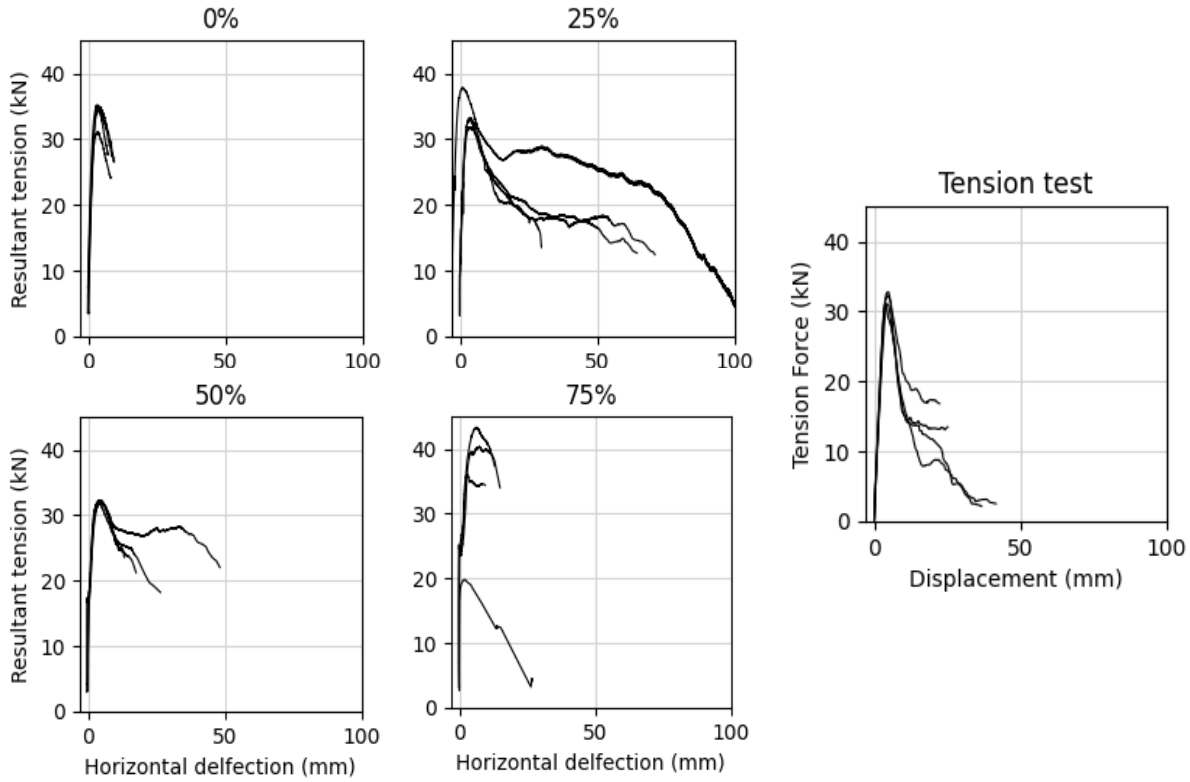

Figure 7. 6 Resultant total tension at the screws in butt joint component tests

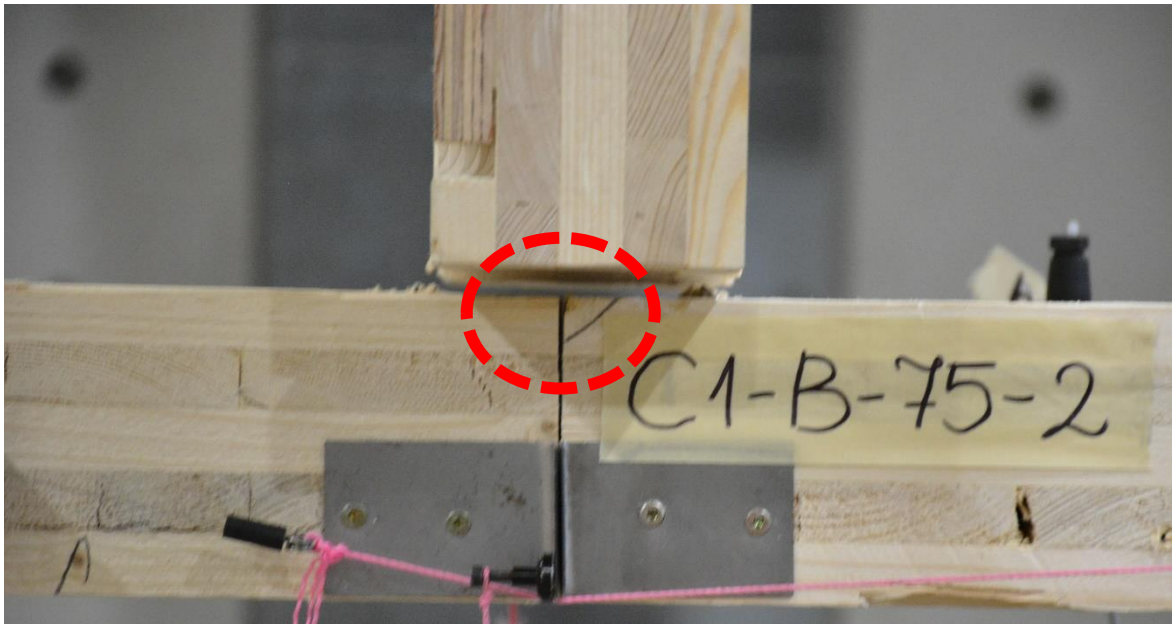

Figure 7. 7 Loss of tight contact point (indicated with red circle) at the top of the connection in 75% r_T series

7.3. Numerical modelling

The aim of the model is to investigate whether the mechanical properties distilled from the component test in combination with the remaining information about the subassembly can reliably predict the experimental results of the large-scale tests. This serves twofold purposes. The main aim is to verify the viability of using the more cost and time effective method as a possible alternative to the large-scale span tests. Moreover, if the model confirms this viability, opens up the possibility for extensive parametric explorations concerning a wide range of subassembly geometries and other influential factors, such as the effects of support conditions on failure modes. This is vital for understanding and successfully implementing efficient design principles for catenary-based ALP load redistribution as unlike in regular design, connections overdesigned to be stiffer than necessary can prevent formation of the necessary displacements. The secondary aim is to draw conclusions as to the sensitivity of the large-scale experiment to inevitable variables distinct from the idealised calculation version, such as the horizontal sway of the midspan and the influence of the overhang over the pin support.

The ABAQUS finite element analysis software was used to allow for the modelling of the interaction of connector stiffness with the compressive contact point in the connections. The software also allows large flexibility in input specifications allowing for use of the experimental data as well as outputs, enabling an easy way of correlating the model results with the empirical results.

7.3.1. Method

7.3.1.1. Subassembly parameters

The model was built in the ABAQUS software utilising 2D beam elements and assigning them the cross sectional properties of the CLT as used in the large-scale tests – 600mm wide and 100mm thick. The model built focused on a single type of connection, the butt joint, as in large scale testing it was investigated with most replicates for the basic pin supoprt cases and most parameter variables and therefore the modelling results can be compared to the most reliable database of experimental results. The beam element engineering properties were implemented using the engineering constants input and the EI_{eff} in each direction was calculated using the modified gamma method (Möhler, 1956; Swedish Wood, 2019).

The main challenge of accurate modelling is reconciling the interactions that the parameters have on one another, particularly the dependence of the rotational spring stiffness on axial load and deformation. This stiffness under combined loading is nonlinear; its value along with maximum moment capacity varies with change in the tension utilisation r_T. This change is illustrated in Figure 7. 8, which shows a comparison between force displacement (a) and moment rotation curves (b) of tests representative of their series.

This parametric change required developing the two spring models shown in Figure 7. 9. The axial stiffness of the fastener and the maximum tension force remain unchanged regardless of the overall maximum tension imposed on the connection (cf. section 7.2.4). Thus, modelling the axial spring along with compressive point at a lever arm seen in the connection (Figure 7. 9a), results in a model that inherently

accounts for rotational stiffness changes and could be used in all tension loading history cases. Figure 7. 9b shows the more classic representation of connection behaviour, where the rotation and axial behaviour are treated as separate parameters. Its benefit is the simplicity, not requiring modelling a contact point. However, given the observed interdependency of moment and tension stiffness in this case, it is only representative of a scenario under specified tension, which is unhelpful in real catenary activation where the tension changes as the deformation changes. Both models were used in the following analysis to investigate their applicability.

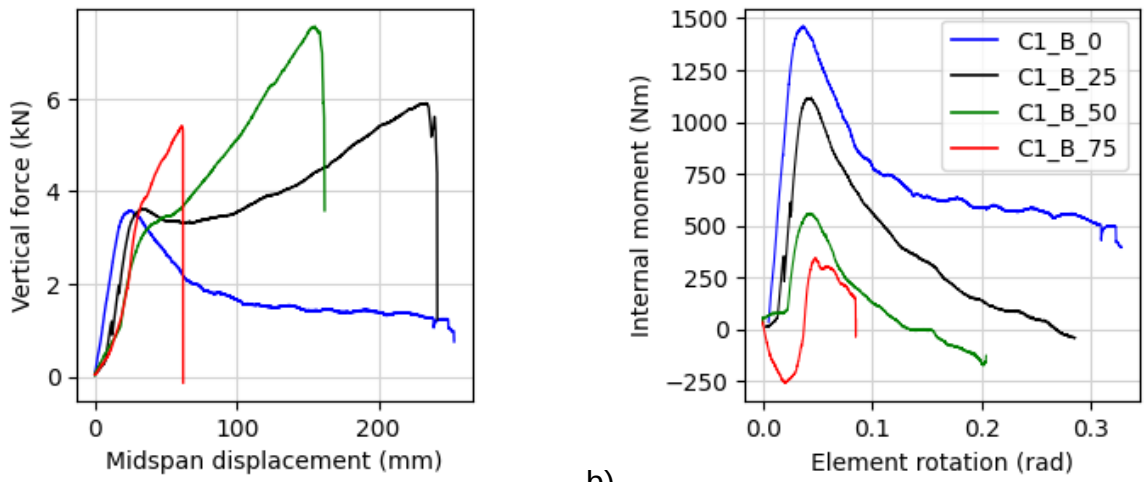

a) b)

Figure 7. 8 Vertical force displacement curve (a) and moment rotation curve (b) of the component tests at r_T of 0, 25, 50 and 75%

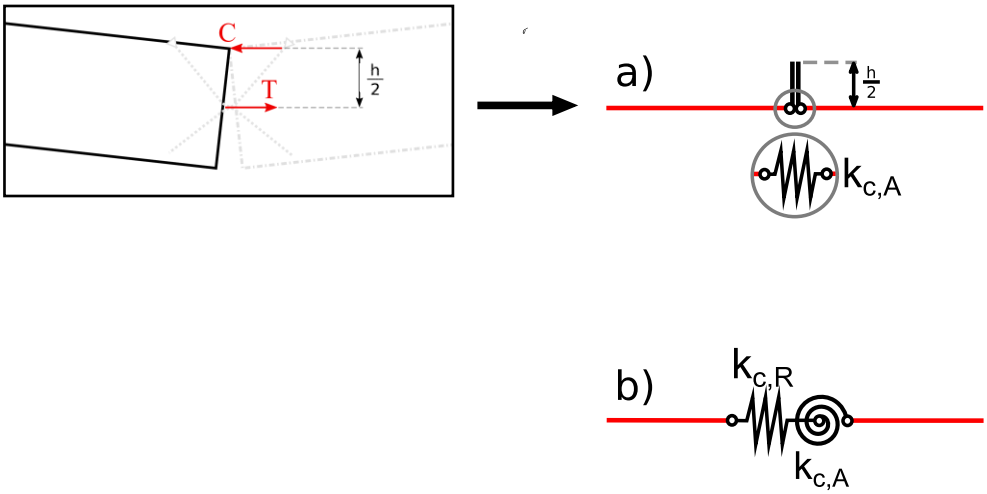

Figure 7. 9 Connection spring models: a) axial spring with lever arm; b) series of rotational and axial non-dimensional spring

7.3.1.2. Spring modelling

Axial spring is modelled based on the experimental data. The numerical average of the tension test results from section 5.3.1 was derived for the purpose of linear regression line fitting, as seen on Figure 7. 10. Based on the fact that the first part of the data follows an approximately linear pattern a combination of linear spring and the failure criterion of maximum force in the connector have been implemented.

Two linear regression lines were fitted, the first following only the linear elastic range of the curve (Linear 2) and the second range including the point up until 10% load drop off (Linear 1). Both can be seen in Figure 7. 10.

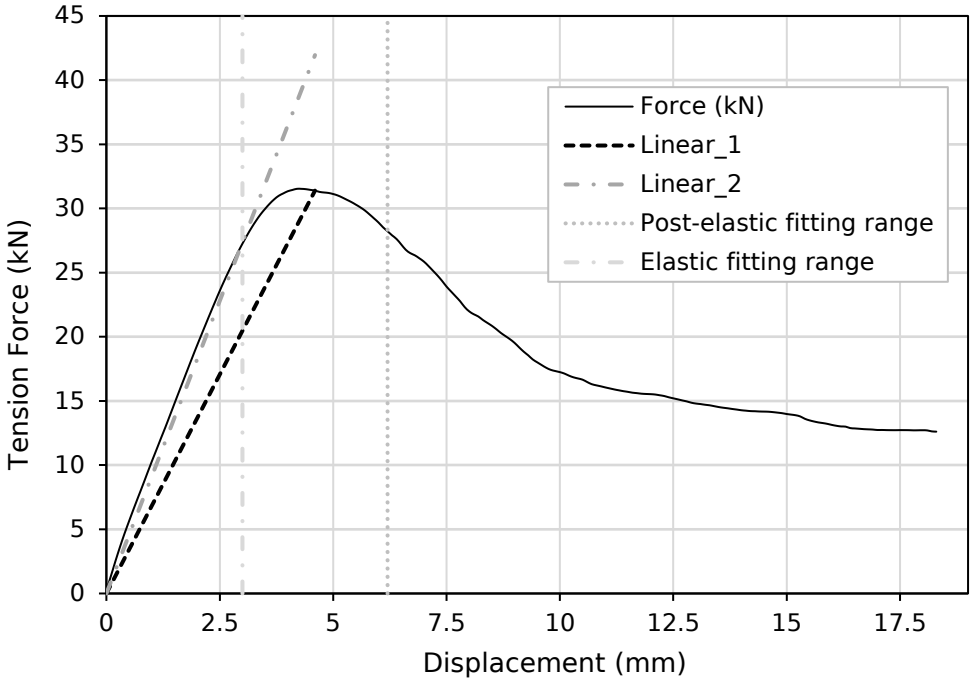

Figure 7. 10 Linear regression lines fitting for axial stiffness

Table 7. 1 shows the numerical stiffness value for both options as well as the corresponding axial forces calculated based on the average maximum displacement. Despite the Linear_2 regression line fitting the data better in the elastic range, it is thought that reaching the maximum axial force at the right displacement will result in a more accurate result. Comparison of both linear stiffness values to the real calculated rolling average stiffness values can be seen in Figure 7. 11. When considering the area under the chart to assess accuracy of the real stiffness to both linear approximations, the total deflection seen at the point of failure will be closer to the real values if utilising Linear_1.

Table 7. 1 Calculation of important values based on the two linear axial stiffness approximations

	Axial stiffness $k_{c,A}$ (N/mm)	**Max displacement (mm)**	**Axial force (N)**
Linear 1	**6824**	4.60	31392
Linear 2	9119	4.60	41949

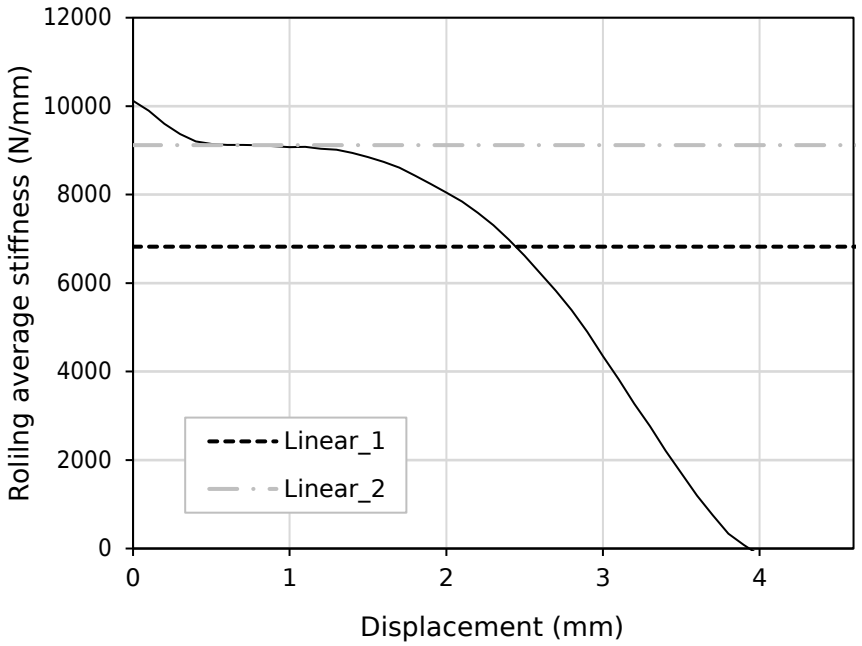

Figure 7. 11 Comparison of two linear stiffnesses approximations

The rotational spring moment rotation curve model for the butt joint is a more challenging task, as this depends directly on the tension present in the connection. The tension utilisation, as visualised in Figure 7. 8 will affect the shape of the moment rotation curve and therefore its rotational stiffness. The two distinct features of the moment rotation curves will be the maximum moment and the rotation capacity of the connection. The direct influence of both of these is discussed at length in sections 7.2.1-7.2.2.

There is a possibility of using the trends derived from this analysis presented in Figure 7. 1 and Figure 7. 3 and interpolate the values in order to obtain the maximum

moment and rotation at any level of utilisation. In modelling a variable tension scenario, this also poses a challenge, as an external script would need to be implemented to take the tension at each timestep and adjust the value of stiffness accordingly. Even in the case where linear approximation is used based on the location of the peak moment, this would be computationally heavy.

However, in the scenario where we can assume a constant tension, such as the load hold tests presented in the thesis, this becomes a case of simple interpolation. Table 7. 2 outlines the rotational stiffness extrapolation for the 15kN load hold. This value was chosen as it was representative of the large-scale test with the most replicates, therefore it was thought to be the best dataset to attempt to model. The following values are based on the component test results.

To complete the model, on top of the linear stiffness approximations, failure criteria also needed to be outlined. Two were of importance here: tension in the connector, and the maximum rotation. Tension in the connector as a failure criterion is the maximum tension that the connector can take based on the axial tension tests. In the result outputs, the locations of the corresponding values were found, and this was marked as the point of failure for the floor subassembly.

The second criterion, maximum rotation, was used for the rotational spring because the model does not account for the resultant tension force in the connection and therefore the first criterion cannot be used. Again, in the load hold scenario this was straightforward, as it only required interpolation of the results at the available tension utilisation ratios r_T. The graph presented in Figure 7. 3 makes it possible to read the corresponding values of peak moment and rotation for the 46% r_T representing 15kN tension and therefore mark the failure at that point.

Table 7. 2 The rotational moment extrapolation for the constant load check

r_T	M (Nm)	$\theta_{M,max}$ (rad)	**Rotational stiffness $k_{c,R}$** (Nm/rad)
25%	1779	0.031	57387
	1336	0.035	38171
	1349	0.036	37472
	1278	0.035	36514
average	1435	0.034	**41912**
50%	910	0.048	18958
	894	0.036	24833
	1068	0.037	28864
	898	0.035	25657
average	942	0.039	**24166**
46%		→	**26296**

7.3.2. Results and discussion

Thorough modelling the geometry and loading conditions of the full-scale testing setups, their behaviour was predicted using the stiffness specification of the connector directly from the processed component test data as described in detail in Section 7.3.1. Models a) is the axial spring with lever arm and model b) is the series of rotational and axial spring.

The comparison of the deflected shapes of models a) and b) under 2.5kN load is presented in Figure 7. 12. The movement of the members is shown to be an almost ideal rigid-body movement, which was confirmed numerically (Chapter 6, section 6.3, Figure 6. 10). The force displacement curves of the models and their failure points

are shown in Figure 7. 13. Both models a) and b) closely represent the test data, with model a) showing higher stiffness and model b) showing lower stiffness. The governing failure criterion for model a) was reaching the ultimate tension force of the axial spring and for model b) it was the maximum rotation based on the values presented in Figure 7. 3c).

Both models closely predict the displacement under gravity loading. Model b) initially provides better results, with the stiffness accuracy dropping off with the increase of mid-span displacement. The failure point in model b) also better aligned with the experimental data. For model a), the idealised lever arm results in a higher stiffness which results in underestimation of the strength. In reality, the top contact point formation in failed specimen consistently shown a contact slip of approximately 10 mm, an example of which can be seen in Figure 7. 14a. It is worth noting that this phenomenon was more prevalent in the samples where no tensile load was introduced (Figure 7. 14b), which appeared to be due to the local crushing of the top contact point, not present in the catenary sample. Based on these observations, an empirical factor of 0.8 was introduced to the half-depth lever arm to account for this effect, resulting in an adjusted model a*). This adjustment allowed for a much better, however still conservative, prediction of the failure point and system stiffness.

Table 7. 3 showcases the statistical summary of the experimental results from the large-scale tests and the numerical models. The location and scale parameters are specific to the Gumbel distribution and were used to calculate all of the corresponding related values. The values across the board (median, mean and coefficient of variation COV) show model b) to be the closest to predicting actual values achieved during the experiments. It did not however perform best at predicting the lower

confidence interval for maximum force – all of the models overestimated these values. The significantly smaller variation exhibited by both models a) and a*) can be attributed to the method of establishing the failure criteria, where in these cases it was the maximum internal connector tension force based on the axial tests. The axial tests have been very consistent in comparison to the combined loading component tests, and which could affect the accuracy of confidence interval predictions.

Table 7. 3 Statistical parameters and lower 95% confidence interval (CI) comparison between the empirical results and models A, A and B*

		Empirical data	Numerical models data		
			a	a*	b
Maximum Force (kN)	*Location parameter μ*	2.84	2.00	2.50	2.90
	Scale parameter β	1.04	0.17	0.16	0.60
	Median	3.22	2.06	2.56	3.10
	Mean	3.44	2.10	2.59	3.25
	COV	39%	10%	8%	24%
	Lower 95% CI	1.48	1.81	2.19	2.10
Maximum Displacement (mm)	*Location parameter μ*	315	155	240	320
	Scale parameter β	80	12	23	77
	Median	344	159	248	348
	Mean	361	162	253	364
	COV	29%	9%	12%	27%
	Lower 95% CI	210	140	210	220

a)

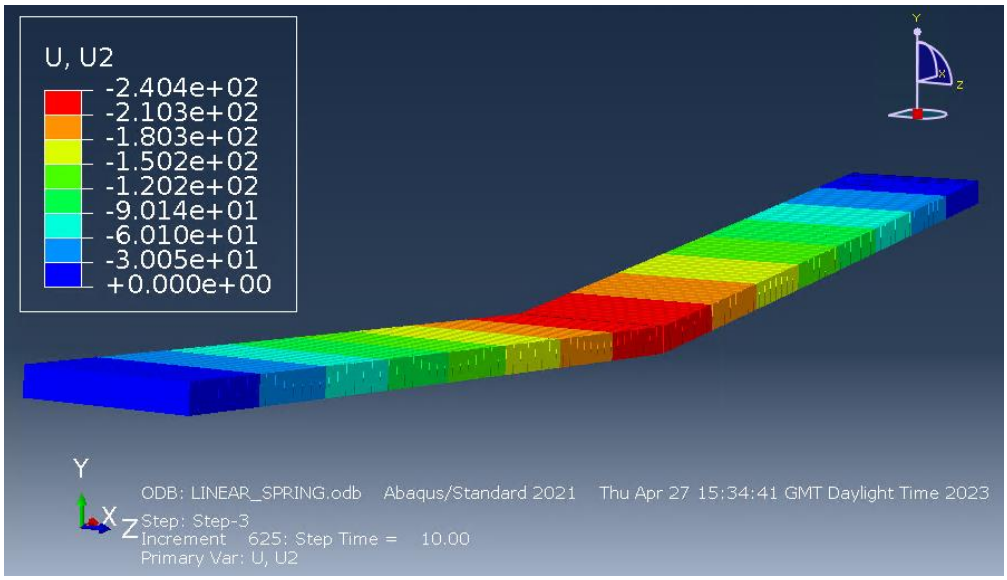

b)

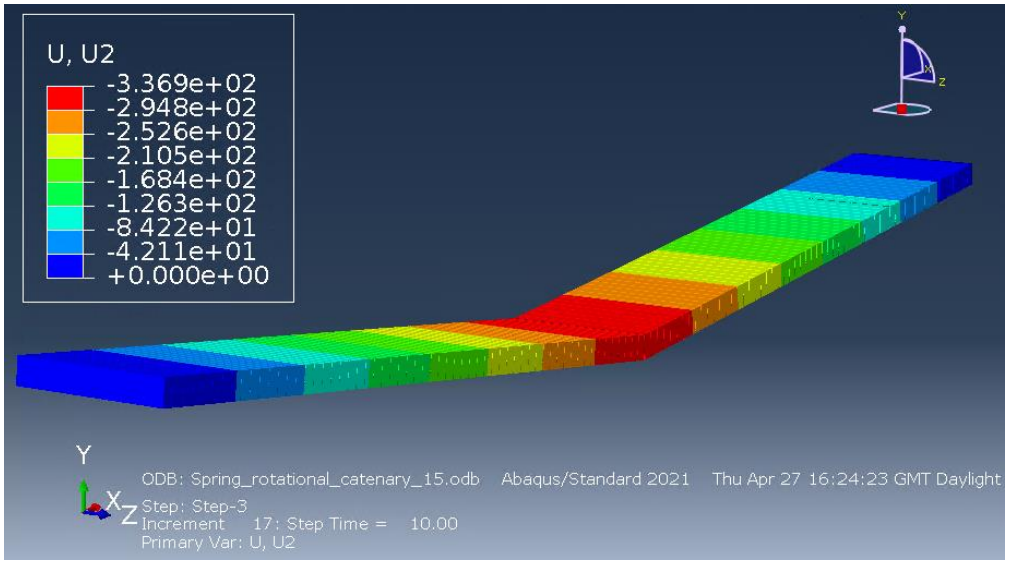

Figure 7. 12 FEA model deformations under 2.5kN of model a) and model b)

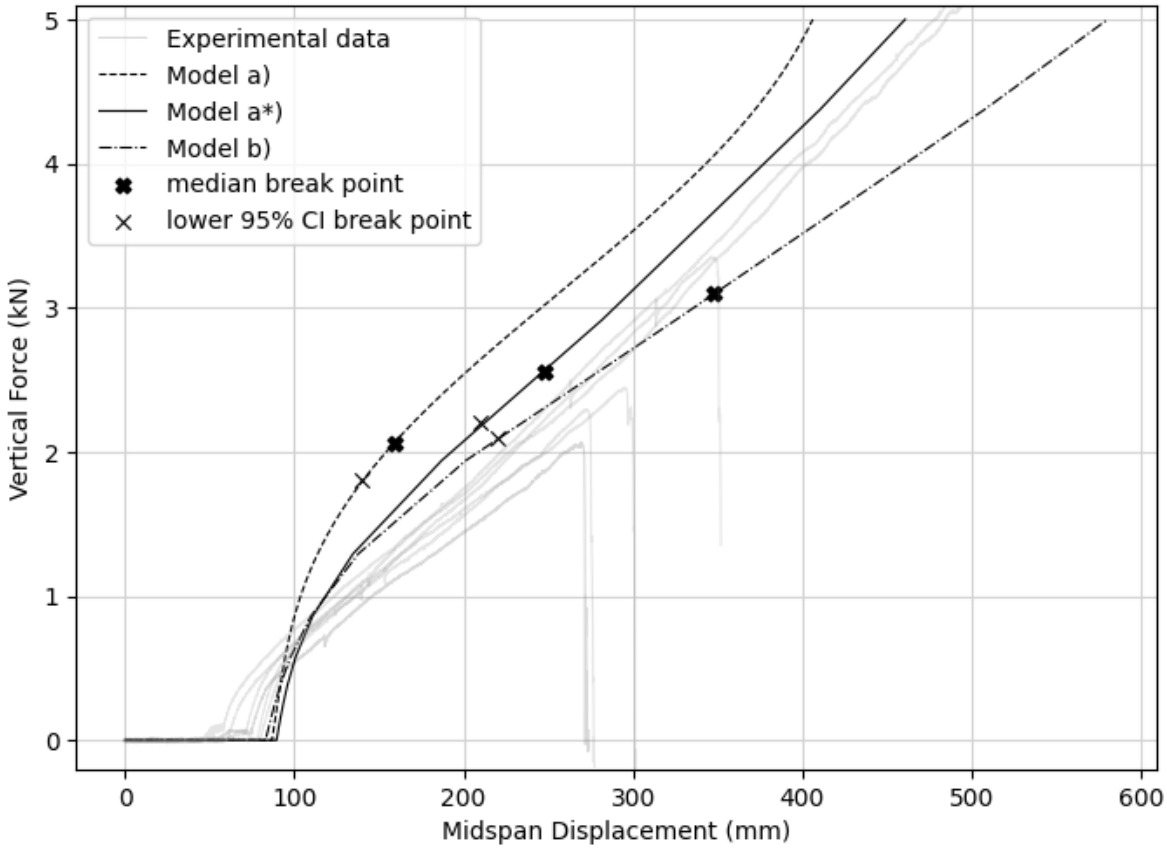

Figure 7. 13 Comparison of ABAQUS and test results for a 15kN load hold

a) b)

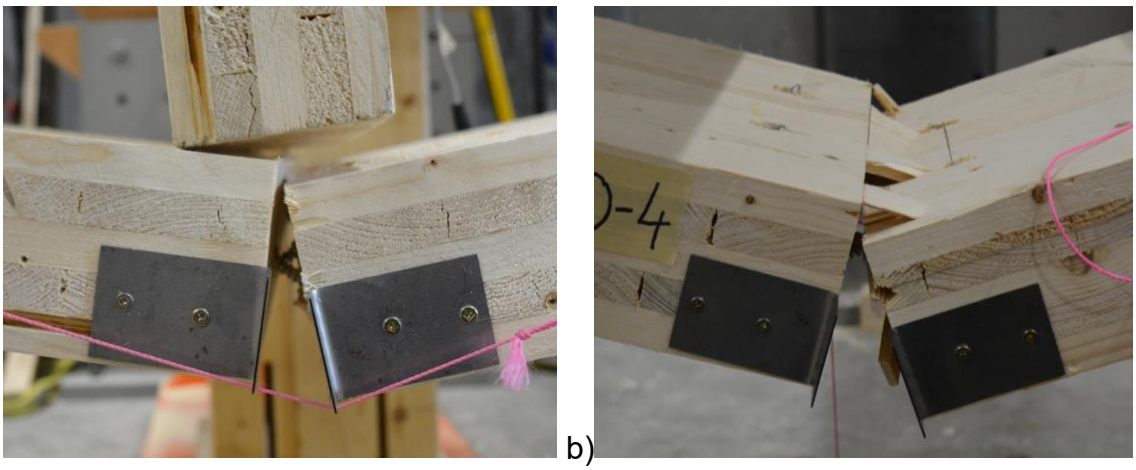

Figure 7. 14 Top contact slip in a failed butt joint component specimen present in combined load specimen (a) and bending only specimen (b).

The main discrepancy of the model, similarly to the direct mapping of the component test results and the full-span test results seen in Figure 7. 4, is that although the predictions of the median and lower end of the confidence interval encapsulate the results, the experimental upper outliers tend to be consistently stronger than the numerically predicted strengths. With this being a trend, more investigation would be needed to investigate the root cause. The rotational spring model could also be improved for use under variable tension, which could be done through introducing parametric variables into the model. This however introduces another level of complexity and time cost, which might not be replicable in a lot of the design scenarios.

The discrepancies in both models can be attributed to the non-linearity of stiffnesses, however the linear approximations used along with the outlined failure criteria are thought to be sufficiently good predictors of the behaviour. The modelling conducted above has shown two methods for predicting the behaviour of the large-scale test with the cheaper, faster, and more easily accessible component test. This model was a proof of concept, allowing for endless implementations in the substructure and structure level studies, this is however out of the scope of this thesis.

7.4. Summary

The results of the performed component tests introduced in Chapter 5 have been further processed into maximum moment versus tension utilisation r_T interaction curves and similarly maximum rotation versus r_T interaction curve. The implementation of just 3 predetermined combined loading combinations allows for

identification the of the trends across the tension spectrum and presentation of the data in this format allows for direct use in ultimate level checks.

To ensure that the component test can be deemed a satisfactory predictor of the larger subassemblies two methods were used to a compare the butt joint test results at both scales. Firstly, the butt joint moment-tension interaction curves based on component tests were analysed statistically to estimate the 95% confidence interval trend lines and the full-span test results were plotted against the resulting range. It was shown that the full-span tests fell largely within the confidence interval, skewing however slightly over the upper bound.

The second method used for comparison was building the full span subassembly model in ABAQUS and giving the connection properties based on the measured values from component tests. Two methods of connection modelling were used, each presenting unique pros and cons. The ultimate limit states constituting failure were read using the previously derived interaction curves. After accounting for the imperfect top contact during bending both models have shown close resemblance to the experimental full-span test results. Overall, the component testing method presented within the thesis shows promise in being a relatively cheap and easy way of testing a large variety of mass timber connections, with the capacity to predict behaviour at larger subassemblies.

Chapter 8: Conclusions

Emphasising the importance of performance-based progressive collapse design methods holds significant weight in shaping the future generation of timber design standards. The research presented here has firstly investigated structural significance of an accidental scenario with a timber specific material response, which was done to show that the assumption of appropriateness of material independent guidance is not a safe approach, thus confirming the need for performance-based design strategies. The thesis goes on to identify the gap in the knowledge that prevents from understanding of the mass timber behaviours under extreme deformations, establishes an empirical foundation and introduces an economical testing approach, known as the "component test method," for effectively measuring these parameters in connections. The component test method was then implemented with the test matrix designed to yield results that could be easily applied in modelling of various subassemblies and even whole structures. Finally, a series of full span floor tests were performed, and numerical methods were used to confirm how well the component level testing was able to predict the large-scale test behaviours, giving validity to the novel proposed test method.

The chapter specific conclusions are as follows:

1. Component test conclusions
    1.1. Moment-tension as well as maximum rotation-tension interaction curves were derived for 3 types of typically used CLT joints. For joints with significant rotational stiffness, a negative correlation was shown between the tension level and moment capacity. Supplementary rotation curves indicated that the best catenary can be achieved for most joints with between 25%-50% of tension utilisation r_T. The spline connection exhibited the greatest benefit from catenary action; however, it did not offer significant bending stiffness in normal conditions. The connection that exhibited the least capacity for developing the catenary action has been a 3-ply half lap connection and this is thought to be due to the type of deflection needed for the significant rotation to develop acting on the screws directly in withdrawal.
    1.2. It is thought that for the connection which has exhibited the most unique behaviour, the spline connection, lack of moment resistance was of benefit to the successful formation of the catenary action. In some cases, the post-peak plastic plateau is not possible to achieve or is considered unreliable – that being the case in the case of stiff wood connections (butt joint, half laps). In contrast connections that are not meant to withstand sagging bending moments can be a good solution, especially when, like in the case of the spline connection, it is thought that its moment resistance achieved in the hogging direction could be significant. Therefore, for part of the structure where hogging is the primary moment direction under regular circumstances, but under catenary action this could be reversed, this kind of design

asymmetrical from top to bottom direction could be a good solution to consider, however more investigation into the reverse bending behaviours in such components is thought to be needed.

1.3. Overall, the analysis has shown that the tension increase in the system has both beneficial and compromising effects on the total force capacity on the system – the tension allows for the load redistribution to form, consequently lessening the bending capacity demand on the system, but at the same time decreases the bending capacity itself. For stiffer connections the maximum moment capacity is consistently being reached at minimal deformations and the subsequent catenary activation occurs on a sample effectively past its failure load. Moreover, the variability of results increases drastically at the higher end of the utilisation scale meaning that relying on that behaviour is not advised.

2. Full span conclusions

2.1. The study revealed similar load combination levels at failures for the results of full-span testing when applying active load-holding methods (active tension) and employing horizontal restraint technique (passive tension). However, displacements achieved in the active tension tests were generally larger (around 50mm). Additionally, active tension tests produced a larger amount of higher end outliers which could cause general overestimation of the ability of the structures for catenary formation and more importantly ability to maintain the catenary state under constant load. Despite this it can be asserted that given the same final force combinations, similar failure is to be

expected irrespective of the loading history. This allows for a higher flexibility in methods of testing.

2.2. The introduction of the wall brackets has had a positive effect on the floor-to-floor performance of the butt joint subassemblies. Between active and passive tension tests, they have shown overall the same trend of increased performance, but this was seen much more prevalent in the passive tension application.

3. Comparative investigation conclusions

3.1. Using the interaction curves presenting moment and tension utilisation on the two axis it was possible to compare the results of the full-span and component tests. The correlation observed between the component and full-span test results show very similar trends, however the full-span tests have overall achieved slightly higher peak moments than the component tests at the same tension utilisation ratio r_T. However, although the upper outliers have gone beyond the 95% confidence interval modelled from the component tests, the lower bound have encompassed all of the test results.

3.2. Numerical modelling of the full-span tests using the empirical data extracted from the component-level tests was also successful in predicting the displacements under gravity loading, shape of the load displacement curves as well as points of failure. Out of the two models presented it is thought that the axial-rotational spring example was easier to implement and predicted the failure well under constant tension, however it is predicted to lose its accuracy once variable tension is introduced. The axial spring with lever

armed contact point model has required more careful modelling to account for the real-life imperfection of the contact point in bending, however the final result was shown to be a good predictor of stiffness and failure and it is a method that will work under every tension utilisation.

3.3. Overall, it can be asserted that on multiple levels of complexity (hand calculations/spreadsheet as well as modelling), with some adjustments, the component tests to be good predictors of the behaviour of the full-span subassemblies.

The construction industry has witnessed a notable increase in the use of mass timber as a primary building material in tall and long-span buildings, thanks to development of EWP technologies and the multidute of positive qualities of the material. Although the accidental actions discussed do not occur often, the conseqences of one occuring can be dire. If such unfortunate event would happen in a large timber building it is still not known whether it could lead to progressive structural failure resulting in loss of life. It is not wise to wait until such event occurs before learning the lesson, as was done after the Ronan Point collapse. Aiming for standardisation of material specific methods of test and modelling and comprehensive, functional design guidance is essential for continuous growth of the industry and use of timber as modern construction material for years to come.

Bibliography

Abrahamsen, R. (2017). Mjøstårnet – Construction of an 81 m tall timber building. *23. Internationales Holzbau-Forum IHF 2017*, 1–13.

Agarwal, J., Blockley, D., & Woodman, N. (2003). Vulnerability of structural systems. *Structural Safety*, *25*(3), 263–286. https://doi.org/10.1016/S0167-4730(02)00068-1

Alshaikh, I. M. H., Bakar, B. H. A., Alwesabi, E. A. H., & Akil, H. M. (2020). Experimental investigation of the progressive collapse of reinforced concrete structures: An overview. In *Structures* (Vol. 25, pp. 881–900). Elsevier Ltd. https://doi.org/10.1016/j.istruc.2020.03.018

ARUP. (2011). Review of International Research on Structural Robustness and Disproportionate Collapse. *Department for Communities and Local Government*, 76. https://www.gov.uk/government/publications/structural-robustness-and-disproportionate-collapse-of-buildings-international-research

ASCE. (2006). Minimum Design Loads for Buildings and Other Structures. In *American Society of Civil Engineers*.

ASCE. (2014). Seismic Evaluation and Retrofit of Existing Buildings, ASCE/SEI 41-13. In *Seismic Evaluation and Retrofit of Existing Buildings*. American Society of Civil Engineers. https://doi.org/10.1061/9780784412855

ASCE. (2017). ASCE 7-16 Minimum Design Loads and Associated Criteria for Buildings and Other Structures. In *American Society of Civil Engineers* .

Baker, J. W., Schubert, M., & Faber, M. H. (2008). On the assessment of robustness. *Structural Safety*, *30*(3), 253–267. https://doi.org/10.1016/J.STRUSAFE.2006.11.004

Big See. (2022). *HoHo Wien*. Big See Wood Design Award 2022 Winner . https://bigsee.eu/hoho-wien/

Breneman, S., Timmers, M., John Martin, S. A., & Dennis Richardson, A. (2021). Tall Wood Buildings in the 2021 IBC - Up to 18 Stories of Mass Timber. In *WoodWorks* .

Brett, C., & Lu, Y. (2013). Assessment of robustness of structures: Current state of research. *Frontiers of Structural and Civil Engineering*, *7*(4), 356–368. https://doi.org/10.1007/s11709-013-0220-z

BS EN 338:2016: Structural timber. Strength classes. (n.d.). [Document]. British Standards Institute.

BS EN 14080:2005: Timber structures. Glued laminated timber. Requirements. (n.d.). [Document]. British Standards Institute.

Callaway, D. S., Newman, M. E. J., Strogatz, S. H., & Watts, D. J. (2000). Network Robustness and Fragility: Percolation on Random Graphs. *Physical Review Letters*, *85*(25), 5468. https://doi.org/10.1103/PhysRevLett.85.5468

Canadian Commission on Building and Fire Codes. (2020). *National Building Code of Canada 2020*.

Cao, A. S., Esser, L., Glarner, B., & Frangi, A. (2023). A nonlinear dynamic model for collapse investigations in tall timber buildings. *World Conference on Timber Engineering*. https://doi.org/10.3929/ethz-b-000619266

Cao, A. S., & Frangi, A. (2023a). Mixed Element Method for Progressive Collapse Analysis: Method Description and Verification. *Lecture Notes in Civil Engineering*, *326 LNCE*, 289–298. https://doi.org/10.1007/978-3-031-30125-4_26/FIGURES/9

Cao, A. S., & Frangi, A. (2023b). Dynamic strength increase of glued laminated timber beams subjected to impact loading. *INTER International Network on Timber Engineering Research*.

Cheng, X., Gilbert, B. P., Guan, H., Underhill, I. D., & Karampour, H. (2021). Experimental dynamic collapse response of post-and-beam mass timber frames under a sudden column removal scenario. *Engineering Structures*, *233*. https://doi.org/10.1016/j.engstruct.2021.111918

Churkina, G., Organschi, A., Reyer, C. P. O., Ruff, A., Vinke, K., Liu, Z., Reck, B. K., Graedel, T. E., & Schellnhuber, H. J. (2020). Buildings as a global carbon sink. *Nature Sustainability 2020 3:4*, *3*(4), 269–276. https://doi.org/10.1038/s41893-019-0462-4

Clifton, G. C. (2001). Collapse of the World Trade Centre Towers. In *HERA Report*.

COST Association AISBL. (2021). *Memorandum of Understanding for the implementation of the COST Action “Holistic design of taller timber buildings” (HELEN) CA20139*.

COST Domain Committee. (2010). *COST Action E55 Modelling of the Performance of Timber Structures - Progress Report*.

Dietsch, P., & Winter, S. (2018). Structural failure in large-span timber structures: A comprehensive analysis of 230 cases. *Structural Safety*. https://doi.org/10.1016/j.strusafe.2017.11.004

Dinu, F., Marginean, I., & Dubina, D. (2017). Experimental testing and numerical modelling of steel moment-frame connections under column loss. *Engineering Structures*, *151*, 861–878. https://doi.org/10.1016/j.engstruct.2017.08.068

Dusenberry, D. O. (2022). New SEI/ASCE Disproportionate Collapse Mitigation Standard. *Journal of Structural Engineering*, *148*(4). https://doi.org/10.1061/(asce)st.1943-541x.0003305

Ellingwood, B. R., Smilowitz, R., Dusenberry, D. O., Duthinh, D., Lew, H. S., & Carino, N. J. (2007). *Best practices for reducing the potential for progressive collapse in buildings*. https://doi.org/10.6028/NIST.IR.7396

Entwicklung Baufeld Delta GmbH. (2021). *Official Website HoHo Wien - Information*. https://www.hoho-wien.at/en/information/

European Committee for Standardisation. (2004a). *Eurocode 5: Design of timber structures - Part 1-1: General - Common rules and rules for buildings BS EN 1995-1-1:2004+A1:2008*.

European Committee for Standardisation. (2004b). *Eurocode 5: Design of timber structures - Part 1-2: General - Structural fire design Eurocode*.

European Committee for Standardization. (2006). *Eurocode 1 - Actions on structures - Part 1-7: General actions - Accidental actions BS EN 1991-1-7:2006* (Vol. 1, p. 66).

Fallahi, A. (2017). *Innovation in Hybrid Mass Timber High-rise Construction: A Case Study of UBC's Brock Commons Project*.

Fink, G., Jockwer, R., Šušteršič, I., Stepinac, M., Palma, P., Bedon, C., Casagrande, D., Franke, S., D'Arenzo, G., Brandon, D., & Viau, C. (2023). *HOLISTIC DESIGN OF TALLER TIMBER BUILDINGS - COST ACTION HELEN (CA20139)*. 1001–1008. https://doi.org/10.52202/069179-0137

Forquin, P., & Chen, W. (2017). An experimental investigation of the progressive collapse resistance of beam-column RC sub-assemblages. *Construction and Building Materials*, *152*, 1068–1084. https://doi.org/10.1016/j.conbuildmat.2017.05.179

Foster, R., Ramage, M., & Reynolds, T. (2017). Rethinking CTBUH Height Criteria In the Context of Tall Timber Rethinking CTBUH Height Criteria In the Context of Tall Timber . *CTBUH Journal*, *IV*. www.natmat.group.cam.ac.uk

FPInnovations. (2013). Cross Laminated Timber Handbook. In *Book*. https://doi.org/10.1017/CBO9781107415324.004

Frühwald, E. (2011). Analysis of structural failures in timber structures: Typical causes for failure and failure modes. *Engineering Structures*, *33*(11), 2978–2982. https://doi.org/10.1016/j.engstruct.2011.02.045

Frühwald, E. ;, Serrano, E. ;, Toratti, T. ;, Emilsson, A. ;, & Thelandersson, S. (2007). *Design of Safe Timber Structures-How Can we Learn from Structural Failures in Concrete, Steel and Timber?* www.kstr.lth.se

General Services Administration. (2013). *Alternate Path Analysis and Design Guidelines for Progressive Collapse Resistance*. GSA Distribution.

Green, M., & Taggart, J. (2020). *Tall Wood Buildings: Design, Construction and Performance*. https://books.google.co.uk/books?hl=pl&lr=&id=8avWDwAAQBAJ&oi=fnd&pg=PA7&dq=hoho+wien&ots=fHkCUkSBFL&sig=0tfHj3mgdLCeVp_MAOhECha9H7A&redir_esc=y#v=onepage&q=hoho%20wien&f=false

Hansson, M., & Larsen, H. J. (2005). Recent failures in glulam structures and their causes. *Engineering Failure Analysis*, *12*(5 SPEC. ISS.), 808–818. https://doi.org/10.1016/j.engfailanal.2004.12.020

Harley, T., White, G., Dowdall, A., Bawcombe, J., Mcrobie, A., & Steinke, R. (2016). Dalston Lane-The world's tallest CLT building. *WCTE 2016 Conference Proceedings*.

Holt, R., & Wardle, K. (2014). LESSONS FROM TALL WOOD BUILDINGS: What We Learned from Ten International Examples Lessons from Tall Wood Buildings. *Perkins & Will Research Journal*, *06*(02), 7–18. http://awc.org/

Hu, Y. C., Tan, Y. H., & Xi, F. (2021). Failure assessment and virtual scenario reproduction of the progressive collapse of the FIU bridge. *Engineering Structures*, *227*. https://doi.org/10.1016/j.engstruct.2020.111423

Huber, J. A. J., Ekevad, M., Girhammar, U. A., & Berg, S. (2020). Finite element analysis of alternative load paths in a platform-framed CLT building. *Proceedings of the Institution of Civil Engineers: Structures and Buildings*, *173*(5), 379–390. https://doi.org/10.1680/jstbu.19.00136

Huber, J., Ekevad, M., Girhammar, A., & Berg, S. (2018). A Review of Structural Robustness with Focus on Timber Buildings. *40th IABSE Symposium*, 32–49.

Huber, J., Ekevad, M., Girhammar, U. A., & Berg, S. (2019). Structural robustness and timber buildings–a review. *Wood Material Science and Engineering*, *14*(2), 107–128. https://doi.org/10.1080/17480272.2018.1446052

Huber, J., Huang, Y., Knutsen, S., Przystup, A., Tannert, T., & Berg, S. (2023). APPLICATION OF A TUBE CONNECTOR FOR CATENARY ACTION IN CLT FLOORS. *World Conference on Timber Engineering*, 1216–1223. https://doi.org/10.52202/069179-0166

International Code Council. (2021). *International Building Code*.

International Organization for Standardization. (2019). *Bases for design of structures — General requirements, ISO 22111:2019(en),* . https://www.iso.org/obp/ui/#iso:std:iso:22111:ed-2:v1:en

Izzuddin, B. A. (2022). Rational Robustness Design of Multistory Building Structures. *Journal of Structural Engineering*, *148*(3). https://doi.org/10.1061/(asce)st.1943-541x.0003254

Izzuddin, B. A., Vlassis, A. G., Elghazouli, A. Y., & Nethercot, D. A. (2008). Progressive collapse of multi-storey buildings due to sudden column loss - Part I: Simplified

assessment framework. *Engineering Structures*, *30*(5), 1308–1318. https://doi.org/10.1016/j.engstruct.2007.07.011

J.D. Sørensen, P. Dietsch, P.H. Kirkegaard, J. Munch-Andersen, D. Čizmar, L. Neves, J. Branco, B. Zhang, G. Fink, R. Steiger, J. Köhler, V. Rajčić, G. Turk, & S. Winter. (2010). *COST Action E55, Guideline : Design for Robustness of Timber Structures* . https://www.researchgate.net/publication/257940714

Johnson, R. B., & Mahamid, M. (2010). Design of steel connections for tie forces. *Structures Congress 2010*, *41130*(May 2010), 943–954. https://doi.org/10.1061/41130(369)86

Kiakojouri, F., de Biagi, V., Chiaia, B., & Sheidaii, M. R. (2020). Progressive collapse of framed building structures: Current knowledge and future prospects. *Engineering Structures*, *206*. https://doi.org/10.1016/j.engstruct.2019.110061

Kiakojouri, F., De Biagi, V., Chiaia, B., & Sheidaii, M. R. (2020). Progressive collapse of framed building structures: Current knowledge and future prospects. In *Engineering Structures* (Vol. 206). Elsevier Ltd. https://doi.org/10.1016/j.engstruct.2019.110061

KLH. (2020). Structural pre-analysis tables. In *Version: 01/2020*.

Kuzmanovska, I. ;, Gasparri, E. ;, Tapias Monné, D., & Aitchison, M. (2018, August 27). TALL TIMBER BUILDINGS: EMERGING TRENDS AND TYPOLOGIES. *World Conference on Timber Engineering 2018 Conference Proceedings* .

Lai, B., Liew, J. Y. R., Hoang, A. Le, & Xiong, M. (2019). A unified approach to evaluate axial force-moment interaction curves of concrete encased steel composite

columns. *Engineering Structures*, *201*. https://doi.org/10.1016/j.engstruct.2019.109841

Lehne, J., & Preston, F. (2018). *Chatham House Report: Making Concrete Change Innovation in Low-carbon Cement and Concrete* . https://www.chathamhouse.org/sites/default/files/publications/2018-06-13-making-concrete-change-cement-lehne-preston-final.pdf

Li, G. Q., Li, L. L., Jiang, B., & Lu, Y. (2018). Experimental study on progressive collapse resistance of steel frames under a sudden column removal scenario. *Journal of Constructional Steel Research*, *147*, 1–15. https://doi.org/10.1016/J.JCSR.2018.03.023

Li, Y., Lu, X., Guan, H., & Ye, L. (2011). An improved tie force method for progressive collapse resistance design of reinforced concrete frame structures. *Engineering Structures*, *33*(10), 2931–2942. https://doi.org/10.1016/j.engstruct.2011.06.017

Lipasti, K., Bendjoia, T., Letzner, M., Minami, A., & Kukkonen, S. (2020). *Treet Tower Tree Tower Norway-Bergen*.

Liu, T., Xiao, ; Y, Asce, F., Yang, ; J, & Chen, B. S. (2017). CFRP Strip Cable Retrofit of RC Frame for Collapse Resistance. *Journal of Composites for Construction*, *21*(1). https://doi.org/10.1061/(ASCE)CC.1943-5614.0000722

Lu, X., Guan, H., Sun, H., Li, Y., Zheng, Z., Fei, Y., Yang, Z., & Zuo, L. (2021). A preliminary analysis and discussion of the condominium building collapse in surfside, Florida, US, June 24, 2021. *Frontiers of Structural and Civil Engineering*, *15*(5), 1097–1110. https://doi.org/10.1007/s11709-021-0766-0

Lyu, C. (2022). *Progressive Collapse Resistance of Post-and-Beam Mass Timber Buildings: Experimental and Numerical Investigations on 2D and 3D Substructures*. https://doi.org/10.25904/1912/4258

Lyu, C., Gilbert, B. P., Guan, H., Karampour, H., Gunalan, S., & Leggate, W. (2023). *AN ACCURATE FINITE ELEMENT MODEL TO STUDY THE PROGRESSIVE COLLAPSE OF POST-AND-BEAM MASS TIMBER BUILDINGS*. 2811–2819. https://doi.org/10.52202/069179-0368

Lyu, C. H., Gilbert, B. P., Guan, H., Underhill, I. D., Gunalan, S., & Karampour, H. (2021). Experimental study on the quasi-static progressive collapse response of post-and-beam mass timber buildings under corner column removal scenarios. *Engineering Structures*, *242*. https://doi.org/10.1016/j.engstruct.2021.112497

Lyu, C. H., Gilbert, B. P., Guan, H., Underhill, I. D., Gunalan, S., Karampour, H., & Masaeli, M. (2020). Experimental collapse response of post-and-beam mass timber frames under a quasi-static column removal scenario. *Engineering Structures*, *213*. https://doi.org/10.1016/j.engstruct.2020.110562

Malo, K. A., Abrahamsen, R. B., & Bjertnæs, M. A. (2016). Some structural design issues of the 14-storey timber framed building “Treet” in Norway. *European Journal of Wood and Wood Products*, *74*(3), 407–424. https://doi.org/10.1007/s00107-016-1022-5

McKenna, S. T., Jones, N., Peck, G., Dickens, K., Pawelec, W., Oradei, S., Harris, S., Stec, A. A., & Hull, T. R. (2019). Fire behaviour of modern façade materials – Understanding the Grenfell Tower fire. *Journal of Hazardous Materials*, *368*, 115–123. https://doi.org/10.1016/J.JHAZMAT.2018.12.077

Möhler, K. (1956). *Über Das Tragverhalten Von Biegeträgern Und Druckstäben Mit Zusammengesetzten Querschnitten Und Nachgiebigen Verbindungsmitteln*.

Mpidi Bita, H., Huber, J. A. J., Palma, P., & Tannert, T. (2022). Prevention of Disproportionate Collapse for Multistory Mass Timber Buildings: Review of Current Practices and Recent Research. *Journal of Structural Engineering*, *148*(7). https://doi.org/10.1061/(asce)st.1943-541x.0003377

Mpidi Bita, H., Huber, J. A. J., Voulpiotis, K., & Tannert, T. (2019). Survey of contemporary practices for disproportionate collapse prevention. *Engineering Structures*, *199*, 109578. https://doi.org/10.1016/j.engstruct.2019.109578

Mpidi Bita, H., Popovski, M., & Tannert, T. (2020). Experimental Study of Disproportionate Collapse Resistance Mechanisms for Mass-Timber Buildings. *ASCE Journal of Structural Engineering*, *146(2)*(04019199). https://doi.org/10.1061/(ASCE)ST.1943-541X.0002485

Mpidi Bita, H., & Tannert, T. (2017). Robustness of multi-storey timber buildings. *IABSE Conference, Vancouver 2017: Engineering the Future - Report*, 1934–1941. https://doi.org/10.2749/vancouver.2017.1934

Mpidi Bita, H., & Tannert, T. (2019a). Disproportionate collapse prevention analysis for a mid-rise flat-plate cross-laminated timber building. *Engineering Structures*, *178*(August 2018), 460–471. https://doi.org/10.1016/j.engstruct.2018.10.048

Mpidi Bita, H., & Tannert, T. (2019b). Experimental Study of Disproportionate Collapse Prevention Mechanisms for Mass-Timber Floor Systems. *Journal of Structural Engineering*, *146*(2), 04019199. https://doi.org/10.1061/(ASCE)ST.1943-541X.0002485

Mpidi Bita, H., & Tannert, T. (2019c). Tie-force procedure for disproportionate collapse prevention of CLT platform-type construction. *Engineering Structures*, *189*(February), 195–205. https://doi.org/10.1016/j.engstruct.2019.03.074

Munch-Andersen, J., & Dietsch, P. (2011). Robustness of large-span timber roof structures - Two examples. *Engineering Structures*, *33*(11), 3113–3117. https://doi.org/10.1016/j.engstruct.2011.03.015

Nam, N., & Luu, H. (2015). Analytical simplify models of the key elements in the alternative load path within the frame in accidental situation. *Transactions of the VŠB-Technical University of Ostrava Civil Engineering Series*, *15*(2). https://doi.org/10.1515/tvsb-2015-0014

Nie, X., Wang, J.-J., Mu, ;, Tao, X., Fan, J.-S., Mo, ; Y L, Asce, F., & Zhang, Z.-Y. (2020). Experimental Study of Shear-Critical Reinforced-Concrete Shear Walls under Tension-Bending Shear-Combined Cyclic Load. *Journal of Structural Engineering*, *146*(5). https://doi.org/10.1061/(ASCE)ST.1943-541X.0002596

Palma, P., Munch-Andersen, J., & Dietsch, P. (2023). *UPDATING EUROCODE 5 - DESIGN GUIDANCE FOR INCREASING THE ROBUSTNESS OF TIMBER STRUCTURES*. 3054–3061. https://doi.org/10.52202/069179-0398

Palmisano, F. (2014). Mitigation of Progressive Collapse by the Activation of the Elasto-Plastic Catenary Behaviour of R.C. Slab Structures. *The Open Construction and Building Technology Journal*, *8*(1), 122–131. https://doi.org/10.2174/1874836801408010122

Pearson, C., & Delatte, N. (2003). Lessons from Progressive Collapse of the Ronan Point Apartment Tower. *Forensic Engineering*, 190–200.

Pearson, C., & Delatte, N. (2005). Ronan Point Apartment Tower Collapse and its Effect on Building Codes. *Journal of Performance of Constructed Facilities*, *19*(2), 172–177. https://doi.org/10.1061/(ASCE)0887-3828(2005)19:2(172)

Pilon, A., Teshnizi, Z., Gilmore, L., Lopez, D., Koleilet, S., Rimland, J., & Herron, T. (2017). *Construction of a Tall Wood Building Brock Commons Tallwood House: Construction Overview*. 28. http://wood-works.ca/wp-content/uploads/brock_commons_-_construction_overview.pdf

Poirier, E., Staub-French, S., Pilon, A., Fallahi, A., Teshnizi, Z., Tannert, T., & Froese, T. (2022a). Design process innovation on brock commons tallwood house. *Construction Innovation*, *22*(1), 23–40. https://doi.org/10.1108/CI-11-2019-0116/FULL/XML

Poirier, E., Staub-French, S., Pilon, A., Fallahi, A., Teshnizi, Z., Tannert, T., & Froese, T. (2022b). Design process innovation on brock commons tallwood house. *Construction Innovation*, *22*(1), 23–40. https://doi.org/10.1108/CI-11-2019-0116

Przystup, A. C., Schrempf, H., Visniauskas, G., & Reynolds, T. P. S. (2020). CLT connection behaviour under extreme deformations and its influence on structural robustness in large timber construction. *IOM3 Tinber 2020 Conference*, 5–18.

Przystup, A., Lu, Y., Przystup, A. C., & Reynolds, T. (2021). *Are current robustness strategies appropriate for large timber structures?* https://www.researchgate.net/publication/360223117

Sasani, M. (2008). Response of a reinforced concrete infilled-frame structure to removal of two adjacent columns. *Engineering Structures*, *30*, 2478–2491. https://doi.org/10.1016/j.engstruct.2008.01.019

SIA. (2004). *Standard SIA 260 - Basis of Structural Design.*

Song, B. I., Giriunas, K. A., & Sezen, H. (2013). Progressive collapse testing and analysis of a steel frame building. *Journal of Constructional Steel Research*, *94*, 76–83. https://doi.org/10.1016/j.jcsr.2013.11.002

Sørensen, J. D. (2011). Framework for robustness assessment of timber structures. *Engineering Structures*, *33*(11), 3087–3092. https://doi.org/10.1016/j.engstruct.2011.02.025

Sørensen, J. D., Dietsch, P., Kirkegaard, P. H., & Köhler, J. (2010). *Design for Robustness of Timber Structures COST Action E55 "Modelling of Performance of Timber Structures."*

Starossek, U. (1999). Progressive collapse study of a multi-span bridge. *Structural Engineering International: Journal of the International Association for Bridge and Structural Engineering (IABSE)*, *9*(2), 121–125. https://doi.org/10.2749/101686699780621127

Starossek, U. (2007a). Disproportionate collapse: a pragmatic approach. *Proceedings of the Institution of Civil Engineers - Structures and Buildings*, *160*(6), 317–325. https://doi.org/10.1680/stbu.2007.160.6.317

Starossek, U. (2007b). Disproportionate collapse: A pragmatic approach. *Proceedings of the Institution of Civil Engineers: Structures and Buildings*, *160*(6), 317–325. https://doi.org/10.1680/stbu.2007.160.6.317

Starossek, U. (2007c). Typology of progressive collapse. *Engineering Structures*, *29*(9), 2302–2307. https://doi.org/10.1016/j.engstruct.2006.11.025

Starossek, U., & Haberland, M. (2008). Measures of Structural Robustness-Requirements and Applications. *Structures Congress 2008*.

Starossek, U., & Haberland, M. (2010). Disproportionate Collapse: Terminology and Procedures. *ASCE*, *24*(6), 519–528. https://doi.org/10.1061/ASCECF.1943-5509.0000138

Starossek, U., & Haberland, M. (2011). Approaches to measures of structural robustness. *Structure and Infrastructure Engineering*, *7*(7–8), 625–631. https://doi.org/10.1080/15732479.2010.501562

Starossek, U., & Haberland, M. (2012a). Robustness of structures. *Int. J. Lifecycle Performance Engineering*, *1*(1), 3–21. https://doi.org/10.1504/IJLCPE.2012.051279

Starossek, U., & Haberland, M. (2012b). Robustness of structures. *Int. J. Lifecycle Performance Engineering*, *1*(1), 3–21. https://doi.org/10.1504/IJLCPE.2012.051279

Structural Timber Association. (2015). Timber Engineering Notebook series. *The Structural Engineer*, *10*, 40–46.

Stylianidis, P. M., & Nethercot, D. A. (2021). Simplified Methods for Progressive Collapse Assessment of Frame Structures. *Journal of Structural Engineering*, *147*(11). https://doi.org/10.1061/(asce)st.1943-541x.0003190

Stylianidis, P. M., Nethercot, D. A., Izzuddin, B. A., & Elghazouli, A. Y. (2016a). Robustness assessment of frame structures using simplified beam and grillage

models. *Engineering Structures*, *115*, 78–95. https://doi.org/10.1016/J.ENGSTRUCT.2016.02.003

Stylianidis, P. M., Nethercot, D. A., Izzuddin, B. A., & Elghazouli, A. Y. (2016b). Study of the mechanics of progressive collapse with simplified beam models. *Engineering Structures*, *117*, 287–304. https://doi.org/10.1016/J.ENGSTRUCT.2016.02.056

Swedish Wood. (2019). *The CLT Handbook*.

Tan, E. L., & Uy, B. (2009). Experimental study on straight composite beams subjected to combined flexure and torsion. *Journal of Constructional Steel Research*, *65*(4), 784–793. https://doi.org/10.1016/J.JCSR.2008.10.006

Thornburg, D. W., & Kimball, C. (2022). *2021 International Building Code Illustrated Handbook*. McGraw-Hill Education. https://www-accessengineeringlibrary-com.ezproxy.is.ed.ac.uk/content/book/9781264270118

UK Building Regulations. (2022). *Approved Document B (fire safety) volume 1: Dwellings, 2019 edition incorporating 2020 and 2022 amendments*. www.gov.uk/guidance/building-regulations-

Unified Facilities Criteria. (2016). Design of Buildings To Resist Progressive Collapse. *Design of Buildings To Resist Progressive Collapse*, *November*.

Unified Facilities Criteria (UFC). (2005). *Structures to Resist the Effect of Accidental Explosions*. http://dod.wbdg.org/.

Viau, C., & Doudak, G. (2019). Behaviour and modelling of cross-laminated timber panels with boundary connections subjected to blast loads. *Engineering Structures*, *197*, 109404. https://doi.org/10.1016/J.ENGSTRUCT.2019.109404

Viau, C., & Doudak, G. (2020). Behavior and Modeling of Glulam Beams with Bolted Connections Subjected to Shock Tube–Simulated Blast Loads. *Journal of Structural Engineering*, *147*(1), 04020305. https://doi.org/10.1061/(ASCE)ST.1943-541X.0002876

Voulpiotis, K., Köhler, J., Jockwer, R., & Frangi, A. (2021a). A holistic framework for designing for structural robustness in tall timber buildings. *Engineering Structures*, *227*, 111432. https://doi.org/10.1016/j.engstruct.2020.111432

Voulpiotis, K., Köhler, J., Jockwer, R., & Frangi, A. (2021b). A holistic framework for designing for structural robustness in tall timber buildings. *Engineering Structures*, *227*. https://doi.org/10.1016/j.engstruct.2020.111432

Voulpiotis, K., Schär, S., & Frangi, A. (2022). Quantifying robustness in tall timber buildings: A case study. *Engineering Structures*, *265*. https://doi.org/10.1016/J.ENGSTRUCT.2022.114427

Wiesner, F. (2019). *Structural behaviour of cross-laminated timber elements in fires*. University of Edinburgh.

Wiesner, F., Bell, D., Chaumont, L., Bisby, L., & Deeny, S. (2018). Rolling shear capacity of CLT at elevated temperature. *WCTE 2018 - World Conference on Timber Engineering*, *August*.

Wiesner, F., Bisby, L. A., Bartlett, A. I., Hidalgo, J. P., Santamaria, S., Deeny, S., & Hadden, R. M. (2019). Structural capacity in fire of laminated timber elements in compartments with exposed timber surfaces. *Engineering Structures*, *179*(November 2018), 284–295. https://doi.org/10.1016/j.engstruct.2018.10.084

Winter, S., & Kreuzinger, H. (2008). The Bad Reichenhall ice-arena collapse and the necessary consequences for wide span timber structures. In *10th World Conference on Timber Engineering* .

Wood Products Council. (2022). *Status of Building Code Allowances for Tall Mass Timber in the IBC*. WoodWorks. https://www.woodworks.org/resources/status-of-building-code-allowances-for-tall-mass-timber-in-the-ibc/

Yang, B., & Tan, K. H. (2013). Robustness of Bolted-Angle Connections against Progressive Collapse: Experimental Tests of Beam-Column Joints and Development of Component-Based Models. *Journal of Structural Engineering*, *139*(9), 1498–1514. https://doi.org/10.1061/(ASCE)ST.1943-541X.0000749

Appendix A: Accidental scenario modelling initial research

A.1. Experimental methods

A linear static finite element analysis was performed in ABAQUS package on an example 5-storey experimental CLT building under multiple different loading scenarios, and the response of the system, in terms of member forces and displacements was compared. First group of scenarios is a series of notional removal of a stretch of load bearing wall, deemed as a statistically independent event. The second scenario group is imitating a fire contained in one compartment at a time, leading to a partial loss of mechanical strength in the adjacent structural elements without the occurrence of combustion (Figure A. 1). The maximum stresses areas are identified and then contraposed against the ultimate limit states of structural components predicting possible modes of failure.

A.1.1. Structure modelling

As this study is concerned with assessing the performance of CLT buildings, a generic arrangement for multi-storey CLT apartment buildings based on the KLH product design guidance was used (KLH, 2020), where dimensioning and structural design was based on Eurocode 5 EN 1995-1-1:2004 and EN 1995-1-2:2004 (European Committee for Standardisation, 2004). The simple single-leaf, one-way spanning arrangement allows for further simplification of the model, as modelling multiple bays in depth of the building is not going to be necessary, as each of the bays are predicted to act in a similar manner. Although the two-way spanning CLT capacity is recognised in this arrangement, where multiple panels are spanning in the same direction and only the fringes are additionally supported, the middle panels will be the most vulnerable for collapse. The choice was hence made that the FEA model will be created in a 2D frame arrangement. This would also allow for adopting the model in the future to simple experimental data from component test modelling.

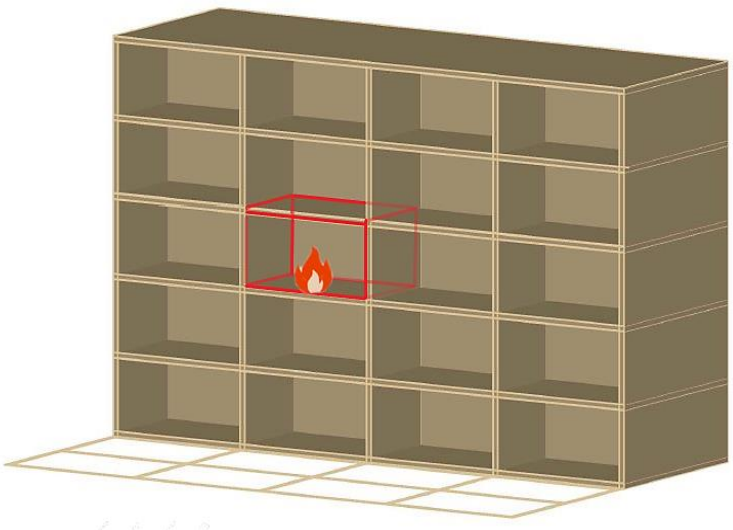

Figure A. 1 Structural elements affected by contained compartment fire.

The floor joints in this arrangement are located over the point of zero moment under regular loading conditions, which results in its location offset slightly from the central wall panel. Recent tests (A. C. Przystup et al., 2020) on the bending capacity of a typical half-lap connection have shown the initial loading rotational stiffness to be low enough to consider negligible in the specific loading conditions investigated, hence connections were modelled as hinges. TRADA pre-scheme design guide was used for wall and floor dimensioning. The building was chosen to be 5 storeys each of a height of 2500mm and 4 bays across, each spanning 5000mm (Figure A. 2). The choice of cross section for the walls was the 5-ply 100mm CLT of 20-20-20-20-20mm layup and for the floors the 5-ply 180mm CLT with the layup of 30-40-40-40-30.

To represent the CLT properties in the ABAQUS an equivalent homogenised material modelling approach was taken, using hand calculations to achieve the elastic and shear moduli of the slabs as a whole. The effective bending stiffness $(EI)_{eff}$ was calculated using the γ −method (Structural Timber Association, 2015) as shown in the Eq. A.1-A.3, where i is the layer number, γ is the connection efficiency factor, E_i is the elastic modulus of the layer i, A_i is the area of layer i, d_{cross} is the thickness of the traverse layer, G_r is the rolling shear modulus of the traverse layer, b is the width and *l* is the effective span of the member. In Equation A.2 I_i is the second moment of area of layer i and a_i is the lever arm to the centroid of layer i. In Eq. A.3, a_{ax} is the distance between two centre axes of top and bottom layers, h_i is the thickness of layer i, G_i is the shear modulus of the layer i, h_n is the thickness of surface layer and G_n is the shear modulus of the surface layer.

The effective shear stiffness $(GA)_{eff}$ was calculated using the shear analogy method (FPInnovations, 2013). Timber and hence the CLT panels are orthotropic and hence the calculations were undertaken in the three different directions, as shown in Table A. 1.

$$\gamma_i = \left[1 + \frac{\pi^2 E_i A_i d_{cross}}{G_r b l^2}\right]^{-1} \quad (A.1)$$

$$(EI)_{eff} = \sum_{i=1}^{3}(E_i I_i + \gamma_i E_i A_i {a_i}^2) \quad (A.2)$$

$$(GA)_{eff} = \frac{a_{ax}^2}{\left[\left(\frac{h_1}{2G_1 b}\right)+\left(\sum_{i=2}^{n-1}\frac{h_i}{G_i b_i}\right)+\left(\frac{h_n}{2G_n b}\right)\right]} \quad (A.3)$$

Table A. 1 Calculated equivalent elastic and shear moduli

	i	1	2	3
Floor 180mm	**E_i** (kPa)	6.92E+6	6.54E+5	4.00E+5
	G_i (kPa)	7.35E+4	8.25E+4	5.00E+4
Wall 100mm	**E_i** (kPa)	7.43E+6	1.95E+5	4.00E+5
	G_i (kPa)	7.46E+4	7.46E+4	5.00E+4

A.1.2. Load case modelling

The structural elements were numbered as shown in Figure A. 2. Two different categories of scenarios were investigated: the fire scenarios in ground floor compartments versus notional removal of ground floor walls (Figure A. 3a). The notional removal scenarios were undertaken for each of the structural walls at the ground level - W1, W2, W3, W4 and W5, resulting in 5 different removal scenarios (Figure A. 3c). These load cases were numbered after to the member lost e.g., removal of wall element 2 resulted in load case Removal 2. The 4 compartments at ground levels were similarly numbered (Figure A. 2) each of them resulting in scenarios Fire

1 through to Fire 4, each corresponding to the numbered compartment (Figure A. 3b). In modelling of the load cases for the fire scenarios, each of these compartments was investigated under three different levels of elastic modulus loss, which as per Eurocode 5 (European Committee for Standardisation, 2004b) occur at temperatures as presented in Table A. 2. Each of these fire scenarios is from now on referred to by the number of compartments it affects and relative modulus in percentage e.g., fire in compartment 2 causing decrease of elastic modulus down to 75% is referred to as be Fire-2-75. Additionally, a control load case was performed where no fire or element removal was present for reference to the other load cases.

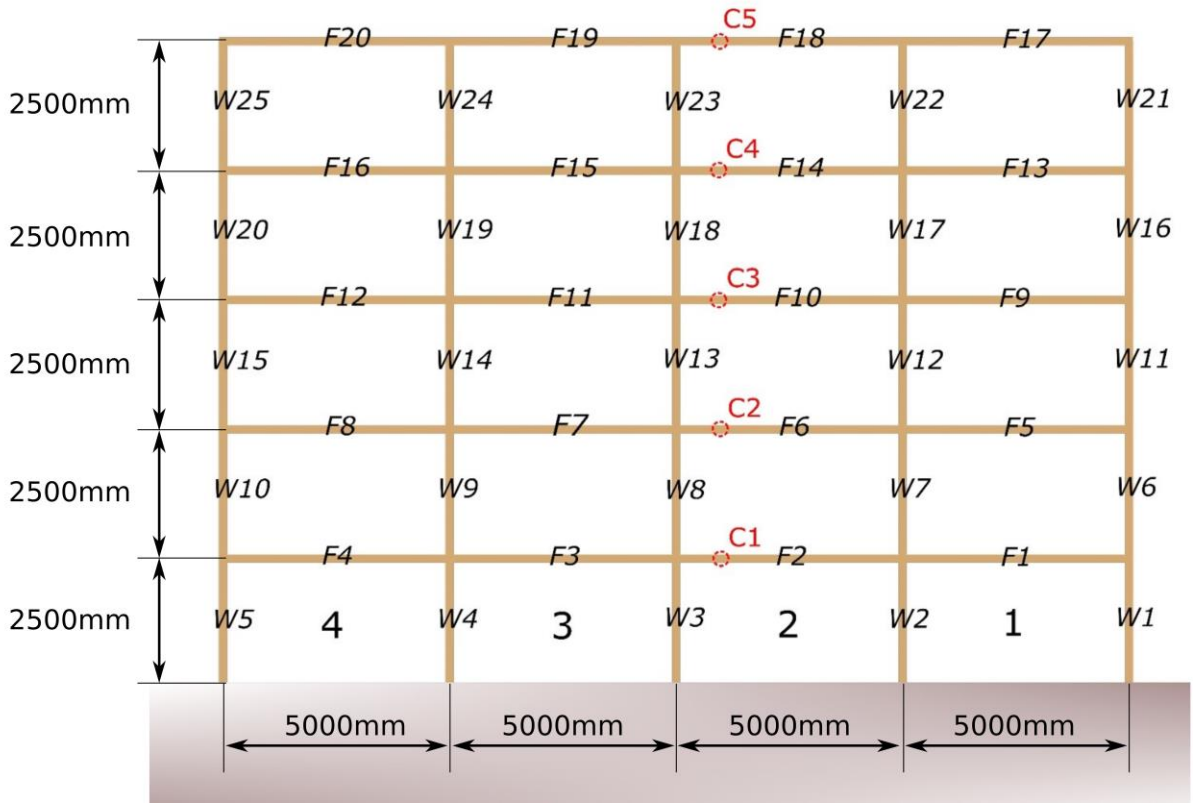

Figure A. 2 The numbering of structural elements, connections, and ground floor bays.

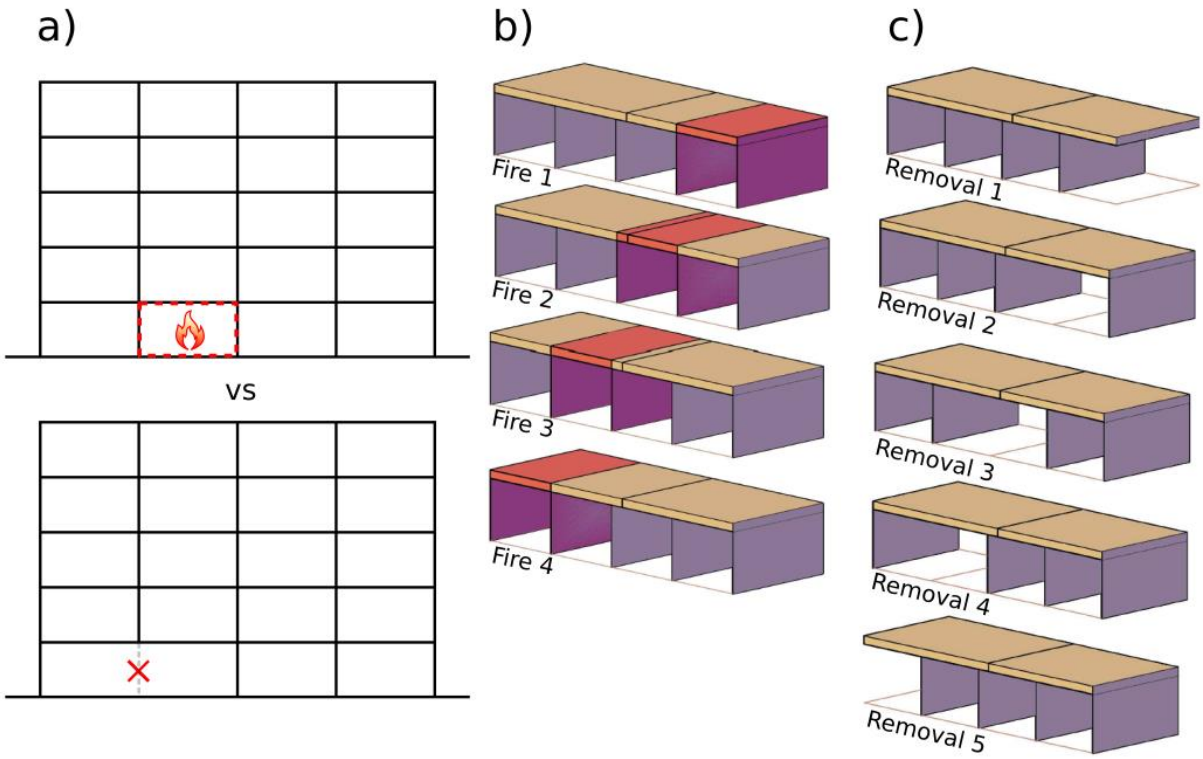

Figure A. 3 Diagram of the accidental loading scenarios investigated; a) fire versus wall removal scenarios in the context of the 5-storey experimental building; b) Fire scenarios 1-4; c) wall removal scenarios 1-5;

Table A. 2 Reduced elastic moduli due to increased temperature and the equivalent temperatures based on tension and compression charts

Relative modulus of elasticity	**Equivalent temperature in tension (˚C)**	**Equivalent temperature in compression (˚C)**
75%	60	50
50%	100	82
25%	175	153

A.2. Results and discussion

A.2.1. Ultimate limit state utilisations

Mechanical strength of the CLT has been experimentally shown (Wiesner, 2019) to decrease with rise in temperatures, approximating the curves outlined in the Eurocode 5 Part 1-2 Structural Fire Design (European Committee for Standardisation, 2004b). As such the reduction factor for compression, tension, and shear in the CLT elements was calculated based on the equivalent temperatures for relative reductions in modulus of elasticity (Table A. 4). The reduction factors were applied to the calculated ultimate strengths of the CLT appropriate to each of the load cases. Results of maximum stresses in each of the members were extracted from the ABAQUS output files for each of the load cases and the utilisation was subsequently calculated based on these values.

Table A. 3: Strength reduction factors

Relative modulus of elasticity	Compression reduction factor	Shear reduction factor	Tension reduction factor
0.75	0.7	0.8	0.87
0.5	0.25	0.55	0.65
0.25	0.18	0.3	0.4

A.2.2. Wall members

These structural elements were analysed based on their compressive force utilisations. The compressive strength in ambient temperatures was calculated as outlined in Eurocode 5 Part 1-1 eq. 6.20 (European Committee for Standardisation, 2004a), yielding the value of $4.12x10^3$ kN/m^2. As presented in Figure A. 4, all of the load cases have shown to reach capacities lower than 12%, staying well within their range to withstand the vertical loading. This is however directly dependent on the design and loading choices of the experimental structure. At corresponding temperatures as low as 50-60℃ (Table A. 2) the compressive force utilisation becomes comparable to one observed after removal of a support. The worst loading case from the ones investigated here is the Fire 1-25, affecting wall members W1, W2. The corresponding temperature as per Eurocode in this case ranges between 153-175℃.

Figure A. 5 shows the trend between the normalised values which were calculated to aid understanding of the relative influence a compartment fire load case model has on the structure in comparison to both the control case as well as the removal scenarios which are represented as horizontal lines on the graph for reference. As the decrease in elastic moduli and hence increase in temperatures is directly connected to the decrease in compressive strength capacity, the higher the reduction in the original elastic moduli the higher the utilisation exhibited. In this case the 75% reduction in their original elastic moduli would exhibit the largest utilisation even in comparison to the highest removal cases. As little as 25% reduction which corresponds to temperatures between 50-60 ℃ shows utilisations comparable to a complete removal of a wall support. Although in this specific case the utilisation is low, should there be a case study in which the walls were designed closer to their ultimate limit states or

compressive forces were distributed differently e.g., around large openings in the wall, special care should be taken.

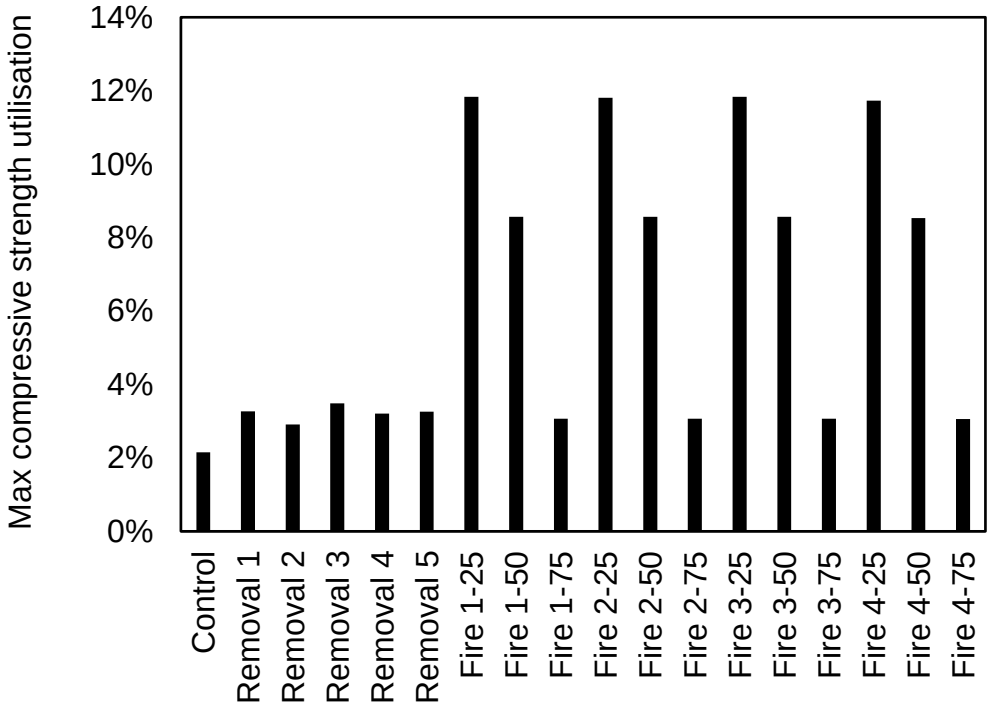

Figure A. 4 Maximum compressive strength utilisation for each of the load cases

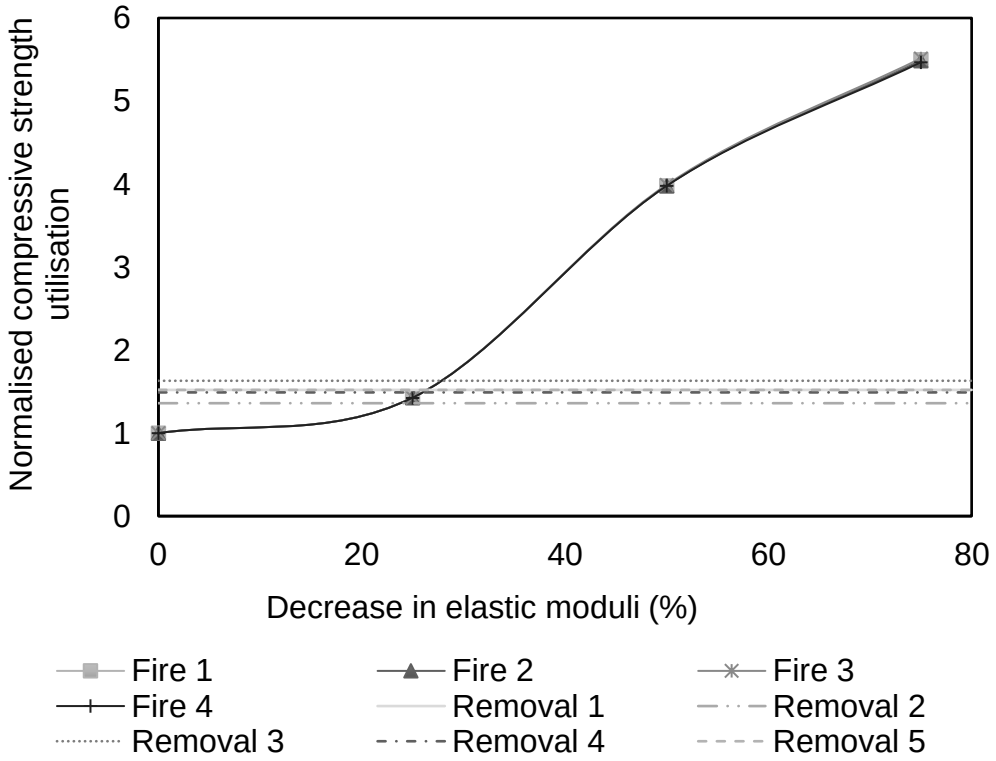

Figure A. 5 Normalised maximum compressive strength utilisation vs decrease in elastic moduli due to increased temperatures

It is also important to note that in case of a compartment fire all compressive elements surrounding this compartment could potentially be affected. The model also assumes that the change in temperatures occurs uniformly throughout the structure, whereas in reality this is expected to be in a form of gradient. As this would result in differential elastic moduli, the additional adverse P-delta effects could further decrease the buckling capacity of the elements.

A.2.3. Floor members

Floor members were investigated under two possible failure modes – bending strength and shear. The bending strength of the floor slabs in ambient temperature was assumed to be 1.45×10^4 kN/m^3, as outlined in BS EN 338:2016 for Class T14 (*BS EN 338:2016: Structural Timber. Strength Classes*, n.d.). The shear and rolling shear strengths were taken as 4×10^3 kN/m^3 and 1.25×10^3 kN/m^3 respectively as advised by Structural Timber Association (Structural Timber Association, 2015) using the BS EN 14080:2005 standard (*BS EN 14080:2005: Timber Structures. Glued Laminated Timber. Requirements*, n.d.). Based on these assumptions the maximum bending strength utilisations from the analysis are presented in Figure A. 6.

The worst load cases here can be identified to be the notional element removal, ranging in maximum bending strength utilisations between 42-58%. The location of the floor slab joint has shown to be of significance here, as the loss of member W2 resulted in the maximum utilisation localised in slab F1 of approximately 10% higher than the loss of W4 in its equivalent floor member F4. Similarly, loss of member W1

caused stresses 13% higher than the member W5. Overall, the fire loading scenarios was identified to cause significantly lower maximum utilisations in comparison to the notional removal of members, staying within the ranges of 12-28%. Figure A. 7 however still shows a notable increase from the control case and should the elements suffer any damage from element combustion and subsequently charring, the utilisation may increase further. The shear utilisations investigated have been found to be in a very low region, all of the rolling shear utilisation showing to be well below 3% and the shear strength utilisation below 1% (Figure A. 8). For a structure with floor spans of 5000mm it is expected for the bending strength to be the governing failure mode, hence the shear failures could be of significance in shorter spans. Normalised shear strength values calculated were the same for rolling and regular shear (Figure A. 9), as the same reduction factor was applied on these strength values. Although the utilisations were in the really low regions, the normalised chart does suggest that in a design case where shear would be the governing failure mode, the section weakening at around 60% loss of elastic moduli (approximately equivalent to temperatures above 90℃) could exceed the maximum utilisation of notional removal cases.

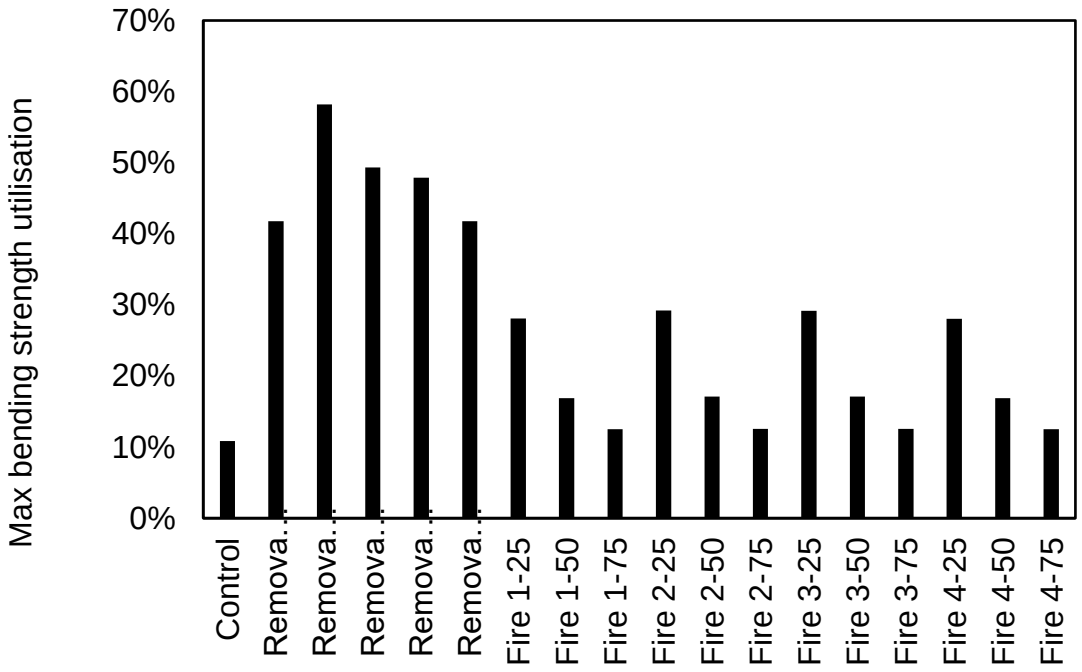

Figure A. 6 Maximum bending strength utilisation for each of the load cases

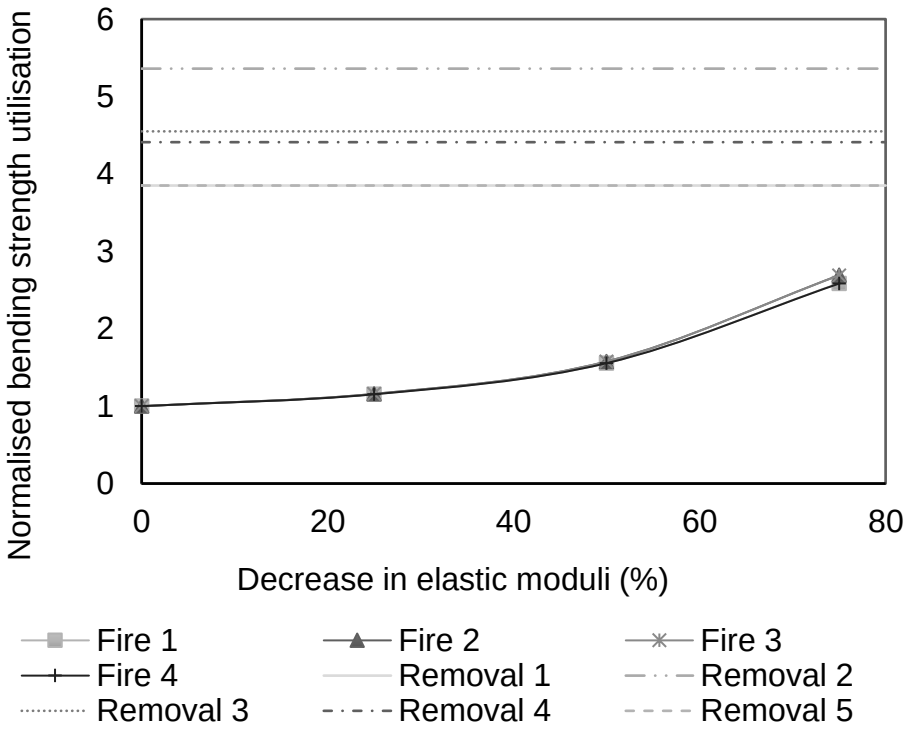

Figure A. 7 Normalised maximum bending strength utilisation vs decrease in elastic moduli due to increased temperatures

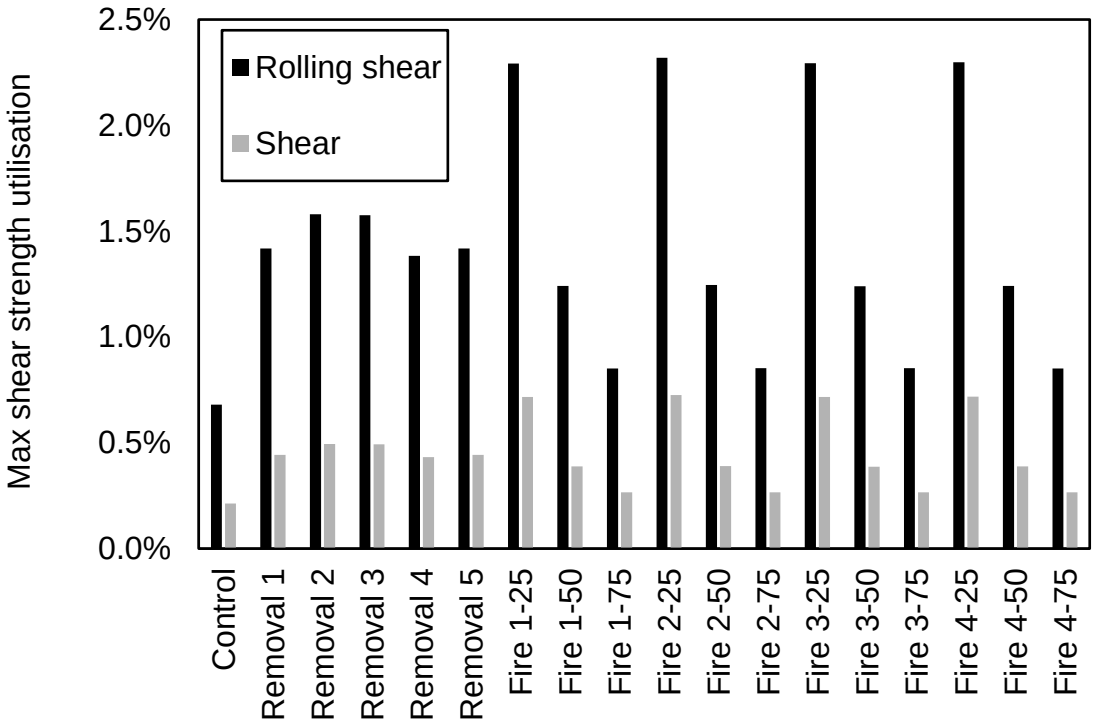

Figure A. 8 Maximum shear and rolling shear strength utilisation for each of the load cases.

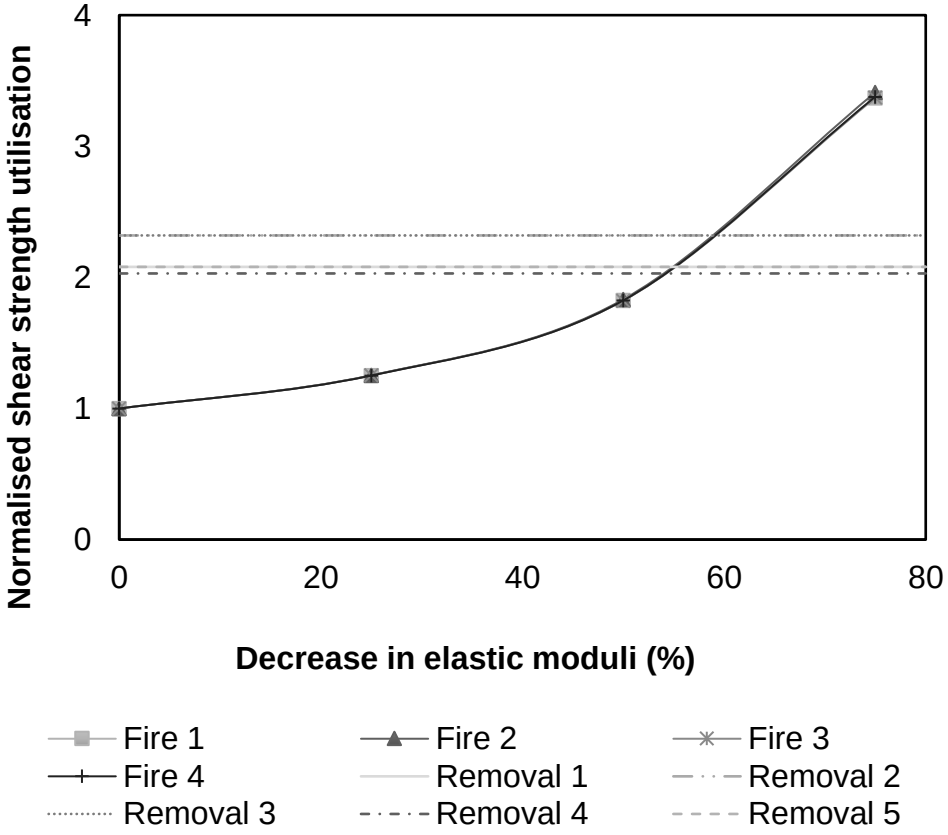

Figure A. 9 Normalised maximum shear and rolling shear strength utilisation vs decrease in elastic moduli due to increased temperatures.

A.3. Conclusions

The approach in this study was taken to use a simplified CLT structure resembling a 2D frame, which is to represent the behaviour of CLT elements under specific conditions rather than a real-life structure. This means that in a 3D case the forces could redistribute differently, especially since CLT elements are two-way spanning. The above scenarios were analysed under linear static column removal scenario and assumed to have kept within the elastic limit of timber, hence dynamic effects as well as second order analysis were here omitted. Inclusion of dynamic effects would be expected to further increase the strength utilisations and the second order analysis to reveal more redistribution of the forces, however in low levels of utilisations observed, these are expected to be insignificant.

The design of section dimensions was undertaken in accordance with a pre-scheme design guide and typical span to depth ratios for buildings used in practice, however, to minimise the assumptions the loading of the structure did not include any building finishes, but solely the CLT gravitational load and basic assumed live load. This kept the utilisations fairly low and may not be representative of the utilisations in real scenario. The equivalent homogeneous properties approach which was taken to model CLT panels in ABAQUS meant that the bending stresses needed to be recalculated to account for the imperfect composite action in the CLT panels.